

UNIVERSITÉ DU QUÉBEC À MONTRÉAL

UTILISATION DES KYSTES DE DINOFAGELLÉS COMME TRACEURS
D'EFFLORESCENCES ALGALES NUISIBLES ET OUTIL DE
RECONSTRUCTIONS PALÉOENVIRONNEMENTALES
DANS LE GOLFE DU MEXIQUE

THÈSE PRÉSENTÉE COMME EXIGENCE PARTIELLE
DU DOCTORAT EN SCIENCES DE L'ENVIRONNEMENT

PAR
AUDREY LIMOGES

FÉVRIER 2015

UNIVERSITÉ DU QUÉBEC À MONTRÉAL
Service des bibliothèques

Avertissement

La diffusion de cette thèse se fait dans le respect des droits de son auteur, qui a signé le formulaire *Autorisation de reproduire et de diffuser un travail de recherche de cycles supérieurs* (SDU-522 – Rév.01-2006). Cette autorisation stipule que «conformément à l'article 11 du Règlement no 8 des études de cycles supérieurs, [l'auteur] concède à l'Université du Québec à Montréal une licence non exclusive d'utilisation et de publication de la totalité ou d'une partie importante de [son] travail de recherche pour des fins pédagogiques et non commerciales. Plus précisément, [l'auteur] autorise l'Université du Québec à Montréal à reproduire, diffuser, prêter, distribuer ou vendre des copies de [son] travail de recherche à des fins non commerciales sur quelque support que ce soit, y compris l'Internet. Cette licence et cette autorisation n'entraînent pas une renonciation de [la] part [de l'auteur] à [ses] droits moraux ni à [ses] droits de propriété intellectuelle. Sauf entente contraire, [l'auteur] conserve la liberté de diffuser et de commercialiser ou non ce travail dont [il] possède un exemplaire.»

REMERCIEMENTS

Je tiens à remercier Anne de Vernal, Yves Gélinas et Ana-Carolina Ruiz-Fernandez pour la co-direction de ce projet de recherche. Cette étude a beaucoup bénéficié de leurs expertises respectives et complémentaires.

Un merci particulier à Anne de Vernal pour son soutien extrêmement précieux tout au long de mon parcours et pour toutes les opportunités d'enseignement, de participations à des expéditions océanographiques et de formation dans différents laboratoires qu'elle m'a offert. Son positivisme et sa confiance m'ont permis de relever plusieurs défis personnels.

Je tiens à remercier Jean-François Hélie, André Poirier et Maryse Henry pour tous les bons conseils, les discussions constructives et l'aide au spectromètre de masse, au laser et au microscope. Un énorme merci également à Laurent Londeix, Kenneth Mertens, André Rochon, Nicolas Van Nieuwenhove et Taoufik Radi pour leur patience et leur aide à l'identification taxonomique des différentes espèces de kystes de dinoflagellés. Merci à Amanda Gabriel pour sa gentillesse et sa patience durant le mois en laboratoire que nous avons partagé à extraire des brévetoxines.

Je voudrais aussi remercier Marie-Yasmine Bottein, John Ramsdell et l'équipe du centre de recherche CCEHBR de Charleston avec qui j'ai passé deux séjours exemplaires en laboratoire.

Un merci tout spécial revient à Sandrine Solignac pour avoir été une super partenaire d'échantillonnage et avoir survécu au *Chaha Coconut Tropical* Golfe du Mexique, épisode qui marque le début officiel de mon projet de doctorat. Je voudrais aussi remercier tous les amis du labo: Jenny, Jean-Baptiste, Laurence, Dimitri, Olivia, Lars, Sandrine, André, Benoît, Christelle, Julien, Jade et Quentin (et Céline & Renaud!).

Merci pour les supers randonnées en raquette, les bons soupers franco-belges québécois et les parties de croquette au lac Limoges, qui ont sans doute tous contribué à améliorer mon esprit analytique. Un énorme merci également à ma famille élargie qui a vécu de près ou de loin les aléas de la thèse: Ariane, Émilie, Geneviève, Martin, et Guillaume, vous êtes géniaux, un énorme merci!

Bien sûr, je tiens à remercier mes parents, mes sœurs, mes beaux-frères, mes neveux et nièces (Gilles, Jeannine, Sophie, Jim, Élyse, Louis, Annie, Louis-David, Alice, Élodie, Lily-Anne, Justine, Matthew, Éloi et Olivia) pour leur soutien, les beaux bricolages et encouragements. Je ne pourrai jamais assez remercier mes parents pour leur patience, leur générosité, leur compréhension et toutes leurs petites attentions qui font tellement plaisir.

Finalement, un gigantesque merci à monsieur Nicolas, qui a vécu la thèse avec moi. Merci pour ta patience, ta compréhension, ton aide, ton support, ta délicieuse lasagne, merci pour le quotidien.

TABLE DES MATIÈRES

LISTE DES FIGURES.....	ix
LISTE DES TABLEAUX.....	xii
LISTE DES PLANCHES PHOTOGRAPHIQUES	xiv
RÉSUMÉ	xv
INTRODUCTION GÉNÉRALE	1
CHAPITRE I	
ORGANIC-WALLED DINOFAGELLATE CYST DISTRIBUTION IN THE GULF OF MEXICO	12
Résumé.....	13
Abstract	14
1. Introduction.....	15
2. Regional Setting.....	17
2.1. Northern Gulf of Mexico (26–29°N; 86–94°W).....	18
2.2. West-central Florida coast (23–27°N; 82°W)	19
2.3. Southwestern Gulf of Mexico (18–19°N; 94–95°W).....	19
2.4. Mexican lagoons.....	20
3. Material and Methods	21
3.1. Palynological analyses	21
3.2. Statistical analyses.....	22
3.2.1. Hydrographical parameters	23
4. Results	24
4.1. Palynological assemblages	24
4.2. Statistical analyses.....	26
5. Discussion	27
5.1. Regional characteristics of palynological assemblages.....	27

5.2. Relationships between dinoflagellate cyst assemblages and environmental conditions	29
5.3. Note on the use of dinocysts as tracers of paleo-harmful blooms.....	30
6. Conclusion	32
7. References	34

CHAPITRE II

LONG-TERM HYDROLOGICAL CHANGES IN THE NORTHEASTERN GULF OF MEXICO (ODP-625B) DURING THE HOLOCENE AND LATE PLEISTOCENE INFERRED FROM ORGANIC-WALLED DINOFLAGELLATE CYSTS	64
Résumé	65
Abstract	66
1. Introduction	67
2. Material and Methods	69
2.1. Regional setting	69
2.2. Core and stratigraphy	70
2.3. Isotopic analyses ($\delta^{18}\text{O}$ and $\delta^{13}\text{C}$)	71
2.4. Mg/Ca ratios	71
2.5. Organic-walled dinoflagellate cysts	73
3. Results	74
3.1. Isotopic analyses ($\delta^{18}\text{O}$ and $\delta^{13}\text{C}$)	74
3.2. Mg/Ca ratios	75
3.3. Palynology and organic-walled dinoflagellate cysts	76
4. Discussion	78
4.1. Long-term changes in dinocyst assemblages	78
4.2. Comparison between Holocene and last interglacial records	79
5. Conclusion	82
6. References	84

CHAPITRE III

HIGH-RESOLUTION RECORD OF DINOFLAGELLATE CYSTS ASSEMBLAGES FROM THE SHALLOW ALVARADO LAGOON (SOUTHEASTERN GULF OF MEXICO)	105
Résumé.....	106
Abstract	107
1. Introduction.....	108
2. Regional setting.....	109
3. Material and methods.....	110
3.1. Age model	111
3.2. Geochemical and grain size analyses	112
3.3. Mg/Ca ratios	113
3.4. Palynological Analyses	113
4. Results.....	114
4.1. Geochemical analyses and grain size analyses.....	114
4.2. Mg/Ca ratios	115
4.3. Palynomorph assemblages	115
5. Discussion	117
5.1. Dinoflagellate cyst assemblages.....	117
5.2. Potential for past and future harmful algal blooms	119
5. Conclusion	121
6. References.....	122
CONCLUSION GÉNÉRALE	141
APPENDICE A	
FIRST REPORT OF SUB-RECENT FOSSILIZED CYSTS PRODUCED BY THE BENTHIC <i>BYSMATHRUM SUBSALSUM</i> (DINOPHYCEAE) FROM A SHALLOW MEXICAN LAGOON IN THE GULF OF MEXICO	145

Résumé.....	146
Abstract	147
Research note	148
References.....	153
APPENDICE B	
RAPPORT DE STAGE : DÉVELOPPEMENT D'UN BIOMARQUEUR POUR LE DINOFLAGELLÉ <i>KARENIA BREVIS</i>	160
BIBLIOGRAPHIE GÉNÉRALE	173

LISTE DES FIGURES

Figure	Page
1.1. Simplified map of seasonal surface currents along the shelves of the Gulf of Mexico	53
1.2. Distribution of winter (January–March) and summer (July–September) temperatures (°C) and salinities (psu) in the study area	54
1.3. Map showing the position of the studied sites and the principal river systems (A) and enlargements of the different study areas: B) Veracruz shelf, C) the Western coast of Florida, D) Laguna Alvarado, E) Laguna Mecoacán and F) Laguna de Terminos	55
1.4. Percentages of phototrophic taxa, dinoflagellate cyst concentrations (cysts·g ⁻¹), pollen grain concentrations (grains·g ⁻¹), foraminifer organic lining concentrations (linings·g ⁻¹) and annual productivity (gC·m ⁻² ·yr ⁻¹)	56
1.5. Percentages of the main dinoflagellate cyst taxa and the ratio of the reworked cysts over modern cysts	57
1.6. Distribution of A) total concentrations of dinoflagellate cysts (cysts·g ⁻¹), B) relative abundances (%) of heterotrophic and phototrophic taxa, C) relative abundances (%) of atypical <i>Operculodinium centrocarpum</i> , D) relative abundances (%) of atypical <i>Spiniferites mirabilis</i> , E) sites where <i>Melitasphaeridium choanophorum</i> was observed, and F) relative abundances (%) of <i>Polysphaeridium zoharyi</i>	58
1.7. Results of redundancy analysis: ordination diagram of species and environmental parameters according to axes 1 (44.7%) and 2 (20%)	59
1.8. Results of redundancy analysis: ordination diagram of sample scores according to axes 1 and 2, which represent respectively 44.7% and 20% of the variance.....	60
2.1. A) Position of site ODP-625B (28.83°N, 87.16°W), B) simplified map of the Loop Current and seasonal (summer and winter) position of the ITCZ, C)	

distribution of summer (July-September) temperatures (°C), D) distribution of winter (January-March) temperatures (°C).....	97
2.2. A) Total concentration of dinoflagellate cysts (cysts·g ⁻¹); B) estimated SST on the basis of Mg/Ca ratios from <i>G. ruber</i> (white) (this study) and Mg/Ca SST from Ziegler et al. (2008); C) stable carbon isotope ($\delta^{13}\text{C}$ in ‰) records of <i>U. peregrina</i> , <i>G. ruber</i> (white) and <i>G. ruber</i> (pink) (this study) and average $\delta^{13}\text{C}$ data from the benthic foraminifer <i>Cibicidoides wuellerstorfi</i> and <i>Cibicidoides</i> spp. from the northeast slope of Ceara Rise (Curry and Oppo, 1997); D) stable oxygen isotope ($\delta^{18}\text{O}$ in ‰) record of <i>U. peregrina</i> ; E) stable oxygen isotope ($\delta^{18}\text{O}$ in ‰) records of <i>G. ruber</i> (white) and <i>G. ruber</i> (pink); F) benthic stable oxygen isotopes ($\delta^{18}\text{O}$ in ‰) from stack LR04 (Lisiecki and Raymo, 2005); G) summer insolation at 30°N.....	98
2.3. 1) The dominant species index (<i>Impagidinium</i> species and <i>Operculodinium centrocarpum</i> over <i>Spiniferites</i> species), relative abundances of the main dinocyst taxa, total cyst concentrations (cysts·g ⁻¹), organic foraminifer lining concentrations (linings·g ⁻¹) and the ratio of cysts over pollen during the Holocene and late Pleistocene intervals.....	99
2.4. Affinity to mean annual temperature (°C) and salinity (psu) for the dominant dinocyst species according to the global dataset.....	100
2.5. Model simulations for different sea-level and the position of the modern and MIS 6 Mississippi delta.....	101
3.1. Study area with position of core site and surface circulation	134
3.2. (a) Records of ^{210}Pb activity (Bq·kg ⁻¹) and (b) ^{237}Cs activity (Bq·kg ⁻¹) as function of depth, (c) age model, (d) sediment accumulation rate (SAR) over depth	135
3.3. Results of geochemical and grain size analyses, and age model: granulometry (%) and relative abundances of carbonate (CaCO ₃ ; %), organic carbon (C _{org} ;%), aluminum (%), titanium (%), chlorine (%) and bromine (μg/g).....	136
3.4. Flux of dinocysts (cysts·cm ⁻² ·yr ⁻¹), organic foraminifer linings (linings·cm ⁻² ·yr ⁻¹), gymnosperm pollen (grains·cm ⁻² ·yr ⁻¹) and angiosperm pollen (grains·cm ⁻² ·yr ⁻¹), temperatures inferred from Mg/Ca ratios of foraminifer shells and age model.....	

.....	137
3.5. Relative abundance of the main dinocyst taxa (%) and total cyst fluxes (cysts· cm ⁻² ·yr ⁻¹).....	138

LISTE DES TABLEAUX

Tableau	Page
1.1. Location of the surface sediment samples investigated in the present study	47
1.2. Environmental parameters included in the statistical analyses corresponding to the database sampling sites: summer, winter and annual temperatures (sSST, wSST, aSST; °C), summer, winter and annual salinity (sSSS, wSSS, aSST), annual, summer (April–September) and winter (October–March) primary productivity estimated by moDIS programs (sP, wP, aP; gC·m ⁻² ·yr ⁻¹), the water depth (m) and the distance to the coast (km)	48
1.3. Dinoflagellate cyst species reported from surface sediment samples, abbreviations and notes.....	50
1.4. Dinoflagellate cyst species reported from surface sediment samples, abbreviations and notes.....	50
1.5. Coefficient of correlation between environmental parameters and the scores of the three first axes of redundancy analysis.....	51
1.6. Scores of dinocyst taxa according to the three first axes of redundancy analysis ..	52
2.1. Results from the radiocarbon analyses for core ODP-625B	93
2.2. Mean Mg/Ca values for each chamber of the analyzed foraminifers and resulting Mg/Ca corresponding to each sample.....	94
2.3. Geochemical data	95
2.4. Affinity to mean annual temperature (°C) and salinity (psu) for the dominant dinocyst species according to the global dataset (Zonneveld et al., 2013) and modern distribution in the Gulf of Mexico (Limoges et al., 2013).....	96

3.1. Records of ^{210}Pb activity ($\text{Bq}\cdot\text{kg}^{-1}$) and ^{237}Cs activity ($\text{Bq}\cdot\text{kg}^{-1}$) as function of depth.....	131
3.2. Geochemical and grain size data.....	132
3.3. Palynomorph concentrations and fluxes over depth	133

LISTE DES PLANCHES PHOTOGRAPHIQUES

Planche	Page
1.1. Bright field light micrographs of selected dinocyst taxa: 1. <i>Selenopemphix nephroides</i> ; 2–3. <i>Selenopemphix quanta</i> ; 4. <i>Votadinium spinosum</i> ; 5. <i>Stelladinium stellatum</i> ; 6. <i>Impagidinium striatum</i> ; 7. <i>Impagidinium aculeatum</i> ; 8. <i>Impagidinium velorum</i> 9–11. <i>Melitasphaeridium choanophorum</i> ; 12. <i>Concentricystes</i> ind.; 13–14. <i>Lingulodinium machaerophorum</i> ; 15. <i>Polysphaeridium zoharyi</i> ; 16. Scanning electron microscope (SEM) image showing the bifurcate process termination of the cyst <i>Polysphaeridium zoharyi</i>	61
1.2. Bright field light micrographs of selected dinocyst taxa: 1–5. <i>Nematosphaeropsis rigida</i> ; 6–7. <i>Operculodinium israelianum</i> ; 8. <i>Operculodinium longispinigerum</i> ; 9–10. Atypical <i>Operculodinium centrocarpum</i> ; 11. <i>O. centrocarpum</i> ; 12–13. <i>Spiniferites belerius</i> ; 14–15. <i>Spiniferites bentorii</i> ; 16–19. Different morphotypes of <i>Spiniferites mirabilis</i> ; 20. Scanning electron microscope (SEM) image of <i>S. mirabilis</i>	62
2.1. Bright field light micrographs of selected dinocyst taxa: 1. <i>Impagidinium aculeatum</i> ; 2. <i>Impagidinium plicatum</i> ; 3. <i>Impagidinium striatum</i> ; 4. <i>Tectatodinium pellitum</i> ; 5–6. cf. <i>Impagidinium sphaericum</i> ; 7–8. <i>Brigantedinium cariacense</i> ; 9. <i>Quinquecuspis concreta</i> ; 10. <i>Tuberculodinium vancampoae</i>	102
2.2. Bright field light micrographs of selected dinocyst taxa: 1. <i>Operculodinium janduchenei</i> ; 2. <i>Operculodinium giganteum</i> ; 3. <i>Operculodinium longispinigerum</i> ; 4. <i>Operculodinium israelianum</i> ; 5. <i>Nematosphaeropsis rigida</i> ; 6. <i>Polysphaeridium zoharyi</i> ; 7. <i>Nematosphaeropsis lemniscata</i>	103
3.1. Bright field light micrographs of selected dinoflagellate cyst species (1–3) <i>Spiniferites mirabilis</i> sensu stricto. Note the important morphological variations that characterize this taxon. (4–6) <i>Spiniferites</i> cf. <i>lenzii</i> . High to low focal planes. (7) <i>Polysphaeridinium zoharyi</i> (8–9) <i>Spiniferites</i> cf. <i>delicatus</i>	139

RÉSUMÉ

Les efflorescences algales nuisibles connaissent une augmentation en fréquence et en intensité dans de nombreux milieux côtiers à travers le monde. En réponse à des conditions environnementales favorables, elles résultent d'une forte densité relative d'espèces toxiques, ou d'une biomasse élevée contribuant à la diminution des concentrations en oxygène des eaux profondes. L'apparente intensification des efflorescences algales nuisibles est un problème environnemental de plus en plus préoccupant. Elle est possiblement liée au forçage anthropique (i.e. réchauffement climatique, pollution, eutrophisation, transport maritime, etc.). Elle pourrait également refléter une surveillance accrue des milieux côtiers. Afin de mieux identifier leurs causes naturelles et/ou anthropiques, il est ainsi nécessaire de retracer leur variation dans le temps, au-delà des quelques décennies d'enregistrements directs, lorsqu'ils existent.

Dans le golfe du Mexique, environ 40 espèces potentiellement toxiques ont été identifiées. Parmi celles-ci, les dinoflagellés sont associés aux conséquences les plus délétères sur les écosystèmes marins. Dans ce contexte, cette thèse a pour principal objectif de caractériser la distribution temporelle et spatiale des espèces de dinoflagellés nuisibles dans le golfe du Mexique. À cette fin, nous explorons le potentiel des microfossiles contenus dans les sédiments comme traceurs d'efflorescences algales nuisibles. Puisque les dinoflagellés occupent un rôle important dans la formation de blooms nuisibles en milieu marin, cette étude s'intéresse à leur forme fossile préservée dans les sédiments à la faveur de leur membrane organique très résistante, soit les kystes de dinoflagellés ou dinokystes.

Dans un premier temps, des analyses palynologiques ont été effectuées sur 44 échantillons de surface provenant de différentes régions du golfe du Mexique. Elles ont permis de définir quantitativement la relation entre les paramètres environnementaux (i.e. température, salinité, profondeur, productivité, etc.) et les assemblages modernes de dinokystes. Des analyses de redondance ont permis d'identifier la profondeur de la colonne d'eau, la distance par rapport à la côte et la température annuelle comme étant les facteurs qui sont le plus liés à la distribution des kystes dans le golfe du Mexique. Ce travail a également permis d'identifier certaines zones susceptibles d'être affectées par des efflorescences causées par le dinoflagellé potentiellement toxique *Pyrodinium bahamense*. Le kyste qu'il produit, *Polysphaeridinium zoharyi*, atteint en effet des abondances très élevées notamment sur la côte ouest de la péninsule de la Floride et dans les lagunes mexicaines. Les réservoirs de kystes dans le sédiment ont le potentiel de constituer l'inoculum primaire à la formation de blooms.

En second lieu, des analyses géochimiques sur la calcite de foraminifères ($\delta^{18}\text{O}$ et ratios Mg/Ca) ont été combinées à des analyses palynologiques sur la séquence sédimentaire ODP-625B, collectée dans le nord-est du golfe et présentant les enregistrements de plusieurs grands cycles climatiques. Elles permettent de documenter la réponse des assemblages de dinokystes vis-à-vis les variations climatiques de l'Holocène et de la fin du Pléistocène, notamment pendant l'optimum du dernier interglaciaire. Les résultats illustrent des assemblages de dinokystes significativement distincts entre les périodes froides et chaudes, mais également entre l'interglaciaire actuel et le dernier interglaciaire, malgré des faibles différences de l'insolation boréale en été et des paléo-températures régionales entre ces deux périodes (~1-2°C selon les températures déduites des ratios Mg/Ca). Les assemblages de dinokystes suggèrent que des différences dans la circulation des masses d'eaux de surface et dans la bathymétrie expliquent les modifications dans les communautés phytoplanctoniques au site d'étude au cours des intervalles étudiés. Les dinokystes montrent un potentiel d'utilisation dans le cadre de reconstitutions paléoenvironnementales en milieu tropical, où les efflorescences algales nuisibles représentent un enjeu considérable.

Finalement, une série chronologique de plus haute résolution a été développée à partir de l'étude d'une carotte sédimentaire prélevée dans la lagune Alvarado (sud-ouest golfe du Mexique). L'enregistrement couvre environ 830 ans, une période au cours de laquelle *Polysphaeridium zoharyi* est resté très abondant. Les dépôts de kystes dans les sédiments indiquent que ce taxon a potentiellement créé des efflorescences algales nuisibles dans le passé et constituent toujours une menace.

En outre, cette thèse fournit des informations originales sur l'autoécologie des dinokystes en milieu tropical. Elle démontre une extension biostratigraphique moderne de *Melitasphaeridium choanophorum* dans les sédiments du golfe du Mexique, alors que cette espèce était considérée éteinte depuis la fin du Pléistocène. Elle a permis de recenser pour la première fois les kystes du dinoflagellé benthique *Bysmatrum subsalsum*. Elle a également permis d'illustrer les variations de la morphologie des kystes produits en milieux peu profonds soumis à des conditions variables de salinité et température.

Finalement, ce projet ouvre la voie à l'utilisation des archives sédimentaires comme outil de surveillance pour les zones susceptibles d'être affectées par des efflorescences algales nuisibles et pour aider à mieux comprendre les facteurs favorables à leur initiation.

Mots-clés: Dinokystes, Efflorescences algales nuisibles, golfe du Mexique, *Melitasphaeridium choanophorum*, *Bysmatrum subsalsum*, *Polysphaeridium zoharyi*

INTRODUCTION GÉNÉRALE

Les efflorescences algales nuisibles se produisent lorsque des augmentations significatives et anormalement élevées de la concentration d'une ou de plusieurs espèces planctoniques induisent des conséquences néfastes sur la qualité du milieu et sur la santé des espèces vivantes. Parmi les quelques 4000 espèces marines planctoniques, environ 300 sont documentées comme potentiellement nuisibles (Sournia, 1995) et comptent notamment parmi elles plusieurs diatomées, cyanobactéries, raphidophytes, haptophytes et dinoflagellés. Chacune de ces espèces présente une niche écologique spécifique et leur multiplication est stimulée lorsque les conditions requises au développement de populations viables sont rencontrées qu'il s'agisse de la température, salinité, ou disponibilité en nutriments, par exemple. Les conséquences écosystémiques des proliférations nuisibles sont donc largement dépendantes des affinités biologiques et écologiques des espèces impliquées ainsi que des propriétés physico-chimiques du milieu (Zingone & Enevoldsen, 2000). Ainsi, le développement d'une forte densité d'espèces toxiques ou d'une biomasse élevée peut, le cas échéant, causer une intoxication de l'ensemble de la chaîne alimentaire et/ou contribuer à la diminution des concentrations en oxygène dissous dans les eaux profondes. Elles peuvent provoquer des mortalités massives chez les poissons, mammifères et invertébrés et potentiellement rendre le milieu impropre au développement de la vie. À l'échelle internationale, 60 000 cas d'intoxication humaine causés par des algues marines toxiques sont relevés chaque année (Van Dolah, 2000a). En plus des conséquences sur les écosystèmes marins et la santé des populations humaines, ces blooms nuisibles représentent des enjeux majeurs pour les industries de la pêche et du tourisme des pays qui en sont affectés.

Les efflorescences algales, au sens strict, se produisent généralement de manière saisonnière et ponctuelle. Cependant, depuis les dernières décennies, l'augmentation de leur fréquence et amplitude, ainsi que de leur expansion géographique sont

souvent attribuées directement ou indirectement aux activités humaines. Les causes qui ont été évoquées pour expliquer l'intensification de cette problématique incluent l'eutrophisation des milieux côtiers, l'augmentation des activités d'aquaculture, le réchauffement climatique et le transfert des organismes envahissants via les activités de transport maritime (e.g. Smayda, 1990, 2008 ; Hallegraeff, 1993; Van Dolah, 2000a; Anderson et al., 2008 ; Landsberg, 2002; Heisler et al., 2008; Rabalais et al., 2009). Elle peut également résulter d'une surveillance plus soutenue des régions côtières.

Parmi la variété d'organismes qui montrent un potentiel pour leur formation, les dinoflagellés constituent le groupe phytoplanctonique le plus fréquemment impliqué dans le développement d'efflorescences algales nuisibles (Van Dolah, 2000b, Smayda & Reynolds, 2003).

1.1 Les dinoflagellés nuisibles

Les dinoflagellés sont des protistes algaires de la division des Dinoflagellata et appartenant à la classe des Dinophyceae. Avec les coccolithophores et les diatomées, ils représentent l'un des constituants majeurs de la productivité primaire marine et sont également rencontrés dans les milieux saumâtres (e.g. Trigueros, 2000) et d'eau douce (Mertens et al., 2012). Environ la moitié des dinoflagellés modernes sont phototrophes ou mixotrophes, c'est-à-dire ayant la capacité de combiner des processus photosynthétiques et hétérotrophiques. L'autre moitié, dépourvue de chloroplaste, est hétérotrophique et dépend de l'abondance d'autres micro-organismes et/ou de matière organique dissoute pour combler ses besoins énergétiques (Jacobson & Anderson, 1986; Taylor & Pollingher, 1987). À cela s'ajoutent, pour certains dinoflagellés, des modes de nutrition plus complexes dont le parasitisme et la symbiose avec d'autres organismes (Pawlowski et al., 2001).

Environ 100 espèces de dinoflagellés sont associées à la formation de blooms nuisibles. À l'exception de quelques taxons (e.g. *Noctiluca*, *Dinophysis*, *Protoperidinium*), les espèces nuisibles se caractérisent par un mode de nutrition photosynthétique ou mixotrophe (de Vernal & Marret, 2007). De ce nombre, environ la moitié (~50 espèces) libèrent des toxines ou des métabolites secondaires qui peuvent causer divers types d'empoisonnement (Sournia, 1995). Le rôle écologique de ces toxines demeure incertain (défense, prédation, etc) (Rice, 1984; Granéli et al., 2008; Sheng et al., 2010), mais il leur confère un avantage compétitif pour l'accès aux ressources du milieu. Puisqu'elles ne peuvent être consommées efficacement par le zooplancton, les efflorescences algales toxiques sont également associées à un pauvre transfert des éléments nutritifs et du carbone vers les niveaux trophiques supérieurs ce qui affecte l'ensemble de la chaîne alimentaire. Ce processus s'ajoute à l'action directe des biotoxines sur les organismes.

Plusieurs études approfondies ont été consacrées à la toxicologie des toxines de dinoflagellés qui peuvent causer un certain nombre de symptômes aigus et chroniques: 1) l'intoxication paralysante par les mollusques (PSP pour *paralytic shellfish poisoning*), 2) l'intoxication neurotoxique par les mollusques (NSP pour *neurotoxic shellfish poisoning*), 3) l'intoxication diarrhéique par les mollusques (DSP pour *diarrhetic shellfish poisoning*), 4) l'intoxication par la ciguatera (CFP pour *ciguatera fish poisoning*) et 5) l'intoxication azaspiracide (AZP pour *azaspiracide shellfish poisoning*) (e.g. Botana, 2000). Certaines de ces toxines peuvent être bioaccumulées par les mollusques – qui constituent par ailleurs le vecteur de contamination principal vers l'Homme – mais également par les poissons et d'autres organismes en fonction des toxines impliquées.

1.2 Le cycle de vie des dinoflagellés et la production de kystes de résistance

Les dinoflagellés présentent des cycles de vie complexes au cours desquels se

succèdent plusieurs stades de développement caractérisés par des transformations aux niveaux de la physiologie, la motilité et la résistance aux conditions du milieu. Le cycle de vie de certaines espèces comporte une phase haploïde végétative ainsi qu'une phase diploïde sexuée (Figure 1). Au cours de la phase haploïde végétative, les cellules sont motiles dans la colonne d'eau et se reproduisent par simple division (mitose). Il s'agit du mode de reproduction le plus répandu. La reproduction sexuée est quant à elle observée chez un nombre plus restreint de dinoflagellés. Elle implique la fusion des gamètes produits lors de la phase végétative ce qui assure la recombinaison du matériel génétique. Chez environ 15% des espèces, des kystes de résistance – communément appelés dinokystes – sont produits suite à la phase de reproduction sexuée et permettent de protéger la cellule durant une période de dormance. Ce stade benthique non-motile assure notamment la survie des organismes en période de stress environnemental (i.e. température, limitation des nutriments, etc.) (Von Stosch, 1973; Anderson & Lindquist, 1985; Anderson et al., 1985; Rengefors & Anderson, 1998; Anderson & Rengefors, 2006 ; Figueroa & Bravo, 2006). Il a été démontré que les kystes peuvent rester viables dans les dépôts sédimentaires jusqu'à un siècle (Lundholm et al., 2011; Ribeiro et al., 2011). Suite à une période de dormance de durée variable, mais obligatoire, la cellule peut sortir du kyste par une ouverture appelée « archéopyle » et se diviser en deux cellules haploïdes par méiose (Evitt, 1985). Un nouveau cycle de reproduction peut alors commencer.

Cette capacité qu'ont certains dinoflagellés de produire des kystes de dormance relève d'une grande importance dans les mécanismes de formation des blooms, car les kystes peuvent constituer l'inoculum primaire à leur formation et permettre une multiplication exponentielle des cellules lorsque les conditions environnementales redeviennent favorables (Wall, 1971; Anderson, 1998; Estrada et al., 2010). Ainsi, le nombre de cellules qui « exkystent » est considéré comme un facteur décisif pour l'étendue et l'intensité des blooms (Hense, 2010). Les kystes jouent un rôle très important pour la dispersion des dinoflagellés par différents vecteurs, incluant les

courants ou les eaux de ballast des navires puisqu'ils les rendent davantage susceptibles d'être transférés d'un milieu vers un autre et de survivre au voyage les menant vers un nouvel habitat (e.g. Lacasse et al., 2013).

Par ailleurs, la paroi de la majorité des dinokystes est composée d'un polymère de carbohydrate complexe (dinosporine) très réfractaire (Versteegh et al., 2012), ce qui permet leur bonne préservation dans le registre fossile. Ces kystes présentent donc un intérêt particulier pour le domaine de la micropaléontologie puisqu'ils sont moins susceptibles d'être affectés par des processus de dissolution que les autres microfossiles à tests siliceux telles les diatomées, ou carbonatés tels les foraminifères et coccolithes. Dans le cadre d'études d'assemblages fossiles de dinokystes, il est toutefois important de considérer la préservation sélective des espèces en conditions oxydantes (e.g. Zonneveld et al., 2008). Bien que les assemblages de dinokystes reflètent une image partielle de la diversité de la communauté de dinoflagellés dont ils sont issus (~15% des espèces produisent des kystes de résistance), ils n'en constituent pas moins d'excellents traceurs des paramètres hydrologiques de surface (de Vernal & Marret, 2007 et les références qui y sont incluses), de productivité primaire (Dale, 2001; Radi et al. 2007), de la pollution liée aux activités humaines (Pospelova et al., 2002) et des processus d'eutrophisation (Dale & Fjellså, 1994; Dale, 1996). Ils sont largement utilisés dans le cadre de reconstitutions paléoenvironnementales et paléocéanographiques, notamment dans les hautes latitudes (e.g. Mudie et al., 2001 et références qui y sont incluses ; de Vernal et al., 2005).

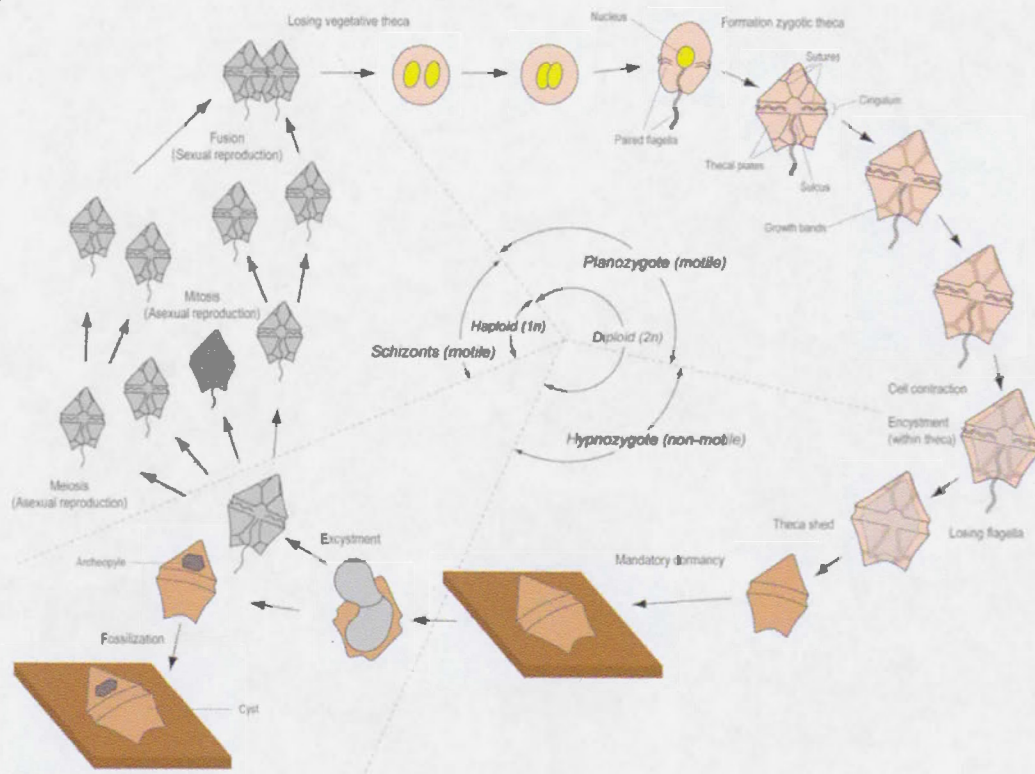


Schéma idéalisé du cycle de vie des espèces de dinoflagellés associées à la production de kystes de résistance (modifié par Verleye (2011) d'après Evitt (1985)).

1.3 Le Golfe du Mexique et les efflorescences algales nuisibles

Le Golfe du Mexique est un bassin océanique semi-isolé adjacent à l'océan Atlantique. Sa circulation de surface forme une boucle: les eaux chaudes et salées des Caraïbes pénètrent par le chenal du Yucatán, s'étendent vers le nord-est et ressortent par le détroit de la Floride, pour finalement alimenter le Gulf Stream (e.g., Oey et al, 2005 et références qui y sont incluses). L'extension longitudinale et latitudinale du courant des Caraïbes à l'intérieur du bassin varie saisonnièrement, entraînant des modifications dans les propriétés des masses d'eau de surface (température, salinité). L'hydrologie régionale est également influencée par le système fluvial Mississippi-

Atchafalaya qui représente 90% de l'apport total d'eau douce dans le Golfe du Mexique.

Les premiers enregistrements d'efflorescences algales nuisibles dans le Golfe du Mexique remontent à 1530, alors que les explorateurs espagnols avaient noté des fortes mortalités de poissons près de Tampa Bay (Floride) (Steidinger et al., 1998). Le long des côtes mexicaines, le premier épisode reporté est survenu en 1875 à proximité de la ville de Veracruz (Magaña et al., 2003). Depuis les dernières décennies, la récurrence accrue des efflorescences algales nuisibles a motivé la création d'un vaste réseau de surveillance et de détection du (micro)plancton toxique. Les zones côtières de la péninsule de la Floride sont parmi les mieux documentées (e.g. Taylor, 1917; Tester & Steidinger, 1997; Steidinger et al., 1998; Kusek et al., 1999; Phlips et al., 1999, 2004, 2006; Magaña et al., 2003; Flewelling et al., 2005; Brand & Compton, 2007; Vargo et al., 2008). Sur l'ensemble du bassin, plus de 40 espèces toxiques ou potentiellement toxiques ont été identifiées parmi lesquelles les dinoflagellés, et particulièrement *Karenia brevis*, sont associés aux conséquences les plus délétères sur les écosystèmes côtiers. La liste de dinoflagellés nuisibles inclut: *Ceratium* sp., *Heterocapsa* sp., *Protoperidinium* sp., *Karlodinium* sp., *Takamaya* sp., *Dinophysis* sp., *Peridinium quinquecorne*, *Prorocentrum* sp., *Pyrodinium* sp. and *Scrippsiella* sp. (Licea et al., 2002; Sierra-Beltrán et al., 2005).

Au-delà des enregistrements historiques ponctuels et des observations récentes sur la distribution des dinoflagellés nuisibles, très peu de données concernent leur composition et évolution à long terme dans le Golfe du Mexique.

2. Objectifs et méthodes

Cette thèse a donc pour principal objectif d'estimer l'évolution à long terme des efflorescences algales nuisibles dans le Golfe du Mexique à partir d'enregistrements

sédimentaires. Ce projet s'inscrit dans une perspective plus large et complémentaire aux observations (micro)planctoniques actuelles, visant à mieux comprendre les paramètres environnementaux qui régissent la prolifération des espèces nuisibles.

Les objectifs spécifiques sont :

- (1) Évaluer le potentiel des kystes organiques de dinoflagellés préservés dans les sédiments, comme traceurs de l'évolution temporelle et spatiale des efflorescences algales nuisibles dans le Golfe du Mexique.
- (2) Développer une base de données régionale sur la distribution moderne des kystes de dinoflagellés et leur relation avec les paramètres environnementaux. Ces données seront intégrées à la base de données globale qui est grandement utilisée dans le cadre de reconstitutions paléoenvironnementales (<http://www.geotop.ca/fr/bases-de-donnees/dinokystes.html>). En outre, cette base de données régionale permet d'élargir nos connaissances sur l'autoécologie des dinokystes en milieux tropicaux.
- (3) Comparer les assemblages de dinokystes contenus dans les intervalles sédimentaires holocènes et du dernier interglaciaire afin d'estimer l'évolution des populations dans un contexte climatique plus chaud que l'actuel et évaluer le potentiel des dinokystes comme traceurs paléocéanographiques en milieu tropical.
- (4) Caractériser l'évolution temporelle des assemblages de dinokystes dans un milieu peu profond affecté par le processus d'eutrophisation.
- (5) Identifier un biomarqueur du dinoflagellé toxique *Karenia brevis*. Ce dinoflagellé ne produit pas de kyste de résistance, mais les toxines qu'il

synthétise constituent de potentiels traceurs moléculaires des populations passées. Les premières démarches méthodologiques réalisées dans le cadre de ce projet, qui ont par la suite motivé de plus amples recherches sur le sujet, sont également présentées.

Afin de répondre à ces objectifs, une approche multidisciplinaire a été privilégiée. Les analyses ont été menées sur 44 échantillons de surface prélevés dans différentes régions du Golfe du Mexique, ainsi que dans 2 carottes sédimentaires : l'une collectée près du bassin *de Soto* lors d'une mission océanographique effectuée en 1985 dans le cadre du programme *Ocean Drilling Program* (carotte ODP-625B) et l'autre prélevée en 2011, dans une lagune peu profonde de l'état mexicain de Veracruz. Suite à des traitements physiques et chimiques effectués sur les sédiments (e.g. de Vernal et al., 1999), les dinokystes peuvent être facilement isolés et identifiés par observation au microscope optique. Une attention particulière est portée aux espèces associées au développement de blooms nuisibles.

La base de données régionales des assemblages de dinokystes repose sur les analyses effectuées sur les échantillons de surface. Des traitements statistiques multivariés sont utilisés pour établir la relation entre les assemblages modernes de dinokystes et les caractéristiques physico-chimiques des masses d'eau. Par ailleurs, les analyses palynologiques effectuées sur la carotte ODP-625B sont combinées à des analyses géochimiques sur les foraminifères aux fins d'établissement d'une stratigraphie isotopique ($\delta^{18}\text{O}$) et d'une (paléo)thermométrie (Mg/Ca). L'utilisation de ces différents traceurs permet d'obtenir une image plus complète de la relation existant entre les assemblages de dinokystes et les paramètres océanographiques. Finalement, les analyses palynologiques effectuées sur la carotte prélevée dans le système lagunaire Alvarado permettent d'obtenir un enregistrement à haute résolution de l'évolution des assemblages de dinokystes sur une échelle historique.

3. Structure de la thèse

Cette thèse se présente sous forme de trois chapitres qui constituent des articles rédigés en anglais, publiés, soumis ou pour soumission dans des revues avec comité de lecture. La mise en forme des articles et des annexes est donc conforme à celle exigée par les différentes revues.

Ma contribution aux publications présentées dans le cadre de cette thèse couvre le traitement des échantillons et l'ensemble du domaine analytique, à l'exception des analyses géochimiques et de ^{210}Pb présentées dans le troisième chapitre. J'ai été responsable d'organiser la collecte d'échantillons le long de la péninsule de la Floride et j'ai participé au prélèvement des échantillons de surface et des carottes sédimentaires dans les lagunes mexicaines. J'ai également interprété l'ensemble des résultats et rédigé les articles. Ces activités ont été réalisées sous la supervision et les conseils d'Anne de Vernal. L'expertise des autres co-auteurs a également été mise à contribution dans les différents chapitres de cette thèse.

Le premier chapitre, intitulé *Organic-walled dinoflagellate cyst distribution in the Gulf of Mexico*, a été publié en 2013 dans la revue *Marine Micropaleontology*. Il a été écrit en collaboration avec Laurent Londeix et Anne de Vernal. Cette étude évalue quantitativement la relation entre les assemblages de dinokystes modernes et les propriétés physico-chimiques des masses d'eau superficielles. Il souligne l'importance du Golfe du Mexique comme refuge potentiel pour des espèces que l'on croyait éteintes depuis la fin du Cénozoïque. Il permet aussi de cibler différentes zones susceptibles d'être affectées par des efflorescences algales nuisibles.

Le deuxième chapitre, intitulé *Long-term hydrological changes in the northeastern Gulf of Mexico (ODP-625B) during the Holocene and late Pleistocene inferred from organic-walled dinoflagellate cysts* est un article accepté pour publication (août 2014)

dans la revue *Palaeogeography, Palaeoclimatology, Palaeoecology*. Écrit en collaboration avec Nicolas Van Nieuwenhove et Anne de Vernal, il présente notamment une étude comparative entre les assemblages de dinokystes du dernier interglaciaire et de l'interglaciaire actuel. Les dinokystes y montrent leur potentiel comme outil de reconstitutions paléocéanographiques.

Le troisième chapitre *High-resolution record of dinoflagellate cysts assemblages from the shallow Alvarado lagoon (Southeast Gulf of Mexico)* a été écrit en collaboration avec Ana-Carolina Ruiz-Fernandez, Joan-Albert Sanchez-Cabeza et Anne de Vernal. Il porte sur l'évolution historique des assemblages palynologiques dans une lagune mexicaine peu profonde fortement soumise aux activités humaines.

En appendices se trouve également un article accepté pour publication dans la revue *Journal of Phycology* et intitulé *First report of sub-recent fossilized cysts produced by the benthic dinoflagellate Bysmatrum subsalsum (Dinophyceae) from a shallow Mexican lagoon in the Gulf of Mexico*. Cet article a été écrit en collaboration avec Kenneth Mertens, Ana-Carolina Ruiz-Fernandez et Anne de Vernal. Il présente la découverte des premiers restes fossiles produits par des dinoflagellés benthiques.

Pour terminer, le rapport d'un stage effectué en automne 2011 au *Center for Coastal Environmental Health and Biomolecular Research* est présenté en appendice B. Ce dernier expose les premières démarches pour le développement d'un biomarqueur du dinoflagellé toxique *Karenia brevis*. Ce volet du projet a été pris en charge par Amanda Gabriel, sous la supervision de Yves Gélinas.

CHAPITRE I

ORGANIC-WALLED DINOFAGELLATE CYST DISTRIBUTION IN THE GULF OF MEXICO

Audrey Limoges¹, Anne de Vernal¹, Laurent Londeix²

¹ Geotop, Université du Québec à Montréal, C.P. 8838, Montréal, QC H3C 3P8, Canada

² Université Bordeaux 1, UMR 5805 EPOC, Avenue Des Facultés, 33405 Talence Cedex, France

Article publié en 2013 dans la revue *Marine Micropaleontology*, Vol. 102, 51-68

<http://dx.doi.org/10.1016/j.marmicro.2013.06.002>

Résumé

Des analyses palynologiques ont été réalisées sur 44 échantillons de sédiment de surface provenant du golfe du Mexique (17°N à 29°N) afin de documenter la distribution régionale des kystes de dinoflagellés (dinokystes) et caractériser leur relation avec les paramètres des masses d'eau de surface (température, salinité, productivité primaire). Les échantillons présentent des concentrations totales en dinokystes faibles à modérées (78 à 3576 dinokystes g^{-1}). Les assemblages sont dominés par *Brigantedinium* spp. et *Polysphaeridium zoharyi*, ainsi que par les taxons phototrophes *Spiniferites* spp. et *Operculodinium* spp. Les analyses de redondance (RDA) ont permis d'identifier la distance par rapport à la côte et/ou la profondeur de la colonne d'eau, et la température annuelle comme étant les paramètres environnementaux ayant la plus grande influence sur la distribution des dinokystes dans le golfe du Mexique. Les deux premiers axes correspondent respectivement à 44.7% et 20% de la variance totale. La distribution de *Impagidinium* spp. est principalement associée au domaine océanique profond, alors que *Polysphaeridium zoharyi* montre une affinité pour les milieux côtiers peu profonds. Cette dernière espèce, produite par le dinoflagellé potentiellement nuisible *Pyrodinium bahamense*, atteint de fortes concentrations notamment le long de la péninsule ouest de la Floride. Par ailleurs, *Melitasphaeridium choanophorum*, une espèce préalablement considérée comme éteinte depuis la fin du Pléistocène, apparaît comme une composante moderne des sédiments marins du nord et du sud-ouest du golfe. Sa présence moderne dans le golfe du Mexique suggère que le bassin ait fonctionné comme refuge permettant la persistance d'espèces endémiques. Elle implique également une modification des limites biostratigraphiques qui étaient assignées à *M. choanophorum*.

Mots-clés: Golfe du Mexique, Kystes de résistance, Efflorescences algales nuisibles, *Melitasphaeridium choanophorum*

Abstract

In order to document the distribution of organic-walled dinoflagellate cysts (dinocysts) and their relationship with sea-surface parameters (temperature, salinity, primary productivity), palynological analyses were performed on 44 surface sediment samples from the Gulf of Mexico (17°N to 29°N). Samples display low to moderate concentrations with values ranging from 78 to 3576 dinocysts·g⁻¹ dry weight sediment. Assemblages are dominated by either *Brigantedinium* spp. or *Polysphaeridium zoharyi* along with the phototrophic taxa *Spiniferites* spp. and *Operculodinium* spp. Redundancy analyses (RDA) identified the distance to the coast and/or water depth and annual temperature as being the most important factors that control cyst distribution in the Gulf of Mexico. The first two axes explain respectively 44.7% and 20% of the total variance. The inshore to offshore trend in cyst distribution emphasized by the RDA involves changes in associations of species with the presence of *Impagidinium* spp. in more oceanic assemblages and higher representation of *Polysphaeridium zoharyi* nearshore. This latter species, produced by the potentially toxic dinoflagellate *Pyrodinium bahamense*, reaches very high abundances notably on the west Florida shelf and in the Mexican lagoons. Additionally, *Melitasphaeridium choanophorum*, which was considered to have gone extinct by the end of the Pleistocene, appears as a modern component of marine sediment from the north and southwestern Gulf. Our results thus demonstrate a biostratigraphical range extending to the present, at least in the study area. This palynological investigation highlights the importance of the Gulf of Mexico as potential refuge for late Cenozoic species thought to be extinct.

Keywords: Gulf of Mexico, Dinoflagellates, Cysts, Harmful algal bloom, *Melitasphaeridium choanophorum*

1. Introduction

A worldwide increase in harmful algal blooms (HABs), including toxic events, has been observed during the past decade (Anderson, 1989; Smayda, 1990; Hallegraeff, 1993; Anderson et al., 2002; Glibert et al., 2005a, 2005b). This tendency of harmful phytoplankton to form blooms is highly influenced by the community composition, local hydrography (stratification, circulation patterns) and diverse environmental parameters such as nutrient concentrations, temperature, salinity and turbidity, which may be altered by human activity (i.e., cultural eutrophication, pollution, climate changes) (Burkholder, 1998; Anderson et al., 2002; Smayda, 2002; Peperzak, 2003; Glibert and Burkholder, 2006; Heisler et al., 2008). In the Gulf of Mexico, recurrent HABs are an issue as they may result in significant economic losses (Anderson et al., 2000). In this region, at least 40 species of toxic or potentially toxic algae are known to occur. These include harmful dinoflagellate species such as *Ceratium* sp., *Heterocapsa* sp., *Protoperidinium* sp., *Karlodinium* sp., *Takamaya* sp., *Dinophysis* sp., *Peridinium quiquecorne*, *Prorocentrum* sp., *Pyrodinium* sp. and *Scrippsiella* sp. (Licea et al., 2002; Sierra-Beltrán et al., 2005). Of all these taxa, the toxic dinoflagellate *Karenia brevis* – previously known as *Gymnodinium breve* – has the greatest impact on marine wildlife, human health, fisheries and tourism (Davis, 1948; Van Dolah, 2000; Magaña et al., 2003; Steidinger, 2009).

Because many dinoflagellates produce resting cysts that settle in bottom sediment for a variable time period (Wall and Dale, 1968; Dale, 1983; Taylor, 1987), interactions between the benthic and pelagic environments play a key role in HAB dynamics. Most dinoflagellate cyst taxa are composed of a complex carbohydrate-based polymer (“dinosporin”) (Versteegh et al., 2012) and some taxa are composed of calcareous material (Matsuoka and Fukuyo, 2000). They represent a dormant stage related to sexual reproduction that also ensures the survival of dinoflagellates through

unfavorable environmental conditions (Itakura et al., 1997). Cysts related to sexual reproduction may survive for decades and even centuries in bottom sediments (Lundholm et al., 2011; Ribeiro et al., 2011). When conditions are suitable, the germination of cysts occurs and the upward migration of cells may contribute significantly to the initiation of blooms (Anderson, 1998; Anderson and Rengefors, 2006; Garcés et al., 2002; Hense, 2010). The seed banks in sediment can therefore initiate blooms and have an important influence on their composition and magnitude. Additionally, species abundance and composition in assemblages from recent sediment offer a (fragmentary) picture of the organic primary production in a given area and may be helpful to document past productivity (Radi and de Vernal, 2008) along with living population diversity and dynamics in regions affected by harmful blooms (Anderson et al., 2005).

In middle to high latitudes of the Northern Hemisphere, numerous studies have shown close relationships between the assemblages of organic-walled dinoflagellate cysts (dinocysts) and the environmental conditions in the upper water column (e.g., Wall et al., 1977; Marret, 1994; Matthiessen, 1995; de Vernal et al., 1997, 2001, 2005; Zonneveld, 1997; Rochon et al., 1999; de Vernal and Marret, 2007; Radi and de Vernal, 2008; Pospelova et al., 2008; Bonnet et al., 2012). Dinocysts have thus been largely used for reconstructions of past sea-surface conditions such as temperature, salinity, sea-ice cover and productivity (e.g., Turon, 1978; Turon and Londeix, 1988; Harland and Howe, 1995; de Vernal et al., 2000; Hillaire-Marcel et al., 2001; Warny et al., 2003; Solignac et al., 2004). These studies rely on the development of extensive datasets of the modern distribution of cysts and corresponding environmental conditions. However, to date, the distribution of dinocyst assemblages from tropical Atlantic areas remains poorly documented despite important taxonomic diversity and their significance in terms of economic and health issues. Only few studies have documented dinocyst Quaternary assemblages from the Gulf of Mexico (e.g., Wall, 1967; Wall et al., 1977; Wrenn, 1988; Edwards, 1986; Edwards and Willard, 2001;

van Soelen et al., 2010). Here, we present the results of palynological analyses undertaken on 44 surface sediment samples from selected areas of the Gulf of Mexico, all affected to a varying degree by harmful algal blooms. Since a few of these harmful species are known to produce fossilizable cysts, the goals of the study are 1) to provide an accurate picture of the cyst distribution in recent sediments with focus on the occurrence of potentially toxic species and their relationship with modern hydrographic parameters, and 2) to develop a regional dinocyst database that could be used for paleoenvironmental and paleoceanographical reconstructions.

2. Regional setting

It is believed that the Gulf of Mexico formed as a semi-enclosed back-arc basin in the Middle to Late Jurassic during a short-lived extensional phase (Stern and Dickinson, 2010). The surface circulation in the central portion of the Gulf is dominated by the Loop Current, its rings and a permanent anticyclonic gyre (Nowlin and McLellan, 1967; Cochrane, 1972; Elliot, 1979; Cherubin et al., 2006). Surface waters enter into the Gulf through the Yucatán channel and exit through the Florida Strait (Elliot, 1982; Blumberg and Mellor, 1985; Hofmann and Worley, 1986; Oey et al., 2005; Jochens and DiMarco, 2008; Auladell et al., 2010) (Figure 1).

The latitudinal and longitudinal extensions of the Yucatán Current into the northeastern Gulf are seasonally variable and may lead to the shedding of mesoscale rings that gain velocity through radial diffusion as they move westward. These eddies which have diameters varying between 200 and 400 km and vertical depth of about 1000 m, have a life span of a couple of months to a year. They can interact with the topography and split into new smaller-scale rings (Ichiye, 1962 ; Nowlin, 1972 ; Elliot, 1982; Vukovich and Crissman, 1986; Cooper et al., 1990; Coats, 1992; Auladell et al., 2010). The surface water circulation results in mostly uniform sea-surface conditions with respect to summer temperature (26-30°C), whereas winter temperatures vary from 18 to 25°C (Figure 2).

Here, we analyze dinocyst assemblages from four areas of the Gulf of Mexico that show particular hydrographic features, notably with respect to upwelling, salinity and stratification.

2.1. Northern Gulf of Mexico (26-29°N; 86-94°W)

The regional hydrology of the northern Gulf is greatly influenced by the Mississippi-Atchafalaya River system ($\sim 10^4 \text{ m}^3 \cdot \text{s}^{-1}$), which accounts for 90% of the total freshwater input into the Gulf of Mexico. The areal extent of the Mississippi River plume fluctuates in relation with changes in river discharge, varying from about 822 km² under low river discharge conditions to 7700 km² under high river discharge conditions (Walker, 1996). The seasonal winds and pressure gradient also influence the dispersal pattern of the plume, forcing it predominantly to the west along the Louisiana-Texas shelf. The average plume length is 18 km eastward, 37 km westward, and 25 km southward (Walker, 1996) and results in a salinity gradient from 0 to 36 from the outlet of the river to the sea.

The inshore circulation is cyclonic throughout the year, except in summer (June to August) during which the currents flow eastward (Cochrane and Kelly, 1986; De Velasco and Winant, 1996; Wang et al., 1998) (Figure 3A) and water column stratification causes oxygen-depletion (Justic et al., 2002; Nowlin et al., 2005). The freshwater plume constitutes the main sediment source for the coastal environment (~210 million tons of sediment) and accounts for a considerable portion of the dissolved nutrients and organic material brought into the area. Sample sites from the northern Gulf of Mexico are not known to be affected by harmful algal blooms on a regular basis.

2.2. West-central Florida coast (23-27°N; 82°W)

The circulation along the West Florida Coast exhibits two principal features: 1) the nutrient-rich water of the Loop Current that flows southward along the Florida shelf and 2) the coastal current, which is driven by seasonal winds. From autumn to spring (October to March), the coastal current flows southward and the circulation is characterized by an offshore surface transport that induces coastal upwelling (Figure 3B). In summer (April to September), the alongshore current flows northwestward and surface circulation is shoreward, generating coastal downwelling (Yand et al., 1999). Surface sediments in this area consist of fine-grained quartz-rich sand and coarse marine biogenic carbonate sand. The west Florida shelf is one of the most frequently affected regions in the world with long-lasting harmful algal blooms. They are mainly caused by *K. brevis* and they typically occur in late summer and fall (Steidinger et al., 1998; Steidinger, 2009).

2.3. Southwestern Gulf of Mexico (18-19°N; 94-95°W)

In addition to the Loop Current and the Loop Current Rings, the circulation off the southwestern Gulf of Mexico is governed by the strong seasonal North winds called the Nortes ($90\text{-}129 \text{ m}\cdot\text{s}^{-1}$) that contribute to the cooling and mixing of the water column from October to April, while it remains stratified during summer (Tapánes and González-Coya, 1980; Alatorre et al., 1987; Vidal et al., 1994; Soto and Escobar, 1995). Along the Mexican shelves of Tamaulipas and Veracruz (between 18.5°N and 26°N) a cyclonic circulation pattern dominates from October to February. This leads to the coastal advection of the low-salinity (~33psu) waters from the Mississippi-Atchafalaya River system (Zavala-Hidalgo et al., 2003) (Figure 3C). Transport reverts northward from May to August, preventing the water plume to reach the Mexican coast during this period (Monreal-Gómez et al., 1992; Nowlin et al., 2001;

Zavala-Hidalgo et al., 2003). On the shallow shelf, local circulation is also influenced by the river discharge, which is maximum in summer and associated with the rivers Coatzacoalcos ($224 \times 10^9 \text{ m}^3 \cdot \text{yr}^{-1}$) and Grijalva-Usumacinta, including the Terminos Lagoon ($105.2 \times 10^9 \text{ m}^3 \cdot \text{yr}^{-1}$) (Carriart-Ganivet and Merino, 2001). Several toxic and potentially toxic dinoflagellate species are a permanent component of the living assemblages in this region (Licea et al., 2002).

2.4. Mexican lagoons

Three Mexican lagoon systems, which are briefly described below, were sampled for this study. They are all affected by harmful algal blooms caused notably by *K. brevis* (Borbolla-Sala et al., 2006).

The Laguna Alvarado (18.79°N - 95.83°W) system includes several lagoons (e.g. Alvarado, Tlalixcoyan, Buen País and Camaronera) and numerous small aquatic bodies (Figure 3D). Formed by the convergence of four important rivers (Papaloapan, Blanco, Acula and Limón), it communicates with the Gulf of Mexico permanently via a 400 m wide channel. The surface area is 62 km^2 , the average depth is 2 meters and the water exchange time is estimated to be semi-diurnal (Moran-Silva et al., 2005; Cruz-Escalona et al., 2007). The mean annual temperature ranges from 22 to 26°C and salinity shows important variations in relation to precipitation. Different types of mangroves occupy the adjacent coastal areas.

The Laguna Mecoacán (18.38°N - 93.15°W) covers 50 km^2 . It is shallow and characterized by a mean depth of 1.2 m. It permanently communicates with the Gulf of Mexico through the Dos Bocas mouth, which is limited by two littoral barriers (Figure 3E). The annual temperature and salinity of the water range respectively from 22.5 to 32.5°C and from 4.7 to 34.1 (Castañeda and Contreras, 2001).

Laguna de Términos (18.61°N - 91.58°W) is the largest coastal lagoon along the Mexican coast. It is ~ 3.5 m deep and covers 2500 km^2 (Figure 3F). It is connected to the Gulf via two major inlets at either extremities of the calcareous-sand barrier island of Isla del Carmen. In addition to mixed diurnal tides of about 0.3 m and currents of $1.3 \text{ m}\cdot\text{s}^{-1}$, the lagoon is influenced by a mean freshwater discharge of $378 \text{ m}^3\cdot\text{s}^{-1}$ associated with the three main rivers: Palizada, Chumpán and Candelaria-Mamantel (David and Kjerfve, 1998). The residence time of water in the lagoon is about 9 days.

3. Material and methods

Marine core-top samples (0-1 cm) from the northern Gulf of Mexico, the Belize coast and the Florida Strait were recovered during the *RV Marion Dufresne* cruise to the area in 2002, whereas those from the inner shelf of Veracruz were recovered during the *El Puma* cruise in 2011, at depths ranging from 476 to 2250 meters. The core-top sediment is mainly composed of calcareous clays. Samples from the inner shelf of the West Florida Coast and the Mexican lagoons were also collected in 2011 at very shallow depths (1 to 32 m) using box cores (Table 1). They are respectively composed of quartz and carbonate-rich sands, and silty-clays. Wet sediments were stored in a cool room (4°C) until palynological treatments were performed. Unfortunately, sediment mass accumulation rates at the study sites are unknown.

3.1. Palynological analyses

Samples were prepared for palynological analyses according to standard laboratory procedures (e.g. de Vernal et al., 1999). In order to determine the absolute dinocyst abundances, one tablet of exotic marker grain *Lycopodium clavatum* was added to each sample before treatment (Stockmarr, 1971). A volume of 3 to 10 cm^3 of wet

sediment was wet sieved between 10 and 106 µm to remove fine silt and clay (<10 µm) and coarse sand (>106 µm). The remaining sediment fraction was subsequently treated with hydrochloric acid (HCl 10%) and hydrofluoric acid (HF 48%) to dissolve calcium carbonates and silicates, respectively. The residual fraction was sieved again. No additional oxidation or heavy liquid separation was applied, but samples were subjected to another washing, filtering and ultrasound bath step to eliminate as much amorphous organic material as possible. The final residues were mixed with glycerin jelly and mounted for microscopic observation. The identification of dinocysts was carried out using an optical microscope at magnifications of 400X and 1000X. In general, 2 to 3 slides were analyzed per sample. However, because sediments were characterized by very low cyst concentrations despite large amounts of organic material (e.g. pollen grains, foraminifer linings, amorphous matter), the total number of counted specimens remains <300 in many samples (see appendix A). We established the minimal count at 60 specimens for inclusion in the dataset and statistical analyses, being aware that such low counts may lead to greater statistical uncertainties on percentage data. All absolute abundances are reported as specimens per unit of dry weight sediment ($\text{specimens}\cdot\text{g}^{-1}$). The error on the counts using the method of Stockmarr (1971) is presented in appendix A. Cyst identification was made following the original description of the holotype of each taxon and the most recent nomenclature was used (Fensome et al., 2008). Identification of the cyst of *Polykrikos kofoidii* and the cyst of *Polykrikos schwartzii* was made according to Rochon et al. (1999).

3.2. Statistical analyses

In order to characterize the relationships between sea-surface parameters and dinocyst abundance in modern sediments on a quantitative basis, statistical analyses were performed using the CANOCO software (Canonical Community Ordination: version 4.0 for Windows, Ter Braak and Smilauer, 1998). A detrended correspondence

analysis (DCA) was done first. The longest gradient was found to be shorter than 3.0 standard deviations, indicating a linear distribution of cyst taxa and justifying the use of redundancy analysis (RDA). A logarithmic transformation of species percentages was made in order to increase the statistical weight of rare species that often show a narrower ecological affinity compared to the dominant taxa. All counted taxa were considered for statistical analyses, even those occurring in low number or occasionally, because their distribution appears characteristic of specific environments. Samples with low cyst counts (<60; sites 1, 2, 4, 32-36, 42 and 44) were not used for statistical analysis. Because hydrographical and productivity data were not available for sites 29-30-31, these sites were also excluded for the statistical analysis. The significance of each environmental parameter was evaluated from the length of its gradient and from the correlation of the main axes with cyst taxa. The hydrographical parameters retained for these analyses included seasonal temperature, salinity and productivity of surface waters, along with water depth and the distance of the sampling sites to the coast (Table 2).

3.2.1 Hydrographical parameters

Sea-surface temperature (SST) and sea-surface salinity (SSS) were extracted from the World Ocean Atlas (WOA, 2001) dataset published by the National Climatic Data Center (NCDC). The average values used here were calculated for a radius of 1° around each station, at a depth of 0 m. The distance to the coast was measured from nautical maps and the Google Earth software (version 7.0). The water depth was measured onboard using a depth sounder and/or according to the length of the cable allowing the boxcore to grab sediment (lagoons). We used productivity (chlorophyll-a) data from the MODerate resolution Imaging Spectroradiometer (moDIS) program, which were calculated following the Vertical Generalized Primary Production Model (VGPM) developed by Behrenfeld and Falkowski (1997). Interpolations were carried out for sampling sites where productivity values were unavailable from this dataset.

4. Results

4.1. Palynological assemblages

Samples were characterized by terrestrial (pollen grains, spores) and marine (foraminifer organic linings and dinocysts) components together with large amounts of amorphous organic material (Table 3; Figure 4). Although they represent only a small proportion of the total palynomorph content (<4%), a great diversity of dinocyst species was found over the whole study area (Table 4; Figure 5; Supplementary material). A total of 54 taxa were identified, including morphotypes of *Spiniferites mirabilis-hyperacanthus* (hereafter named *S. mirabilis* s.l.) and *Operculodinium centrocarpum* sensu Wall and Dale (1966) (cf. Table 3). Cyst concentrations were generally low to moderate with values ranging from 78 to 3576 dinocysts·g⁻¹ dry weight sediment (errors on concentrations are shown in supplementary material). The highest concentrations were recorded in the Mexican lagoons (sites 23 to 31), in the northern Gulf of Mexico (site 8) and in the Florida Strait (site 11).

Phototrophic species dominated over heterotrophic species in most studied sites (Figure 4). However, *Brigantedinium* spp. also reaches very high concentrations (up to 90%) and dominates some assemblages together with *Polysphaeridium zoharyi* (up to 70%) and *Spiniferites* spp. (maximum 66%) and diverse *Operculodinium* species (maximum 43%) including *O. centrocarpum*, *O. israelianum* and *O. longispinigerum*. Other common taxa include *Impagidinium* spp. (0-53%), *Lingulodinium machaerophorum* (0-13%), *Nematosphaeropsis rigida* (0-11%), *Selenopemphix quanta* (0-13%), *Selenopemphix nephroides* (0-10%) and *Echinidinium* spp. (0-13%). Finally, *Melitasphaeridium choanophorum*, *Bitectatodinium spongium*, *Islandinium minutum*, *Lejeunecysta* spp., *Operculodinium janduchenei*, cyst of

Pentapharsodinium dalei, *Polykrikos* spp., *Stelladinium stellatum* and *Tuberculodinium vancampoae* accounted for less than 6% of assemblages.

Important morphological variations (size, spine length and morphology, and surface features) characterized specimens of *Operculodinium centrocarpum* (*sensu* Wall and Dale, 1966), notably along the Florida coast (Figure 6C). When compared to the specimen illustrated by Wall and Dale (1966), many cysts appear more robust with well-developed processes and irregular granulation (Plate 2; Micrographs 9-10). In addition, the scattered granules typically observed on the holotype wall were not always visible or were absent. Further observations are required for a thorough comparison with other *Operculodinium* species. Nevertheless, it is clear that specimens differ from *O. crassum* (Harland and Hill, 1979) by having longer processes and a thinner non-spongy wall. They are also distinguished from *O. aguinawense* (Marret and Kim, 2009) by having a granulated wall surface and bearing stout processes with capitate terminations instead of tetrafurcate to multifurcate tips. Since the occurrence of these specimens is concomitant with *O. centrocarpum*, we assumed that they are eco-morphotypes and they were named “atypical *Operculodinium centrocarpum*”.

Important intraspecific morphological variations also characterized *Spiniferites* taxa. The proportion of *Spiniferites* specimens showing uncommon features was higher in the Mexican lagoons and in the northern Gulf of Mexico than elsewhere. In general, the cysts were smaller with highly variable process numbers and length (see Plate 2). In many cases, identification to species levels of specimens belonging to the genus *Spiniferites* was difficult because it was impossible to determine whether it was just aberrant or if it presented the uniqueness required for the establishment of a separate morphotype or new species. Particularly large morphological variations characterized specimens attributed to *S. mirabilis* and *S. hyperacanthus* and are referred to as “atypical *S. mirabilis*”. These specimens were sometimes characterized by

exceptionally well-expressed septae and tabulations. They were counted separately and their distribution in the study area is illustrated in Figure 6D.

4.2. Statistical analyses

The RDA results showed that the first two axes explain respectively 44.7 and 20% of the total variance. The distance to the coast and/or water depth correlate with the first axis ($R^2=0.5210$ and 0.5497), whereas the annual temperature is linked to axis 2 ($R^2=0.8410$) (Table 5). Axis 1 is defined by negative scores of *Brigantedinium* spp. and *Impagidinium aculeatum* and by positive scores of *Polysphaeridium zoharyi* and atypical *Spiniferites mirabilis* (Table 6; Figure 7). Axis 2 is characterized by an opposition between most heterotrophic taxa having positive scores and phototrophic species characterized by negative scores.

Three distinct assemblages were defined from the ordination diagram (Figure 8).

- The Group 1 comprises sites from the north and southwestern Gulf of Mexico as well as the Florida Strait. The dominant dinoflagellate cyst species are *Spiniferites* spp. (*S. ramosus* and *S. mirabilis* s.l.) and *Brigantedinium* spp. along with *Impagidinium* spp. and *Operculodinium* spp. Other characteristic species include *Nematospaeropsis rigida* and *Melitasphaeridium choanophorum* (see below for discussion) (Figure 6E).
- The Group 2 corresponds to sites located along the western coast of Florida. The main species are the heterotrophic *Brigantedinium* spp. and the phototrophic taxa *Spiniferites* spp. (mainly *S. ramosus* and *S. mirabilis* s.l), *Polysphaeridium zoharyi* and *Operculodinium* spp. In contrast with other sites from the open Gulf of Mexico, *Impagidinium* is rare. This region is also characterized by a significant number of *Operculodinium centrocarpum* specimens showing atypical features.

- Group 3 represents the Mexican lagoons, where *Polysphaeridium zoharyi* reaches its peak abundance (around 70%) (Figure 6F). The other dominant species is atypical *Spiniferites mirabilis*, which exhibits large variations in size and septae features within the same slide. Assemblages also comprise a combination of marine and freshwater taxa belonging to chlorophytes or other categories such as *Pediastrum* and *Concentricystes* ind. (Plate 1). In addition, visible cellular material in several specimens from sediment of the lagoons suggests exceptional dinocyst preservation and/or recent cyst production.

5. Discussion

5.1. Regional characteristics of palynological assemblages

Surface sediment assemblages analyzed in this work represent a large variety of environmental conditions from the Gulf of Mexico. Cyst assemblages from offshore sites show a species composition typical of warm and oligotrophic environments, whereas assemblages from the coast of Florida are more typical of moderately high productivity (Marret and Zonneveld, 2003). In the Mexican lagoons, the euryhaline *P. zoharyi* is largely dominant. This is consistent with previous studies reporting this species from restricted warm and shallow marine environments including mangroves where it can reach high concentrations (Maclean, 1989; Usup et al., 2012). The list of species in assemblages is generally similar with that of previous works from the Mississippi Sound (Edwards and Willard, 2001), Tampa Bay (van Soelen et al., 2010) and the inner continental shelf of the Caribbean Sea (Deflandre and Cookson, 1955). Also of note is the similarity between the modern assemblages described in this work and those from Neogene sedimentary sequences of the area. For example, the main taxa recorded in sequences from the Bahamas bank (Head and Westphal, 1999) and

the Yucatan channel (Wall and Dale, 1969) were *Polysphaeridium zoharyi*, *Spiniferites* spp., *Lingulodinium machaerophorum* and *Operculodinium* spp. including *O. israelianum*. Their relative abundance fluctuations were associated with changes in relative sea-level. Our results supports the hypothesis raised in these studies stipulating that *Polysphaeridium zoharyi* may be qualitatively used as indicator of more restricted nearshore environment.

Noteworthy is also the presence of the phototrophic *Melitasphaeridium choanophorum*, which is common in late Cenozoic marine sediment with first and last occurrences reported to occur in the Late Miocene (~10 Ma) and Late Pleistocene (> 11 ka) respectively (Wrenn and Kokinos, 1986; Powell, 1992). We furthermore note that this species occurs in a core from the Cariaco Basin covering the last 30 000 years (Mertens et al., 2009a), but to the best of our knowledge, no published records exist that show its occurrence in modern sediments. Associated with warm climate episodes in many biostratigraphic reports, it has been recorded notably in sequences from the continental shelf off the United States in the Gulf of Mexico (Duffield and Stein, 1986; Lenoir and Hart, 1986; Wrenn and Kokinos, 1986), the eastern United States (Edwards, 1986) and the Bahamas bank (Head and Westphal, 1999). In this study, several specimens were observed in the surface sediment of 14 sites scattered throughout the northern and southwestern parts of the Gulf (Figure 6E). Because all specimens are well preserved and because the samples contain almost no reworked pre-Quaternary palynomorphs (e.g. Figure 4), our data suggest a biostratigraphical range that extends to the present day, at least regionally in the Gulf of Mexico. This lead us to hypothesize that semi-enclosed basins such as the Gulf of Mexico may have been a refugium for some tropical to subtropical dinoflagellate taxa. This is further illustrated by the presence of *Operculodinium longispinigerum* in a few sites from the northern Gulf of Mexico. This species, recently also observed in tropical oligotrophic environments from the south of the Indonesian island Java (Zonneveld et al., in press), has been known as a significant component of dinocyst assemblages

from Early Miocene to Early Pleistocene sediments (Manum et al., 1989 ; Head and Wrenn, 1992; de Verteuil and Norris, 1996).

5.2. Relationships between dinoflagellate cyst assemblages and environmental conditions

The most prominent environmental factor that explains the distribution of dinocyst assemblages in the Gulf of Mexico is the distance to the coast and/or water depth, allowing the distinction between oceanic and coastal assemblages. *Impagidinium* spp. yields higher relative abundance with larger distance to the coast, whereas *Polysphaeridium zoharyi* shows a clear trend of increasing relative abundance at shallower depths. According to RDA results, the opportunistic *Brigantedinium* spp. is also well-correlated to increasing distance to the coast. However, this species shows a widespread distribution and its lower percentage in nearshore assemblages may result from an increasing concentration of *P. zoharyi*. The affinity of *P. zoharyi* for nearshore settings in our data set may be related to a number of parameters linked to such environments, including turbulence and light penetration, water stratification and nutrient availability. However, these parameters are difficult to quantify.

According to RDA results, the second most determining parameter for the dinocyst distribution in the Gulf of Mexico is the annual temperature, and the summer and winter temperatures are in opposition in the ordination diagram. However, seasonal temperatures are very similar from one site to another (summer $29\pm1^{\circ}\text{C}$; winter $22\pm2.5^{\circ}\text{C}$), except for those along the coast of Florida, which are characterized by comparably lower temperatures during winter ($18.5\pm0.5^{\circ}\text{C}$). This may be caused by the coastal upwelling that occurs from October to March and which allows deeper cold and nutrient-rich water to replace the surface water. Therefore, the second axis may be explained by a relationship between dinocyst assemblages and the high

productivity level at sites from the Florida coast. This would justify the opposition between heterotrophic taxa and winter temperature.

Spiniferites mirabilis has a coastal to oceanic global distribution that extends from temperate to equatorial regions (Zonneveld et al., in press). In the high latitudes (e.g. North Atlantic), this species occurs mostly in open oceanic environments and is usually associated with warm and relatively saline waters (Rochon et al., 1999). High relative abundances of *S. mirabilis* have occasionally been reported from specific coastal equatorial regions having high productivity and/or under the influence of riverine input (e.g. Black Sea and Marmara Sea; Zonneveld et al., in press), but these regions however have average seasonal and annual salinity >32. The fact that, in our study, concentrations of this species show a clear shoreward increase with maximal concentrations in lagoons implies that its distribution also extends to very shallow coastal environments. These lagoonal settings are prone to significant seasonal changes in salinity, but their average annual salinity is still high, in line with the global observations for the species' distribution (Zonneveld et al., in press). The ordination diagram further reveals that the number of aberrant morphotypes increases as the distance to the coast decreases (Figure 7). Such morphotypes are commonly noticed among dinoflagellate cysts in areas with variable salinity (Ellegaard, 2000; Mertens et al., 2009b; Verleye et al., 2012). However, in the case of the Gulf of Mexico, we suggest that other factors related to the shallow depositional environment may have caused variations in the morphological development of the cysts, notably growth obstruction due to turbulence or cyst formation in benthic situations (cf. Kokinos and Anderson, 1995).

5.3. Note on the use of dinocysts as tracers of paleo-harmful blooms

In the Gulf of Mexico, cyst-forming dinoflagellates represent a small part of the total flora associated with harmful blooms: only the potentially toxic species

Polysphaeridium zoharyi (i.e. *Pyrodinium bahamense*) was identified in recent sediments, and on a historical basis, it has not been related to important harmful events in the study area. Maximal concentrations of this species were observed close to shore, at shallow depths, notably along the west Florida shelf and in the Mexican lagoons. In other tropical and subtropical coastal areas around the world (e.g. Indo-Pacific and Pacific coast of Central America), *P. bahamense* is an important cause of seafood toxicity and is considered more harmful than any other Paralytic Shellfish (PS) toxin producer (Usup et al., 2012). Since Landsberg et al. (2006) reported that the Atlantic strain of *P. bahamense* might also be associated with the production of PS toxins (most likely saxitoxins), the distribution of *P. zoharyi* cysts in sediments from the Gulf of Mexico deserves special attention. In Manila Bay (Phillipines), blooms of *P. bahamense* tend to occur after periods of heavy rain and have been associated to the resuspension of resting cysts by turbulence in shallow environments (Villanoy et al., 1996). This mechanism was also observed in the Indian Lagoon in Florida (Phlips et al., 2006). Since furthermore the motile forms are not present throughout the year and may thus be missed by plankton studies (Usup et al., 2012), palynological studies especially can help highlighting regions more susceptible to harmful proliferations in the future. Besides, such an approach combined with, for instance, biomarker analyses, can represent an interesting avenue for analyzing the evolution through time of species involved in the formation of harmful algal blooms.

Our work provides useful information that strengthens our understanding of low latitude ecology. It also represents an important complement to the standardized modern database of the Northern Hemisphere that presently includes 1492 sites (de Vernal et al., submitted). In terms of temperature, salinity and productivity, the study sites are very comparable to those from similar latitudes in the Pacific Ocean (Limoges et al., 2010). However, they are characterized by large taxonomic differences. In particular, protoperidiniales and gymnodiniales taxa including

Brigantedinium spp., *Echinidinium* spp., *Polykrikos kofoidii* and *Selenopemphix quanta* are dominant in the eastern Pacific, whereas gonyaulacoids are dominant with large species diversity in the Gulf of Mexico. These differences and the occurrence of *Melitasphaeridium choanophorum* emphasize the endemic and particular character of the Gulf of Mexico as semi-enclosed basin.

6. Conclusions

This study provides an overview of the spatial distribution of organic-walled dinoflagellate cysts from recent sediment of the Gulf of Mexico. Empirical observations coupled with statistical analyses allow a clear distinction between assemblages from the upwelling area, lagoons and offshore low productivity environments. The main environmental parameter controlling cyst assemblages is the distance to the coast and/or water depth. This is notably evidenced by a steady shoreward increase of *Polysphaeridium zoharyi* and a decrease of *Impagidinium* spp. Statistical analyses also pointed out temperature as a controlling parameter, but because of the very small gradient in sea-surface temperature throughout the study area, we believe it rather reflects upwelling, thus productivity.

Our results reveal the richness and the thermophilic nature of the modern dinocyst assemblages from the Gulf of Mexico. They include typical taxa of tropical and subtropical environments such as *Operculodinium israelianum* and *Polysphaeridium zoharyi*. This latter species, produced by the potentially toxic dinoflagellate *Pyrodinium bahamense*, was abundant notably along the west Florida shelf and in the Mexican lagoons. In recent times, a global scale increase in the importance of this species as toxin(s) producer may indicate a potential future environmental threat for the Gulf of Mexico, therefore emphasizing the relevance of studying cyst banks in sediment.

In addition, assemblages include species that had not or rarely been observed in the dinocyst flora from the mid-latitudes of the North Atlantic since the Pliocene period (e.g. *Operculodinium longispinigerum*, *Melitasphaeridium choanophorum*). Among these species *Melitasphaeridium choanophorum* deserves special attention, because its appearance as a minor component of the assemblages at several sites would imply that this species is currently still living in the Gulf of Mexico, and suggests that the basin may have functioned as a sheltered environment allowing the persistence of endemic species. This seems to be substantiated by the occurrence of several species in the surface assemblages that also characterize Pliocene assemblages from the Gulf of Mexico and surrounding areas.

Acknowledgements

This study was possible through the financial support of *Fonds de Recherche Nature et Technologies* of Quebec. We thank Ana-Carolina Ruiz-Fernandez, Rosalba Alonso-Rodriguez and Marie-Yasmine Bottein for the organization of the sampling campaign in the Mexican lagoons and along the Florida coast. We are grateful to Captain Dean and Charles for their help and assistance at sea along the Florida coast and Maria Luisa Machain Castillo for providing sediments from the southwestern Gulf of Mexico. Special thanks go to Maryse Henry, Taoufik Radi, Nicolas van Nieuwenhove and André Rochon for their help with the dinocyst identifications. We also gratefully acknowledge Stijn De Schepper and Sophie Warny for their helpful and constructive review comments.

7. References

- Alatorre, M.A., Ruiz, F., Salas de León, D., 1987. Efecto del paso de frentes fríos atmosféricos sobre la Bahía de Campeche (Effect of cold atmospheric fronts on the Bay of Campeche). In: Memoria Reunión Anual 1987, (Eds.) J.F. González, M. Medina and M. Martínez, Unión Geofísica Mexicana, México, 186-193.
- Anderson, D.M., 1989. Toxic algal bloom and red tides: a global perspective. In: Okaichi, T., Anderson, D.M., Nemoto, T. (Eds.), Red Tides: Biology, Environmental Science and Technology, 11-16.
- Anderson, D.M. 1998. Physiology and bloom dynamics of toxic *Alexandrium* species, with emphasis on life cycle transitions, p. 29-48. In: Anderson et al. (Eds.), Physiological ecology of harmful algal blooms. NATO ASI series. Springer-Verlag, Berlin, Germany.
- Anderson, D.M., Rengefors, K., 2006. Community assembly and seasonal succession of marine dinoflagellates in a temperate estuary: The importance of life cycle events. Limnology and Oceanography 51(2), 860-873.
- Anderson, D.M., Hoagland, P., Kauru, Y., White, A.W., 2000. Estimated annual economic impacts from harmful algal blooms (HABs) in the US. Woods Hole Oceanographic Institute, Woods Hole, MA.
- Anderson, D.M., Glibert, P.M., Burkholder, J.M., 2002. Harmful algal blooms and eutrophication: nutrient sources, composition and consequences. Estuaries 25, 562-584.
- Anderson D.M., Stock, C.A., Keafer, B.A., Nelson, A.B., McGillicuddy, D.J., Keller, M., Thompson, B., Matrai, P.A., Martin, J., 2005. *Alexandrium fundyense* cyst dynamics in the Gulf of Maine Deep-Sea Research II 52, 2522-2542.
- Antonov, J. I., D. Seidov, T. P. Boyer, R. A. Locarnini, A. V. Mishonov, and H. E. Garcia, 2010. World Ocean Atlas 2009 Volume 2: Salinity. S. Levitus, (Ed.), NOAA Atlas NESDIS 69, U.S. Government Printing Office, Washington, D.C., 184 pp.
- Auladell, M., Pelegrí, J.L., García-Olivares, A., Kirwand Jr., A.D., Liphardt Jr., B.L., Martín, J.M., Pascual, A., Sangrà, P., Zweng, M., 2010. Modelling the early evolution of a Loop Current ring. Journal of Marine Systems 80, 160-171.
- Behrenfeld, M., Falkowski, P., 1997. Photosynthetic rates derived from satellite based chlorophyll concentration. Limnology and Oceanography 42 (1), 1-20.

- Blumberg, A.F., Mellor, G.L., 1985. A simulation of the circulation in the Gulf of Mexico. Israel Journal of Earth Sciences 34, 122-144.
- Bonnet, S., de Vernal, A., Gersonde, R., Lembke-Jene, L., 2012. Modern distribution of dinocysts from the North Pacific Ocean (37-64°N, 144°E-148°W) in relation to hydrographic conditions, sea-ice and productivity. Marine Micropaleontology 84-85 (1), 87-103.
- Borbolla-Sala, M., Colín Osorio, F.A., Vidal Pérez, M.R., Jimérez, M.M., 2006. Marea Roja de Tabasco 2005, *Karenia brevis*. Salud en Tabasco 12 (2), 425-433.
- Burkholder, J.M., 1998. Implications of harmful microalgae and heterotrophic dinoflagellates in management of sustainable marine fisheries. Ecological Applications 8, 37-62.
- Carricart-Ganivet, J.P., Merino, M., 2001. Growth responses of the reef-building coral *Montastraea annularis* along a gradient of continental influence in the southern Gulf of Mexico. Bulletin of Marine Science 68, 133-146.
- Castañeda L.O., Contreras, F.E., 2001. Serie: Bibliografia Comentada sobre ecosistemas costeros mexicanos 2001. Centro de Documentación Ecosistemas Litorales Mexicanos. Universidad Autónoma Metropolitana, Unidad Iztapalapa, División C. B. S. Depto. de Hidrología. Publicación electrónica (CD). ISBN: 970-654-912-9. Mexico, D.F.
- Cherubin, L.M., Morel, Y., Chassagnet, E.P., 2006. Loop Current Ring Shedding : The Formation of Cyclones and the Effect of Topography. Journal of Physical Oceanography (36), 569-591.
- Coats, D.A., 1992. The Loop Current. In: Milliman, J.D., Imamura, E. (Eds.), The Physical Oceanography of the U.S. Atlantic and Eastern Gulf of Mexico, U.S. Department of Interior, Atlantic OCS Region, Mineral Management Service.
- Cochrane, J.D., Kelly, F. J., 1986: Low-frequency circulation on the Texas-Louisiana continental shelf. Journal of Geophysical Research 91 (10), 645-659.
- Cochrane, J.D., 1972. Separation of an anticyclone and subsequent developments in the Loop Current. Contributions on the Physical Oceanography of the Gulf of Mexico, L.R.A. Capurro and J. L. Reid, (Eds.), Gulf Publishing, 91-106.
- Cooper, C., Forristall, G. Z., Joyce, T. M., 1990. Velocity and hydrographic structure of two Gulf of Mexico warm-core rings. Journal of Geophysical Research 95, 663-679.

- Cruz-Escalona, V.H., Arreguín-Sánchez, F., Zetina-Rejón, 2007. Analysis of the ecosystem structure of Laguna Alvarado, western Gulf of Mexico, by means of a mass balance model. *Estuarine, Coastal and Shelf Science* 72, 155-167.
- Dale, B., 1983. Dinoflagellate resting cysts: “benthic plankton”. In: Fryxell, G.A. (Ed.), *Survival Strategies of the Algae*. Cambridge University Press, Cambridge, 69-136.
- David, L.T., Kjerfve, B., 1998. Tides and currents in a two-inlet coastal lagoon: Laguna de Términos, México. *Continental Shelf Research* 18, 1057-1079.
- Davis, C., 1948. *Gymnodinium breve*: a cause of discolored water and animal mortality in the Gulf of Mexico. *Botanical Gazette* 109, 358-360.
- Deflandre, G., Cookson, I.C., 1955. Fossil microplankton from Australian Late Mesozoic and Tertiary sediments. *Australian Journal of Marine and Freshwater Research* 6 (2), 242-313.
- de Velasco, G. G., & Winant, C. D., 1996. Seasonal patterns of wind stress and wind stress curl over the Gulf of Mexico. *Journal of Geophysical Research-Oceans* 101 (18), 127-140.
- de Vernal, A., Marret, F., 2007. Organic-walled dinoflagellate cysts: tracers of sea-surface conditions. *Developments in Marine Geology* 1, 371-408.
- de Vernal, A., Rochon, A., Turon, J.-L., Matthiessen, J., 1997. Organic-walled dinoflagellate cysts: palynological tracers of sea-surface conditions in middle to high latitude marine environments. *Geobios* 30, 905-920.
- de Vernal, A., Henry, M., Bilodeau, G., 1999. Techniques de préparation et d'analyse en micropaléontologie. *Les Cahiers du GEOTOP*, p. 28.
- de Vernal, A., Hillaire-Marcel, C., Turon, J.-L., Matthiessen, J., 2000. Reconstruction of sea-surface temperature, salinity, and sea-ice cover in the northern North Atlantic during the last glacial maximum based on dinocyst assemblages. *Canadian Journal of Earth Sciences*, 37(5), 725-750.
- de Vernal, A., Henry, M., Matthiessen, J., Mudie, P.J., Rochon, A., Boessenkool, K., Eynaud, F., Grøsfjeld, K., Guiot, J., Hamel, D., Harland, R., Head, M.J., Kunz-Pirring, M., Levac, E., Loucheur, V., Peyron, O., Pospelova, V., Radi, T., Turon, J.-L., Voronina, E., 2001. Cyst assemblages as tracer of sea-surface conditions in the northern North Atlantic, Arctic and sub-Arctic seas: the “n=677” database and

- derived transfer functions. *Journal of Quaternary Science* 16, 681-698.
- de Vernal, A., Eynaud, F., Henry, M., Hillaire-Marcel, C., Londeix, L., Mangin, S., Matthiessen, J., Marret, F., Radi, T., Rochon, A., Solignac, S., Turon, J.-L., 2005. Reconstruction of sea-surface conditions at middle to high latitudes of the Northern Hemisphere during the Last Glacial Maximum (LGM) based on dinoflagellate cyst assemblages. *Quaternary Science Reviews* 24, 897-924.
- de Vernal, A., Rochon, A., Fréchette, B., Henry, M., Radi, T., Solignac, S., 2013. Reconstructing past sea ice cover of the Northern hemisphere from dinocyst assemblages: status of the approach. *Quaternary Science Reviews*, accepted.
- de Verteuil de L., Norris, G., 1996. Miocene dinoflagellate stratigraphy and systematics of Maryland and Virginia. *Micropaleontology* 42, 172 pp.
- Duffield, S., Stein, J. A., 1986. Peridiniacean-dominated dinoflagellate cyst assemblages from the Miocene of the Gulf of Mexico shelf, offshore Louisiana. In : Wrenn J., et al. (Eds.), *1st Symposium Neogene Dinoflagellate Cyst Biostratigraphy*. AASP Contribution Series (17), 27-46.
- Edwards, L.E., 1986. Late Cenozoic dinoflagellate cysts from South Carolina, U.S.A.. U.S. Geological Survey, AASP Contribution Series (17), 47-51.
- Edwards, L.E., Willard, D.A. 2001. Dinoflagellate cysts and pollen from sediment samples, Mississippi Sound and Gulf of Mexico. In : Gohn, G.S., (Ed.), Paleontology and geology of Mississippi Sound sediments, US Geological Survey Open-File Report 01-415.
- Ellegaard, M., 2000. Variations in dinoflagellate cyst morphology under conditions of changing salinity during the last 2000 years in the Limfjord, Denmark. *Review of Palaeobotany and Palynology* 109, 65-81.
- Elliot, B. A., 1979. Anticyclonic rings and the energetics of the circulation of the Gulf of Mexico. Ph.D. dissertation, Texas A&M University, College Station, TX, 188 pp.
- Elliott, B.A., 1982. Anticyclonic rings in the Gulf of Mexico. *Journal of Physical Oceanography* 12, 1292-1309.
- Fensome, R.A., MacRae, R.A., Williams, G.L., 2008. DINOFALAJ2, Version 1. American Association of Stratigraphic Palynologists, Data Series no. 1.

- Garcés, E., Masó, M., Camp, J., 2002. Role of temporary cysts in the population dynamics of *Alexandrium taylori* (Dinophyceae). Journal of Plankton Research 24, 681-686.
- Garcia, H.E., Locarnini, R.A., Boyer, T.P., Antonov, J. I., 2010a. World Ocean Atlas 2009 Volume 3: Dissolved Oxygen, Apparent Oxygen Utilization, and Oxygen Saturation. S. Levitus, Ed., NOAA Atlas NESDIS 70, U.S. Government Printing Office, Washington, D.C., 344 pp.
- Garcia, H.E., Locarnini, R.A., Boyer, T.P., Antonov, J. I., 2010b. World Ocean Atlas 2009, Volume 4: Nutrients (phosphate, nitrate, and silicate). S. Levitus, Ed., NOAA Atlas NESDIS 71, U.S. Government Printing Office, Washington, D.C., 398 pp.
- Glibert, P.M., Burkholder, J.M., 2006. The complex relationships between increasing fertilization of the earth, coastal eutrophication and proliferation of harmful algal blooms. In: Graneli, E., Turner, J. (Eds.), Ecology of Harmful Algae. Springer, 341-354.
- Glibert, P.M., Anderson, D.A., Gentien, P., Granéli, E., Sellner, K.G., 2005a. The global, complex phenomena of harmful algal blooms. Oceanography 18 (2), 136-147.
- Glibert, P.M., Seitzinger, S., Heil, C.A., Burkholder, J.M., Parrow, M.W., Codispoti, L.A., Kelly, V., 2005b. The role of eutrophication in the global proliferation of harmful algal blooms. Oceanography 18, 198-209.
- Hallegraeff, G.M., 1993. A review of harmful algal blooms and their apparent global increase. Phycologia 32, 79-99.
- Harland, R., Hill, J., 1979. Dinoflagellate biostratigraphy of Neogene and Quaternary sediments at holes 400/400A in the Bay of Biscay (Deep Sea Drilling Project Leg 48). In: Montadert, L. et al., Deep Sea Drilling Project, Washington, Initial Reports 48, 531-545.
- Harland, R., Howe, J.A., 1995. Dinoflagellate cyst and Holocene oceanography of the northeastern Atlantic Ocean. The Holocene 5 (2), 220-228.
- Head, M.J., Westphal, H. 1999. Palynology and paleoenvironments of a Pliocene carbonate platform: the Clino Core, Bahamas. Journal of Paleontology 73(1), 1-25.
- Head, M.J., Wrenn, J.H., 1992: A forum on Neogene and Quaternary dinoflagellate cysts. In Head, M.J. and Wrenn, J.H. (Eds.), Neogene and Quaternary Dinoflagellate Cysts and Acritarchs, p.1-31; American Association of Stratigraphic Palynologists Foundation, Dallas, U.S.A.

- Heisler, J., Glibert, P.M., Burkholder, J.M., Anderson, W., Cochlan, W., Dennison, W.C., Dortch, Q., Gobler, C.J., Heil, C.A., Humphries, E., Lewitus, A., Magnien, R., Marshall, H.G., Sellner, K., Stockwell, D.A., Stoecker, D.K., Suddleson, M., 2008. Eutrophication and harmful algal blooms : A scientific consensus. *Harmful Algae* 8 (1), 3-13.
- Hense, I., 2010. Approaches to model the life cycle of harmful algae. *Journal of Marine Systems* 83, 108-114.
- Hillaire-Marcel, C., de Vernal, A., Bilodeau, G., Weaver, A.J., 2001. Absence of deep water formation in the Labrador Sea during the last interglacial period. *Nature* 410, 1073-1077.
- Hofmann, E.E., Worley, S.J., 1986. An investigation of the circulation of the Gulf of Mexico. *Journal of Geophysical Research* 9 (14), 221-238.
- Ichiye, T., 1962. Circulation and water-mass distribution in the Gulf of Mexico. *Geofisica Internacional* 2, 47-76.
- Itakura, S., Imai, I., Itoh, K., 1997. "Seed bank" of coastal planktonic diatoms in bottom sediments of Hiroshima Bay, Seto Inland Sea, Japan. *Marine Biology* 128, 497-508.
- Jochens, A.E., DiMarco, S.F., 2008. Physical oceanographic conditions of the deepwater Gulf of Mexico in summer 2000-2002. *Deep-Sea Research Part II: Topical Studies in Oceanography* 55, 2541-2554.
- Justic, D., Rabalais, N.N., Turner, R.E., 2002. Modeling the impacts of decadal changes in riverine nutrient fluxes on coastal eutrophication near the Mississippi River Delta. *Ecological Modelling* 152, 33-46.
- Kokinos, J.P., Anderson, D.M., 1995. Morphological development of resting cysts in cultures of the marine dinoflagellate *Lingulodinium polyedrum* (=*L. machaeophorum*). *Palynology* 19, 143-166.
- Landsberg, J.H., Sherwood, H., Johannessen, J.N., White, K.D., Conrad, S.M., Abbott, J.P., Flewlling, L.J., Richardson, R.W., Dickey, R.W., Jester, E.L.E., Etheridge, S.M., Deeds, J.R., Van Dolah, F.M., Leifield, T.A., Zou, Y., Beaudry, C.G., Benner, R.A., Rogers, P.L., Scott, P.S., Kawabata, K., Wolny, J.L., Steidinger, K.A., 2006. Saxitoxin puffer fish poisoning in the United States, with the first report of *Pyrodinium bahamense* as the putative toxin source. *Environmental Health Perspectives* 114, 1502-1507.

- Lenoir, E.A., Hart, G.F., 1986. Burdigalian (early Miocene) dinocysts from offshore Louisiana. In: Wrenn, J.H., Duffield, S.L., and Stein, J.A. (Eds), AASP Contribution Series Papers. 17, 59-81.
- Licea, S., Zamudio, M.E., Luna, R., Okolodkov, Y., Gomez Aguirre, S., 2002. Toxic and harmful dinoflagellates in the southern Gulf of Mexico. In: Proceedings of the X International Conference on Harmful Algae. St. Petersburg, FL, 21-25 October, (Abstracts), p. 170.
- Limoges, A., Kielt, J-F., Radi, T., Ruiz-Fernandez, A. C., de Vernal, A., 2010. Dinoflagellate cyst distribution in surface sediments along the south-western Mexican coast (14.76°N to 24.75°N). *Marine Micropaleontology* 76, 104-123.
- Locarnini, R.A., Mishonov, A.V., Antonov, J.I., Boyer, T.P., Garcia, H.E., 2010. World Ocean Atlas 2009, Volume 1: Temperature. S. Levitus, (Ed.), NOAA Atlas NESDIS 68, U.S. Government Printing Office, Washington, D.C., 184 pp.
- Lundholm, N., Ribeiro, S., Andersen, T.J., Koch, T.A., Godhe, A., Ekelund, F., Ellegaard, M., 2011. Buried alive-germination of up to a century-old marine protist resting stages. *Phycologia* 50 (6), 629-640.
- Maclean, J.L., 1989. An overview of *Pyrodinium* red tides in the Western Pacific. In: G. M. Hallegraeff and J. L. Maclean (Eds.), Biology, epidemiology and management of *Pyrodinium* red tides. ICLARM Conference Proceedings 21. International Center for Living Aquatic Resources Management, Manila, Philippines, 1-7.
- Magaña, H.A., Contreras, C., Villareal, T.A., 2003. A historical assessment of *Karenia brevis* in the western Gulf of Mexico. *Harmful Algae* 2, 163–171.
- Manum, S.B., Boulter, M.C., Gunnarsdottir, H., Rangnes, K., Scholze, A., 1989. Eocene to Miocene palynology of the Norwegian Sea (ODP Leg 104). *Proceedings of Ocean Drilling Program-Scientific Results* 104, 611-662.
- Marret, F., 1994. Distribution of dinoflagellate cysts in recent marine sediments from the east Equatorial Atlantic (Gulf of Guinea). *Review of Palaeobotany and Palynology* 84, 1-22.
- Marret, F., Zonneveld, K.A.F., 2003. Atlas of modern organic-walled dinoflagellate cyst distribution. *Review of Palaeobotany and Palynology* 125 (1-2), 1-200.

Marret, F., Kim, S-Y., 2009. *Opercudodinium aguinawense* sp. nov., dinoflagellate cyst from the late Pleistocene and recent sediments of the east equatorial Atlantic ocean. *Palynology* 33 (1), 125-139.

Matsuoka, K., Fukuyo, Y., 2000. Technical guide for modern dinoflagellate cyst study. WESTPAC-HAB/WESTPAC/IOC, Japan Society of the Promotion Science, Tokyo, p. 29.

Matthiessen, J., 1995. Distribution patterns of dinoflagellate cysts and other organic-walled microfossils in recent Norwegian-Greenland Sea sediments. *Marine Micropaleontology* 24, 307-334.

Mertens, K.N., González, C., Delusina, I., Louwye, S., 2009a. 30 000 years of productivity and salinity variations in the late Quaternary Cariaco Basin revealed by dinoflagellate cysts. *Boreas* 38, pp. 647-662

Mertens, K.N., Ribeiro, S., Bouimetarhan, I., Caner, H., Combourieu Nebout, N., Dale, B., de Vernal, A., Ellegaard, M., Filipova, M., Godhe, A., Goubert, E., Grøsfjeld, K., Holzwarth, U., Kotthoff, U., Leroy, S.A.G., Londeix, L., Marret, F., Matsuoka, K., Mudie, P.J., Naudts, L., Peña-Manjarrez, J.L., Persson, A., Popescu, S.-M., Pospelova, V., Sangiorgi, F., van der Meer, M.T.J., Vink, A., Zonneveld, K.A.F., Vercauteren, D. Vlassenbroeck, J., Louwye, S., 2009b. Process length variation in cysts of a dinoflagellate, *Lingulodinium machaerophorum*, in surface sediments: Investigating its potential as salinity proxy. *Marine Micropaleontology* 70, 54-69.

Monreal-Gómez, M.A., Salas de León, D.A., Padilla, A.R., Alatorre, M.A., 1992. Hydrography and estimation of density currents in the southern part of the Bay of Campeche, Mexico. *Ciencias Marinas* 18, 115-133.

Moran-Silva, A., Martínez Franco, L.A., Chávez-López, R., Franco-López, J., Bedia Sánchez, C. M., Contreras Espinosa, F., Gutiérrez Mendieta, F., Brown-Peterson, N.J., Peterson, M.S., 2005. Seasonal and spatial patterns in salinity, nutrients, and chlorophyll a in the Alvarado Lagoonal system, Veracruz, Mexico. *Gulf and Caribbean Research* 17, 33-143.

Nowlin, W.D. Jr., 1972. Winter circulation patterns and property distributions. *Texas A&M University Oceanographical Studies* 2, L.R.A. Capurro and J.L. Reid, (Eds.), Gulf Publication Company, Houston, 3-52.

Nowlin, W.D., Jr., McLellan, H.J., 1967. A characterization of the Gulf of Mexico waters in winter. *Journal of Marine Research* 25, 29-59.

- Nowlin, W.D., Jr., A.E. Jochens, S.F. DiMarco, R.O. Reid, and M.K. Howard. 2001. Deepwater Physical Oceanography Reanalysis and Synthesis of Historical Data: Synthesis Report. OCS Study MMS 2001-064, U.S. Department of the Interior, Minerals Management Service, Gulf of Mexico OCS Region, New Orleans, LA. 528 pp.
- Nowlin, W.D., Jochens, A.E., DiMarco, S.F., Reid, R.O., Howard, M. K., 2005. Low-frequency circulation over the Texas–Louisiana continental shelf. In: Wilton, Lugo-Fernandez, A. (Eds.), Circulation in the Gulf of Mexico. American Geophysical Union, 219-240.
- Oey, L.-Y., Ezer, T., Lee, H.-C., 2005. Loop current, rings and related circulation in the Gulf of Mexico : A review of numerical models and future challenges. In: Circulation in the Gulf of Mexico : Observations and models, Sturges, W., Lugo-Fernandez, A. (Eds.), Geophysical Monograph Series 161, American Geophysical Union, Washington, DC, 31-56.
- Peperzak, L., 2003. Climate change and harmful algal blooms in the North Sea. *Acta Oecologica* 24, 139-144.
- Phlips, E.J., Badylak, S., Bledsoe, E., Cichra, M., 2006. Factors affecting the distribution of *Pyrodinium bahamense* var. *bahamense* in coastal waters of Florida. *Marine Ecology Progress Series* 322, 99-115.
- Pospelova, V., de Vernal, A., Pedersen, T.F., 2008. Distribution of dinoflagellate cysts in surface sediments from the northeastern Pacific Ocean (43–25°N) in relation to sea-surface temperature, salinity, productivity and coastal upwelling. *Marine Micropaleontology* 68, 21-48.
- Powell, A.J., 1992. Dinoflagellate cysts of the tertiary system. In : Powell, A.J. (Ed.) : A stratigraphic index of dinoflagellate cysts. British Micropaleontological Society Publication Series, London (Chapman and Hall), 155-251.
- Radi, T., de Vernal, A., 2008. Dinocysts as proxy of primary productivity in mid-high latitudes of the Northern Hemisphere. *Marine Micropaleontology* 68, 84-114.
- Ribeiro, S. Berge, T., Lundholm, N., Andersen, T., Abrantes, F., Ellegaard, M. 2011. Phytoplankton growth after a century of dormancy illuminates past resilience to catastrophic darkness. *Nature Communications* 2 (311), doi:10.1038/ncomms1314.
- Rochon, A., de Vernal, A., Turon, J. L., Matthiessen, J., et Head, M.J., 1999. Distribution of dinoflagellate cysts in surface sediments from the North Atlantic

Ocean and adjacent basin and quantitative reconstruction of sea-surface parameters. American Association of Stratigraphic Palynologists, Dallas, Contribution Series 35, pp. 152.

Schlitzer, R., 2012. Ocean Data View, <http://odv.awi.de>

Sierra-Beltrán, A.P., Cortés-Altamirano, R., Cortés-Lara, M.C., 2005. Occurrences of *Prorocentrum minimum* (Pavillard) in México. Harmful Algae 4, 507-517.

Smayda, T.J., 1990. Novel and nuisance phytoplankton blooms in the sea: evidence for a global epidemic. In: Granéli, E., Sundstrom, B., Edler, L., Anderson, D.M. (Eds.), Toxic Marine Phytoplankton, New York, 29-40.

Smayda, T.J., 2002. Adaptive ecology, growth strategies, and the global bloom expansion of dinoflagellates. Journal of Oceanography 58, 281-294.

Solignac, S., de Vernal, A., Hillaire-Marcel, C., 2004. Holocene sea-surface conditions in the North Atlantic-Contrasted trends and regimes in the western and eastern sectors (Labrador Sea vs. Iceland Basin). Quaternary Sciences Reviews 23(3-4), 319.

Soto, L. A., Escobar, E., 1995. Coupling mechanisms related to benthic production in the SW Gulf of Mexico. In: Biology and Ecology of Shallow Coastal Waters (Eds.), A. Eleftheriou, A. D. Ansell, and J. Smith, pp. 233-242, Olsen and Olsen, Fredensborg, Denmark.

Steidinger, K.A., 2009. Historical perspective on *Karenia brevis* red tide research in the Gulf of Mexico. Harmful Algae 8, 549-561.

Steidinger, K.A., Vargo, G.A., Tester, P.A., Tomas, C.R., 1998. Bloom dynamics and physiology of *Gymnodinium breve* with emphasis on the Gulf of Mexico. In: Anderson DM, Cembella AD, Hallegraeff GM, (Eds.), Physiological Ecology of Harmful Algal Blooms. Springer-Verlag; Berlin, 133-153.

Stern, R.J., Dickinson, W.R., 2010. The Gulf of Mexico is a Jurassic backarc basin. Geosphere 6 (6), 739-754

Stockmarr, J., 1971. Tablets with spores used in absolute pollen analysis. Pollen et Spores, 13, 615-621.

Tapáñes, J.J., González-Coya, F., 1980. Hidrometeorología del Golfo de México y Banco de Campeche (Hydrometeorology of the Gulf of Mexico and Campeche Bank). Geofisica Internacional, 19, 335-354.

Taylor, F.J.R. (Ed.), 1987. The Biology of Dinoflagellates. Botanical Monographs 21. Blackwell Scientific Publications, Oxford. p. 785.

Ter Braak, C.J.F., Smilauer, P., 1998. Canoco reference manual and user's guide for Canoco for Windows. Software for Canonical Community Ordination (Version 4). Centre for Biometry, Wageningen, p. 351.

Turon, J.-L., 1978. Les dinoflagellés témoins des paléoenvironnements durant l'Holocène dans l'Atlantique Nord Oriental. Signification paléohydrologique et paléoclimatique. Comptes Rendus de l'Académie des Sciences, Paris 286, 1861-1864.

Turon, J.L., Londeix, L., 1988. Les assemblages de kystes de dinoflagellés en méditerranée occidentale (mer d'Alboran) mise en évidence de l'évolution des paléoenvironnements depuis le dernier maximum glaciaire. Bulletin des Centres de Recherches Exploration-Production Elf-Aquitaine 12 (1), 313-344.

Usup, G., Ahmad, A., Matsuoka, K., Lim, P.T., Leaw, C.P., 2012. Biology, ecology and bloom dynamics of the toxic marine dinoflagellate *Pyrodinium bahamense*. Harmful Algae 14, 301-312.

Van Dolah, F. M., 2000. Marine algal toxins: origins, health effects, and their increased occurrence. Environmental Health Perspectives 108, 133-141.

Van Soelen, E.E., Lammertsma, E.I., Cremer, H., Donders, T.H., Sangiorgi, F., Brooks, G.R., Larson, R.A., Sinninghe Damsté, J.S., Wagner-Cremer, F., Reichart, G.J., 2010. Late Holocene sea-level rise in Tampa Bay: Integrated reconstruction using biomarkers, pollen, organic-walled dinoflagellate cysts, and diatoms. Estuarine, Coastal and Shelf Science 86, 216-224.

Verleye, T.J., Mertens, K.N., Young, M.D., Dale, B., McMinn, A., Scott, L., Zonneveld, K.A.F., Louwye, S., 2012. Average process length variation of the marine dinoflagellate cyst *Operculodinium centrocarpum* in the tropical and Southern Hemisphere Oceans: Assessing its potential as a palaeosalinity proxy. Marine Micropaleontology 86-87, 45-58.

Versteegh, G.J.M., Blokker, P., Bogus, K.A., Harding, I.C., Lewis, J., Oltmanns, S., Rochon, A., Zonneveld, K.A.F., 2012. Infra red spectroscopy, flash pyrolysis, thermally assisted hydrolysis and methylation (THM) in the presence of tetramethylammonium hydroxide (TMAH) of cultured and sediment-derived *Lingulodinium polyedrum* (Dinoflagellata) cyst walls. Organic Geochemistry 43, 92-102.

- Vidal, V.M.V., Vidal, F.V., Hernández, A.F., Meza, E. and Pérez-Molero, J.M., 1994. Baroclinic flows, transports, and kinematic properties in a cyclonic-anticyclonic-cyclonic ring triad in the Gulf of Mexico. *Journal of Geophysical Research* 99 (C4), 7471-7497.
- Villanoy, C.L., Corrales, R.A., Jacinto, G.S., Cuaresma Jr., N.T., Crisostomo, R.P., 1996. Towards the development of a cyst-based model for *Pyrodinium* red tides in Manila Bay, Philippines. In: Yasumoto, T., Oshima, Y., Fukuyo, Y. (Eds.), Harmful and Toxic Algal Blooms. Intergovernmental Oceanographic Commission (IOC) of UNESCO, Paris, pp. 189–192.
- Vukovich, F. M., Crissman, B.W., 1986. Aspects of warm rings in the Gulf of Mexico. *Journal of Geophysical Research* 91, 2645-2660.
- Wall, D., Dale, B. 1966. Living fossils in Western Atlantic plankton. *Nature* 211, 1025-1026.
- Wall, D., 1967. Fossil microplankton in deep-sea cores from the Caribbean Sea. *Palaeontology* 10 (1), 5-123.
- Wall, D., Dale, B., 1968. Modern dinoflagellate cysts and evolution of the Peridiniales. *Micropaleontology* 14, 265–304.
- Wall, D., Dale, B., 1969. The “*Hystrichosphaerid*” resting spore of the dinoflagellate *Pyrodinium bahamense*. *Journal of Phycology* 5, 140-149.
- Wall, D., Dale, B., Lohmann, G.P., Smith, W.K., 1977. The environmental and climatic distribution of dinoflagellate cysts in modern marine sediments from regions in the North and South Atlantic Oceans and adjacent seas. *Marine Micropaleontology* 2, 121-200.
- Walker, N.D., 1996. Satellite assessment of Mississippi River plume variability: Causes and predictability. *Remote Sensing of Environment* 58 (1), 21-35.
- Wang, W., Nowlin, W. D., & Reid, R. O., 1998. Analyzed surface meteorological fields over the northwestern Gulf of Mexico for 1992–94: mean, seasonal, and monthly patterns. *Monthly Weather Review* 126, 2864-2883.
- Warny, S., Bart, P.J., Suc, J-P., 2003. Timing and progression of climatic, tectonic and glacioeustatic influences on the Messinian Salinity Crisis. *Palaeogeography, Palaeoclimatology and Palaeoecology* 202(1-2), 59-66.

World Ocean Atlas, 2001. CD-ROMs Data Set. National Oceanographic Data Center, Silver Spring, MD.

Wrenn, J.H., 1988. Differentiating species of the dinoflagellate cyst genus *Nematosphaeropsis*. Deflandre & Cookson 1955. *Palynology* 12, 129-150.

Wrenn, J.H., Kokinos, J.P., 1986. Preliminary comments on Miocene through Pleistocene dinoflagellate cysts from De Soto Canyon, Gulf of Mexico. In: Wrenn, J.H., Duffield, S.L., and Stein, J.A. (Eds.), AASP Contribution Series 17, 169-225.

Yang, H., Weisberg, R.H., Niiler, P.P., Sturges, W., Johnson, W., 1999. Lagrangian circulation and forbidden zone on the West Florida Shelf. *Continental Shelf Research* 19, 1221-1245.

Zavala-Hidalgo, J., S. L., Morey, and J. J. O'Brien, 2003. Seasonal circulation on the western shelf of the Gulf of Mexico using a high resolution numerical model. *Journal of Geophysical Research* 108 (C12), 3389.

Zonneveld, K.A.F., 1997. Dinoflagellate cyst distribution in surface sediments from the Arabian Sea (northwestern Indian Ocean) in relation to temperature and salinity gradients in the upper water column. *Deep-Sea Research II* 6-7, 1411-1443.

Zonneveld, K.A.F., Marret, F., Versteegh, G.J.M., Bonnet, S., Bouimetarhan, I., Crouch, E., de Vernal, A., Elshanawany, R., Edwards, L., Esper, O., Forke, S., Grøsfjeld, K., Henry, M., Holzwarth, U., Kielt, J.-F., Kim, S.-Y., Ladouceur, S., Ledu, D., Chen, L., Limoges, A., Londeix, L., Lu, S.-H., Mahmoud, M.S., Marino, G., Matsuoka, K., Matthiessen, J., Mildenhall, D.C., Mudie, P., Neil, H.L., Pospelova, V., Qi, Y., Radi, T., Richerol, T., Rochon, A., Sangiorgi, F., Solignac, S., Turon, J.-L., Verleye, T., Wang, Y., Wang, Z., Young, M., In Press. Atlas of modern dinoflagellate cyst distribution based on 2405 datapoints. Review of Palaeobotany and Palynology.

	Sample number	Site	Lab number	Cruise	Latitude (N)	Longitude (W)
B Northern Gulf	1	2532	2887-1	MD-02	16.7718	88.0083
	2	2534	2815-1	MD-02	26.7405	94.0290
	3	2548	2815-4	MD-02	27.6375	92.1995
	4	2549	2815-5	MD-02	26.4280	92.5657
	5	2550	2815-6	MD-02	26.9462	91.3457
	6	2558	2817-1	MD-02	28.0830	89.4892
	7	2574	2817-2	MD-02	28.6267	88.2248
	8	2576	2817-3	MD-02	29.0015	87.1190
	9	2577	2817-4	MD-02	28.8373	88.6592
	10	2578	2817-5	MD-02	28.8377	86.6592
F Florida Coast	11	2581	2817-6	MD-02	23.8780	82.4433
	12	A1	2857-1	SAR-11	27.3210	82.6136
	13	C1	2857-2	SAR-11	27.2334	82.6289
	14	C2	2857-3	SAR-11	27.2002	82.6668
	15	C9	2857-4	SAR-11	27.1168	82.9000
	16	C8	2857-5	SAR-11	27.1169	82.8668
	17	D7	2857-6	SAR-11	27.3322	82.5886
	18	B10	2858-1	SAR-11	27.2918	83.1503
	19	B3	2858-2	SAR-11	27.3049	82.6284
	20	B1	2858-3	SAR-11	27.3049	82.6000
	21	B2	2858-4	SAR-11	27.3050	82.6216
	22	A2	2858-6	SAR-11	27.3200	82.6573
Mexican lagoons	23	1	2872-1	MEX-11	18.8584	95.9111
	24	2	2872-2	MEX-11	18.8470	95.9225
	25	3	2872-3	MEX-11	18.8365	95.9323
	26	4	2872-4	MEX-11	18.8153	95.8588
	27	5	2872-5	MEX-11	18.7979	95.8579
	28	6	2872-6	MEX-11	18.7248	95.8222
	29	7	2873-1	MEX-11	18.6281	91.8271
	30	8	2873-2	MEX-11	18.5904	91.5617
	31	9	2873-3	MEX-11	18.7809	91.4700
	32	12	2873-4	MEX-11	18.4338	93.1289
	33	13	2873-5	MEX-11	18.4295	93.1487
	34	14	2873-6	MEX-11	18.4230	93.1470
	35	E41	2885-1	GDM-11	18.9730	94.6820
	36	E48	2885-2	GDM-11	19.0403	94.8227
	37	E50	2885-3	GDM-11	19.1647	94.8960
	38	E51	2885-4	GDM-11	19.0640	94.8777
	39	E52	2885-5	GDM-11	19.0048	94.9267
	40	E54	2885-6	GDM-11	19.1595	94.9920
	41	E55	2886-1	GDM-11	19.0743	94.9897
	42	E57	2886-2	GDM-11	19.1170	94.0362
	43	E58	2886-3	GDM-11	19.1603	94.0688
	44	E42	2886-4	GDM-11	18.9878	94.6692

Table 1. Location of the surface sediment samples investigated in the present study. Abbreviations: B: Belize, F: Florida Strait.

	#	NOAA						MODIS			Depth (m)	Distance to the coast (km)
		sSST	wSST	aSST	sSSS	wSSS	aSSS	aP	sP	wP		
B	1	28,75	26,66	28,06	36,07	36,04	36,06	104,21	49,90	54,31	333	27,29
	2	29,39	21,84	24,94	35,92	35,46	35,16	114,86	51,87	62,98	1350	271,85
	3	29,31	21,18	25,16	34,07	35,8	34,98	124,69	53,47	71,22	610	199,97
	4	29,35	21,8	25,51	35,67	35,94	34,81	109,95	48,57	61,39	2049	336,4
	5	29,35	21,76	25,45	34,98	36,02	35,62	108,45	48,06	60,40	2248	250,22
	6	29,37	21,02	24,91	32,94	35,23	34,24	120,13	51,03	69,09	1125	99,23
	7	29,39	19,85	25,87	34,1	34,85	34,43	149,23	71,46	77,77	1963	96,65
	8	29,09	20,53	25,82	34,38	35,97	35,07	143,05	67,14	75,91	848	147,2
	9	29,12	19,63	24,96	31,42	33,15	32,54	201,37	98,52	102,85	476	48,55
	10	29,09	20,87	25,67	34,7	35,79	35,27	143,05	67,14	75,91	476	159,59
F	11	29,17	24,48	26,64	35,82	36,11	36,04	80,93	35,77	45,16	1063	76,09
	12	29,94	17,92	23,89	35,3	34,89	35,27	229,37	88,30	141,07	8,87	2,36
	13	29,95	18,12	23,97	35,34	34,97	35,33	229,37	88,30	141,07	10,91	7,61
	14	29,94	18,31	24,11	35,37	35,14	35,38	229,37	88,30	141,07	12,95	12,84
	15	29,89	19,05	24,24	35,39	35,48	35,52	229,37	88,30	141,07	25,36	37,42
	16	29,91	19,04	24,23	35,39	35,48	35,51	229,37	88,30	141,07	26,52	34,4
	17	29,94	17,91	23,89	35,3	34,89	35,27	229,37	88,30	141,07	6,10	0,06
	18	29,75	18,8	24,15	35,34	35,68	35,55	229,37	88,30	141,07	32	48,32
	19	29,94	18,01	23,89	35,3	34,89	35,28	229,37	88,30	141,07	9,02	4,46
	20	29,94	17,95	23,87	35,3	34,89	35,27	229,37	88,30	141,07	8,08	2,06
	21	29,94	18,01	23,89	35,3	34,89	35,28	229,37	88,30	141,07	9,30	3,86
	22	29,93	18,09	23,94	35,3	34,97	35,3	229,37	88,30	141,07	11,49	10,3
Mexican lagoons	23	28,4	24,13	26,67	34,97	35,06	35,3	272,65	134,16	138,50	1,50	0,21
	24	28,4	24,13	26,67	34,97	35,06	35,3	272,65	63,68	70,48	1,50	0,22
	25	28,4	24,13	26,54	34,97	35,06	35,21	272,65	134,16	138,50	2,50	1,93
	26	28,27	24,06	26,48	34,97	35,06	35,26	272,65	134,16	138,50	1,50	0,6
	27	28,17	24,07	26,39	34,97	35,06	35,26	272,65	134,16	138,50	1,25	0,24
	28	28,4	23,91	26,3	34,97	35,06	35,3	272,65	134,16	138,50	1,50	0,39
	29	n/a	n/a	27,36	n/a	n/a	36,87	n/a	n/a	n/a	1,15	0,81
	30	n/a	n/a	27,36	n/a	n/a	36,87	n/a	n/a	n/a	1,20	0,08
	31	n/a	26,27	27,02	n/a	n/a	36,42	n/a	n/a	n/a	3,50	0,33
	32	26,34	24,93	25,61	n/a	35,62	35,97	n/a	n/a	n/a	1	12,57
	33	26,34	24,93	25,54	n/a	35,62	35,82	n/a	n/a	n/a	1	0,01
	34	26,34	24,93	25,54	n/a	35,62	35,82	n/a	n/a	n/a	1	0,07
Southwestern Gulf	35	28,42	24,2	25,82	35,17	35,88	35,72	234,31	104,87	129,44	1	0,01
	36	28,46	24,17	26	35,41	35,93	35,83	234,31	104,87	129,44	821	49,91
	37	28,64	24,18	26,01	36,38	35,96	36,03	234,31	104,87	129,44	1350	51,68
	38	28,55	24,14	26,01	35,41	35,96	35,86	234,31	104,87	129,44	1785,11	58,6
	39	28,43	24,2	25,95	35,17	35,93	35,83	234,31	104,87	129,44	1442	50,93
	40	28,61	24,23	26,04	36,28	35,96	35,96	234,31	104,87	129,44	1263	42,46
	41	28,55	24,19	26,08	35,41	35,96	35,81	234,31	104,87	129,44	1750	53,74
	42	28,48	24,37	25,95	36,26	35,93	35,94	343,04	129,14	213,90	1525,36	45,16
	43	28,53	24,35	26,04	36,35	36,07	36	343,04	129,14	213,90	1647	91,17
	44	28,42	24,23	25,85	35,17	35,92	35,74	234,31	104,87	129,44	1785	97,55

Table 2. Environmental parameters included in the statistical analyses corresponding to the database sampling sites: summer, winter and annual temperatures (sSST, wSST, aSST; °C), summer, winter and annual salinity (sSSS, wSSS, aSSS), annual, summer (April-September) and winter (October-March) primary productivity estimated by moDIS programs (sP, wP, aP; gC·m⁻²·yr⁻¹), the water depth (m) and the distance to the coast (km). Abbreviations: B : Belize, F: Florida Strait.

#	Cyst concentration (cysts·g ⁻¹)	Reworked cyst concentration (cysts·g ⁻¹)	Relative abundance phototrophic specimens (%)	Pollen grain concentrations (grains·g ⁻¹)	Organic lining concentrations (linings·g ⁻¹)
B Northern Gulf	1	198	16	88	707
	2	113	0	100	274
	3	298	7	67	1412
	4	436	25	100	1310
	5	2430	62	6	14301
	6	535	27	58	2396
	7	886	4	88	963
	8	2297	9	78	2849
	9	2028	19	79	4636
	10	820	0	75	486
F Florida Coast	11	1653	7	85	2038
	12	333	0	69	1368
	13	493	0	64	2795
	14	127	0	69	812
	15	385	0	67	2480
	16	170	4	33	2041
	17	1059	0	42	118566
	18	614	0	82	2550
	19	75	0	93	440
	20	412	0	58	1729
	21	152	0	61	1097
	22	290	0	55	1090
M Mexican lagoons	23	3016	0	88	15839
	24	3287	0	88	13619
	25	3331	0	92	12403
	26	1459	0	96	6041
	27	3576	0	98	4389
	28	1727	0	99	8366
	29	2043	0	86	3061
	30	2232	0	92	3027
	31	2121	0	69	4142
	32	239	0	33	4769
	33	163	0	58	4586
	34	78	0	27	2800
	35	317	14	67	3333
	36	171	0	52	1469
G Southwestern Gulf	37	296	2	67	1017
	38	404	7	45	1673
	39	412	18	62	2382
	40	279	0	57	1546
	41	316	8	80	797
	42	167	0	89	1726
	43	485	14	51	2341
	44	113	0	82	3124
					100

Table 3. Dinoflagellate cyst concentrations (cysts·g⁻¹), reworked dinoflagellate cyst concentrations (cysts·g⁻¹), relative abundance of phototrophic species (%), pollen grain concentrations (grains·g⁻¹) and foraminifer organic lining concentrations (linings·g⁻¹). Abbreviations: B: Belize, F: Florida Strait.

Dinoflagellate cyst species	Abbreviations	Notes
Gonyaulacales		
<i>Bitectatodinium spongium</i>	BSPO	
<i>Impagidinium aculeatum</i>	IACU	
<i>Impagidinium paradoxum</i>	IPAR	
<i>Impagidinium patulum</i>	IPAT	
<i>Impagidinium sphaericum</i>	ISPH	
<i>Impagidinium striatum</i>	ISTR	
<i>Impagidinium velorum</i>	IVEL	
<i>Lingulodinium machaerophorum</i>	LMAC	
<i>Melitasphaeridium choanophorum</i>	MCHO	
<i>Nematosphaeropsis rigida</i>	NRIG	
<i>Operculodinium cf. bahamense</i>	OBAH	
<i>Operculodinium centrocarpum</i>	OCEN	sensu Wall & Dale, 1966
Atypical <i>Operculodinium centrocarpum</i>	*OCEN	
<i>Operculodinium cezare</i>	OCEZ	
<i>Operculodinium giganteum</i>	OGIG	
<i>Operculodinium israelianum</i>	OISR	
<i>Operculodinium janduchenei</i>	OJAN	
<i>Operculodinium longispinigerum</i>	OLON	
<i>Polysphaeridium zoharyi</i>	PZOH	
<i>Spiniferites membranaceus</i>	SMEM	
<i>Spiniferites mirabilis</i> s.l.	SMIR s.l.	
<i>Spiniferites hyperacanthus</i>	SHYP	grouped with <i>S. mirabilis</i>
Atypical <i>Spiniferites mirabilis</i>	*SMIR	
<i>Spiniferites ramosus</i>	SRAM	
<i>Spiniferites belerius</i>	SBEL	
<i>Spiniferites bentorii</i>	SBEN	
<i>Spiniferites bulloideus</i>	SBUL	
Granular <i>Spiniferites</i>	SGRA	
<i>Spiniferites</i> spp.	SSPP	
<i>Tuberculodinium vancampoae</i>	TVAN	
Peridiniales		
<i>Brigantedidium</i> spp.	BSPP	
Cyst of <i>Pentapharsodinium dalei</i>	PDAL	
<i>Echinidinium aculeatum</i>	EACU	
<i>Echinidinium delicatun</i>	EDEL	
<i>Echinidinium granulatum</i>	EGRA	
<i>Echinidinium transparantum</i>	ETRA	
<i>Echinidinium</i> sp. Z	ESPZ	
<i>Echinidinium</i> spp.	ESPP	
<i>Islandinium brevispinosum</i>	IBRE	
<i>Islandinium minutum</i>	IMIN	
<i>Lejeuneacysta</i> spp.	LSPP	
Protoperdinoids	PERI	
<i>Quinquecupsis concreta</i>	QCON	
<i>Selenopemphix nephroides</i>	SNEP	
<i>Selenopemphix quanta</i>	SQUA	
<i>Stelladinium stellatum</i>	SSTE	
<i>Votadinium spinosum</i>	VSPI	
Gymnodiniales		
<i>Polykrikos kofoeldii</i>	PKOF	sensu Rochon et al., 1999
<i>Polykrikos schwartzii</i>	PSCH	sensu Rochon et al., 1999

Table 4. Dinoflagellate cyst species reported from surface sediment samples, abbreviations (cf. Fig. 7) and notes.

Environmental parameters	AXIS 1	AXIS 2	AXIS 3
sSST	-0.2580	0.7754	-0.3476
wSST	0.1178	-0.7493	0.4099
aSST	0.2378	-0.8410	0.2463
sSSS	-0.0439	0.2112	0.3931
wSSS	-0.4331	-0.2307	0.3721
aSSS	-0.1273	0.0914	0.4702
aP	0.4212	0.1383	0.3558
sP	0.4572	-0.1098	0.3104
wP	0.1379	0.3660	0.2735
Water Depth	-0.5497	-0.5032	0.1843
Distance to the coast	-0.5210	-0.3196	0.0727

Table 5. Coefficient of correlation between environmental parameters and the scores of the three first axes of redundancy analysis. Parameter abbreviations are: summer sea-surface temperature (sSST), winter sea-surface temperature (wSST), annual sea-surface temperature (aSST), summer sea-surface salinity (sSSS), winter sea-surface salinity (wSSS), annual sea-surface salinity (aSSS), annual productivity (aP), summer productivity (sP), winter productivity (wP). Bold numbers correspond to parameters which are best correlated to axes.

Dinocyst taxa	AXIS 1	AXIS 2	AXIS 3
<i>Bitectatodinium spongium</i>	-0.2706	-0.1561	0.2835
<i>Impagidinium aculeatum</i>	-0.6406	-0.6622	0.0287
<i>Impagidinium paradoxum</i>	-0.4885	-0.5014	0.2647
<i>Impagidinium patulum</i>	-0.3260	-0.2767	-0.3980
<i>Impagidinium sphaericum</i>	-0.0970	-0.1416	0.1067
<i>Impagidinium strialatum</i>	-0.4357	-0.3904	0.0297
<i>Impagidinium velorum</i>	-0.1598	-0.1991	0.0693
<i>Lingulodinium machaerophorum</i>	-0.2295	0.1804	-0.5902
<i>Nematosphaeropsis rigida</i>	0.2957	-0.4044	-0.3680
<i>Nematosphaeropsis</i> spp.	-0.0351	-0.2083	-0.2096
<i>Operculodinium centrocarpum</i>	-0.4935	0.1329	-0.3461
<i>Operculodinium centrocarpum</i> atypical	-0.0919	0.5104	-0.0511
<i>Operculodinium israelianum</i>	-0.1115	-0.0037	-0.2662
<i>Operculodinium janduchenei</i>	-0.2694	-0.1520	0.0665
<i>Operculodinium longispinigerum</i>	-0.1088	-0.0970	-0.1049
<i>Operculodinium</i> conf. <i>bahamense</i>	-0.0044	-0.1431	-0.1215
<i>Operculodinium giganteum</i>	0.0368	-0.1840	-0.3117
<i>Operculodinium?</i> sp.1	0.1411	0.2097	0.1173
<i>Polysphaeridium zoharyi</i>	0.6326	0.0847	-0.0543
<i>Spiniferites membranaceus</i>	-0.0027	0.2430	-0.3483
<i>Spiniferites ramosus</i>	-0.1489	0.0180	-0.4057
<i>Spiniferites belerius</i>	0.6927	-0.2496	0.1684
<i>Spiniferites bentonii</i>	0.0980	-0.0625	-0.0310
<i>Spiniferites mirabilis</i> s.l.	0.7153	-0.2758	-0.2393
<i>Spiniferites mirabilis</i> atypical	0.6490	-0.2712	-0.0446
Granular <i>Spiniferites</i>	0.7208	0.0829	-0.0281
<i>Spiniferites</i> spp.	0.2828	-0.0206	-0.3027
Cyst of <i>Pentapharsodinium dalei</i>	-0.2727	-0.1582	-0.3619
<i>Tuberculodinium vancampoae</i>	-0.1599	-0.1810	0.0622
<i>Melitasphaerodinium choanophorum</i>	-0.3372	-0.4605	-0.5240
<i>Islandinium brevispinosum</i>	0.3253	-0.0867	0.1231
<i>Islandinium minutum</i>	-0.0046	0.3476	-0.0239
<i>Brigantedinium</i> spp.	-0.7062	0.2067	0.0693
Protoperidinoids	0.0040	-0.2983	-0.0534
<i>Lejeuneaecysta</i> spp.	0.0171	-0.0305	-0.1012
<i>Selenopemphix nephroides</i>	-0.4392	0.0672	0.1963
<i>Selenopemphix quanta</i>	0.1300	0.5523	-0.0475
<i>Stelladinium stellatum</i>	-0.0495	0.3903	-0.1011
<i>Votadinium spinosum</i>	0.3933	-0.0740	0.1123
<i>Polykrikos kofoidii</i>	0.1575	0.0814	0.0621
<i>Polykrikos schwartzii</i>	-0.0131	0.3743	-0.0879
<i>Echinidinium aculeatum</i>	-0.0279	0.4342	-0.2536
<i>Echinidinium dellicatulum</i>	-0.0135	0.5084	-0.1594
<i>Echinidinium transparentum</i>	-0.0910	0.2294	-0.1713
<i>Echinidinium granulatum</i>	0.0133	0.5711	-0.1820
<i>Echinidinium?</i> sp.Z	-0.0347	0.1294	-0.1328
<i>Echinidinium</i> spp.	-0.0644	0.4662	0.0072

Table 6. Scores of dinocyst taxa according to the three first axes of redundancy analysis.

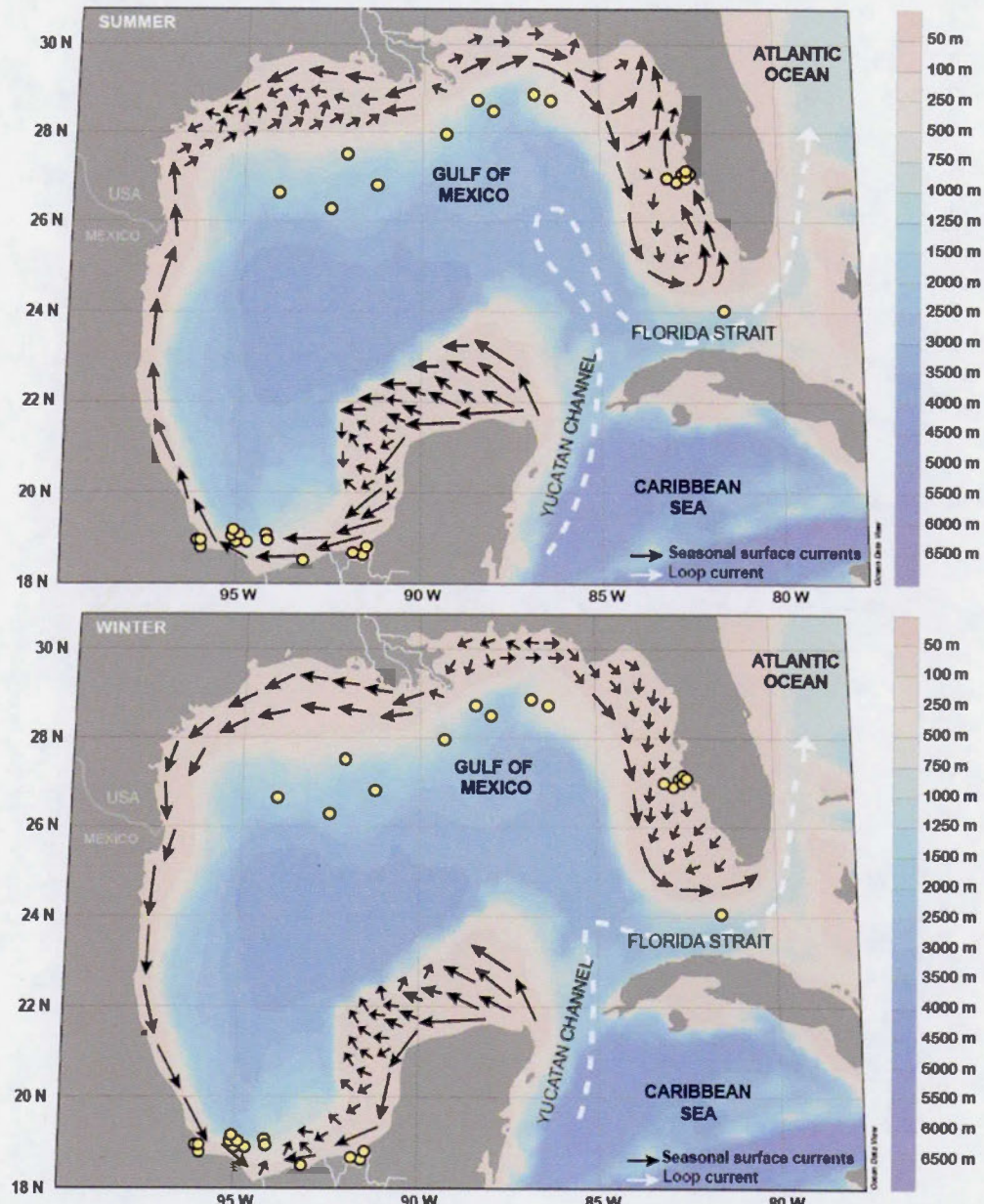


Figure 1. Simplified map of seasonal surface currents along the shelves of the Gulf of Mexico. Modified from Zavala-Hidalgo et al. (2003; western shelves) and Yang et al. (1999; Florida coast).

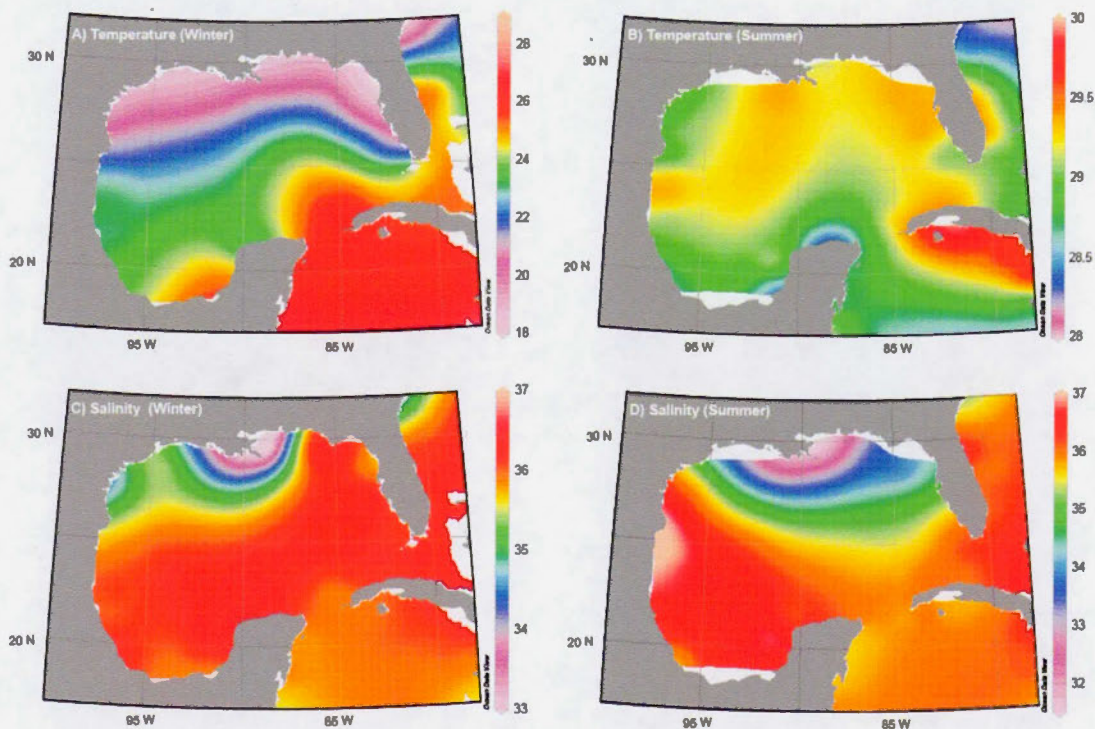


Figure 2. Distribution of winter (January-March) and summer (July-September) temperatures ($^{\circ}\text{C}$) and salinities (psu) in the study area (Ocean Data View (Schlitzer, 2012); Locarnini et al., 2010; Antonov et al., 2010; Garcia et al., 2010a,b).

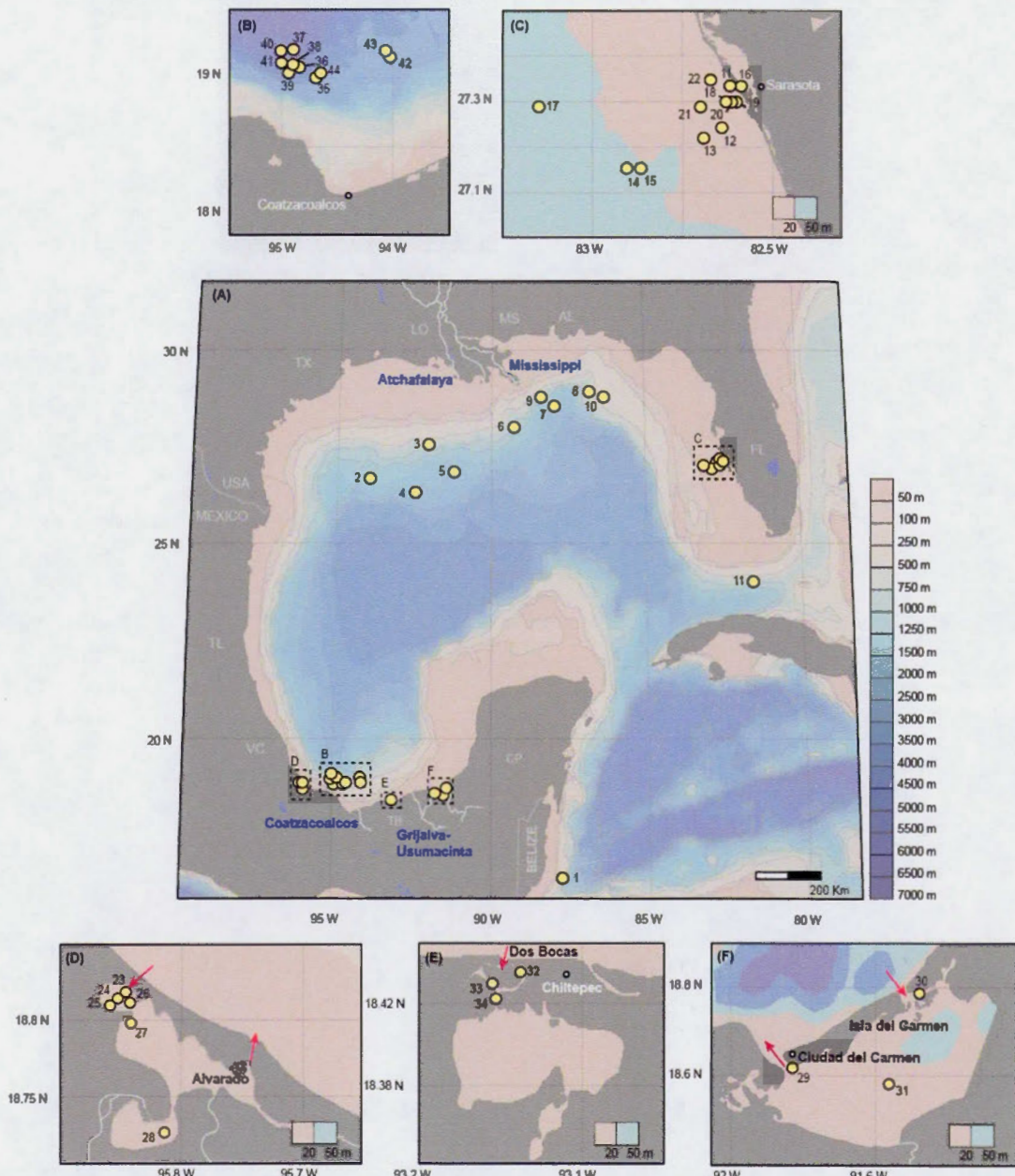


Figure 3. Map showing the position of the studied sites (yellow circles) and the principal river systems (A) and enlargements of the different study areas: B) Veracruz shelf, C) the Western coast of Florida, D) Laguna Alvarado, E) Laguna Mecoacán and F) Laguna de Terminos. Abbreviations: FL: Florida, AL: Alabama, MS: Mississippi, LO: Louisiana, TX: Texas, TL: Tamaulipas, VC: Veracruz, TB: Tabasco, CP: Campeche.

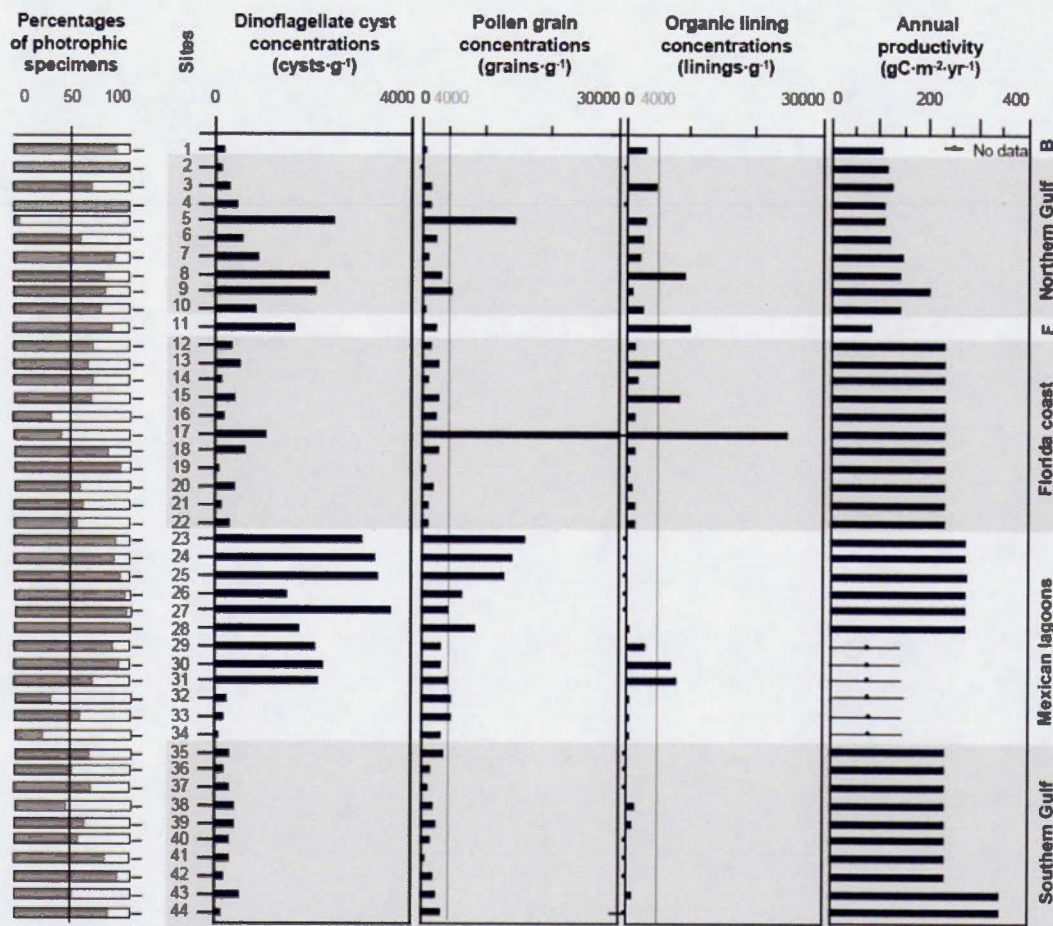


Figure 4. Percentages of phototrophic taxa, dinoflagellate cyst concentrations ($\text{cysts}\cdot\text{g}^{-1}$), pollen grain concentrations ($\text{grains}\cdot\text{g}^{-1}$), foraminifer organic lining concentrations ($\text{linings}\cdot\text{g}^{-1}$) and annual productivity estimated ($\text{gC}\cdot\text{m}^{-2}\cdot\text{yr}^{-1}$). Abbreviations: B: Belize Coast, F: Florida Strait.

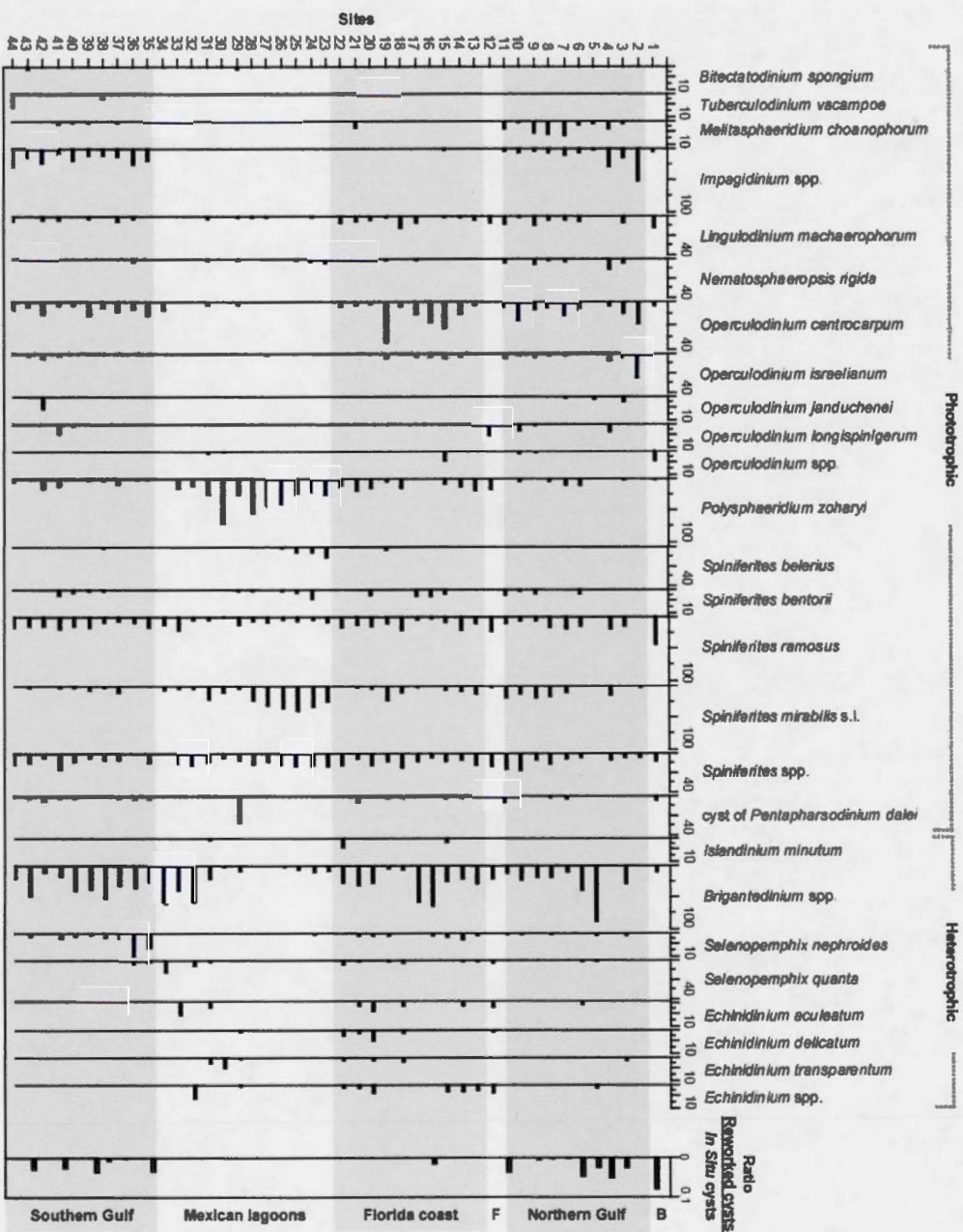


Figure 5. Percentages of the main dinoflagellate cyst taxa and the ratio of reworked cysts over modern cysts.

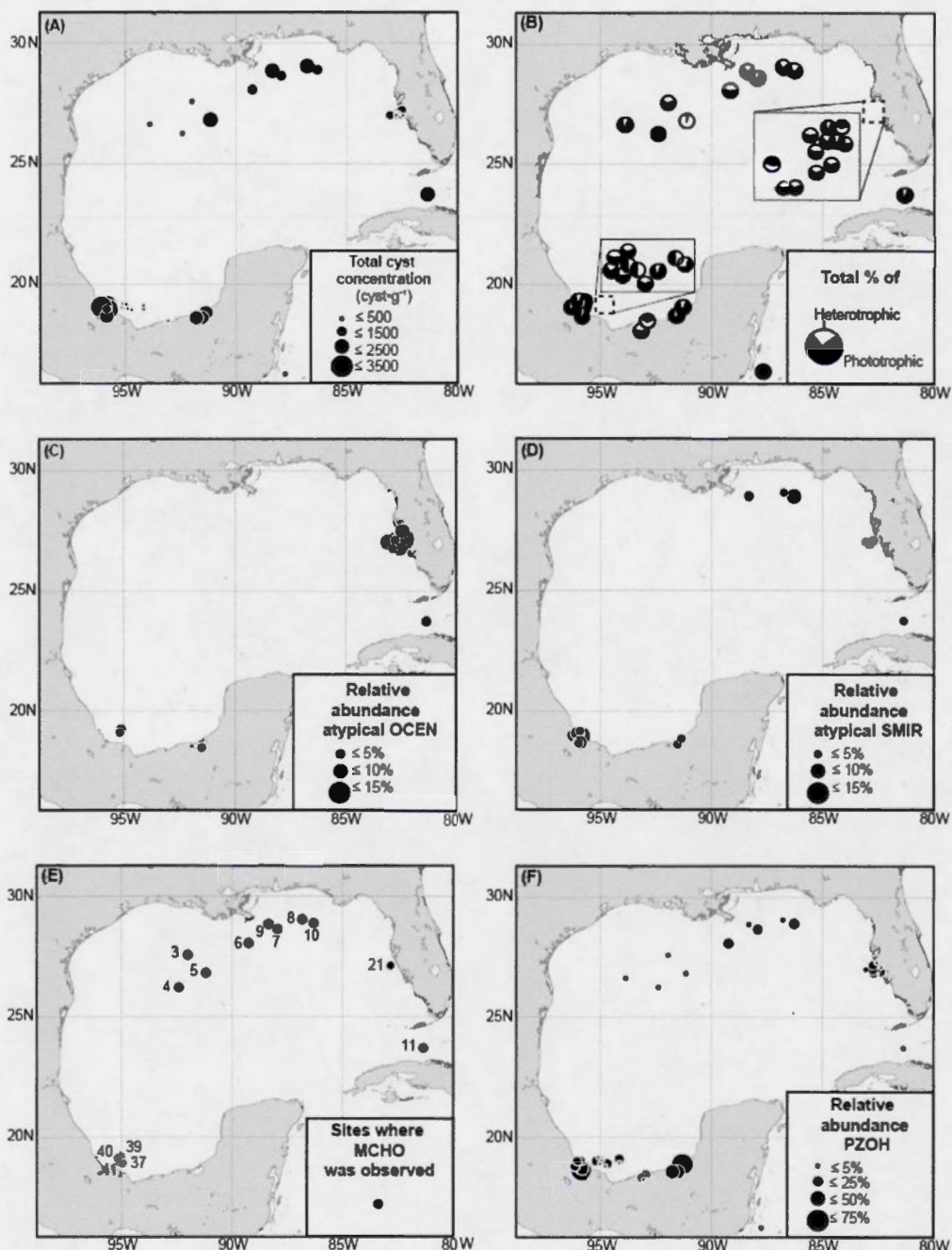


Figure 6. Distribution of A) total concentrations of dinoflagellate cysts (cysts·g⁻¹), B) relative abundances (%) of heterotrophic and phototrophic taxa, C) relative abundances (%) of atypical *Operculodinium centrocarpum*, D) relative abundances (%) of atypical *Spiniferites mirabilis*, E) sites where *Melitasphaeridium choanophorum* was observed, and F) relative abundances (%) of *Polysphaeridium zoharyi*.

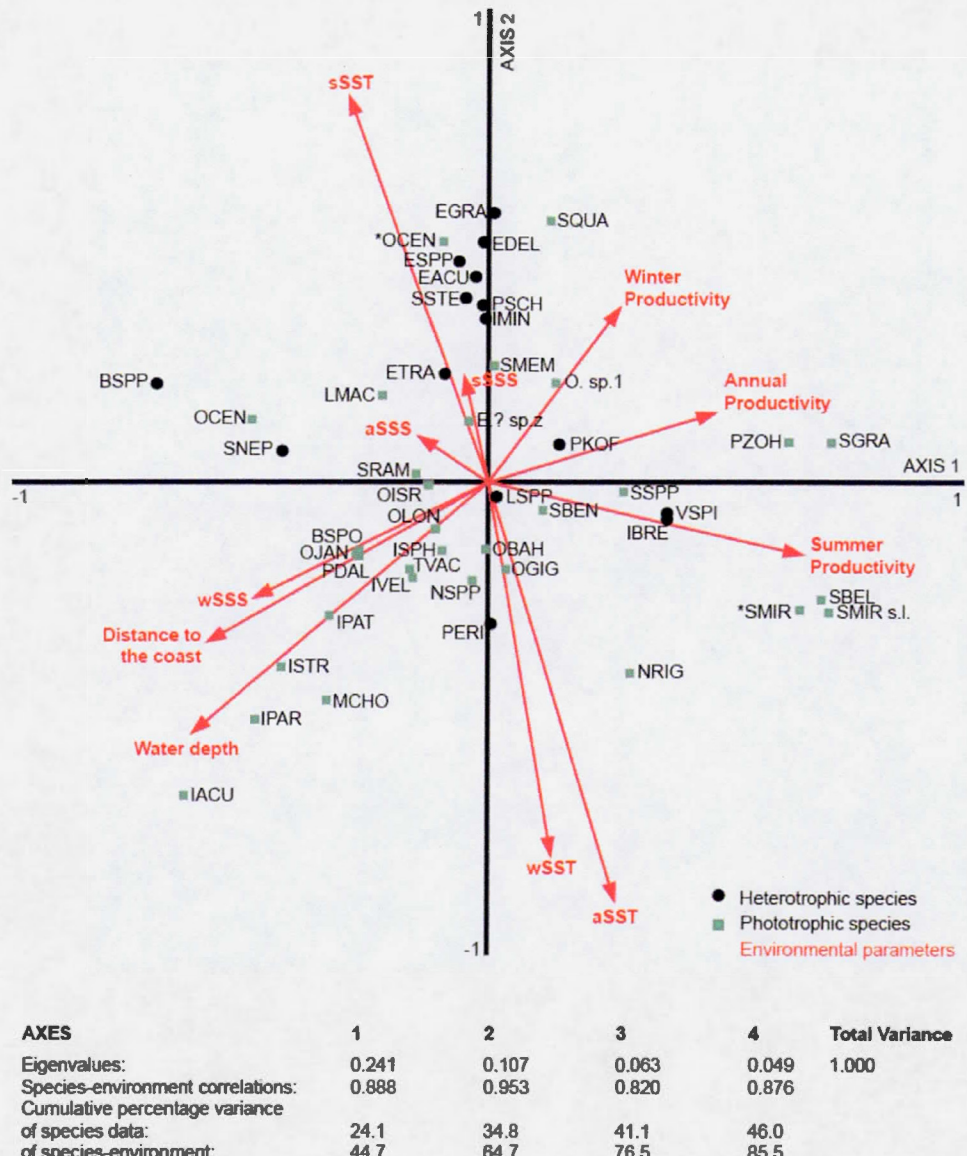


Figure 7. Results of redundancy analysis: ordination diagram of species and environmental parameters according to axes 1 (44.7%) and 2 (20%). The abbreviations of taxa names are from tables 4 and 5.

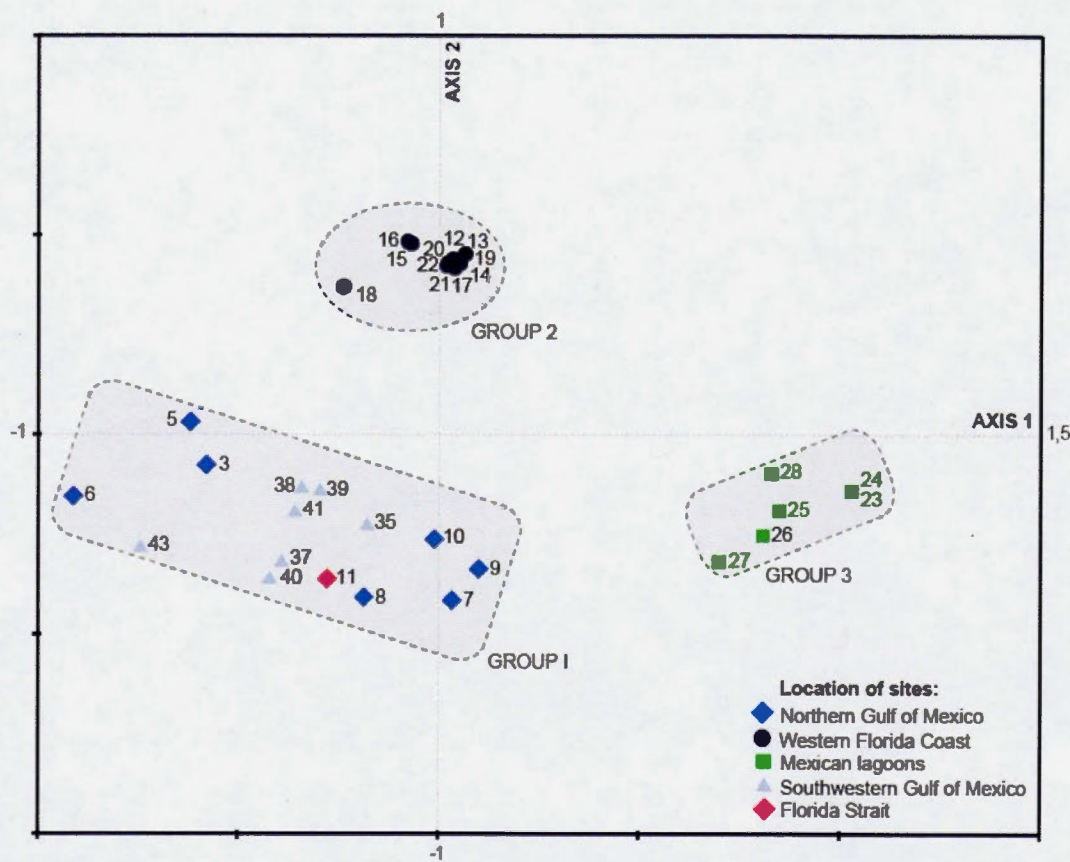


Figure 8. Results of redundancy analysis: ordination diagram of sample scores according to axes 1 and 2, which represent respectively 44.7% and 20% of the variance.

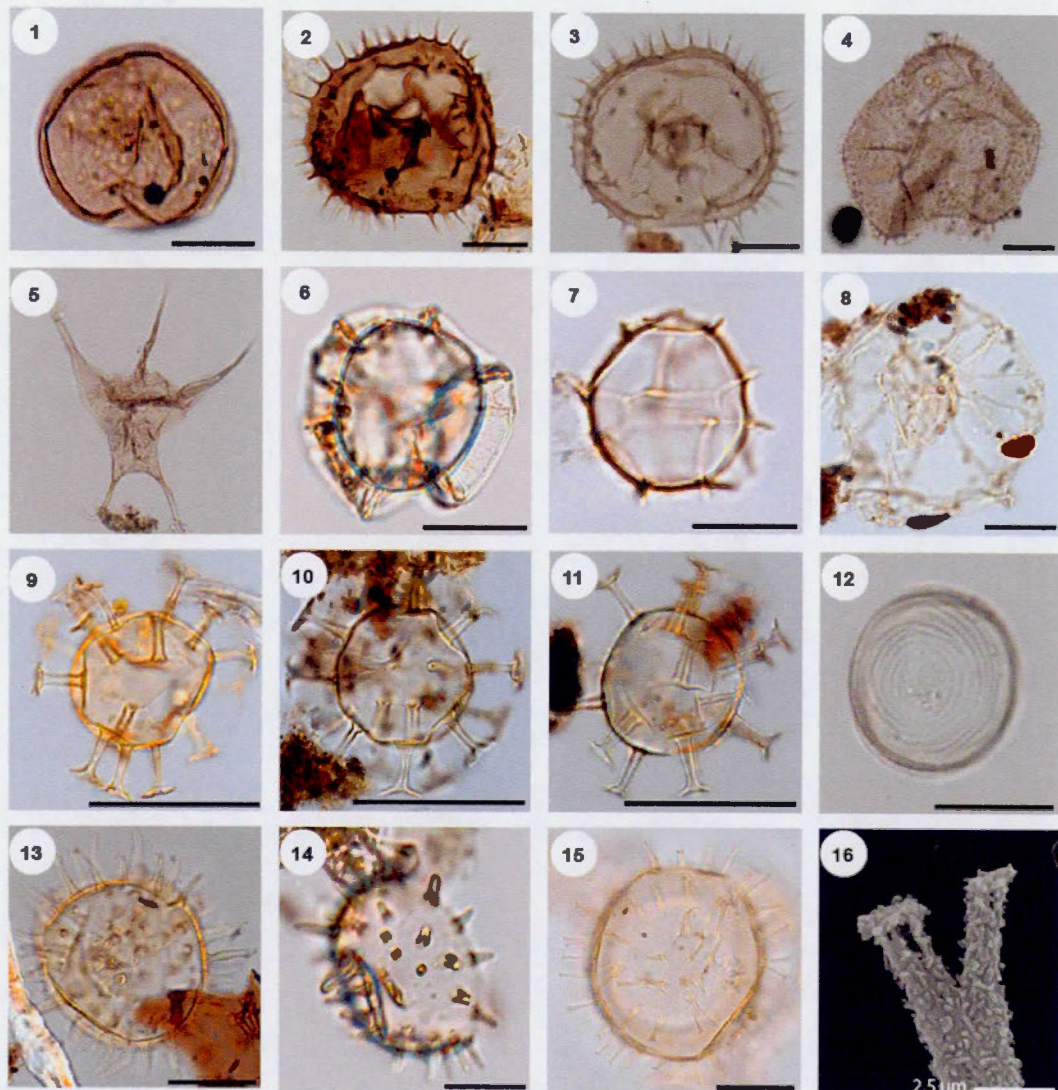


Plate 1. Bright field light micrographs of selected dinocyst taxa: 1. *Selenopemphix nephroides*; 2-3. *Selenopemphix quanta*; 4. *Votadinium spinosum*; 5. *Stelladinium stellatum*; 6. *Impagidinium striatum*; 7. *Impagidinium aculeatum*; 8. *Impagidinium velorum* 9-11. *Melitasphaeridium choanophorum*; 12. *Concentricystes* ind.; 13-14. *Lingulodinium machaerophorum*; 15. *Polysphaeridium zoharyi*; 16. Scanning electron microscope (SEM) image showing the bifurcate process termination of the cyst *Polysphaeridium zoharyi*. Scales bars: 20 μ m.

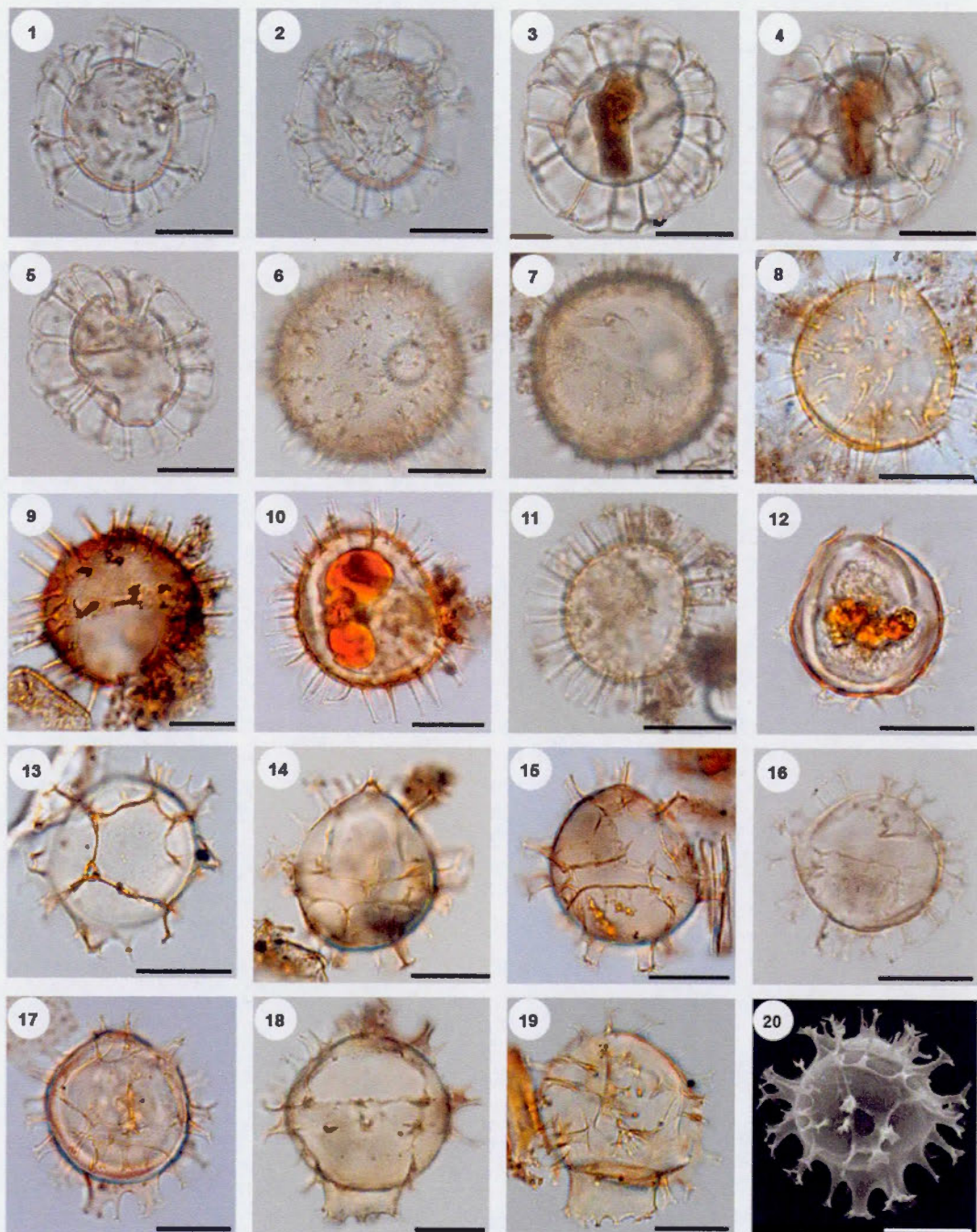


Plate 2. Bright field light micrographs of selected dinocyst taxa : 1-5. *Nematospaeropsis rigida*; 6-7. *Operculodinium israelianum*; 8. *Operculodinium longispinigerum*; 9-10. Atypical *Operculodinium centrocarpum*; 11. *Operculodinium centrocarpum*; 12-13. *Spiniferites belerius*; 14-15. *Spiniferites bentorii*; 16-19. Different morphotypes of *Spiniferites mirabilis* ; 20. Scanning electron microscope (SEM) image of *Spiniferites mirabilis*. Scales bars: 20 μ m.

Supplementary material. Dinocyst raw counts and the error on the counts using the method of Stockmarr (1971).

Benthos mean	Benthos SD	Benthos n	Wetland Site	Wetland SD	Wetland n	Estuarine Site	Estuarine SD	Estuarine n
11	19	26	44	56	24	23	37	35
12	20	13	24	40	27	15	31	32
13	21	15	12	39	16	11	20	19
14	21	10	12	37	13	11	19	20
15	22	10	13	37	14	10	19	20
16	23	10	13	36	13	10	18	18
17	23	11	12	36	12	10	18	18
18	24	11	11	36	12	10	18	18
19	25	11	11	35	11	10	18	18
20	26	12	10	34	11	9	18	17
21	26	12	10	33	11	9	18	17
22	26	12	12	32	12	11	17	16
23	26	12	12	32	12	10	17	16
24	26	12	12	32	12	10	17	16
25	26	12	12	32	12	10	17	16
26	27	12	13	31	13	10	16	15
27	27	13	13	31	13	10	16	15
28	28	13	13	31	13	10	16	15
29	28	13	13	31	13	10	16	15
30	28	13	13	31	13	10	16	15
31	28	13	13	31	13	10	16	15
32	28	13	13	31	13	10	16	15
33	29	13	12	30	13	10	16	15
34	29	13	12	30	13	10	16	15
35	29	13	12	30	13	10	16	15
36	29	13	12	30	13	10	16	15
37	29	13	12	30	13	10	16	15
38	29	13	12	30	13	10	16	15
39	29	13	12	30	13	10	16	15
40	30	13	12	30	13	10	16	15
41	30	12	12	29	12	10	16	15
42	30	12	12	29	12	10	16	15
43	30	12	12	29	12	10	16	15
44	30	12	12	29	12	10	16	15

CHAPITRE II

LONG-TERM HYDROLOGICAL CHANGES IN THE NORTHEASTERN GULF OF MEXICO (ODP-625B) DURING THE HOLOCENE AND LATE PLEISTOCENE INFERRED FROM ORGANIC-WALLED DINOFLAGELLATE CYSTS

Audrey Limoges¹, Nicolas Van Nieuwenhove¹, Anne de Vernal¹

¹ Geotop, Université du Québec à Montréal, C.P. 8888, Montréal, QC H3C 3P8, Canada

Article publié en 2014 dans la revue *Palaeogeography, Palaeoclimatology, Palaeoecology*, Vol. 414, 178-191.

<http://dx.doi.org/10.1016/j.palaeo.2014.08.019>

Résumé

Des analyses palynologiques ont été combinées à des analyses géochimiques sur des foraminifères ($\delta^{18}\text{O}$ et ratio Mg/Ca) afin de documenter la réponse des assemblages de kystes de dinoflagellés (dinokystes) aux changements climatiques de l'Holocène et de la fin du Pléistocène, dans le nord-est du golfe du Mexique. Au cours du stade isotopique marin (SIM) 6 et durant les périodes plus froides du SIM 5, *Impagidinium* spp. et *Operculodinium centrocarpum* dominent les assemblages de dinokystes. Par ailleurs, au cours du dernier interglaciaire et de l'Holocène, les assemblages sont principalement composés de *Spiniferites* spp. et sont caractérisés par des abondances relatives très élevées en *Spiniferites mirabilis-hyperacanthus*, *Operculodinium israelianum* et/ou *Polysphaeridium zoharyi*. Les températures des eaux de surface estimées à partir du rapport Mg/Ca de la calcite des foraminifères indiquent une différence de ~1-2°C entre ces deux interglaciaires. Alors que le dernier interglaciaire montre des fortes abondances de *S. mirabilis*, l'Holocène est caractérisé par des pourcentages élevés de *P. zoharyi*. Nos enregistrements suggèrent des hétérogénéités dans les conditions hydrogéographiques entre ces deux périodes (e.g. circulation de surface, configuration bathymétrique) et illustrent l'importance des paramètres environnementaux autres que la température et la salinité pour la distribution des dinokystes dans la région d'étude.

Mots-clés: Golfe du Mexique, Dernier interglaciaire, Holocène, Kystes de dinoflagellés, Reconstructions paléocéanographiques

Abstract

Palynological analyses are used in conjunction with oxygen isotopes and Mg/Ca ratios in foraminifers in order to document the response of dinoflagellate cysts (dinocysts) assemblages to changing climate conditions in the northeastern Gulf of Mexico over the Holocene and late Pleistocene. During MIS 6, but also during the cooler phases of MIS 5, *Impagidinium* species and *Operculodinium centrocarpum* were dominating the assemblages. By contrast, during the last interglacial (LIG) and the Holocene, assemblages were mainly composed of *Spiniferites* taxa and characterized by high relative abundance of *Spiniferites mirabilis-hyperacanthus*, *Operculodinium israelianum* and/or *Polysphaeridium zoharyi*. These two periods exhibit ~1-2°C difference in temperature as inferred from Mg/Ca ratios and show significantly distinct assemblages, with higher percentages of *S. mirabilis* during the LIG and higher percentages of *P. zoharyi* during the Holocene. This likely denotes important differences in the hydrogeographical conditions (e.g. surface circulation, bathymetric configuration) between the present and last interglacial. The importance of environmental parameters other than temperature and salinity for dinocyst assemblage dynamics is furthermore illustrated.

Keywords: Gulf of Mexico, Last interglacial, Holocene, Dinoflagellate cysts, Paleoceanographic reconstructions

1. Introduction

In the Gulf of Mexico, the interplay between the Mississippi River discharge, open ocean water masses and atmospheric circulation creates a complex dynamic system responsible for hydrological fluctuations on both annual and long-term timescales. To better understand the impact of these parameters on the regional climate, a number of marine sediment studies has focused on the hydrologic evolution of the basin during the Holocene (Poore et al., 2003; Lo Dico et al., 2006; Richey et al., 2007; Meckler et al., 2008; Montero-Serrano, 2010) and the last interglacial (LIG) interval (Joyce et al., 1990, 1993; Tripsanas et al., 2007; Nürnberg et al., 2008; Ziegler et al., 2008; Kujau et al., 2010; Montero-Serrano, 2011; Simms et al., 2013). The LIG, referred to as Marine Isotope Stage (MIS) 5e in marine sediments and spanning the interval between ~130 and 115 kyrs (Liebecki and Raymo, 2005), has experienced conditions warmer than those of the current interglacial in response to higher levels of insolation during boreal summer (e.g., CAPE, 2006; Otto-Bliesner et al., 2006; Hearty et al., 2007). Regional data from the Gulf of Mexico indicate that overall sea-surface temperatures were generally warmer by 1-2°C (Nürnberg et al., 2008; Ziegler et al., 2008; Montero-Serrano et al., 2011) and relative sea-level was approximately 4-6, possibly 9 meters above the present limit (Simms et al., 2013, and references therein). Numerous paleoceanographic investigations therefore stem on the recognition that this interval may represent a possible analogue for future climate and could help infer potential changes in hydrographic conditions in the context of global warming.

Dinoflagellate cysts (dinocysts), which are the organic-walled remains of unicellular algae routinely recovered in palynological preparations, have proven to be a good proxy for paleoenvironmental changes in the upper water column (e.g. Rochon et al., 1999; de Vernal and Marret, 2007). Their assemblages are not only controlled by temperature, but also depend on other environmental parameters (e.g., productivity,

salinity, sea-ice cover, seasonality, sea-level etc) as shown by multivariate analyses of distribution patterns in middle to high latitudes of the Northern Hemisphere (e.g., de Vernal et al., 1997; Devillers and de Vernal, 2000; Pospelova et al., 2008; Radi and de Vernal, 2008; Price and Pospelova, 2011; Bonnet et al., 2012) and in the Gulf of Mexico (Limoges et al., 2013). Therefore, the analysis of dinocyst assemblages has the potential to assess past hydrographic conditions in a fairly nuanced way. While dinocysts have been widely used in paleoceanographic reconstructions for the high latitudes (Mudie et al., 2001 and references therein; de Vernal et al., 2005), they remain a less-exploited tool for such reconstructions in the tropical areas, which is in part due to the lower availability of modern reference datapoints for these regions. For the Gulf of Mexico, the relationship between dinocyst assemblages and modern sea-surface parameters was documented by Limoges et al. (2013) allowing for a more comprehensive interpretation of their regional distribution.

Here, we combine the analyses of stable isotopes ($\delta^{18}\text{O}$ and $\delta^{13}\text{C}$) and Mg/Ca ratios in planktic foraminiferal carbonate with palynological analyses from sediments collected at the Ocean Drilling Program (ODP) site 625B in the Gulf of Mexico (Fig. 1A), in order to document long-term changes in hydrological conditions over the MIS 1 (0 - 11 kyr), MIS 5 (b-e) (90 - 130 kyr) as well as the glacial-interglacial transition MIS 6/5 (130 - 160 kyr). Located in the northeastern part of the Gulf of Mexico, at the outer reaches of the seasonal influence of the Loop Current and near to the Mississippi River Mouth, site ODP-625B is ideally positioned to record changes in paleoproductivity and sea-surface conditions related to long-term hydroclimatic changes. Our study also evaluates the potential of dinocysts as paleoceanographic proxy in tropical areas.

2. Material and Methods

2.1 Regional setting

The Gulf of Mexico is an oceanic basin located on the northwestern edge of the Atlantic Ocean. Its dominant surface current is the Loop Current: warm and salty waters originating from the Caribbean Sea enter into the Gulf via the Yucatán channel, loop northwest and exit through the Florida Strait as the Florida Current, eventually feeding the Gulf Stream (Fig. 1B) (Elliot, 1982; Blumberg and Mellor, 1985; Hofmann and Worley, 1986; Oey et al., 2005; Jochens and DiMarco, 2008; Auladell et al., 2010). The latitudinal extension of the Caribbean water inflow into the basin is seasonally modulated by the position of the Intertropical Convergence Zone (ITCZ) (Fig. 1B). A northward migration of the ITCZ during boreal summer causes the Loop Current to propagate farther north, influencing the hydrological properties of the entire basin (temperature, salinity). Consequently, in the modern climate system, the Atlantic Warm Pool reaches into the Gulf of Mexico during late summer, with temperatures above 28.5°C in the entire basin during this period (Fig. 1C). Conversely, during boreal fall/winter, the tropical waters exit directly through the Florida Strait (Fig. 1D). Current mean annual sea-surface temperature is ~25.85°C with a large seasonal amplitude (~8.5°C), whereas salinity varies from about 34.38 to 35.97 (WOA, 2001). In addition to the Loop Current, the hydrology (salinity, stratification) of the northern Gulf is largely impacted by the freshwater input from the Mississippi River system, which has, at present, an annual mean discharge of over 13 000 m³s⁻¹ (Morey et al., 2003). Currently draining the continental U.S. from the Rockies to the Appalachians, the drainage area of the Mississippi River System intermittently included the meltwater inputs from the Laurentide Ice Sheet throughout the last glacial stages and Terminations (e.g., Teller, 1990; Aharon, 2006; Montero-Serrano et al., 2009; Sionneau et al., 2010, 2013), with potential consequences for the North Atlantic thermohaline circulation (e.g., Broecker et al., 1990; Bond, 1995;

Manabe and Stouffer, 1995, 1997; Fanning and Weaver, 1997; Aharon, 2003; but see also Nürnberg et al., 2008). During interglacial phases, most of the Mississippi outflow is diverted westward (Nürnberg et al., 2008).

2.2 Core and stratigraphy

Core site ODP-625B was drilled in the northeastern Gulf of Mexico (28.83°N , 87.16°W) during the Ocean Drilling Program (ODP) Leg 100, in 1985 (Fig. 1A). The site is located at 889 m water depth on the western Florida continental slope, near the De Soto basin, and ~200 km from the current Mississippi River delta, whose position is thought to have remained the same since either MIS 5 or the beginning of the last glaciation (Coleman et al., 1983; Bouma and Coleman, 1985; Bouma et al., 1985). The complete sequence of site 625B is 231 m long and provides a nearly complete stratigraphic record of the Quaternary and Pliocene, from which we studied the sections corresponding to the MIS 1 and part of MIS 5 and MIS 6, with an average sampling interval of 10 cm. The sampling resolution was increased to 5 cm for palynological analyses in the section corresponding to the LIG, in order to parallel the number of samples representing the Holocene and LIG intervals.

In the section corresponding to MIS 1, three accelerator mass spectrometer radiocarbon dates were obtained from monospecific *Globigerinoides ruber* (white) populations at the NOSAMS-Woods Hole Oceanographic Institution (Table 1). According to these control points, the upper 98 cm of the studied sequence cover the last 10 600 ^{14}C years, which corresponds to the last 11 909 cal. years according to Calib 7.0 with a 400 years reservoir correction (Reimer et al., 2013). This constant reservoir age was used to enable an easy comparison with data from previous studies in the Gulf of Mexico (Nürnberg et al., 2008; Flower et al., 2004). The ages indicate a mean sediment accumulation rate of approximately 8 cm/kyr during the Holocene, a value that appears to be fairly stable based on the radiocarbon dates and the core

lithology. For the interval covering MIS 5 and 6, we used the age model developed by Dowsett (1999), which in turn is based on a low-resolution planktonic stable isotope record (developed by Joyce et al., 1990) and cyclic changes in the relative spectral reflectance of the sediments. The age model validity is illustrated by the good correlation between the LR04 stack (Lisiecki and Raymo, 2005) and our own $\delta^{18}\text{O}$ profiles recovered from the benthic foraminifera *Uvigerina peregrina* and the planktic *Globigerinoides ruber* (pink) and *Globigerinoides ruber* (white) (Fig. 2). Accordingly, the Pleistocene section we analyzed encompasses approximately 157 to 93 kyrs, thus spanning from late MIS 6 to MIS 5b.

2.3 Isotopic analyses ($\delta^{18}\text{O}$ and $\delta^{13}\text{C}$)

Isotopic analyses were conducted on 15-30 specimens (120 µg) of the shallow endobenthic species *U. peregrina* (< 1 cm sediment depth) and the surface-dwelling foraminifera *G. ruber* (white) and *G. ruber* (pink) picked from the 150 to 250 µm size fraction. In order to avoid possible organic matter contamination, benthic tests were burned under vacuum (residual pressure ~8Pa) in an oven at 200°C for one hour. The analyses were carried out using a Micromass Isoprime dual inlet isotope ratio mass spectrometer coupled to a Multicarb system. The $\delta^{13}\text{C}$ and $\delta^{18}\text{O}$ raw data were normalized to VSMOW-SLAP ($\delta^{18}\text{O}$) and NBS19-LSVEC ($\delta^{13}\text{C}$) using an inhouse reference calcium carbonate ($\delta^{18}\text{O}$: -1,40; $\delta^{13}\text{C}$: +2,25). Values are reported in δ -notation in ‰ vs. Vienna-Pee Dee belemnite (VPDB). Analytical uncertainty is ± 0.05 ‰ (1 σ) for both measurements.

2.4 Mg/Ca ratios

Individual shells of the planktic *G. ruber* (white) were picked within a narrow range of size (specimens from 220 to 300 µm; foraminifers were measured), in order to

minimize variations related to changes in calcification rate and/or depth habitat during their evolution from small to large individuals (Elderfield et al., 2002). Since *G. ruber* has a nearly uniform annual occurrence, it is a valuable species for reconstructing past temperature in tropical environments (Tedesco and Thunell, 2003). Prior to analysis, specimens were gently cleaned without crushing the tests: shells were repeatedly rinsed and sonicated for ~3 seconds with MilliQ water and methanol in order to release the silicate phases (clays) attached to the surface (Barker et al., 2003). Mg/Ca analyses were conducted on selected samples from the Holocene, MIS 5e and MIS 6 using laser ablation inductively coupled plasma mass spectrometry (LA-ICP-MS: instrument used was a Photon Machine G2 with 193nm wavelength laser, ran at low energy output (0.6 mJ) with elemental acquisition on a Nu Attom HR-ICP-MS). Laser ablation measurements were performed using spot size of 30 μ m diameter at a pulse repetition rate of 2Hz. Calibration was made against the international glass standard (NIST610). In order to avoid bias due to residual superficial and internal clay contamination and/or diagenetic coatings, the data integration interval was adjusted to exclude zones of manganese, iron and/or aluminum enrichments (see Fhlaithearta et al., 2010). Off-line data reduction was carried on as time resolved analysis using the Iolite software (Paton et al., 2011). Four to ten foraminifer specimens were measured per sediment sample and six ablation spots were made on each foraminifer shell, two per chamber. This allowed the determination of single foraminifer test heterogeneity.

A bias linked to natural differences in composition between chambers of a single individual (Table 2) was eliminated by calculating an average value for each chamber, and these values were then used to calculate an average Mg/Ca value for each foraminifer. In this way, equal weight was given to each chamber in the final foraminifer's Mg/Ca value. Temperature estimates from Mg/Ca ratios were calculated using the calibration curve based on a sediment trap from the Sargasso Sea: $T^{\circ}\text{C} = \text{Ln}(\text{Mg/Ca}/0.38)/0.09$ (Anand et al., 2003). For almost all planktic

foraminifers, culture and core top calibrations indicate a temperature dependence of Mg uptake into calcite of the order of $9.0 \pm 0.3\%$ per $^{\circ}\text{C}$ (Anand et al., 2003). Absolute temperatures are difficult to obtain by such in situ technique, as our external calibration of the elemental Mg/Ca ratio relies on the analysis of a mineralogically different material (NIST610 is a polished synthetic glass), which will behave differently from calcitic unpolished foraminiferal material during laser ablation. We believe our double averaging technique realistically yields the uncertainty budget for one single foraminifer's Mg/Ca, and that the differences between foraminifer (levels) are robust. Using analytical errors obtained from Iolite data reduction for individual laser spots, the reported final precision for Mg/Ca is 0.02, which corresponds to $\pm 0.16^{\circ}\text{C}$ or less.

2.5 Organic-walled dinoflagellate cysts

Sample treatment was made according to standard laboratory procedures (e.g. de Vernal et al., 1999). One calibrated *Lycopodium* tablet ($\sim 18\ 584$ spores) was added to every sample before sieving to allow estimation of the absolute dinocyst abundances (Stockmarr, 1971). A volume of 5 cm³ of sediment was wet-sieved to eliminate fine silt and clay (mesh size of 10 μm) and coarse sand (mesh size of 106 μm). The fraction $>10\ \mu\text{m}$ was treated with hydrochloric acid (HCl 10%) and hydrofluoric acid (HF 48%) to dissolve respectively carbonate and siliceous material. The remaining residue was re-sieved after chemical treatment in order to remove the fine fraction from the residue and subsequently mounted in glycerin jelly for microscopic observation. Cyst identification was made at magnifications ranging from 400 to 1000X and follows the most recent nomenclature (Fensome et al., 2008). Note that *Operculodinium centrocarpum* sensu Wall and Dale (1966) will be referred to simply as *Operculodinium centrocarpum* from here on. For most samples, 2 to 4 slides were analyzed. In order to insure statistical robustness, the palynological results of all

samples with less than 100 dinocyst specimens counted were not used for percentage calculation and were omitted from figure 2 (see Appendix A for exhaustive data).

3. Results

3.1 Isotopic analyses ($\delta^{18}\text{O}$ and $\delta^{13}\text{C}$)

On the whole, the oxygen isotopes series clearly reflect the Pleistocene and Holocene climate variations (Fig. 2; Table 3). The *G. ruber* (white) and *G. ruber* (pink) $\delta^{18}\text{O}$ profiles follow the same pattern during the different studied intervals, but the white variety show slightly lighter values than its pink counterpart. This divergence can be explained by the fact that *G. ruber* (pink) calcifies near-surface and is representative of summer temperatures, whereas *G. ruber* (white) habitat may extent deeper and records an average annual to summer temperature signal (Anand et al., 2003; Richey et al., 2012). In the section corresponding to the Pleistocene, both benthic and planktic $\delta^{18}\text{O}$ profiles display a pronounced excursion from around 128 to 116 kyr, the amplitude of the signal obviously being higher for the planktic species. When comparing our data to the standard LR04 reference stack (Lisiecki and Raymo, 2005), this interval is easily identified as the interglacial MIS 5e. These light values contrast with those from the preceding, isotopically heavy MIS 6, which is interrupted however, by a short excursion of isotopically lighter values in both planktic profiles, suggesting a brief hydrographic event centered around 144 kyr. The MIS 5 b-d interval is characterized by small-amplitude fluctuations in the $\delta^{18}\text{O}$ values (-1.36 to -1.95‰ for *G. ruber* (pink), -0.77 to -1.62 ‰ for *G. ruber* (white) and 3.59 to 2.90 ‰ for *Uvigerina peregrina*) in contrast to the deep-sea records, which reflect the successive warmer and colder substages somewhat more clearly. During the Holocene, all profiles yield minor variations: *G. ruber* (white) and *G. ruber* (pink)

values respectively range from -0.86 to -1.18 ‰ and -1.29 to -1.79 ‰, while they vary from +3.28 to +2.53 ‰ for the benthic *U. peregrina*.

From MIS 6 to MIS 5, a general trend toward increasing $\delta^{13}\text{C}$ values characterizes the profiles (Fig. 2). Such general trend is also observed in the benthic $\delta^{13}\text{C}$ dataset of the Ceara Rise, offshore Brazil (Curry and Otto, 1997) (Fig. 2). However, $\delta^{13}\text{C}$ data from the Gulf of Mexico yield slightly lighter values during the LIG and Holocene, which may be interpreted as increased productivity during warmer periods. *G. ruber* (white) and *G. ruber* (pink) values range from -0.14 to 0.66‰ and 0.21 to 1.37‰ respectively, whereas *U. peregrina* values average between -1.5 and -0.44 ‰. During the Holocene, *G. ruber* (white) and *U. peregrina* display similar $\delta^{13}\text{C}$ profiles with values rather constant in the early part, a fairly abrupt increase at mid-Holocene and a gradual decrease towards the core top. Overall values range from 0.54 to 0.89‰ (*G. ruber* (white)), 0.49 to 1.18‰ (*G. ruber* (pink)) and -0.74 to -0.21‰ (*U. peregrina*).

3.2 Mg/Ca ratios

Significant differences were measured in the Mg/Ca ratios within one sample and between the different foraminiferal chambers (Table 2). Such differences between chambers have been reported from many studies (see Rosenthal, 2007, and references therein). They may be attributed to a number of different factors, amongst which vertical migration in the water column during calcification. They can result from temporal discrepancies (from a few weeks to a few months) recorded by each individual foraminiferal shell. Moreover, as mentioned by Rosenthal (2007), metabolic effects in symbiotic foraminifers such as *G. ruber* cannot be ruled out.

During the Pleistocene interval, Mg/Ca records from the monospecific *G. ruber* (white) are generally in phase with the corresponding $\delta^{18}\text{O}$ profile (Fig. 2). Raw Mg/Ca data range from 2.61 to 4.02 mmol/mol during the MIS 6 and are followed by

a rapid transition to higher values (3.69 to 5.60 mmol/mol) during the MIS 5e, suggesting a sea-surface warming of approximately 6°C during the glacial to interglacial transition. These records also show that SST culminated in the very beginning of MIS 5e. Besides, the peak in Mg/Ca ratios around 146 kyr appears to be somewhat concomitant with the excursion observed within the $\delta^{18}\text{O}$ values, reinforcing the hypothesis of a brief (sub)surface warming event shortly before the onset of the penultimate deglaciation. The Holocene interval is characterized by a continual warming in its early phase and a subsequent cooling towards the top of the section. These results agree with previous work which linked the change in the average position of the ITCZ during the Holocene to increased summer insolation in the early phase of the interval and decreased summer insolation after ca. 6000 ^{14}C yrs B.P. (Hodell et al., 1991; Haug et al., 2001; Poore et al., 2005; Montero-Serrano et al., 2010, 2011). Conversion of the Mg/Ca ratios to temperature yields a mean SST of ~26°C during the Holocene and ~28°C during the last Interglacial. These values are therefore consistent with data from Ziegler et al. (2008) and previous Mg/Ca SST estimates for the Atlantic tropical regions, suggesting that the LIG was approximately 2°C warmer than the Holocene (Schmidt et al., 2004; Nürnberg et al., 2008; Montero-Serrano et al., 2011; Bahr et al., 2013).

3.3. Palynology and organic-walled dinoflagellate cysts

Sediments from the studied sections are characterized by diverse palynological assemblages with abundant terrestrial palynomorphs (pollen grains of gymnosperms and angiosperms, spores of seedless plants), organic linings of foraminifers, and dinocysts (Fig. 3; Plates 1-2;). Although they represent only a small proportion of the total palynomorphs, the dinocyst assemblages are characterized by high species diversity. Gonyaulacoid taxa, which usually correspond to phototrophic productivity, dominate the assemblages (60-100% of total taxa). A total of 47 species was

recognized (Appendix A) but only seven taxa alternatively dominate the assemblages and account together for more than 70% of total population: *Brigantedinium* spp. (1-40%), *Impagidinium aculeatum* (3-34%), *Polysphaeridium zoharyi* (1-32%), *Spiniferites mirabilis-hyperacanthus* (1-32%), *Operculodinium centrocarpum* (1-28%), *Spiniferites ramosus* (3-26%) and *Spiniferites* spp. (0-25%) (*S. membranaceus*, *S. belerius*, *S. bentorii*, *S. bulloideus*, granular *Spiniferites*, unidentifiable and unknown *Spiniferites*). Accompanying taxa (0-12%) include *Impagidinium* spp. (*I. patulum*, *I. plicatum*, *I. paradoxum*, *I. striatum*), *Lingulodinium machaerophorum*, *Nematosphaeropsis lemniscata*, *Nematosphaeropsis rigida*, *Operculodinium* spp. (*O. giganteum*, *O. longispinigerum*, *O. israelianum*), cyst of *Pentapharsodinium dalei*, *Melitasphaeridium choanophorum*, *Tuberculodinium vancampoe*, *Selenopemphix nephroides* and Protoperidinoids. The present study thus confirms the recent occurrence of *M. choanophorum*, which is a species previously believed to be extinct (cf. Limoges et al., 2013).

Total cyst concentrations range from 297 to 3808 cysts · g⁻¹ dry weight sediment. Fluctuations in these values are generally paired with changes in dinocyst associations and coincide with climate transitions. This is particularly well expressed by a major peak in cyst concentrations during the last interglacial (MIS 5e), compared to generally low cyst numbers throughout MIS 6 and the remainder of the MIS 5 interval (MIS 5b-d). The peak in total concentrations is associated with an abrupt rise in *S. mirabilis-hyperacanthus* and a decrease in *Brigantedinium* spp. In addition, *Spiniferites* spp. are by far dominating the assemblages during this time interval. Worth mentioning is also the presence of *O. giganteum*, which is nearly exclusively recorded during this period, and higher relative abundances of the high-salinity stenohaline species *O. israelianum*. Holocene assemblages are characterized by comparable species richness. However, they show high abundances of *P. zoharyi* in the early part of the section and an increase of *L. machaerophorum* towards the top of

the core. *O. centrocarpum* occurs in low number in the Holocene section. *Spiniferites* taxa are common during the Holocene interval, but *S. mirabilis-hyperacanthus* does not reach relative abundances as high as during MIS 5e.

The LIG assemblages contrast significantly with those of the MIS 6 and MIS 5 b-d. *Brigantedinium* spp. records generally high abundances during the latter two intervals, with *Impagidinium aculeatum* and *Operculodinium centrocarpum* furthermore being major constituents of the assemblages. Other cysts belonging to *Impagidinium* such as *I. patulum* and *I. paradoxum* are also more frequently observed during MIS 6. Moreover, *O. centrocarpum* shows a marked increase in percentages towards the top of MIS 5, whereas *S. mirabilis-hyperacanthus* records show decreasing abundance.

4. Discussion

4.1 Long-term changes in dinocyst assemblages

The maximum in dinocyst concentrations during the LIG and at the base of the Holocene indicates high marine productivity during these warmer periods, which can also be inferred from the dinocyst/pollen grains ratio and coeval high amounts of foraminifer organic linings, especially during the Holocene. By contrast, productivity appears to have been reduced during cooler episodes. Assemblage changes from MIS 6 to MIS 5 reflect a shift from oligotrophic conditions to warm and more productive environments: while MIS 6 is characterized by high relative abundances of *Operculodinium centrocarpum* and the typically fully-marine *Impagidinium aculeatum*, MIS 5 shows an increase of *Spiniferites* taxa as well as *O. israelianum* (Fig. 4, Table 4). Furthermore, since *Spiniferites* species have a wider tolerance for variation in salinity than *Impagidinium* species do, these important changes in

dominant species might further suggest strengthened seasonality during the interglacial intervals, that may in turn be related to the regional circulation (Loop Current and/or Mississippi discharge).

Plotting the ratio between the dominant species (*Impagidinium* spp. and *O. centrocarpum* as colder and oligotrophic representatives over *Spiniferites* spp. as more typical of productive environments) yields a semi-quantitative indicator that clearly illustrates the long-term assemblage shifts that coincide with the main climatic phases (Fig. 3). As such, the recurrence of cooler conditions after MIS 5e is evidenced by the increase of *Impagidinium* spp. and *O. centrocarpum* as well as an important drop in absolute cyst concentrations. By contrast, “warmer” index values are shown for the Holocene, which furthermore shows high occurrences of *Polysphaeridium zoharyi*, in line with the species’ common modern-day presence in subtropical to equatorial regions (Head and Westphal, 1999). The Holocene behavior of *P. zoharyi* will be discussed in more detail in section 4.2.

Thus, sharp changes in the relative abundance of the dominant index species in the studied core clearly reflect shifts from glacial to interglacial periods, an observation that is further corroborated by synchronous changes in the dinocyst total concentrations. This demonstrates that dinocyst assemblages from the Gulf of Mexico provide a good proxy for long-term changes in hydrological conditions.

4.2. Comparison between Holocene and last interglacial records

In spite of the general dominance of *Spiniferites* species in the Holocene and last interglacial sediments, the overall species composition of the assemblages shows features that distinct the two interglacial episodes and point to differences in surface water properties in the Gulf of Mexico. The LIG assemblages are marked by higher percentages of *S. mirabilis* sensu lato than during the Holocene. Interestingly,

increased abundances of this species, whose highest occurrences at present are observed in the warm temperate to temperate regions of the eastern North Atlantic (Rochon et al., 1999; Penaud et al., 2008), have also been associated with the LIG climatic optimum in the high latitudes of the northern North Atlantic (Eynaud et al., 2004; Van Nieuwenhove et al., 2011; 2013). However, since Holocene temperatures (Mg/Ca SST: ~24–28°C) are always higher in the Gulf of Mexico than in the present thriving area for this species in the North Atlantic, its high percentages during the LIG may not exclusively reflect temperature. These records imply that other parameters associated with warmer conditions may also have played a significant role on its distribution.

Another important observation is the increase in the relative abundance *O. israelianum* prior to the onset of the last interglacial maximum (~ 135 kyr) and its absence during the Holocene. Generally associated with fully marine equatorial environments, this species shows its highest concentrations in regions characterized by rather elevated salinity (Fig. 4, Table 4) (Zonneveld et al., 2013). Although it has been shown that the volume of freshwater discharged by the Mississippi river was not higher during the LIG than during the Holocene (Nürnberg et al., 2008; Montero-Serrano et al., 2010), the occurrence of *O. israelianum* exclusive to the LIG may highlight differences in sea-surface salinity between the present and last interglacial. It has been suggested that during the LIG, the higher insolation during boreal summer caused a northern shift of the ITCZ as compared to the early Holocene (Ziegler et al., 2008; Montero-Serrano et al., 2011; Nikolova et al., 2013). This would have fostered the warm and salty water from the Caribbean to penetrate further into the Gulf of Mexico during the last interglacial (Nürnberg et al., 2008; Ziegler et al., 2008; Montero-Serrano et al., 2011), heating up the entire basin and leading to saltier conditions, especially during the warm season. In this respect, the paired highest occurrence of *S. mirabilis* and *O. israelianum* during the LIG, as opposed to higher relative abundances of *P. zoharyi* and *L. machaerophorum* during the Holocene are in

line with the hypothesis of a farther-north propagation of the Loop Current during LIG (see scenarios in Montero-Serrano et al., 2011). Furthermore, it is interesting to note that both the high-salinity *O. israelianum* and dinocyst concentrations increase before the onset of optimal condition during the last interglacial (Fig. 3). This would denote a rapid regional response to changes in insolation, likely through the changing impact of the Loop Current in relation with the average position of the ITCZ. Such rapid response of dinocysts to insolation contrasts with observations from the high latitudes of the Atlantic Ocean, where other boundary conditions related to the deglaciation (e.g. surface ocean freshening) also may have played a major role in the development of optimal conditions during the LIG (Van Nieuwenhove et al., 2011; Govin et al., 2012).

Finally, a more coastal character typifies early Holocene dinocyst assemblages compared to those of the last interglacial. This is notably evidenced by the occurrence of *P. zoharyi*, which is nearly absent in the LIG sediments. Since this species is presently associated with warm shallow and nearshore environments (Wall and Dale, 1969; Zonneveld et al., 2013; Limoges et al., 2013), its high relative abundance in the early part of the Holocene and its subsequent decline toward the top of the core may reflect the paired impact of 1) a slight decrease in temperature from early to late Holocene, as also indicated by Mg/Ca SST and, 2) the gradually rising sea-level associated with the reduction of global land-based ice during the early Holocene. Indeed, following the Last Glacial Maximum (LGM), the eustatic sea-level has steadily increased from 20-19 kyr ago until approximately 6 kyr ago, when it attained its present-day level (Clark et al., 2004, 2009, 2012). For the Gulf of Mexico, taking into account the subsidence process, the minimum LGM sea level has been estimated to have stood about 90 m below present level (Bart and Ghoshal, 2003; Simms et al., 2007) leading to an important migration of the shoreline towards the outer shelf (see Fig. 5) and thus reducing the distance between the site location and the paleo-shoreline. During the early Holocene transgression, shallow environments

(cf. lagoons) may have developed on the continental shelf and fostered *P. zoharyi*. Conversely, it has been recognized that a more rapid eustatic sea-level rise, due to a more rapid increase in insolation, has occurred during the penultimate deglaciation (e.g., Otto-Bliesner, 2006; Hearty et al. 2007). The establishment of a high interglacial sea level stand (4-9 m above present) may therefore account for very limited abundance of *P. zoharyi* during the LIG, as ODP site 625 is located further away from the preferred shallow near-shore environment of the species. Such interpretations are in line with the observations of Wall and Dale (1969) from a marine sequence from the Bermudas, showing that sea level changes were associated with alternations between littoral and neritic facies, with *Pyrodinium* (i.e. *P. zoharyi*) likely associated with the former and *Gonyaulax* (i.e. *Spiniferites*) with the latter. Similarly, a reduced area of shallow habitats during glacial sea level lowstands might explain the dominance of oceanic *Impagidinium* species over more shelf-dwelling dinoflagellate species during MIS 6.

5. Conclusions

Phytoplanktonic records from the Gulf of Mexico have shown to document long-term oscillations in climatic conditions over the late Quaternary and to respond to differences in hydrological conditions that existed during the present and last interglacial. Changes from glacial to interglacial stages are marked by shifts from dinocyst assemblages dominated by *Impagidinium* and *O. centrocarpum* to assemblages largely dominated by *Spiniferites* taxa, high abundances of *S. mirabilis-hyperacanthus*, *O. israelianum* and/or *P. zoharyi*. Furthermore, the composition of the dinocyst assemblages indicates distinct phytoplanktonic signatures for the two interstadial stages, which likely underline differences in the hydrological settings of the northeastern Gulf of Mexico during the present and last interglacial intervals:

- The peak in the relative abundance of the coastal *P. zoharyi* shortly after the onset of the Holocene matches with the culminating Mg/Ca SSTs and may indicate the phase when sea-level was still rising, allowing the development of very shallow habitats on the continental shelf during the early part of the Holocene. Moreover, the absence of this coastal taxon in the LIG assemblages agrees with the rapid establishment of high sea-level stand.
- The relatively high occurrences of *S. mirabilis-hyperacanthus* and *O. israelianum* during the LIG suggest that summer sea-surface salinity was higher during the LIG than during the Holocene. This is in line with the hypothesis of a further-northward extension of the ITCZ during the LIG that would have fostered enhanced penetration of Caribbean water into the northern part of Gulf of Mexico.

Finally, this study shows that despite small differences in temperature between interglacial phases in low latitudes such as the Gulf of Mexico, dinocyst assemblages may still provide clues on the disparities in hydrographic conditions that characterize these late Quaternary major climatic phases.

Acknowledgements

This study was possible through the financial support of Fonds de Recherche Nature et Technologies of Quebec. We gratefully acknowledge Jean-François Hélie, André Poirier and Maryse Henry for their technical and scientific support with isotopic, trace element and palynological analyses. We also thank Charlène Manceau for her help with foraminifer picking. Helpful comments by two anonymous reviewers and the associate editor Thierry Corrège are thankfully acknowledged.

6. References

- Aharon, P., 2003. Meltwater flooding events in the Gulf of Mexico revisited: implications for rapid climate changes during the last deglaciation. *Paleoceanography* 18 (4), PA1079.
- Aharon, P., 2006. Entrainment of meltwaters in hyperpycnal flows during deglaciation superfloods in the Gulf of Mexico. *Earth and Planetary Science Letter* 241, 260-270.
- Anand, P., Elderfield, H., Conte, M.H., 2003. Calibration of Mg/Ca thermometry in planktonic foraminifera from a sediment trap time series. *Paleoceanography* 18 (2), 1050. doi:10.1029/2002PA000846, 2003
- Antonov, J.I., Seidov, D., Boyer, T.P., Locarnini, R.A., Mishonov, A.V., Garcia, H.E., 2010. World ocean atlas 2009 volume 2: salinity. In: Levitus, S. (Ed.), NOAA Atlas NESDIS 69. U.S. Government Printing Office, Washington, D.C. (184 pp.).
- Auladell, M., Pelegri, J.L., García-Olivares, A., Kirwand Jr, A.D., Liphardt Jr, B.L., Martín, J.M., Pascual, A., Sangrà, P., Zweng, M., 2010. Modelling the early evolution of a Loop Current ring. *Journal of Marine Systems* 80, 160-171.
- Barker, S., Greaves, M., Elderfield, H., 2003. A study of cleaning procedures used for foraminiferal Mg/Ca paleothermometry. *Geochemistry, Geophysics, Geosystems* 4 (9), 8407. doi : 10.1029/2003GC000559
- Bart, P.J., Ghoshal, S., 2003. Late Quaternary shelf-margin deltas in the northern Gulf of Mexico: implications for the Late Quaternary sea-level elevation at the culmination of the Last Glacial Maximum. In: Roberts, H.H., Rosen, N.C., Fillon, R.H., Anderson, J.B. (Eds.), Shelf Margin Deltas and Linked Down Slope Petroleum Systems: Global Significance and Future Exploration Potential. 23rd Annual GCSSEPM Foundation Bob F. Perkins Research Conference, Programs and Abstracts, p. 19.
- Blumberg, A.F., Mellor, G.L., 1985. A simulation of the circulation in the Gulf of Mexico. *Israel Journal of Earth Sciences* 34, 122-144.
- Bonnet, S., de Vernal, A., Gersonde, R., Lembke-Jene, L., 2012. Modern distribution of dinocysts from the North Pacific Ocean (37–64°N, 144°E–148°W) in relation to hydrographic conditions, sea-ice and productivity. *Marine Micropaleontology* 84–85 (1), 87–103.

- Bouma, A.H., Coleman, J.M., 1985. Mississippi Fan: Leg 96 program and principal results. In: Bouma, A.H., Barnes, N.E., Normark, W.R. (Eds.), Submarine Fans and Related Sequences. Springer-Verlag, New York, pp. 247–252.
- Bouma, A.H., Sterling, C.E., Coleman, J.M., 1985. Mississippi Fan, Gulf of Mexico. In: Bouma, A.H., Barnes, N.E., Normark, W.R. (Eds.), Submarine Fans and Related Sequences. Springer-Verlag, New York, pp. 143–150.
- Bond, G.C., 1995. Climate and the conveyor. *Nature* 377, 383–384.
- Broecker, W.S., Bond, G., Klas, M., Bonani, G., Wolfli, W., 1990. A salt oscillator in the glacial Atlantic? The concept. *Paleoceanography* 5 (4), 469–477.
- CAPE Last Interglacial Project Members (2006). Last interglacial Arctic warmth confirms polar amplification of climate change. *Quaternary Science Review*, 25, 1383-1400, doi:10.1016/j.quascirev.2006.01.033
- Clark, P. U. et al., 2012. Global climate evolution during the last deglaciation. *Proceedings of the National Academy of Sciences of the United States of America* 109 (19), E1134–E1142. doi: 10.1073/pnas.1116619109
- Clark, P. U., Dyke, A.S., Shakun, J.D., Carlson, A.E., Clark, J., Wohlfarth, B., Mitrovica, J., Hostetler, S.W., McCabe, A.M., 2009. The Last Glacial Maximum. *Science* 325, 710-714.
- Clark, P.U., McCabe, A.M., Mix, A.C., Weaver, A.J., 2004. Rapid rise of sea level 19,000 years ago and its global implications. *Science* 304, 1141-1144.
- Coleman, J. M., Prior, D. B., and Lindsay, J. F., 1983. Deltaic influences on shelf edge instability processes. In: Stanley, D. J., and Moore, G. T. (Eds.), *The Shelfbreak: Critical Interface on Continental Margins. Soc. Econ. Paleontol. Mineral. Spec. Publication*, 33: 121-137.
- de Vernal, A., Henry, M., Bilodeau, G., 1999. Techniques de préparation et d'analyse en micropaléontologie. *Les Cahiers du GEOTOP*, p. 28.
- de Vernal, A., Marret, F., 2007. Organic-walled dinoflagellate cysts: tracers of sea-surface conditions. In: C. Hillaire-Marcel and A. de Vernal (eds.) *Proxies in late Cenozoic paleoceanography*, Elsevier, 371–408.
- de Vernal, A., Rochon, A., Turon, J.-L., Matthiessen, J., 1997. Organic-walled dinoflagellate cysts: palynological tracers of sea-surface conditions in middle to high latitude marine environments. *Geobios* 30, 905-920.

- de Vernal, A., Eynaud, F. Henry, M., Hillaire-Marcel, C., Londeix, L., Magin, S., Matthiessen, J., Marret, F., Radi, T., Rochon, A., Solignac, S., Turon, J.-L. (2005). Reconstruction of sea-surface conditions at middle to high latitudes of the Northern Hemisphere during the Last Glacial Maximum (LGM) based on dinoflagellate cyst assemblages. *Quaternary Science Reviews* 24 (7–9), 897–924.
- Devillers, R., de Vernal, A., 2000. Distribution of dinoflagellate cysts in surface sediments of the northern North Atlantic in relation to nutrient content and productivity in surface waters. *Marine Geology* 166, 103–124.
- Dowsett, H.J., 1999. Sediment color and reflectance record from Ocean Drilling Program Hole 625B, Gulf of Mexico (marine isotope stage 5 interval). USGS Open-File Report, 99-413.
- Elderfield, H., Vautravers, M., Cooper, M., 2002. The relationship between shell size and Mg/Ca, Sr/Ca, $d^{18}\text{O}$, and $d^{13}\text{C}$ of species of planktonic foraminifera. *Geochemistry, Geophysics, and Geosystems* 3 (8), 13.
- Elliott, B.A., 1982. Anticyclonic rings in the Gulf of Mexico. *Journal of Physical Oceanography* 12, 1292–1309.
- Eynaud, F., Turon, J.L., Duprat, J., 2004. Comparison of the Holocene and Eemian palaeoenvironments in the South Icelandic Basin: dinoflagellate cysts as proxies for the North Atlantic surface circulation. *Review of Palaeobotany and Palynology* 128, 55–79.
- Fanning, A.F., Weaver, A.J., 1997. Temporal-geographical meltwater influences on the North Atlantic Conveyor: implications for the Younger Dryas. *Paleoceanography* 12, 307–320.
- Fensome, R.A., MacRae, R.A., Williams, G.L., 2008. DINOFLAJ2, version 1. Data Series no. 1. American Association of Stratigraphic Palynologists.
- Fhlaithearta, S.N., Reichart, G.J., Jorissen, F.J., Fontanier, E.J., Rohling, E.J., Thomson, J., De Lange, G.J., 2010. Reconstructing the seafloor environment during sapropel formation using benthic foraminiferal trace metals, stable isotopes, and sediment composition. *Paleoceanography* 25, PA4225, doi:10.1029/2009PA001869
- Flower, B.P., Hastings, D.W., Hill, H.W., Quinn, T.M., 2004. Phasing of deglacial warming and laurentide ice sheet meltwater in the Gulf of Mexico. *Geology* 32, 597–600.

- Garcia, H.E., Locarnini, R.A., Boyer, T.P., Antonov, J.I., 2010a. World ocean atlas 2009 volume 3: dissolved oxygen, apparent oxygen utilization, and oxygen saturation. In: Levitus, S. (Ed.), NOAA Atlas NESDIS 70. U.S. Government Printing Office, Washington, D.C. (344 pp.).
- Garcia, H.E., Locarnini, R.A., Boyer, T.P., Antonov, J.I., 2010b. World ocean atlas 2009, volume 4: nutrients (phosphate, nitrate, and silicate). In: Levitus, S. (Ed.), NOAA Atlas NESDIS 71. U.S. Government Printing Office, Washington, D.C. (398 pp.).
- Govin, A., Braconnot, P., Capron, E., Cortijo, E., Duplessy, J.-C., Jansen, E., Labeyrie, L., Landais, A., Marti, O., Michel, E., Mosquet, E., Risebrobakken, B., Swingedouw, D., Waelbroeck, C., 2012. Persistent influence of ice sheet melting on high northern latitude climate during the early Last Interglacial. *Climate of the Past* 8, 483-507.
- Haug, G.H., Hughen, K.A., Sigman, D.M., Peterson, L.C., Röhl, U., 2001 Southward Migration of the Intertropical Convergence Zone Through the Holocene. *Science* 293 (5533), 1304-1308. doi: 10.1126/science.1059725
- Head, M.J., Westphal, A., 1999. Palynology and paleoenvironment of a Pliocene Carbonate Platform: The Clino Core, Bahamas. *Journal of Paleontology* 73 (1), 1-25.
- Hearty, P.J., Hollin, J.T., Neumann, A.C., O'Leary, M.J., McCulloch, M., 2007. Global sea-level fluctuation during the Last Interglaciation (MIS 5e). *Quaternary Science Reviews* 26, 2090-2112.
- Hodell, D.A., Curtis, J.H., Jones, G.A., Higuera- Gundy, A., Brenner, M., Binford, M.W., Dorsey, K.T., 1991. Reconstruction of Caribbean climate change over the past 10,500 years. *Nature* 352, 790–793.
- Hofmann, E. E. and S. J. Worley, 1986. An investigation of the circulation of the Gulf of Mexico. *Journal of Geophysical Research* 9 (14), 221-238.
- Jochens, A.E., DiMarco, S.F., 2008. Physical oceanographic conditions of the deepwater Gulf of Mexico in summer 2000-2002. *Deep-Sea Research Part II: Topical Studies in Oceanography* 55, 2541-2554.
- Joyce, J.E., Tjalsma, L.R.C., Prutzman, J.M., 1990. High-resolution planktic stable isotope record and spectral analysis for the last 5.35 M.Y.: Ocean drilling program site 625 northeast Gulf of Mexico. *Paleoceanography* 5 (4), 507-529.

- Joyce, J.E., Tjaisma, L.R.C., Prutzman, J.M., 1993. North American glacial meltwater history for the past 2.3 m.y.: Oxygen isotope evidence from the Gulf of Mexico. *Geology* 21, 483-486.
- Kujau, A., Nürnberg, D., Zielhofer, C., Bahr, A., Röhl, U., 2010. Mississippi River discharge over the last ~560,000 years - Indications from X-ray fluorescence core-scanning. *Palaeogeography, Palaeoclimatology, Palaeoecology* 298, 311-318
- Limoges, A., Londeix, L., de Vernal, A., 2013. Organic-walled dinoflagellate cyst distribution in the Gulf of Mexico. *Marine Micropaleontology* 102, 51-68
- Lisiecki, L.E., Raymo, M.E., 2005. A Pliocene-Pleistocene stack of 57 globally distributed benthic $d^{18}\text{O}$ records. *Paleoceanography* 20 (PA1003), doi:10.1029/2004PA001071
- Locarnini, R.A., Mishonov, A.V., Antonov, J.I., Boyer, T.P., Garcia, H.E., 2010. World ocean atlas 2009, volume 1: temperature. In: Levitus, S. (Ed.), NOAA Atlas NESDIS 68. U.S. Government Printing Office, Washington, D.C. (184 pp.).
- LoDico, J.M., Flower, B.P., Quinn, T.M., 2006. Subcentennial-scale climatic and hydrologic variability in the Gulf of Mexico during the early Holocene. *Paleoceanography* 21 (3), PA3015. doi:10.1029/2005PA001243, 2006
- Manabe, S., Stouffer, R.J., 1995. Simulation of abrupt climate change induced by freshwater input to the North Atlantic Ocean. *Nature* 378, 165–167.
- Manabe, S., Stouffer, R.J., 1997. Coupled ocean-atmosphere model response to freshwater input: comparison to Younger Dryas event. *Paleoceanography* 12, 321–336.
- Meckler, A.N., Schubert, C.J., Hochuli, P.A., Plessen, B., Birgel, D., Flower, B.P., Hinrichs, K.-U., Haug, G.H., 2008. Glacial to Holocene terrigenous organic matter input to sediments from Orca Basin, Gulf of Mexico - A combined optical and biomarker approach. *Earth and Planetary Science Letters* 272, 251-263
- Montero-Serrano, J.C., Bout-Roumazeilles, V., Tribouillard, N., Sionneau, T., Riboulleau, A., Bory, A., Flower, B.P., 2009. Sedimentary evidence of deglacial megafloods in northern Gulf of Mexico (Pigmy Basin). *Quat. Sci. Rev.* 28, 3333-3347.
- Montero-Serrano, J.C., Bout-Roumazeilles, V., Sionneau, T., Tribouillard, N., Bory, A., Flower, B.P., Riboulleau, A., Martinez, P., Billy, I., 2010. Changes in precipitation regimes over North America during the Holocene as recorded by

mineralogy and geochemistry of Gulf of Mexico sediments. *Global and Planetary Change*, 74, 132–143, doi:10.1016/j.gloplacha.2010.09.004.

Montero-Serrano, J.C., Bout-Roumazeilles, V., Carlson, A.E., Tribouillard, N., Bory, A., Meunier, G., Sionneau, T., Flower, B.P., Martinez, P., Billy, I., Riboulleau, A., 2011. Contrasting rainfall patterns over North America during the Holocene and Last Interglacial as recorded by sediments of the northern Gulf of Mexico. *Geophysical research letters* 38, 1-6. doi:10.1029/2011GL048194

Morey, S.L., Martin, P.J., O'Brian, J.J., Wallcraft, A.A., Zavala-Hidalgo, J., 2003. Export pathways for river discharged fresh water in the northern Gulf of Mexico. *Journal of Geophysical Research* 108 (C10), 3303. doi:10.1029/2002JC001674.

Mudie, P.J., Harland, R., Matthiessen, J., de Vernal, A., 2001. Marine dinoflagellate cysts and high latitude Quaternary paleoenvironmental reconstructions: an introduction. *Journal of Quaternary Science* 16, 595–602.

Nikolova, I., Yin, Q., Berger, A., Singh, U.K., Karami, M.P., 2013. The last interglacial (Eemian) climate simulated by LOVECLIM and CCSM2. *Climate of the Past* 9, 1789–1806.

Nürnberg, D., Ziegler, M., Karas, C., Tiedemann, R., Schmidt, M.W., 2008. Interacting Loop Current variability and Mississippi River discharge over the past 400kyrs. *Earth and Planetary Science Letters* 272, 278-289

Oey, L.-Y., Ezer, T., Lee, H.-C., 2005. Loop current, rings and related circulation in the Gulf of Mexico : A review of numerical models and future challenges. In, Circulation in the Gulf of Mexico: Observations and models, Sturges, W., Lugo-Fernandez, A. (Eds.), Geophysical Monograph Series 161, American Geophysical Union, Washington, DC, 31-56.

Otto-Bliesner, B.L., Marshall, S.J., Overpeck, J.T., Miller, G.H., Hu, A., CAPE Last Interglacial Project members, 2006. Simulating Arctic Climate Warmth and Icefield Retreat in the Last Interglaciation. *Science* 311, 1751. DOI: 10.1126/science.1120808

Paton, C., Hellstrom, J., Paul, B., Woodhead, J. and Hergt, J. 2011. Iolite: Freeware for the visualisation and processing of mass spectrometric data. *Journal of Analytical Atomic Spectrometry* 26. 2508-2518. doi:10.1039/c1ja10172b.

Penaud, A., Eynaud, F., Turon, J.L., Zaragosi, S., Marret, F., Bourillet, J.F., 2008. Interglacial variability (MIS 5 and MIS 7) and dinoflagellate cyst assemblages in the Bay of Biscay (North Atlantic). *Marine Micropaleontology* 68, 136-155.

Poore, R.Z., Dowsett, H.J., Verardo, S., Quinn, T.M., 2003. Millenial-to century-scale variability in Gulf of Mexico Holocene climate records. *Paleoceanography* 18 (2), 1048. doi:10.1029/2002PA000868

Poore, R.Z., Pavich, M.J., Grissino-Mayer, H.D., 2005. Record of the North American southwest monsoon from Gulf of Mexico sediment cores. *Geology* 33 (3), 209-212. doi : 10.1130/G21040.1

Pospelova, V., de Vernal, A., Pedersen, T.F., 2008. Distribution of dinoflagellate cysts in surface sediments from the northeastern Pacific Ocean (43–25°N) in relation to sea-surface temperature, salinity, productivity and coastal upwelling. *Marine Micropaleontology* 68, 21–48.

Price, A.M., Pospelova, V., 2011. High-resolution sediment trap study of organic-walled dinoflagellate cyst production and biogenic silica flux in Saanich Inlet (BC, Canada). *Marine Micropaleontology* 80, 18-43.

Radi, T., de Vernal, A., 2008. Dinocysts as proxy of primary productivity in mid-high latitudes of the Northern Hemisphere. *Marine Micropaleontology* 68, 84–114.

Reimer, P.J., Bard, E., Bayliss, A., Beck, J.W., Blackwell, P.G., Bronk Ramsey, C., Buck, C.E., Cheng, H., Edwards, R.L., Friedrich, M., Grootes, P.M., Guilderson, T.P., Haflidason, H., Hajdas, I., Hatté, C., Heaton, T.J., Hoffmann, D.L., Hogg, A.G., Hughen, K.A., Kaiser, K.F., Kromer, B., Manning, S.W., Niu, M., Reimer, R.W., Richards, D.A., Scott, E.M., Southon, J.R., Staff, R.A., Turney, C.S.M., van der Plicht, J., 2013, INTCAL13 and MARINE13 radiocarbon age calibration curves 0–50,000 years cal BP. *Radiocarbon* 55 (4), 1869-1887.

Richey, J.N., Poore, R.Z., Flower, B.P., Quinn, T.M., 2007. 1400 yrs multiproxy record of climate variability from the northern Gulf of Mexico. *Geology* 35, 423-426

Richey, J.N., Poore, R.Z., Flower, B.P., Hollander, D.J., 2012. Ecological controls on the shell geochemistry of pink and white *Globigerinoides ruber* in the northern Gulf of Mexico: Implications for paleoceanographic reconstruction. *Marine Micropaleontology* 82-83, 28-37.

Rochon, A., de Vernal, A., Turon, J.L., Matthiessen, J., Head, M.J., 1999. Distribution of Dinoflagellate Cysts in Surface Sediments from the North Atlantic Ocean and Adjacent Basin and Quantitative Reconstruction of Sea-Surface Parameters. Contribution Series, 35. American Association of Stratigraphic Palynologists, Dallas, p. 152.

- Rosenthal, Y., 2007. Elemental proxies for reconstructing Cenozoic seawater paleotemperatures from Calcareous Fossils. In C. Hillaire-Marcel and A. de Vernal (eds.) *Proxies in Late Cenozoic Paleoceanography*, Elsevier, 765-797.
- Schlitzer, R., 2012. Ocean Data View. <http://odv.awi.de>.
- Schmidt, M.W., Spero, H.J., Lea, D.W., 2004. Links between salinity variation in the Caribbean and North Atlantic thermohaline circulation. *Nature* 428 (6979), 160-163.
- Simms, A.R., Lambeck, K., Purcell, A., Anderson, J.B., Rodriguez, A.B., 2007. Sea-level history of the Gulf of Mexico since the Last Glacial Maximum with implications for the melting history of the Laurentide Ice Sheet. *Quaternary Science Reviews* 26, 920-940.
- Simms, A.R., Anderson, J.B., DeWitt, R., Lambeck, K., Purcell, A., 2013. Quantifying rates of coastal subsidence since the last interglacial and the role of sediment loading. *Global and Planetary Change* 111, 296-308.
- Sionneau, T., Bout-Roumazeilles, V., Flower, B.P., Bory, A., Tribouillard, N., Kissel, C., Van Vliet-Lanoë, B., Montero-Serrano, J.C., 2010. Provenance of freshwater pulses in the Gulf of Mexico during the last deglaciation. *Quaternary Research* 74, 235-245.
- Sionneau, T., Bout-Roumazeilles, V., Meunier, G., Kissel, C., Flower, B.P., Bory, A., Tribouillard, N., 2013. Atmospheric re-organization during Marine Isotope Stage 3 over the North American continent: sedimentological and mineralogical evidence from the Gulf of Mexico. *Quaternary Science Reviews* 81, 62-73.
- Stockmarr, J., 1971. Tablets with spores used in absolute pollen analysis. *Pollen et Spores* 13, 615-621.
- Tedesco, K.A., Thunell, R.C., 2003. Seasonal and interannual variations in planktonic foraminiferal flux and assemblage composition in the Cariaco Basin, Venezuela. *The Journal of Foraminiferal Research* 33 (3), 192–210.
- Teller, J.T., 1990. Volume and routing of late-glacial runoff from the southern Laurentide Ice Sheet. *Quaternary Research* 34, 12–23.
- Tripsanas, E.K., Bryant, W.R., Slowey, N.C., Bouma, A.H., Karageorgi, A.P., Berti, D., 2007. Sedimentological history of Bryant Canyon area, northwest Gulf of Mexico, during the last 135 kyr (Marine Isotope Stages 1-6): A proxy record of Mississippi River discharge. *Palaeogeography, Palaeoclimatology, Palaeoecology* 246, 137-161.

Van Nieuwenhove, N., Bauch, H.A., Eynaud, F., Kandiano, E., Cortijo, E., Turon, J.-L., 2011. Evidence for delayed poleward expansion of North Atlantic surface waters during the last interglacial (MIS 5e). *Quaternary Science Reviews* 30, 934-946.

Van Nieuwenhove, N., Bauch, H.A., Andrleit, H., 2013. Multiproxy fossil comparison reveals contrasting surface ocean conditions in the western Iceland Sea for the last two interglacials. *Palaeogeography, Palaeoclimatology, Palaeoecology* 370, 247-259.

Wall, D., Dale, B., 1966. Living fossils in Western Atlantic plankton. *Nature* 211, 1025–1026.

Wall, D., Dale, B., 1969. The « Hystrichosphaerid » resting spore of the dinoflagellate *Pyrodinium bahamense*, Platf, 1906. *Journal of Phycology* 5, 140-149.

World Ocean Atlas, 2001. CD-ROMs Data Set. National Oceanographic Data Center, Silver Spring, MD.

Ziegler, M., Nürnberg, D., Karas, C., Tiedemann, R., Lourens, L.J., 2008. Persistent summer expansion of the Atlantic Warm Pool during glacial abrupt cold events. *Nature Geoscience* 1, 601-605.

Zonneveld, K.A.F., Marret, F., Versteegh, G.J.M., Bonnet, S., Bouimetarhan, I., Crouch, E., de Vernal, A., Elshanawany, R., Edwards, L., Esper, O., Forke, S., Grøsfjeld, K., Henry, M., Holzwarth, U., Kielt, J.-F., Kim, S.-Y., Ladouceur, S., Ledu, D., Chen, L., Limoges, A., Londeix, L., Lu, S.-H., Mahmoud, M.S., Marino, G., Matsuoka, K., Matthiessen, J., Mildenhall, D.C., Mudie, P., Neil, H.L., Pospelova, V., Qi, Y., Radi, T., Richerol, T., Rochon, A., Sangiorgi, F., Solignac, S., Turon, J.-L., Verleye, T., Wang, Y., Wang, Z., Young, M., 2013. Atlas of modern dinoflagellate cyst distribution based on 2405 datapoints. *Review of Palaeobotany and Palynology* 191, 1–197.

Sample	Depth	NOSAMS Lab #	Type	^{14}C Age (yr)	^{14}C Age error (yr)	Calibrated Age (yr)
100-625B-1H-01W-	(1-2 cm)	OS-107192	Foraminifera	1 970	25	1 529
100-625B-1H-01W-	(50-51 cm)	OS-107193	Foraminifera	5 300	30	5 652
100-625B-1H-01W-	(98-100 cm)	OS-107194	Foraminifera	10 600	40	11 909

Table 1. Results from the radiocarbon analyses for core ODP-625B.

Samples	100-6258-1H-QIW (0-1 cm)	100-6258-1H-QIW (20-22 cm)	100-6258-1H-QIW (50-52 cm)	100-6258-1H-QIW (40-42 cm)	100-6258-1H-QIW (58-60 cm)	100-6258-1H-QIW (78-80 cm)	100-6258-1H-QIW (88-90 cm)	100-6258-2H-05W (130-131 cm)	100-6258-2H-05W (139-140 cm)	100-6258-2H-06W (10-11 cm)	100-6258-2H-06W (15-16 cm)	100-6258-2H-06W (30-31 cm)	100-6258-2H-06W (35-36 cm)	100-6258-2H-06W (45-46 cm)	100-6258-2H-06W (75-76 cm)	100-6258-2H-06W (95-96 cm)	100-6258-2H-06W (105-106 cm)	100-6258-2H-06W (115-116 cm)				
# LAB	2923-6	2924-1	3071-2	2924-4	2924-5	2925-1	2925-2	2925-3	2927-5	2927-6	2928-1	3062-2	2928-2	2928-3	3062-4	2928-4	2928-5	2929-2	2929-4	2929-5	2929-6	
Mg/Ca ratios (mmol/mol)																						
CHAMBER 3	2,78 3,23 3,54 3,22	1,90 3,43 4,43 2,22	2,68 2,53 3,45 4,10	2,75 4,10 4,15 4,02	2,87 4,15 4,15 4,04	1,59 3,50 3,76 2,58	3,96 3,78 2,58 2,58	2,30 5,72 5,72 5,64	3,26 4,56 4,56 4,33	2,74 1,49 1,49 3,71	4,38 3,82 3,82 2,18	7,36 2,63 2,63 5,44	3,43 2,13 2,13 4,28	2,65 4,36 4,36 3,16	2,65 3,35 3,35 2,93	3,24 1,92 1,92 1,58	3,91 1,94 1,94 1,57	1,66 3,36 3,36 3,07	2,73 2,48 2,48 2,57	1,67 2,36 2,36 5,07	1,96 2,36 2,36 2,53	
MEAN VALUE	3,19 5,13 4,41 3,43	2,88 3,96 4,02 3,22	4,01 2,10 3,20 5,53	3,75 1,93 4,34 4,60	3,74 5,34 4,52 4,10	3,65 2,63 4,53 5,32	3,42 6,58 6,05 5,49	2,88 2,67 5,26 5,32	4,02 5,16 5,10 5,10	4,04 3,20 6,22 6,22	3,33 5,42 4,22 5,43	4,36 5,15 5,43 7,09	4,45 5,15 5,43 7,09	4,32 4,26 4,26 3,77	3,95 3,66 4,23 5,60	2,87 4,35 4,26 4,23	2,93 3,56 3,56 3,38	2,64 1,83 1,83 4,30	2,98 2,47 2,47 3,27	2,91 2,47 2,47 3,35	2,15 2,47 2,47 2,26	
Mg/Ca ratios (mmol/mol)																						
CHAMBER 2	2,80 6,76 6,76 4,00 5,39 7,13 3,68	5,09 3,43 3,43 3,48 5,19 3,54 6,14	3,58 8,23 8,23 5,03 4,68 7,13 6,14	5,61 6,14 6,14 5,03 4,81 7,13 6,14	3,68 6,14 6,14 7,22 4,81 5,18 4,36	3,45 4,60 4,60 4,25 3,75 5,18 4,36	3,02 5,32 5,32 3,45 2,53 5,18 4,36	4,28 4,28 4,28 4,35 3,75 6,55 4,85	5,68 5,68 5,68 7,05 4,99 6,42 4,85	6,91 6,47 6,47 7,09 4,99 7,36 4,90	4,99 4,99 4,99 7,09 5,77 5,02 4,13	5,77 5,77 5,77 5,77 4,30 5,02 3,97	4,99 4,99 4,99 4,99 4,30 5,02 3,97	4,32 4,26 4,26 4,26 3,70 5,05 4,82	3,95 3,66 3,66 3,66 3,66 5,05 4,82	2,87 3,56 3,56 3,56 3,70 5,05 4,82	2,93 3,56 3,56 3,56 3,70 5,05 4,82	2,64 1,83 1,83 1,83 2,37 3,08 2,64	2,98 2,47 2,47 2,47 3,27 3,08 2,64	2,91 2,47 2,47 2,47 3,35 3,08 2,64	2,15 2,47 2,47 2,47 3,35 3,08 2,64	
Mg/Ca ratios (mmol/mol)																						
CHAMBER 1	6,62 3,34 3,41 4,18 3,45 6,62	6,66 3,51 3,77 3,93 5,60 3,10	4,06 5,25 5,25 4,10 5,86 5,01	7,52 2,77 2,77 5,77 4,70 3,24	5,69 2,52 2,52 3,43 6,08 3,24	5,69 2,52 2,52 3,43 4,51 3,24	5,69 2,24 2,24 3,25 4,02 3,25	4,06 4,44 4,44 4,51 4,81 4,06	6,44 4,61 4,61 4,74 4,92 5,76	6,44 4,60 4,60 5,57 6,26 6,64	3,92 5,11 5,11 5,31 6,30 6,69	5,00 5,11 5,11 5,31 6,08 6,69	8,91 8,91 8,91 9,00 9,00 9,31	8,91 8,91 8,91 8,91 8,91 9,31	4,90 4,43 4,43 4,37 4,23 5,47	4,52 4,43 4,43 4,37 4,23 4,26	4,03 3,11 3,11 3,40 2,33 4,26	4,08 3,26 3,26 3,40 2,33 4,22	3,20 2,26 2,26 2,30 2,30 4,53	3,63 2,36 2,36 2,36 2,36 4,53	4,12 2,36 2,36 2,36 2,36 4,53	2,70 2,36 2,36 2,36 2,36 4,53
MEAN VALUE	4,32 3,34 3,41 4,18 3,45 6,62	3,50 3,51 3,77 3,93 5,60 6,66	4,77 5,25 5,01 4,10 5,86 4,06	3,68 2,77 2,77 4,31 5,77 5,25	5,08 2,52 2,52 4,31 5,77 3,43	4,88 2,52 2,52 4,31 5,77 3,43	5,03 2,52 2,52 4,31 5,77 3,43	4,18 4,29 4,29 4,29 4,29 4,29	4,64 4,64 4,64 4,74 4,92 4,76	4,64 4,64 4,64 5,57 5,57 5,75	4,07 4,07 4,07 5,05 5,05 5,05	6,33 5,77 5,77 5,77 5,77 5,77	5,37 5,79 5,79 5,79 5,79 5,79	5,96 5,96 5,96 6,55 6,55 6,55	4,57 4,57 4,57 5,32 5,32 5,32	4,03 3,25 3,25 3,90 3,90 <br;></br;>	4,08 3,26 3,26 3,40 3,40 3,40	3,20 2,26 2,26 2,30 2,30 2,30	3,63 2,36 2,36 2,36 2,36 4,53	4,12 2,36 2,36 2,36 2,36 4,53	2,70 2,36 2,36 2,36 2,36 4,53	
MEAN VALUE	4,20 3,91	3,35 3,25	4,72 4,50	4,30 3,91	4,80 4,54	4,74 4,42	4,96 3,6	3,98 4,42	4,60 4,41	5,12 5,38	6,51 6,89	5,23 5,83	6,56 5,83	4,17 4,39	3,93 3,69	3,14 3,65	3,98 3,65	5,01 5,02	2,98 2,61			
Mg/Ca	Temperature (°C)	25,89 25,90	23,84 27,46	27,27 27,56	27,27 27,39	27,25 25,24	27,25 27,23	27,25 29,48	28,60 29,89	29,43 29,89	27,61 27,61	25,25 25,25	25,13 25,13	22,94 22,94	24,77 24,77	26,20 26,20	21,40 21,40					

Table 2. Mean Mg/Ca values for each chamber of the analyzed foraminifers and resulting Mg/Ca corresponding to each sample.

		Samples	Lab number	Depth	Age (ka)	<i>U. peregrina</i>		<i>G. ruber</i> (pink)		<i>G. ruber</i> (white)		Mg/Ca (mmol/mol)	Temperature (°C)
						d18O (‰)	d13C (‰)	d18O (‰)	d13C (‰)	d18O (‰)	d13C (‰)		
Holocene	MIS 1	100-625B-1H-01W (1-2 cm)	2923-6	0,015	1,53	2,65	-0,56	-1,29	1,07	-1,16	0,58	3,91	25,89
		100-625B-1H-01W (20-22 cm)	2924-1	0,21	3,15	-	-	-1,79	0,79	-1,1	0,71	3,25	23,84
		100-625B-1H-01W (29-31 cm)	3071-1	0,295	3,86	2,77	-0,28	-1,68	1,18	-0,86	0,89	-	-
		100-625B-1H-01W (40-42 cm)	3071-2	0,205	4,78	2,79	-0,21	-1,32	0,73	-	-	4,50	27,46
		100-625B-1H-01W (50-52 cm)	2924-4	0,51	5,65	2,53	-0,56	-1,64	0,76	-1,07	0,85	3,91	25,90
		100-625B-1H-01W (58-60 cm)	2924-5	0,59	6,69	2,77	-0,66	-1,47	0,87	-0,88	0,64	4,54	27,56
		100-625B-1H-01W (70-72 cm)	2924-6	0,71	8,26	-	-	-1,59	0,58	-1,09	0,54	-	-
		100-625B-1H-01W (78-80 cm)	2925-1	0,79	9,30	2,78	-0,63	-1,50	0,64	-1,18	0,72	4,42	27,27
		100-625B-1H-01W (88-90 cm)	2925-2	0,89	10,61	2,79	-0,68	-	-	-	-	4,47	27,39
		100-625B-1H-01W (98-100 cm)	2925-3	0,99	11,91	3,28	-0,74	-1,74	0,49	-	-	3,68	25,24
Pleistocene	MIS 5	100-625B-2H-05W (0-1 cm)	2925-4	13,9	93,06	3,59	-0,57	-1,64	1,34	-0,83	0,45	-	-
		100-625B-2H-05W (10-11 cm)	2925-5	14	94,90	3,6	-0,63	-1,85	1,4	-0,81	0,62	-	-
		100-625B-2H-05W (20-21 cm)	2925-6	14,1	96,74	3,5	-0,45	-1,44	0,89	-1,24	0,66	-	-
		100-625B-2H-05W (30-31 cm)	2926-1	14,2	98,58	3,3	-0,44	-1,95	1,37	-	-	-	-
		100-625B-2H-05W (40-41 cm)	2926-2	14,3	100,41	3,46	-0,57	-1,36	0,93	-1,62	0,39	-	-
		100-625B-2H-05W (50-51 cm)	2926-3	14,4	102,25	-	-	-1,43	0,69	-0,96	0,36	-	-
		100-625B-2H-05W (60-61 cm)	2926-4	14,5	104,09	3,01	-0,72	-1,61	1,09	-1,2	0,35	-	-
		100-625B-2H-05W (70-71 cm)	2926-5	14,6	105,93	3,16	-0,79	-1,72	0,94	-1,15	0,34	-	-
		100-625B-2H-05W (80-81 cm)	2926-6	14,7	107,77	3,31	-0,6	-1,39	1,12	-1,2	0,59	-	-
		100-625B-2H-05W (90-91 cm)	2927-1	14,8	109,61	3,34	-0,64	-1,5	0,85	-0,77	0,13	-	-
	MIS 6	100-625B-2H-05W (100-101 cm)	2927-2	14,9	111,45	3,23	-0,75	-1,74	0,86	-0,91	0,25	-	-
		100-625B-2H-05W (110-111 cm)	2927-3	15	113,29	3,14	-0,69	-1,54	0,88	-1,04	0,29	-	-
		100-625B-2H-05W (120-121 cm)	2927-4	15,1	115,12	2,9	-0,62	-1,86	0,56	-1,3	0,26	-	-
		100-625B-2H-05W (130-131 cm)	2927-5	15,2	116,96	-	-	-	-	-1,3	-0,04	4,42	27,25
		100-625B-2H-05W (139-140 cm)	2927-6	15,29	118,62	-	-	-2,04	0,73	-1,31	0,45	4,41	27,23
		100-625B-2H-06W (0-1 cm)	3062-1	15,4	120,64	-	-	-	-	-	-	-	-
		100-625B-2H-06W (5-6 cm)	2928-1	15,45	121,56	2,34	-1,02	-2,11	0,21	-1,77	0,33	5,39	29,48
		100-625B-2H-06W (10-11 cm)	3062-2	15,5	122,4785	-	-	-	-	-	-	4,99	28,60
		100-625B-2H-06W (15-16 cm)	2928-2	15,55	123,40	2,81	-0,78	-	-	-1,91	0,05	5,60	29,89
		100-625B-2H-06W (20-21 cm)	3062-3	15,6	124,32	-	-	-	-	-	-	-	-
Holocene	MIS 6	100-625B-2H-06W (25-26 cm)	2928-3	15,65	125,24	2,51	-0,87	-2,06	0,52	-1,65	0,19	5,37	29,43
		100-625B-2H-06W (30-31 cm)	3062-4	15,7	126,16	-	-	-	-	-	-	4,56	27,61
		100-625B-2H-06W (35-36 cm)	2928-4	15,75	127,08	2,82	-1,1	-2,38	0,41	-1,6	0,1	3,69	25,25
		100-625B-2H-06W (40-41 cm)	3062-5	15,8	128	-	-	-	-	-	-	-	-
		100-625B-2H-06W (45-48 cm)	2928-5	15,85	129,7692	3,19	-0,92	-1,35	0,89	-0,74	0,39	3,65	25,13
		100-625B-2H-06W (50-51 cm)	3062-6	15,9	131,5268	-	-	-	-	-	-	-	-
		100-625B-2H-06W (55-56 cm)	2928-6	15,95	133,2844	3,56	-0,79	-1,05	0,53	-0,83	0,35	-	-
		100-625B-2H-06W (65-66 cm)	2929-1	16,05	136,7996	3,32	-1,26	-1	0,6	0,35	0,19	-	-
		100-625B-2H-06W (75-76 cm)	2929-2	16,15	140,3148	3,44	-1,09	-0,9	0,65	0,15	0,02	2,99	22,94
		100-625B-2H-06W (85-86 cm)	2929-3	16,25	143,83	3,45	-1,02	-1,98	0,24	-1,24	-0,14	-	-
Pleistocene	MIS 6	100-625B-2H-06W (95-96 cm)	2929-4	16,35	147,3452	3,53	-1,08	-1,87	0,46	0,55	0,2	3,53	24,77
		100-625B-2H-06W (105-106 cm)	2929-5	16,45	150,8604	3,49	-1,45	-0,55	0,54	0,26	0,26	4,02	26,20
		100-625B-2H-06W (115-116 cm)	2929-6	16,55	154,3756	3,82	-1,25	-0,55	0,48	0,54	0,15	2,61	21,40
		100-625B-2H-06W (125-126 cm)	2930-1	16,65	157,8908	3,52	-1,5	-0,59	0,52	0,57	0,39	-	-
		100-625B-2H-06W (135-136 cm)	2930-2	16,75	161,406	-	-	-	-	-	-	-	-
		100-625B-2H-06W (145-146 cm)	2930-3	16,85	164,9212	-	-	-	-	-	-	-	-

Table 3. Geochemical data.

Dominant dinocyst species	Complete range T [°C]	Optimum global dataset T [°C]	Complete range S [psu]	Optimum global dataset S [psu]	Comments and regional modern distribution
<i>Impagidinium aculeatum</i>	-1.6 - 29.6	18 - 21	31.0 - 39.4	35 - 39	Highest relative abundances in oligotrophic environments. Offshore regions of the Gulf of Mexico
<i>Operculodinium centrocarpum</i>	-2.1 - 29.8	-2 - 23	9.8 - 39.4	32 - 36	Cosmopolitan
<i>Polysphaeridium zoharyi</i>	8.9 - 29.8	24 - 27	28.4 - 39.4	33 - 36	Typical for tropical shallow and productive coastal environments. Warm-water species.
<i>Spiarinifera mirabilis</i> sensu stricto	-0.8 - 29.8	18 - 19 & 27 - 29	17.5 - 39.4	35 - 37	Dominant in warm productive coastal environments of the Gulf of Mexico.
<i>Operculodinium israelianum</i>	1.8 - 29.8	18 - 27	30.3 - 39.4	37 - 39	Warm-water and high salinity species.
<i>Lingulodinium machaeophorum</i>	0 - 29.8	17 - 20	8.5 - 39.4	35 - 37	Highest relative abundances close to river mouths.

Table 4. Affinity to mean annual temperature (°C) and salinity (psu) for the dominant dinocyst species according to the global dataset (Zonneveld et al., 2013) and modern distribution in the Gulf of Mexico (Limoges et al., 2013).

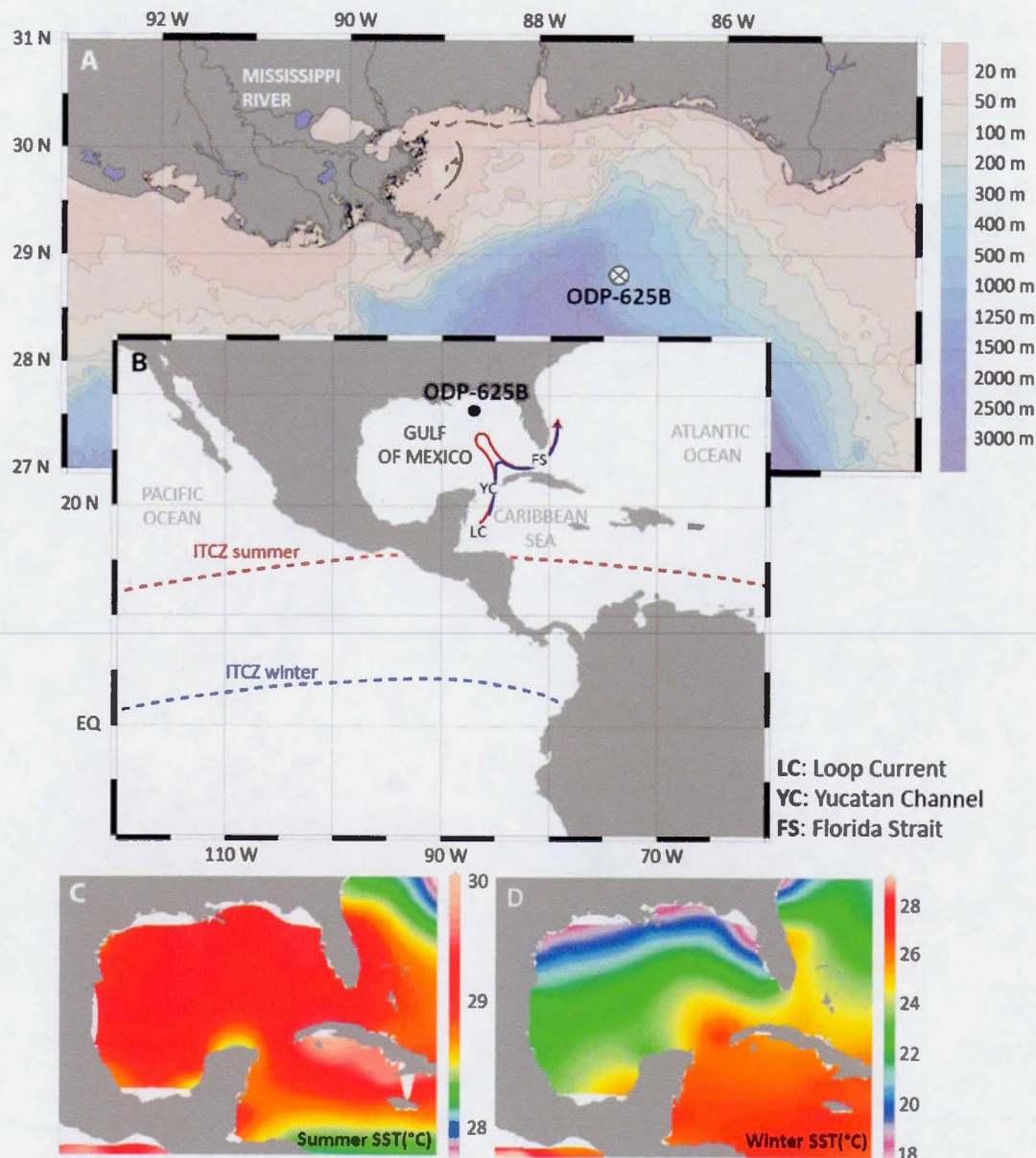


Figure 1. A) Position of site ODP-625B (28.83°N, 87.16°W), B) Simplified map of the Loop Current (dashed line in the inset) and seasonal (summer and winter) position of the ITCZ. Abbreviations: LC: Loop Current, YC: Yucatan Channel, FS: Florida Strait, C) Distribution of summer (July-September) temperatures (°C), D) Distribution of winter (January-March) temperatures (°C) (Ocean data view (Antonov et al., 2010; Garcia et al., 2010a, 2010b; Locarnini et al., 2010; Schlitzer, 2012)).

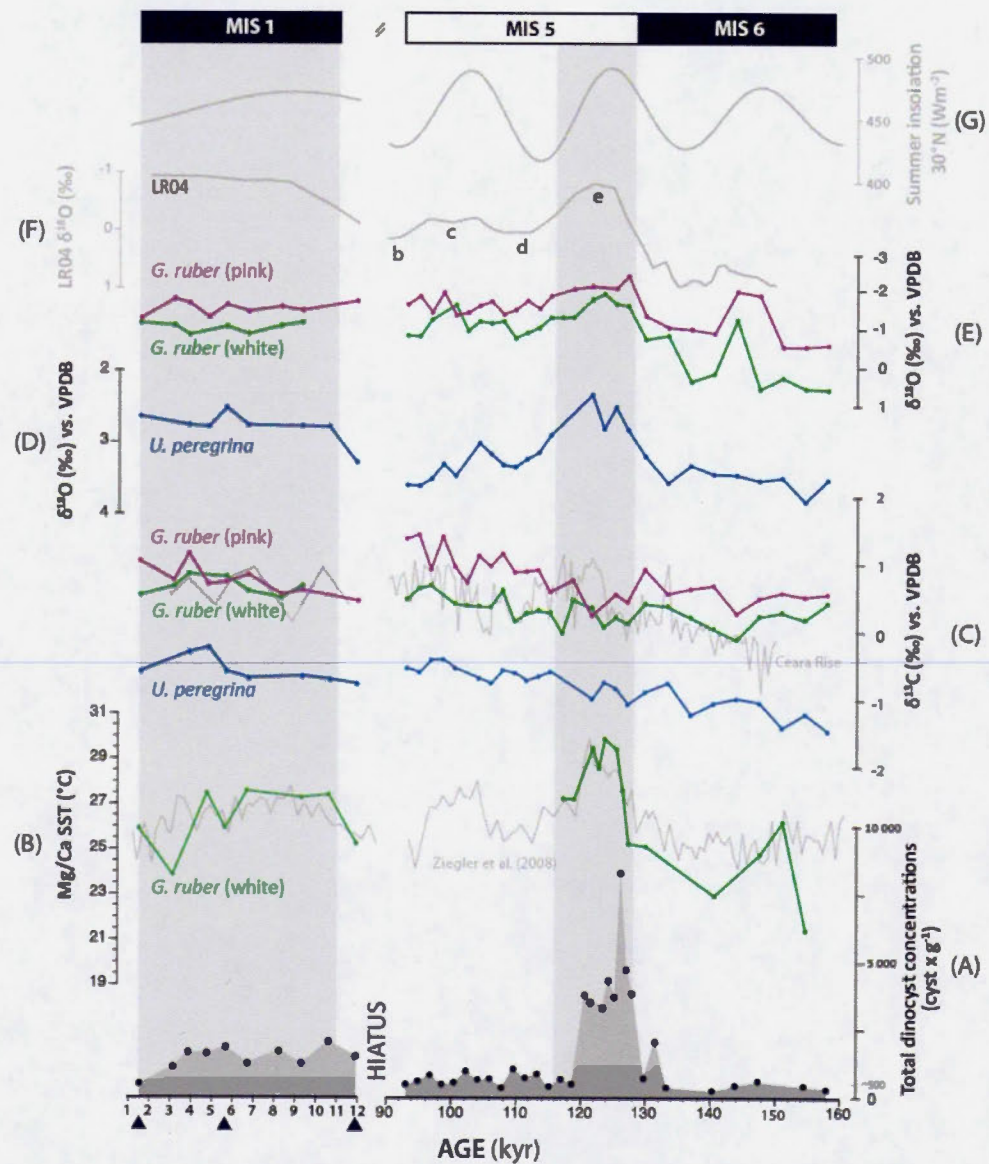


Figure 2. A) Total concentration of dinoflagellate cysts ($\text{cyst} \times \text{g}^{-1}$); B) Estimated SST on the basis of Mg/Ca ratios from *G. ruber* (white) (this study) and Mg/Ca SST from Ziegler et al. (2008); C) Stable carbon isotope ($\delta^{13}\text{C}$ in ‰) records of *U. peregrina*, *G. ruber* (white) and *G. ruber* (pink) (this study) and average $\delta^{13}\text{C}$ data from the benthic foraminifer *Cibicidoides wuellerstorfi* and *Cibicidoides* spp. from the northeast slope of Ceara Rise (Curry and Oppo, 1997); D) Stable oxygen isotope ($\delta^{18}\text{O}$ in ‰) record of *U. peregrina*; E) Stable oxygen isotope ($\delta^{18}\text{O}$ in ‰) records of *G. ruber* (white) and *G. ruber* (pink); F) Benthic stable oxygen isotopes ($\delta^{18}\text{O}$ in ‰) from stack LR04 (Lisicki and Raymo, 2005); G) Summer insolation at 30°N (Laskar, 2004). Shaded areas indicate the Holocene and last interglacial intervals. Black triangles represent calibrated radiocarbon dates.

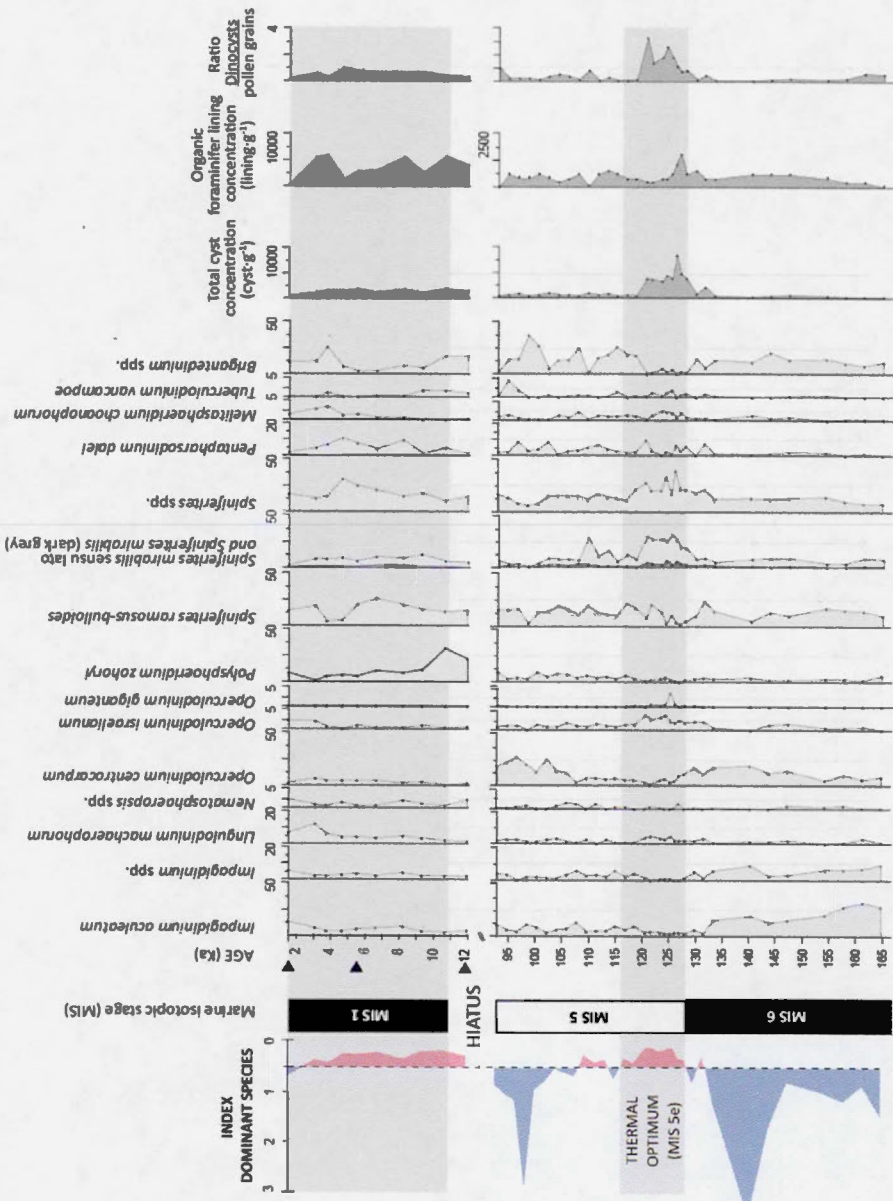


Figure 3. The dominant species index (*Impagidinium* species and *Operculodinium centrocarpum* over *Spiniferites* species; the line at 0.5 demarks when one species group or the other becomes dominant), relative abundances of the main dinocyst taxa, total cyst concentrations (cysts·g⁻¹), organic foraminifer lining concentrations (liming·g⁻¹) and the ratio of cysts over pollen during the Holocene and late Pleistocene intervals.

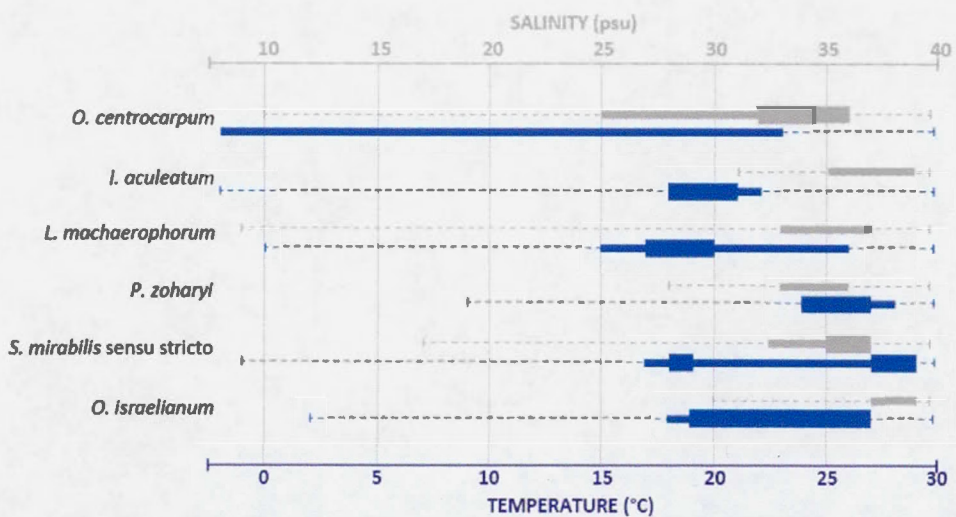


Figure 4. Affinity to mean annual temperature ($^{\circ}\text{C}$) and salinity (psu) for the dominant dinocyst species according to the global dataset (Zonneveld et al., 2013). Thicker bars represent higher relative abundances in the modern assemblages.

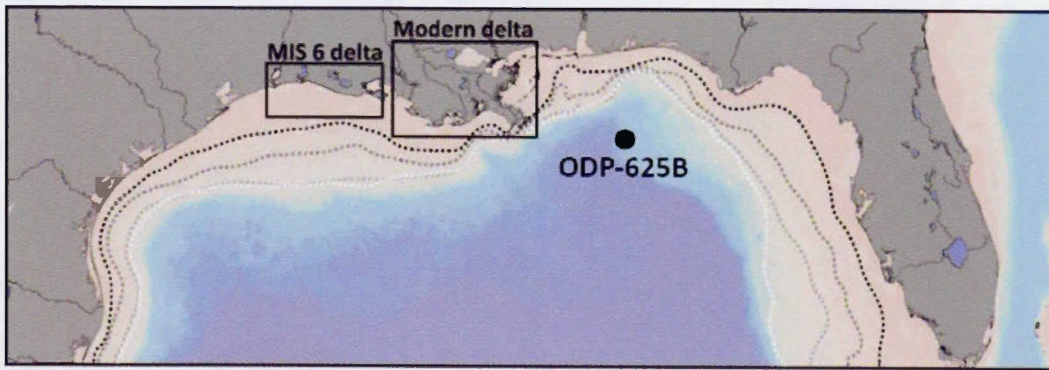


Figure 5. Model simulations for different sea-level (white: -100 mbsl; light grey: -80 mbsl; dark grey: -40 mbsl; black: -20 mbsl) (Lamont-Doherty Earth Observatory of Columbia University) and the position of the modern and MIS 6 Mississippi delta (Tripnasas, 2007).

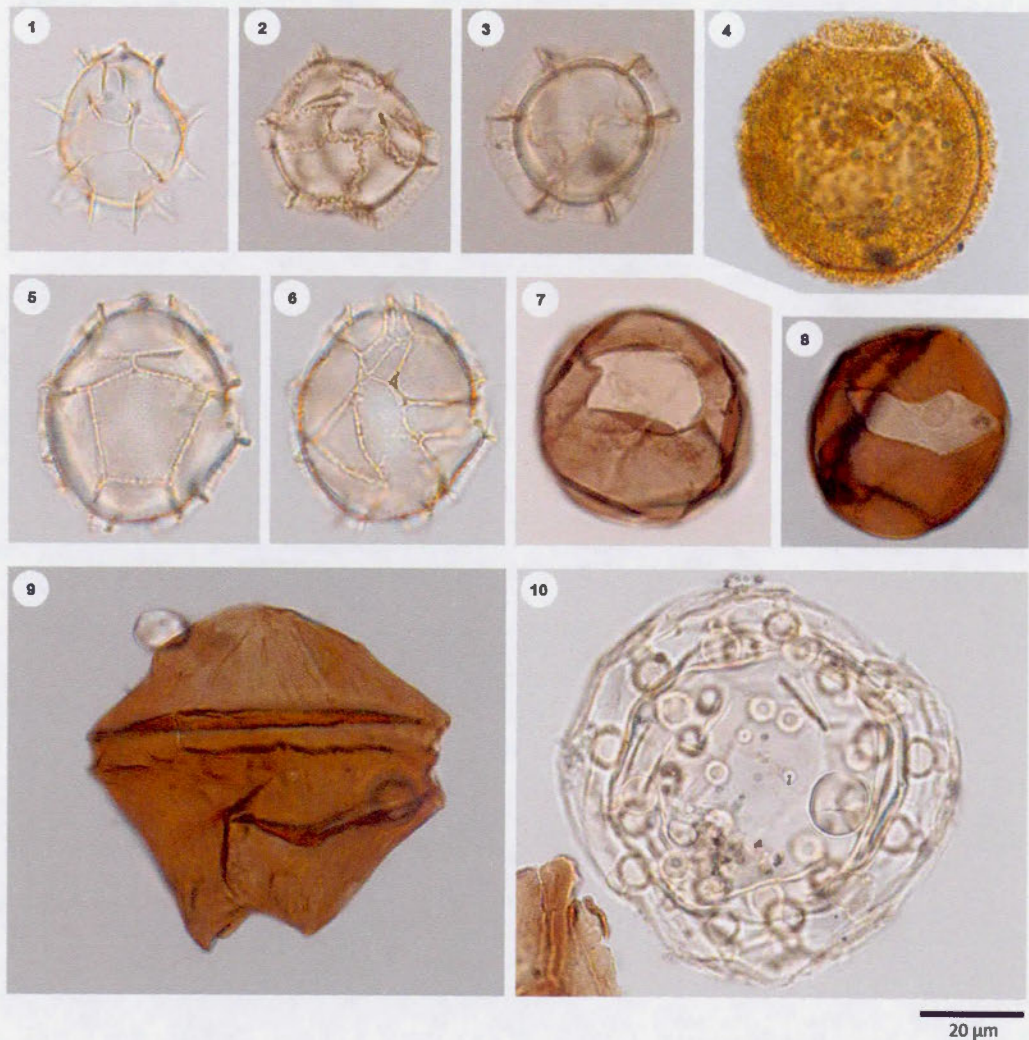


Plate 1. Bright field light micrographs of selected dinocyst taxa: 1. *Impagidinium aculeatum*; 2. *Impagidinium plicatum*; 3. *Impagidinium striatum*; 4. *Tectatodinium pellitum*; 5-6. cf. *Impagidinium sphaericum*; 7-8. *Brigantedinium cariacense*; 9. *Quinquecuspis concreta*; 10. *Tuberculodinium vancampoae*. Scale bar: 20 µm.

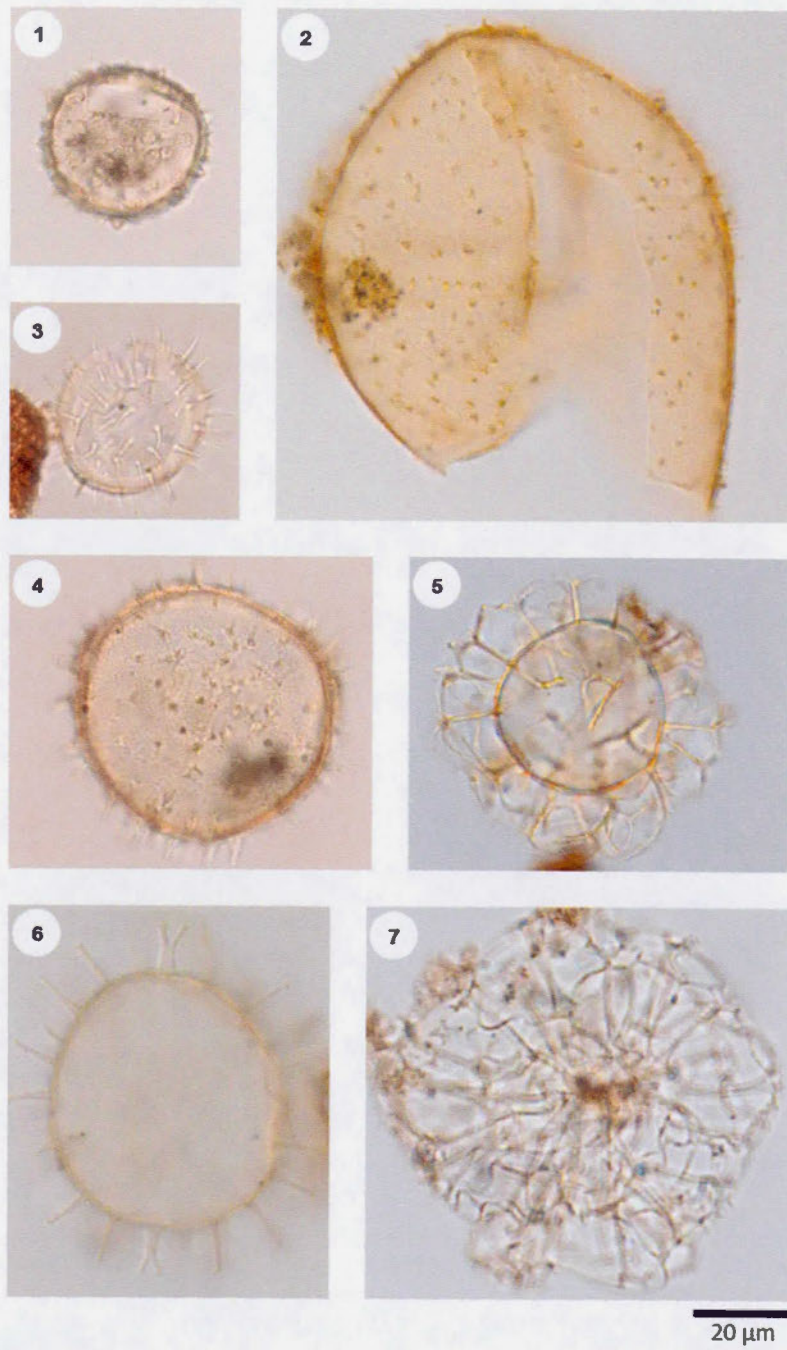


Plate 2. Bright field light micrographs of selected dinocyst taxa: 1. *Operculodinium janduchenei*; 2. *Operculodinium giganteum*; 3. *Operculodinium longispinigerum*; 4. *Operculodinium israelianum*; 5. *Nematosphaeropsis rigida*; 6. *Polysphaeridium zoharyi*; 7. *Nematosphaeropsis lemniscata*. Scale bar: 20 µm.

Supplementary material. Raw dinocyst counts.

HOLECINE		PLIOCENE		MS 1		MS 2		MS 3	
Sample number	HOLECINE	PLIOCENE	MS 1	MS 2	MS 3	PLIOCENE	MS 1	MS 2	MS 3
100-6258-1H-01W 1-2	2924-6	0	30	4	0	1	4	3	0
100-6258-1H-01W 26-22	2924-4	0	22	3	1	1	0	0	0
100-6258-1H-01W 26-31	3071-1	0	8	2	0	1	0	1	0
100-6258-1H-01W 40-42	3071-2	0	8	1	0	0	0	0	0
100-6258-1H-01W 50-52	2924-4	0	12	5	0	0	0	0	0
100-6258-1H-01W 54-60	2924-5	0	25	2	0	0	0	0	0
100-6258-1H-01W 70-72	2924-6	0	26	2	0	0	0	0	0
100-6258-1H-01W 88-90	2925-2	0	10	1	0	0	1	0	0
100-6258-1H-01W 98-100	2925-3	0	16	2	0	3	0	0	0
100-6258-2H-05W 1-2	2924-4	0	30	4	0	1	4	3	0
100-6258-2H-05W 26-22	2924-4	0	22	3	1	1	0	0	0
100-6258-2H-05W 26-31	3071-1	0	8	2	0	1	0	1	0
100-6258-2H-05W 40-42	3071-2	0	8	1	0	0	0	0	0
100-6258-2H-05W 50-52	2925-1	0	26	1	0	0	0	0	0
100-6258-2H-05W 60-61	2925-2	0	25	4	0	0	0	0	0
100-6258-2H-05W 70-71	2925-1	0	22	1	0	0	0	0	0
100-6258-2H-05W 80-81	2925-6	0	35	5	0	0	0	0	0
100-6258-2H-05W 90-91	2927-1	1	19	3	0	0	1	0	0
100-6258-2H-05W 100-101	2927-2	1	19	3	0	1	0	0	0
100-6258-2H-05W 110-111	2927-3	0	24	4	0	0	0	0	0
100-6258-2H-05W 120-121	2927-4	0	1	25	0	0	0	0	0
100-6258-2H-05W 130-131	2927-5	0	2	19	1	0	0	0	0
100-6258-2H-05W 130-140	2927-6	0	0	32	0	0	0	0	0
100-6258-2H-05W 61	3062-6	0	11	2	0	0	0	0	0
100-6258-2H-06W 10-11	2928-1	0	13	0	0	0	0	0	0
100-6258-2H-06W 15-16	2928-2	0	19	0	0	0	0	0	0
100-6258-2H-06W 20-21	3062-3	0	7	2	0	0	0	0	0
100-6258-2H-06W 25-26	2928-1	0	9	0	0	0	0	0	0
100-6258-2H-06W 30-31	3062-4	0	12	0	0	0	0	0	0
100-6258-2H-06W 55-56	2928-4	0	15	1	0	0	0	0	0
100-6258-2H-06W 40-41	3062-5	0	9	2	0	0	0	0	0
100-6258-2H-06W 45-46	2928-5	0	17	2	0	0	0	0	0
100-6258-2H-06W 50-51	3062-6	0	7	0	0	0	0	0	0
100-6258-2H-06W 55-56	2928-6	1	49	5	0	0	0	0	0
100-6258-2H-06W 65-66	2929-1	0	23	3	1	0	0	0	0
100-6258-2H-06W 75-76	2929-2	0	26	4	1	0	0	0	0
100-6258-2H-06W 65-66	2929-3	4	46	2	0	0	0	0	0
100-6258-2H-06W 55-56	2929-4	1	35	1	0	0	0	0	0
100-6258-2H-06W 105-106	2929-5	1	13	0	0	0	0	0	0
100-6258-2H-06W 115-116	2929-6	0	30	1	0	0	0	0	0
100-6258-2H-06W 125-126	2930-1	0	60	4	1	0	0	0	0
100-6258-2H-06W 135-136	2930-2	0	92	2	10	0	0	0	0
100-6258-2H-06W 145-146	2930-3	0	67	6	0	1	0	0	0

CHAPITRE III

HIGH-RESOLUTION RECORD OF DINOFLAGELLATE CYSTS ASSEMBLAGES FROM THE SHALLOW ALVARADO LAGOON (SOUTHEASTERN GULF OF MEXICO)

Audrey Limoges¹, Ana-Carolina Ruiz-Fernandez², Joan-Albert Sánchez-Cabeza²,
Anne de Vernal¹

¹ Geotop, Université du Québec à Montréal, Canada

² Instituto de Ciencias del Mar y Limnología, Universidad Nacional Autónoma de México, Mexico

Résumé

Des analyses palynologiques ont été menées sur une carotte sédimentaire collectée dans la lagune Alvarado dans le but de retracer l'évolution historique des efflorescences algales nuisibles causées par des dinoflagellés. L'enregistrement sédimentaire couvre les derniers ~830 ans, une période durant laquelle *Polysphaeridium zoharyi*, un kyste produit par le dinoflagellé potentiellement toxique *Pyrodinium bahamense*, montre de très fortes abondances relatives. Ses flux élevés dans les différents niveaux sédimentaires indiquent également que ce taxon ait potentiellement formé des efflorescences dans le passé. Les dépôts de kystes dans les sédiments modernes auraient également le potentiel de supporter l'initiation de blooms dans le futur. En outre, cette étude fournit des enregistrements peu communs sur la distribution de *Spiniferites mirabilis* en milieu peu profond de faible salinité et illustre la forte représentation de *Spiniferites* sp. dans ce domaine environnemental.

Mots-clés: Dinokystes, Efflorescences algales nuisibles, *Polysphaeridium zoharyi*, *Pyrodinium bahamense*, golfe du Mexique

Abstract

Palynological assemblages were examined from a sediment core collected in the shallow Alvarado lagoon in order to evaluate the historical evolution of potential harmful algal blooms caused by cyst-producing dinoflagellates. The sedimentary record spans the last ~830 years (CE), a period during which *Polysphaeridium zoharyi*, a cyst produced by the potentially toxic dinoflagellate *Pyrodinium bahamense*, records high relative abundances. The elevated cyst fluxes in sediment also indicate that this taxon likely bloomed in the past and that the modern cyst bank in sediment still has the potential to support the initiation of harmful blooms. This study furthermore provides an unusual record of *Spiniferites mirabilis* from shallow, low salinity tropical environments and illustrates high abundances of *Spiniferites* spp. in these types of settings.

Keywords: Dinocysts, Harmful Algal Bloom, *Polysphaeridium zoharyi*, *Pyrodinium bahamense*, Gulf of Mexico

1. Introduction

Coastal lagoon systems are very productive areas that support a mosaic of habitats with various environmental gradients. In addition to the nutrient inputs from the watershed and through exchanges with the sea, the rapid nutrient cycling that generally characterizes such shallow environments stimulates primary production, which in turn exerts an important influence on the higher trophic levels. These systems therefore frequently offer exceptional fishery resources with nursery areas for commercial shellfish and fishes. They also provide numerous ecosystem services (Costanza et al., 1997; Basset et al., 2006) that promote urban development along the coasts and are therefore under increasing anthropogenic stress (Lotze et al., 2006) and susceptible to be affected by pollution and/or cultural eutrophication.

Phytoplankton communities are very sensitive to environmental changes and anthropogenic pressures (Revilla et al., 2010). Modifications in hydrogeographical conditions (temperature, salinity, turbidity, water depth) may cause compositional shifts in the phytoplankton communities, while exogenous inputs of nutrients may change the nutrient ratios and concentrations and led to the development of harmful algal blooms (HAB) (Anderson, 1989; Hallegraeff, 1993; Burkholder, 1998; Glibert et al., 2005; Glibert & Burkholder, 2006; Smayda, 2002; Anderson et al., 2008). In coastal and estuarine environments, major HABs are caused by opportunistic dinoflagellates that can ultimately replace the most sensitive species, impact the aquatic biota and cause human illness by producing potent toxins. Dinoflagellate blooms may thus represent a major concern for local economy and society.

Among the nearly 2000 dinoflagellates species described, approximately 15% are known to produce resting cysts as part of their sexual reproduction cycle (e.g. Dale, 1976; Taylor & Pollingher, 1987; Head, 1996). These cysts represent a dormant stage during the normal planktonic life-cycle and can remain viable in the sediment for

decades and even centuries before germination (Lundholm et al., 2011; Ribeiro et al., 2011). This capability of forming seedbeds in sediment and surviving under unfavorable conditions are important as they may play key roles in the dynamics of blooms (Dale, 1983; Nehring, 1993; Anderson et al., 1983, 2002; Cembella et al., 1988; Ishikawa and Taniguchi, 1996). Composed of a complex carbohydrate-based polymer (Versteegh et al., 2012) or more rarely of calcareous material (Matsuoka & Fukuyo, 2000), these cysts also are generally well fossilized and may provide micropaleontological sedimentary archives of past primary productivity. It is thereby possible to obtain retrospective information on the evolution of dinoflagellate communities in a given environment and evaluate the influence of environmental changes and anthropogenic activities on their diversity and abundance, as well as the formation of harmful blooms.

In this study, we report on high-resolution analyses of organic-walled dinoflagellate cyst (dinocyst) assemblages from Alvarado Lagoon (southwest Gulf of Mexico). The main objective of this work is to characterize the historical evolution of dinocysts and their use as proxy of red tides. Owing to the potential of *Pyrodinium bahamense* to form toxic blooms in similar warm coastal lagoons (Landsberg et al., 2006), special attention was given to the behavior of its cyst stage, *Polysphaeridium zoharyi*.

2. Regional setting

The Alvarado Lagoon system is located in the southwestern Gulf of Mexico, in the Mexican state of Veracruz. Formed at the confluence of three important rivers (Papaloapan, Blanco and Acula) that bring large volumes of freshwater ($\sim 50 \times 10^9 \text{ m}^3 \cdot \text{yr}^{-1}$; Cruz-Escalona et al., 2007), the lagoon system actually comprises several interconnected lagoons (Alvarado, Camaronera, Buen País and Tlalixcoyan) and numerous smaller aquatic bodies (Fig. 1). The main connection to the Gulf of Mexico is situated in the northeastern part of Alvarado Lagoon (inlet), but an artificial

opening was also constructed in 1982 in Camaronera Lagoon (outlet) (see Fig. 1) (Morán-Silva et al., 2005). The water residence time is about 0.5 day, leading to rapid exchanges of nutrients with adjacent systems (Morán-Silva et al., 2005; Cruz-Escalona et al., 2007). Oriented parallel to the coastline, the lagoon has an average depth of approximately 2 meters and is almost entirely surrounded by different types of mangroves. The tidal range for the regions is ~0.75 m

Primary production is enhanced during the rainy season (June to October) in relation with the high organic- and nutrient-rich river discharges (Abarca-Arenas et al., 2002; Moran-Silva et al., 2005), but also from November to February, when strong northern winds ("Nortes") blow off the Gulf of Mexico and drive resuspension of sediments and nutrients into the water column (Contreras et al., 1994). Conversely, the dry season (March-June) is generally characterized by lower and more stable primary production. The tropical precipitation-drought regime and the hydrological behaviour of the lagoonal system therefore induce significant seasonal variations in productivity (chlorophyll- α : ~4.3 to 92.6 $\mu\text{g/L}$; Morán-Silva et al., 2005) in addition to temperature and salinity changes, with values respectively ranging from ~18 to 32°C and ~ 0 to 17 psu in the area of the study site (Garcia, 1973; Castañeda Chávez et al., 2005; Morán-Silva et al., 2005). Salinity can reach 33.5 psu during the month of June near the Alvarado lagoon inlet (Calva Benítez & Torres Alvarado, 2011).

3. Material and methods

Two sediment cores were collected in October 2011 from Alvarado lagoon, Mexico (18.7979 °N; 95.8579 °W) using a gravity corer UWITEC. The complete sequences were *in-situ* sub-sampled into 1 cm sections. One core was used for palynological analyses and sections were kept refrigerated at 4°C until analysis. The other core was used for geochemical analyses and ^{210}Pb dating and sections were stored at -18°C.

3.1 Age model

For the upper part of the sediment core, the chronology was established using the ^{210}Pb dating technique (Krishnaswamy et al., 1971; Appleby and Oldfield, 1971; Robbins, 1978; Sanchez-Cabeza and Ruiz-Fernández, 2012) at the *Servicio Académico de Fechado* (SAF) at *Universidad Nacional Autónoma de México* (UNAM). In each section, the total ^{210}Pb activity was determined by measuring its daughter product ^{210}Po by alpha spectrometry, assuming secular equilibrium between the two isotopes (for analytical details, see Ruiz-Fernández et al., 2009). The total ^{210}Pb activity profile (Fig. 2, Table 1) showed a clear diminishing trend with depth down to 22 cm. The supported ^{210}Pb activity ($21.3 \pm 1.8 \text{ Bq kg}^{-1}$) was estimated as the mean of 13 samples below that depth. In order to avoid compaction effects, the chronology was established based on the accumulated mass (g cm^{-2}).

The sediment core age-model (Fig. 2) was established using the constant flux (CF) model (Sanchez-Cabeza & Ruiz-Fernández, 2012) and uncertainties were calculated using a Monte Carlo approach (Sanchez-Cabeza et al., 2014). The maximum ^{137}Cs activity (Fig. 2) was observed in section 11-12 cm, corresponding to ages ranging from 1954 to 1963, in good agreement with the maximum deposition of nuclear weapons fallout in the early 1960s (UNSCEAR, 2000). For the section of the core older than 110 years, three accelerator mass spectrometer radiocarbon dates were obtained from shells of the bivalve *Rangia Flexuosa* at the Beta Analytic Inc. laboratory (Miami) (Table 1). Calibration was performed with CALIB 7.0 (Reimer et al., 2013) using the marine reservoir and a correction of 209 years (ΔR), which corresponds to the difference between the radiocarbon age of section 17-18 cm and its ^{210}Pb age. Mass accumulation rates (MAR) for each section showed an upward increasing trend, ranging one order of magnitude (from 0.024 to $0.234 \text{ g cm}^{-2} \text{ yr}^{-1}$) and showing a subsurface maximum for year 2007. Fluxes shown in this work were obtained by multiplying mass concentrations by MAR for each section (Sanchez-

Cabeza et al., 2014). Sediment accumulation rates (SAR) increased upwards from ~0.03 cm yr⁻¹ in the core bottom to 0.61 cm yr⁻¹ in the core surface (Fig. 2). The complete sedimentary sequence covers ca. 830 years.

3.2 Geochemical and grain size analyses

Geochemical and grain size analyses were carried out at SAF-UNAM. Prior to analyses, samples were freeze-dried and ground to homogeneous powders. Percentages of calcium carbonate (in wt. %) in the bulk sediment were determined on subsamples of 500 mg using a colorimetric procedure that includes treatment of sediment with HCl (1N) and a back-titration of the acid excess with NaOH (0.5 N) (Stuardo & Villarroel, 1976). Organic carbon (OC) concentration was determined by treating 250 mg of dry sediments with 10 mL of an oxidant mixture of K₂Cr₂O₇ + Ag₂SO₄ + H₂SO₄ and the acid excess was back-tritrated with Fe(NH₄)₂(SO₄)₂ (Loring & Rantala, 1992). Relative analytical precision is estimated to 2% for CaCO₃ and 5% for OC. Grain size analyses were carried out on samples previously treated with H₂O₂ (30%) to remove organic matter, using a MalvernTM Mastersizer HydroTM 2000 MU grain size analyzer.

The sedimentary relative content of aluminum (Al), bromine (Br), chlorine (Cl) and titanium (Ti), was determined by X-ray fluorescence (XRF) (Xepos-3, Spectro Analytical Instruments) on 4 g of compressed dried sediments, contained in low-density polyethylene cells bottom-covered with ProleneTM membrane film (Fig. 3). Replicate analysis (n=4) of the reference material IAEA-356 “Polluted marine sediments” indicated good agreement between certified and analytical values for Al, Br and Ti (Cl values non-available), with accuracies above 95% and uncertainties below 5% for both of the metals determined.

3.3 Mg/Ca ratios

The shallow-water benthic foraminifer *Ammonia beccarii* is capable of thriving under conditions of varying temperature and salinity (Toyofuku et al., 2011) and represents an important component of the foraminifer assemblages at the study site. Furthermore, the relation between Mg uptake into the foraminiferal calcite and temperature has been calibrated for this species (Toyofuku et al., 2011), making it suited as proxy of (paleo)temperature. Three to five specimens of *Ammonia beccarii* (size ranging from 250 to 300 µm) were picked from each analyzed sample. Mg/Ca analyses were performed using ablation inductively coupled mass spectrometry (LA-ICP-MS). Instruments used was a Photon Machine G2 with 193nm wavelength laser, ran at low energy output (0.6 mJ) with elemental acquisition on a Nu Attom HR-ICP-MS. Multiple ablations were performed on every individual shell (~7) using a spot size of 30 µm diameter at a pulse repetition rate of 2Hz. Calibration was made against the international glass standard (NIST610). To avoid bias linked to diagenetic coatings and/or clay contamination, time-resolved sample signals were cautiously selected to exclude zones of manganese, iron and/or aluminum enrichments (see Fhlaithearta et al., 2010). These off-line data reductions were carried out using the Iolite software (Paton et al., 2011). Final Mg/Ca ratios were calculated by averaging all the measurements from foraminifers belonging to the same sedimentary level (see Limoges et al., 2014 for discussion concerning the application of this method). The calibration curve linking Mg/Ca ratios to temperature was based on culture specimens of *A. beccarii* by Toyofuku et al. (2011): $T(^{\circ}\text{C}) = (\ln ((\text{Mg/Ca}) / 0.575)) / 0.0531$.

3.4 Palynological Analyses

Sediments were processed for palynological analyses following standard laboratory procedures (e.g. de Vernal et al., 1999). A calibrated tablet of *Lycopodium clavatum* spores was added to each sample before treatment in order to estimate the absolute

dinocyst concentrations (Stockmarr, 1971). Wet sediments were then sieved between 106 and 10 µm to remove coarse sand, fine silt and clay. The remaining fraction was repeatedly treated with warm HCl (10%) and warm HF (40%) to remove carbonates and silicates respectively. The final residues were mixed with glycerin jelly and mounted for microscopic observation. The identification of dinocysts was carried out using an optical microscope at magnifications of 400 × and 1000 ×. Cyst identification was made following the original description of the holotype of each taxon and the most recent nomenclature was used (Fensome et al., 2008). Total cyst fluxes were calculated by multiplying the MAR ($\text{g cm}^{-2} \text{ yr}^{-1}$) by the total dinocyst concentration ($\text{cyst} \cdot \text{g}^{-1}$) corresponding to each sample. Since cysts of *Polysphaeridium zoharyi* tend to break in two, half cysts of this species were counted as such.

4. Results

4.1 Geochemical analyses and grain size analyses

The carbonate (CaCO_3) content of the sediment decreases from the deepest sediment horizon until approximately 25.5 cm (1691 CE), from whereon values remain rather constant towards the top of the core. Percentages range from 1.47 to 7.18 (wt. %) with a mean value of 4.19% (Fig. 3, Table 2). Total organic carbon (TOC) oscillates between 0.41 and 1.16 (wt %) (Fig. 3, Table 2). Since the increase in TOC towards the top of the core is neither correlated with higher CaCO_3 nor total cyst fluxes, it may indicate a more important delivery of land-derived organic carbon and/or the formation of seagrass beds (Morán-Silva et al., 2005). It can also be related to an early diagenetic curve.

The physical and chemical properties of the sediments are fairly constant for the complete sequence. Only the sediment accumulation rate (SAR) increases drastically from 7.5 cm depth towards the top of the core, indicating significantly higher supplies of sediment since the 1980s (Fig. 3, Table 2).

4.2 Mg/Ca ratios

Because of a very low number of foraminifer shells within the sediment retrieved, only a few samples could be analyzed (8 samples corresponding to 8 different levels) for Mg/Ca ratios. Raw Mg/Ca data vary from 2.41 to 2.91 mmol/mol. Conversion of these ratios into temperatures (Mg/Ca SST) yields values ranging from ~27 to 30.5 °C (Fig. 4). These values may suggest either a general decrease in temperature from ~1670 to 1931 (CE), or that the blooming behaviour of *A. beccarii* shifted towards a more important growth during a colder period. Furthermore, although no clear correlation may be drawn between the calculated Mg/Ca SST and the total cyst flux in the sediment, the general trend of Mg/Ca SST is similar to that of the sedimentary carbonate (CaCO_3) content. Hence, colder temperatures inferred from foraminifer shell Mg/Ca ratios coincide with decreased accumulation rates of calcareous material.

4.3 Palynomorph assemblages

Dinocysts dominate the marine (organic linings of foraminifers) and terrestrial (pollen grains of gymnosperms and angiosperms) palynological assemblages throughout the complete sedimentary record (see Fig. 4, Table 3). The assemblages are nearly exclusively composed of phototrophic taxa belonging to the Gonyaulacales (Fig. 5, supplementary material). A total of 22 species was recorded, but *Polysphaeridium zoharyi*, *Spiniferites mirabilis* sensu stricto, *Spiniferites hyperacanthus* (hereafter grouped with *S. mirabilis* sensu stricto and named *S. mirabilis* sensu lato) and diverse *Spiniferites* species (*S. belerius*, *S. bentori*, *S. cf.*

delicatus, *S. cf. lenzii*, *S. membranaceous* and *S. ramosus*) represent more than 92 % of total assemblages (Fig. 5). The proportion of *Spiniferites* showing uncommon features was extremely high and identification to species level was often difficult. Therefore, *Spiniferites* spp. encompasses a large number of specimens. Though *S. mirabilis* sensu stricto also exhibits important morphological variations, especially regarding the number of processes included in the flange and its length (Plate 1, micrographs 1-3), specimens characterized by the presence of intergonal processes and a broad conspicuous flange between antapical processes were grouped in *S. mirabilis* sensu stricto.

Accompanying species including *Lingulodinium machaerophorum*, *Nematosphaeropsis rigida*, *Operculodinium israelianum*, *Operculodinium janduchenei*, *Brigantedinium* spp., *Lejeuneacysta* spp., *Echinidinium transparantum* and *Tectatodinium pellitum* were present in low relative abundances (0-6%). Noteworthy is also the presence of well-preserved remains belonging to the benthic dinoflagellate *Bysmatrum subsalsum* (0-2%) (see Limoges et al., 2014).

Cyst concentrations in the sediment samples vary between 1588 and 16 509 cysts·g⁻¹. This translates into high total cyst fluxes (~122 to 1316 cysts·cm⁻²·yr⁻¹) (Table 3). Variations in the flux are concomitant with changes in the relative abundance of the dominant species, in particular with those of the potentially harmful *P. zoharyi* (motile stage: *Pyrodinium bahamense*): the highest total cyst fluxes are associated with increased relative abundances of this species. In addition to *P. zoharyi*, resting cysts belonging to two other potentially harmful dinoflagellates species were recorded: *Lingulodinium machaerophorum* (motile stage of *Lingulodinium polyedrum*) and *Bysmatrum subsalsum*. *L. machaerophorum* occurs in low concentrations throughout the whole sequence, but the first appearance of *B. bysmatum* occurs around 1801 CE (21.5 cm).

5. Discussion

5.1 Dinoflagellate cyst assemblages

While the total number of species is fairly constant over the complete sedimentary sequence, their relative abundance and cyst flux show notable fluctuations through time, suggesting that environmental parameters have been periodically more or less favorable to large cyst-producing dinoflagellate populations. The very low number of heterotrophic taxa is somewhat intriguing since these normally thrive in estuarine environments characterized by high productivity and nutrient availability (Pospelova et al, 2008; Radi & de Vernal, 2008). However, the distribution of heterotrophic taxa is strongly dependent upon diatoms and other microorganisms on which they prey (Jacobson and Anderson, 1986) and the scarcity of heterotrophic species may rather reflect low prey availability. This would also be favorable to phototrophic species as a low number of diatoms, for instance, would induce less competition for the access to nutrients. Given the organic carbon content and the generally good preservation of palynomorphs, we have no reason to believe that the low number of heterotrophic cysts is a preservational bias.

The significant representation of *P. zoharyi* is consistent with its association with shallow tropical environments surrounded by mangrove forests (Head & Wesphal, 1999; Usup et al., 2012). In contrast, the high abundance of *Spiniferites mirabilis* sensu lato reveals a wider-than-thought range of ecological niches for this species, since it has previously mostly been associated to fully marine environments (Marret and Zonneveld, 2003). On the other hand, the large dominance of *Spiniferites* spp. is in agreement with observations from other lagoon environments, where this taxon also forms an important part of the assemblages (Wall et al., 1977; Pospelova et al., 2004). The marine character of our assemblages is somewhat surprising given the very low salinity generally associated to the study site area (i.e. a maximum of

<20%; Morán-Silva et al., 2005). Among abundant palynomorphs, only *Concentricystes* ind. and *Lingulodinium machaerophorum* are typically associated to brackish waters (Mudie et al., 2002; Zonneveld et al., 2009, 2012), and both are recorded in relative abundances lower than 5%. Even the freshwater algae *Pediastrum* sp. was recorded in negligible amounts. This led us think that living cells may have been advected from the coastal region into the lagoon via tidal exchange processes and/or ship transfer, and cysts were then formed in response to environmental stress. However, the high cyst concentrations encountered in the sediment, as well as the fact that dinocysts fluxes are continuously higher than other palynomorphs rather suggest local productivity. We thus postulate that dinoflagellates rather grow during the dry or the “Nortes” seasons, when evaporation causes the salinity to increase, or that the euryhaline character of these species has been underestimated for such tropical nutrient-rich environments. The assumption of seasonal increase in salinity would be coherent with other observations (Calva Benítez & Torres Alvarado, 2011) showing values reaching 33.5 near the Alvarado inlet during the dry season. Plankton tow studies might help to better understand the dinocyst distribution in such coastal settings.

The recovered *Spiniferites* taxa exhibit a particularly large range of morphological variations. Most of these concern the number of processes that form the flange in *S. mirabilis* sensu stricto, the length of the processes and the size of the central body. Other specimens were also classified as *Spiniferites* spp. on the basis of their uncommon features such as the development of high sutural crests. We suggest that low salinity and/or variable conditions in the shallow depositional environment have caused variations in the morphological development of the cysts. Laboratory cultures have shown that growth obstruction can give rise to a wide range of (aberrant) morphologies (e.g., Kokinos & Anderson, 1995). Such growth obstruction can also be assumed to occur in turbulent and shallow environments. Furthermore, the highly variable environmental conditions may also contribute to the development of unusual

morphologies on several taxa, as again shown by several laboratory and field studies (e.g., Lewis et al., 1999, Mertens et al., 2009, 2012). In particular, Ellegaard (2002) has illustrated how changing salinity may cause *Spiniferites* spp. morphology to vary markedly. Such relation was also established with *S. cruciformis* from the Black Sea (Wall et al., 1973; Mudie et al., 1998, 2001; Kouli et al., 2001).

5.2 Potential for past and future harmful algal blooms

An important feature of the study record is the high cyst fluxes, which reflect high productivity throughout the recovered sedimentation period. The predominance of the potentially toxic species *Polysphaeridium zoharyi*, whose peak abundances (~52% of total assemblages), is further associated with high cysts deposition rates. Though the number of motile cells that produce cysts may be variable (Dale, 1976; Lewis, 1988; Anderson & Keafer, 1985), such cyst concentration in the sediment demonstrates that this species has contributed to a large proportion of phytoplankton populations since at least 830 years. Cultures isolated from Florida have recently proven that the Atlantic strains of *Pyrodinium bahamense* (motile stage of *P. zoharyi*) can produce Paralytic Shellfish (PS) toxins (saxitoxins) (Landsberg, 2006). Although it has not been investigated whether this also applies to the strain occurring in Alvarado Lagoon, our cyst records illustrate that past populations may have attained bloom size. It also shows the potential for Alvarado Lagoon to be affected by future blooms as very few cysts may yield the initiation of blooms under favorable conditions (Lewis et al., 1985), especially if physical processes (winds, high precipitation) trigger their resuspension into the water column (Franks & Anderson, 1992; Villanoy et al., 1996; Philips et al., 2006). In this respect, *Lingulodinium machaerophorum* should also be considered, since the vegetative cells (*L. polyedrum*) are characterized by a low cyst formation rate (Lewis, 1988) – implying much higher cell numbers in the water column compared to cyst numbers in the sediment – and has a well-

documented history of bloom formation in coastal waters (Morales-Ramírez, 2001; Benouna et al., 2002; Peña-Manjarrez et al., 2005).

The Atlantic strain of *Pyrodinium bahamense* has been mostly observed from coastal tropical to subtropical environments, notably from Puerto Rico (Margalef, 1961), Jamaica (Seliger et al., 1970) and several estuaries and lagoons along the Florida coasts (Steidinger et al., 1980; Phlips & Badylak, 1996; Badylak & Phlips, 2004; Phlips et al., 2006). In the Gulf of Mexico, the modern distribution of its cyst (*P. zoharyi*) is not limited to shallow coastal environments and low abundances were also recorded offshore (Limoges et al., 2013). Field data from the Indian River Lagoon (Florida) indicate that this species is tolerant to variable salinity regimes, but likely proliferates when SSSs and SSTs exceed 16 and 25°C respectively (Phlips et al., 2006). It has also been noticed that blooms frequently occur after periods of heavy rain and/or in relation with climatic cycles such as El Niño and La Niña (Phlips et al., 2004, 2006) as these may cause increased nutrient-rich runoff from the continental shelf and/or resuspension of resting cysts from the sediment into the water column. These mechanisms were also observed with the Pacific strain of *P. bahamense* in Southeast Asia (Maclean, 1989; Usup & Lung, 1991; Villanoy et al., 1996), where harmful blooms caused by *P. bahamense* represent a major ecosystemic and societal problem (Abuso et al., 1999). Unfortunately, we lack historical information to link our fossil assemblages with short time scale fluctuations. In any case, the Alvarado region deserves special attention. It is seasonally subject to strong northern winds and heavy rain, which make it prone to the resuspension of the resting cysts into the water column, promoting the initiation of seasonal blooms. In addition, the high abundances of potentially harmful resting cysts in such protected environment may play an important role as seed population from which cells may be entrained offshore and reach other growing habitats (Anglès et al., 2010). Furthermore, since the Alvarado lagoon is a region of intense fishing and shipping activities, transport of cells by boats may also represent a potential vector of transfer.

6. Conclusion

Our study provides information on the evolution of cyst-producing dinoflagellate communities during the last centuries. It notably reveals that the potentially harmful *Pyrodininium bahamense* has been an important part of the assemblages since at least 830 years. Given the observed increase in the recent dinocyst fluxes, in particular that of *Polysphaeridium zoharyi*, which may be at the origin of toxic bloom formation, special attention has to be paid to the climate and hydrological regimes of the area. Finally, the beginning of the industrial period (~1958) coincides with changes in the sediment accumulation rate as well as dinocyst assemblage composition and flux. Additional work would be however needed to verify if such relation is also recorded in other areas of the Alvarado lagoon. It would also be interesting to characterize the cyst production in such shallow environments characterized by seasonal resuspension events.

Acknowledgements

This study was possible through the financial support of *Fonds de Recherche Nature et Technologies* of Quebec. We would like to thank Nicolas Van Nieuwenhove, Kenneth Mertens and Maryse Henry for assistance with cyst identification and helpful comments. Special thanks go to Jade Falardeau and Cynthia Leduc for help with foraminifera picking.

7. References

- Abarca-Arenas, L.G., J. Franco-Lopez, R. Chavez-Lopez, D. Arceo-Carranza, and A. Moran-Silva. 2002. Trophic analysis of the fish community taken as bycatch of the shrimp trawls off the coast of Alvarado, Mexico. *Proceedings of the Gulf and Caribbean Fisheries Institute* 55: 384–94.
- Abuso, Z.V., Cabella, L.M.T., Tuazon, L.C., 1999. Red tide monitoring in Maqueda and Villareal bays, Samar, Central Phillipines. In Watson, I., Vigers, G., Ong, K.-S. [Eds.], ASEAN Marine Environmental Management. Proceedings Fourth ASEAN-CANADA, Technical Conference on Marine Science, Langkawi, October 26-30, pp. 488–98.
- Anderson, D.M., Chisholm, S.W., Watras, C.J., 1983. Importance of life cycle events in the population dynamics of *Gonyaulax tamarensis*. *Mar. Biol.* 76: 179–89.
- Anderson, D.M. & Keafer, B.A., 1985. Dinoflagellate cyst dynamics in coastal and estuarine waters. In Anderson, D.M., White, A.W., Baden, D.G. [Eds.], *Toxic Dinoflagellates*. Elsevier Science Publishing, pp. 219–24.
- Anderson, D.M., 1989. Toxic algal blooms and red tides: a global perspective. In Okaichi, T., Anderson, D.M., Nemoto, T. [Eds.] *Red Tides: Biology, Environmental Science and Toxicology*. Elsevier, pp. 11–16.
- Anderson, D.M., Glibert, P.M., Burkholder, J.M., 2002. Harmful algal blooms and eutrophication : nutrient sources, composition, and consequences. *Estuaries* 25: 704–726.
- Anderson, D.M., Burkholder, J.M., Cochlan, W.P., Glibert, P.M., Gobler, C.J., Heil, C.A., Kudela, R.M., Parsons, M.L., Rensel, J.E.J., Townsend, D.W., Trainer, V.L., Vargo, G.A., 2008. Harmful algal blooms and eutrophication: Examining linkages from selected coastal regions of the United States. *Harmful Algae* 8: 39–53.
- Anglès, S., Jordi, A., Garcés, E., Basterretxea, G., Palanques, A., 2010. *Alexandrium minutum* resting cyst distribution dynamics in a confined site. *Deep-Sea Res. II* 57 (3–4): 210–221.
- Appleby, P. G. & Oldfield, F., 1978. The calculation of ^{210}Pb dates assuming a constant rate of supply of unsupported ^{210}Pb to the sediment. *Catena* 5: 1–8.

- Badylak, S. & Phlips, E.J., 2004. Spatial and temporal patterns of phytoplankton abundance and composition in a subtropical lagoon, the Indian River Lagoon, Florida, USA. *Journal of Plankton Research* 26: 1–22.
- Basset, A., Sabetta, L., Carrada, G.C., 2006. Conservation of transitional water ecosystems in the Mediterranean area: bridging basic ecological research and theories with requirements of application. *Aquatic Conservation: Marine and Freshwater Ecosystems* 16: 439–440.
- Bennouna, A., Berland, B., El Attar, J., Assobhei, O., 2002. Eau colorée à *Lingulodinium polyedrum* (Stein) Dodge, dans une zone aquacole du littoral du Doukkala (Atlantique marocain) *Lingulodinium polyedrum* (Stein) Dodge red tide in shellfish areas along Doukkala coast (Moroccan Atlantic). *Oceanologica Acta* 25: 159–170.
- Burkholder, J.M., 1998. Implications of harmful microalgae and heterotrophic dinoflagellates in management of sustainable marine fisheries. *Ecological Applications* 8 : 37–62.
- Calva Benítez, L. G. & Torres Alvarado, M.R. (2011). Textura de sedimentos y carbono orgánico en el sistema costero lagunar Alvarado, Veracruz. *Contactos* 81: 11–16
- Castañeda Chávez, M.d.R., Sedas, V.P., Borunda, E.O., Reynoso, F.L., 2005. Influence of water temperature and salinity on seasonal occurrences of *Vibrio cholerae* and enteric bacteria in oyster-producing areas of Veracruz, México. *Marine Pollution Bulletin* 50: 1641–1648.
- Cembella, A.D., Turgeon, J., Theriault, J.C., Béland, P., 1988. Spatial distribution of *Protogonyaulax tamarensis* resting cysts in nearshore sediments along the north coast of the lower St. Lawrence estuary. *Journal of Shellfish Research* 7: 597–609.
- Contreras, E.F., García, A., Castañeda, O., 1994. La clorofila como base para un índice trófico en lagunas costeras mexicanas. Anales del Instituto de Ciencias del Mar y Limnología. Universidad Nacional Autónoma de México. Volumen 2. Número 21, pp. 1–15.
- Costanza, R., d'Arge, R., de Groot, R., Farberk, S., Grasso, M., Hannon, B., Limburg, K., Naeem, S., O'Neill, R.V., Paruelo, J., Raskin, R.G., Sutton, P., van den Belt, M., 1997. The value of the world's ecosystem services and natural capital. *Nature* 387: 253–60.

- Cruz-Escalona, V., Arreguin-Sánchez, F., Zetina-Rejon, M., 2007. Analysis of the ecosystem structure of Laguna Alvarado, western Gulf of Mexico, by means of a mass balance model. *Estuarine, Coastal and Shelf Sciences* 72 : 155–67.
- Dale, B., 1976. Cyst formation, sedimentation and preservation: factors affecting dinoflagellate assemblages in recent sediments from Trondheimsfjord, Norway. *Review of Palaeobotany and Palynology* 22: 39–60.
- Dale, B., 1983. Dinoflagellate resting cysts: “benthic plankton”. In Fryxell, G.A. [Ed.], *Survival Strategies of the Algae*. Cambridge University Press, Cambridge, pp. 69–136.
- de Vernal, A., Henry, M., Bilodeau, G., 1999. Techniques de préparation et d'analyse en micropaléontologie. *Les Cahiers du GEOTOP*, p. 28.
- Ellegaard, M., 2002. Variations in dinoflagellate cyst morphology under conditions of changing salinity during the last 2000 years in the Limfjord, Denmark. *Review of Palaeobotany and Palynology* 109: 65–81.
- Fensome, R.A., MacRae, R.A., Williams, G.L., 2008. DINOFLAJ2, version 1. Data Series no. 1. American Association of Stratigraphic Palynologists.
- Fhlaithearta, S.N., Reichart, G.J., Jorissen, F.J., Fontanier, E.J., Rohling, E.J., Thomson, J., De Lange, G.J., 2010. Reconstructing the seafloor environment during sapropel formation using benthic foraminiferal trace metals, stable isotopes, and sediment composition. *Paleoceanography* 25, PA4225.
- Franks, P.J.S. & Anderson, D.M., 1992. Toxic phytoplankton blooms in the southwestern Gulf of Maine: testing hypotheses of physical control using historical data. *Marine Biology* 112: 165–174.
- Garcia, E., 1973. Modificaciones al sistema de Clasificación Climática de Köppen para adaptarlo a las condiciones de la República Mexicana. *Inst. Geofísica, Univ. Nal. Autónoma de México*, 246 p.
- Glibert, P.M., Seitzinger, S., Heil, C.A., Burkholder, J.M., Parrow, M.W., Codispoti, L.A., Kelly, V., 2005. The role of eutrophication in the global proliferation of harmful algal blooms. *Oceanography* 18: 198–209.
- Glibert, P.M. & Burkholder, J.M., 2006. The complex relationships between increasing fertilization of the earth, coastal eutrophication and proliferation of harmful algal blooms. In Graneli, E., Turner, J. [Eds.], *Ecology of Harmful Algae*. Springer, pp. 341–354.

- Hallegraeff, G.M., 1993. A review of harmful algal blooms and their apparent global increase. *Phycologia* 32: 79–99.
- Head, M.J., 1996. Modern dinoflagellate cysts and their biological affinities. In Jansonius, J., Mc Gregor, D.C. [Eds.], *Palynology: Principles and Applications*, vol. 3. AASP Foundation, Salt Lake City, UT, pp. 1197–1248.
- Head, M.J. & Westphal, A., 1999. Palynology and paleoenvironment of a Pliocene Carbonate Platform: The Clino Core, Bahamas. *Journal of Paleontology* 73: 1–25.
- Ishikawa, A., Taniguchi, A., 1996. Contribution of benthic cysts to the population dynamics of *Scrippsiella* spp. (Dinophyceae) in Onagawa Bay, northeast Japan. *Marine Ecology Progress Series* 140: 169–78.
- Jacobson, D. & Anderson, D., 1986. Thecate heterotrophic dinoflagellates: feeding behaviour and mechanics. *Journal of Phycology* 22, 249–258.
- Kokinos, J.P. & Anderson, D., 1995. Morphological development of resting cysts in cultures of the marine dinoflagellate *Lingulodinium polyedrum* (=*L. machaerophorum*). *Palynology* 19: 143–166.
- Kouli, K., Brinkhuis, H., Dale, B., 2001. *Spiniferites cruciformis*: a fresh water dinoflagellate cyst? *Review of Palaeobotany and Palynology* 113: 273–286.
- Krishnaswamy, S., Lal, D., Martin, J., Meybeck, M., 1971. Geochronology of lake sediments. *Earth Planetary and Science Letters* 11: 407–414.
- Landsberg, J.H., Sherwood, H., Johannessen, J.N., White, K.D., Conrad, S.M., Abbott, J.P., Flewlling, L.J., Richardson, R.W., Dickey, R.W., Jester, E.L.E., Etheridge, S.M., Deeds, J.R., Van Dolah, F.M., Leifield, T.A., Zou, Y., Beaudry, C.G., Benner, R.A., Rogers, P.L., Scott, P.S., Kawabata, K., Wolny, J.L., Steidinger, K.A., 2006. Saxitoxin puffer fish poisoning in the United States, with the first report of *Pyrodinium bahamense* as the putative toxin source. *Environmental Health Perspectives* 114: 1502–1507.
- Lewis, J., Tett, P., Dodge, J.D., 1985. The cyst-theca cycle of *Gonyaulax polyedra* (*Lingulodinium machaerophorum*) in Creran, a Scottish west coast loch. In Anderson, D.M., White, A.W., Baden, D.G. [Eds.], *Toxic Dinoflagellates*. Elsevier Science Publishing Company, pp. 85–90.
- Lewis, J., 1988. Cysts and sediments: *Gonyaulax polyedra* (*Lingulodinium machaerophorum*) in Loch Creran. *Journal of the Marine Biological Association* 68, 701–14.

- Lewis, J., Rochon, A., Harding, I., 1999. Preliminary observations of cyst-theca relationship in *Spiniferites ramosus* and *Spiniferites membranaceus* (Dinophyceae). *Grana* 38: 113–24.
- Limoges, A., Londeix, L., de Vernal, A., 2013. Organic-walled dinoflagellate cyst distribution in the Gulf of Mexico. *Marine Micropaleontology* 102, 51–68.
- Limoges, A., de Vernal, A., Van Nieuwenhove, N., 2014. Organic-walled dinoflagellate cyst distribution in the Gulf of Mexico, accepted in *Palaeogeography, Palaeoclimatology, Palaeoecology*. PALAEO7859
- Loring, D.H. & Rantala, R.T.T., 1992. Geochemical analyses of marine sediments and suspended particulate matter. *Earth-Science Reviews* 32, 235–283.
- Lotze, H.K., Lenihan, H.S., Bourque, B.J., Bradbury, R.H., Cooke, R.G., Kay, M.C., Kidwell, S.M., Kirby, M.X., Peterson, C.H., Jackson, J.B.C., 2006. Depletion, degradation, and recovery potential of estuaries and coastal seas. *Science* 312 : 1806–1809.
- Lundholm, N., Ribeiro, S., Andersen, T.J., Koch, T.A., Godhe, A., Ekelund, F., Ellegaard, M., 2011. Buried alive-germination of up to a century-old marine protist resting stages. *Phycologia* 50: 629–640.
- Maclean, J.L., 1989. An overview of *Pyrodinium* red tides in the western Pacific. In Hallegraeff, G.M., Maclean, J.L. [Eds.], *Biology, Epidemiology and Management of Pyrodinium Red Tides*. ICLARM Conference Proceedings 21. Fisheries Department, Ministry of Development, Brunei Darussalam, and International Center for Living Aquatic Resources Management, Manila, Philippines, pp. 1–8.
- Marret, F. & Zonneveld, K.A.F., 2003. Atlas of modern organic-walled dinoflagellate cyst distribution. *Review of Palaeobotany and Palynology* 123, 1–200.
- Margalef, R., 1961. Hidrografía y fitoplancton de un área marina de la costa meridional de Puerto Rico. *Investig Pesq*. 18: 33–96.
- Matsuoka, K. & Fukuyo, Y., 2000. Technical guide for modern dinoflagellate cyst study. WESTPAC-HAB/WESTPAC/IOC. Japan Society of the Promotion Science, Tokyo, p. 29.
- Mertens, K.N., Ribeiro, S., Bouimetarhan, I., Canerd, H., Nebout, N.C., Dale, B., de Vernal, A., Ellegaard, M., Filipova, M., Godhe, A., Goubert, E., Grøsfjeld, K., Holzwarth, U., Kotthoff, U., Leroy, S.A.G., Londeix, L., Marret, F., Matsuoka, K., Mudie, P.J., Naudts, L., Peña-Manjarrez, J.S., Persson, A., Popescu, S.M., Pospelova,

- V., Sangiorgi, F., van der Meer, M.T.J., Vink, A., Zonneveld, K.A.F., Vercauteren, D., Vlassenbroeck, Louwey, S., 2009. Process length variation in cysts of a dinoflagellate, *Lingulodinium machaerophorum*, in surface sediments: Investigating its potential as salinity proxy. *Marine Micropaleontology* 70: 54–69.
- Mertens, K.N., Bringué, M., Van Nieuwenhove, N., Takano, Y., Pospelova, V., Rochon, A., de Vernal, A., Radi, T., Dale, B., Patterson, T., Weckström, K., André, E., Louwey, S., Matsuoka, K., 2012. Process length variation of the cyst of the dinoflagellate *Protoceratium reticulatum* in the North Pacific and Baltic-Skagerrak region: calibration as an annual density proxy and first evidence of pseudo-cryptic speciation. *Journal of Quaternary Science* 27: 734–744.
- Morales-Ramírez, A., Víquez, R., Rodríguez, K., Vargas, M., 2001. Red tide bloom produced by *Lingulodinium polyedrum* (Peridiniales, Dinophyceae) in Bahía Culebra, Papagayo Gulf, Costa Rica. *Revista de Biología Tropical*: 19–23.
- Morán-Silva, A., Martínez Franco, L.A., Chávez-López, J.R., Franco-López, J., Bedia-Sánchez, C.M., Contreras Espinosa, F., Gutiérrez-M., F., Brown-Peterson, N.J., Petersons, M.S., 2005. Seasonal and spatial patterns in salinity, nutrients and chlorophyll- α in the Alvarado Lagoonal system, Veracruz, Mexico. *Gulf and Caribbean Research* 17: 133–143.
- Mudie, P.J., Aksu, A.E., Duman, M., 1998. Late Quaternary dinocysts from the Black, Marmara and Aegean seas: variations in assemblages, morphology and paleosalinity, NTNU Vitensk. Mus. Rapp. Bot. Ser, 1998-1, Trondheim, p. 116.
- Mudie, P.J., Aksu, A.E., Duman, M., 2001. Quaternary dinocysts from the Black, Marmara and Aegean seas: variations in assemblages, morphology and paleosalinity. *Marine Micropaleontology* 43: 155–178.
- Mudie, P.J., Rochon, A., Aksu, A.E., Gillespie, H., 2002. Dinoflagellate cysts, freshwater algae and fungal spores as salinity indicators in Late Quaternary cores from Marmara and Black seas. *Marine Geology* 190: 203–231.
- Nehring, S., 1993. Mechanisms for recurrent nuisance algal blooms in coastal zones: resting cyst formation as life-strategy of dinoflagellates. In Sterr, H., Hofstade, J., Plag, H.-P. [Eds.], *Proceedings of the International Coastal Congress on Interdisciplinary Discussion of Coastal Research and Coastal Management Issues and Problems*, Kiel, 1992, Lang, Frankfurt/M, pp. 454–467.

- Paton, C., Hellstrom, J., Paul, B., Woodhead, J. and Hergt, J. 2011. Iolite: Freeware for the visualisation and processing of mass spectrometric data. *Journal of Analytical Atomic Spectrometry* 26: 2508–18.
- Peña-Manjarrez, Hélenes, J., Gaxiola-Castro, Orellana-Cepeda, E., 2005. Dinoflagellate cysts and bloom events at Todos Santos Bay, Baja California, México, 1999-2000. *Continental Shelf Research* 25: 1375–1393.
- Philips, E.J., Badylak, S., Youn, S., Kelley, K., 2004. The occurrence of potentially toxic dinoflagellates and diatoms in a subtropical lagoon, the Indian River Lagoon, Florida, USA. *Harmful Algae* 3: 39–49.
- Philips, E.J. & Badylak, S., 1996. Spatial variability in phytoplankton standing crop and composition in a shallow inner shelf lagoon, Florida Bay, Florida. *Bulletin of Marine Sciences* 58: 203–206.
- Philips, E.J., Badylak, S., Bledsoe, E., Cichra, M., 2006. Factors affecting the distribution of *Pyrodinium bahamense* var. *bahamense* in coastal waters of Florida. *Marine Ecology Progress Series* 322: 99–115.
- Pospelova, V., Chmura, G.L., Walker, H.A., 2004. Environmental factors influencing the spatial distribution of dinoflagellate cyst assemblages in shallow lagoons of southern New England (USA). *Review of Palaeobotany and Palynology* 128: 7–34.
- Pospelova, V., de Vernal, A., Pedersen, T.F., 2008. Distribution of dinoflagellate cysts in surface sediments from the northeastern Pacific Ocean (43–25°N) in relation to sea-surface temperature, salinity, productivity and coastal upwelling, *Marine Micropaleontology* 68: 21–48.
- Radi, T. & de Vernal, A., 2008. Dinocysts as proxy of primary productivity in mid-high latitudes of the Northern Hemisphere. *Marine Micropaleontology* 68: 84–114.
- Revilla, M., Franco, J., Garmendia, M., Borja, A., 2010. A new method for phytoplankton quality assessment in the Basque estuaries (northern Spain), within the European Water Framework Directive. *Revista de Investigación Marina* 17: 150–64.
- Ribeiro, S., Berge, T., Lundholm, N., Andersen, T., Abrantes, F., Ellegaard, M., 2011. Phytoplankton growth after a century of dormancy illuminates past resilience to catastrophic darkness. *Nature Communications* 2: 311.
- Robbins, J.A., 1978. Geochemical and geophysical applications of radioactive lead isotopes. In Nriagu, J.O. (Ed.), *Biochemistry of Lead*, Elsevier, Amsterdam, pp. 85–393.

- Ruiz-Fernández, A.C., Hillaire-Marcel, C., de Vernal, A., Machain-Castillo, M.L., Vásquez, L., Ghaleb, B., Aspiazu-Fabián, J.A., Páez-Osuna, F., 2009. Changes of coastal sedimentation in the Gulf of Tehuantepec, South Pacific Mexico, over the last 100 years from short-lived radionuclide measurements. *Estuarine Coastal and Shelf Science* 823: 525–536.
- Sanchez-Cabeza, J.A. & Ruiz-Fernández, A.C., 2012. ^{210}Pb Sediment radiochronology : An integrated formulation and classification of dating models. *Geochimica et Cosmochimica Acta* 82: 183–200.
- Sanchez-Cabeza J.A., Ruiz-Fernández A.C., Ontiveros Cuadras J.F., Pérez Bernal L.H., 2014. Monte Carlo uncertainty calculation of ^{210}Pb sediment dating chronologies and accumulation rates. *Quaternary Geochronology*, DOI 10.1016/j.quageo.2014.06.002.
- Seliger, H.H., Carpenter, J.H., Loftus, M., McElroy, W.D., 1970. Mechanisms for the accumulation of high concentrations of dinoflagellates in a bioluminescent bay. *Limnology and Oceanography* 15: 234–245.
- Smayda, T.J., 2002. Adaptive ecology, growth strategies, and the global bloom expansion of dinoflagellates. *Journal of Oceanography* 58: 281–294.
- Steidinger, K.A., Tester, L.S., Taylor, F.J.R., 1980. A redescription of *Pyrodinium bahamense* var. *compressa* (Böhm) stat. nov. from Pacific red tides. *Phycologia* 19: 329–337.
- Stockmarr, J., 1971. Tablets with spores used in absolute pollen analysis. *Pollen et Spores* 13: 615–621.
- Stuardo, J. & Villarroel, M., 1976. Lagunas costeras del estado de Guerrero. *Anales ICMyl* 3: 1–180.
- Taylor, F.J.R., Pollingher, U., 1987. The ecology of dinoflagellates. In Taylor, F.J.R. [Ed.], *The Biology of Dinoflagellates*. Blackwell Scientific Publications, Oxford, p. 398–533.
- Toyofuku, T., Suzuki, M., Suga, H., Sakai, S., Szuki, A., Ishikawa, T., de Nooijer, L.J., Schiebel, R., Kawahata, H., Kitazato, H., 2011. Mg/Ca and ^{18}O in the brashish shallow-water benthic foraminifer *Ammonia beccarii*. *Marine Micropaleontology* 78: 113–120.

UNSCEAR (United Nations Scientific Committee on the Effects of Atomic Radiation), 2000. Report to the General Assembly, with scientific annexes. United Nations, New York.

Usup, G. & Lung, Y.K., 1991. Effects of meteorological factors on toxic red tide events in Sabah, Malaysia. *Marine Ecology* 12: 331–339.

Usup, G., Ahmad, A., Matsuoka, K., Teen Lim, P., Pin Leaw, C., 2012. Biology, ecology and bloom dynamic of the toxic marine dinoflagellate *Pyrodinium bahamense*. *Harmful Algae* 14: 301–312.

Versteegh, G.J.M., Blokker, P., Bogus, K.A., Harding, I.C., Lewis, J., Oltmanns, S., Rochon, A., Zonneveld, K.A.F., 2012. Infra red spectroscopy, flash pyrolysis, thermally assisted hydrolysis and methylation (THM) in the presence of tetramethylammonium hydroxide (TMAH) of cultured and sediment-derived *Lingulodinium polyedrum* (Dinoflagellata) cyst walls. *Organic Geochemistry* 43: 92–102.

Villanoy, C.L., Corrales, R.A., Jacinto, G.S., Cuaresma Jr., N.T., Crisostomo, R.P., 1996. Towards the development of a cyst-based model for *Pyrodinium* red tides in Manila Bay, Philippines. In Yasumoto, T., Oshima, Y., Fukuyo, Y. [Eds.], *Harmful and Toxic Algal Blooms*. Intergovernmental Oceanographic Commission (IOC) of UNESCO, Paris, pp. 189–192.

Wall, D., Dale, B., Harada, K., 1973. Descriptions of new fossil dinoflagellates from the Late Quaternary of the Black Sea. *Micropaleontology* 19: 18–31.

Wall, D., Dale, B., Lohmann, G.P., Smith, W.K., 1977. The environmental and climatic distribution of dinoflagellate cysts in modern marine sediments from regions in the North and South Atlantic Oceans and adjacent seas. *Marine Micropaleontology* 2: 121–200.

Zonneveld, K.A.F., Chen, L., Möbius, J., Mahmoud, M.S., 2009. Environmental significance of dinoflagellate cysts from the proximal part of the Po-river discharge plume (off southern Italy, Eastern Mediterranean). *Journal of Sea Research* 52: 189–213.

Zonneveld, K.A.F., Chen, L., Elshanawany, R., Fischer, H.W., Hoins, M., Ibrahim, M.I., Pittauerova, D., Versteegh, G.J.M., 2012. The use of dinoflagellate cysts to separate human-induced from natural variability in the trophic state of the Po River discharge plume over the last two centuries. *Marine Pollution Bulletin* 64: 114–132.

Depth (cm)	Accumulated mass (g cm ⁻²)	²¹⁰ Pb activity (Bq kg ⁻¹)	Uncertainty ²¹⁰ Pb activity (Bq kg ⁻¹)	²³⁷ Cs activity (Bq kg ⁻¹)	Uncertainty ²³⁷ Cs activity (Bq kg ⁻¹)
0,5	0,17	75,96	5,5	2,57	0,20
1,5	0,60	68,37	4,6		
2,5	1,17	64,18	4,2		
3,5	1,82	65,19	4,8		
4,5	2,61	66,03	4,9		
5,5	3,36	56,69	3,7	1,74	0,14
6,5	4,11	56,85	4,3		
7,5	4,97	64,19	4,7		
8,5	5,76	54,69	3,8		
9,5	6,57	52,73	3,8	2,45	0,20
10,5	7,37	41,07	2,7	4,15	0,21
11,5	8,19	45,48	3,7	4,58	0,27
13,5	9,71	36,96	3,0	3,18	0,22
14,5	10,52	33,83	2,7	2,80	0,21
15,5	11,32	29,84	2,0	2,70	0,20
16,5	12,17	28,35	2,1		
17,5	13,08	28,24	2,2	1,19	0,14
18,5	13,81	28,09	2,2		
19,5	14,51	23,83	1,8		
20,5	15,29	25,47	1,7		
21,5		26,28	1,9		
22,5		23,68	1,5		
23,5		18,48	1,4		
25,5		19,79	1,3		
26,5		22,45	1,5		
27,5		24,24	1,7		
30,5		19,55	1,3		
32,5		23,97	1,7		
33,5		23,52	1,7		
40,5		19,15	1,3		
43,5		22,16	1,7		
45,5		21,39	1,5		
47,5		20,67	1,6		
55,5		21,25	1,6		
56,5		19,91	1,3		

Table 1. Records of ²¹⁰Pb activity (Bq·kg⁻¹) and ²³⁷Cs activity (Bq·kg⁻¹) as function of depth.

Depth (cm)	CaCO ₃ (%)	C _{org} (%)	Granulometry			Al (%)	TI (%)	Cl (%)	Br (µg g ⁻¹)
			Clays (%)	Silt (%)	Sand (%)				
0,5	4,12	1,19	6,62	83,1	10,28	9,41	0,70	0,93	25,7
1,5	2,33	0,9	6,14	82,19	11,67	9,44	0,67	0,76	17,1
2,5	2,61	1,13	5,73	80,61	13,67	8,99	0,68	0,62	11,9
3,5	2,66	0,76	5,32	80,94	13,74	8,96	0,66	0,50	7,9
4,5	3,24	0,65	6,19	82,22	11,59	9,08	0,65	0,44	3,5
5,5	3,28	0,77	5,45	80,89	13,66	9,20	0,66	0,45	1,3
6,5	3,02	0,66	5,12	79,03	15,85	8,97	0,66	0,41	0,9
7,5	1,47	0,6	5,62	83,75	10,63	9,03	0,66	0,46	1,6
8,5	3,36	0,8	5,27	82,31	12,42	8,89	0,65	0,44	
9,5	3,42	0,52	5,59	83,36	11,05	9,21	0,64	0,52	
10,5	3,20	0,41	5,2	78,36	16,44	9,35	0,65	0,58	
11,5	3,96	0,57	5,61	83,77	10,62	9,26	0,64	0,57	
12,5	2,72	0,63	6,31	84,02	9,67	9,28	0,65	0,60	
13,5	3,68	0,63	5,87	83,8	10,32	9,19	0,65	0,61	
14,5	3,23	0,77	6,01	81,4	12,6	9,36	0,64	0,61	
15,5	3,36	0,7	9,75	90,25	0	9,47	0,64	0,64	
16,5	3,24	0,44	7,48	85,56	6,96	9,24	0,63	0,58	
17,5	3,18	0,53	7,24	85,03	7,72	9,18	0,65	0,58	
18,5	2,93	0,53	9,37	86,04	4,59	9,19	0,65	0,55	
19,5	3,37	0,89	7,9	87,04	5,05	9,34	0,66	0,55	
20,5	4,79	0,92	8,56	84,16	7,28	9,04	0,65	0,55	
21,5	2,98	0,95	7,84	81,61	10,56	9,48	0,64	0,53	
22,5			7,98	78,24	13,78	9,45	0,64	0,53	
23,5	4,18	0,64	8	76,45	15,55	9,67	0,66	0,52	
24,5			7,5	69,13	23,37	9,42	0,65	0,46	
25,5	2,96	0,8	8,32	75,1	16,58	9,73	0,66	0,56	
26,5	3,39	0,89	9,73	80,08	10,19	9,43	0,66	0,55	
27,5	3,84	0,82	10,29	84,79	4,92	9,72	0,67	0,60	
28,5			9,59	83,71	6,69	9,73	0,68	0,62	
29,5			8,86	87,34	3,81	9,67	0,69	0,65	1,4
30,5	4,75	1,04	10,4	85,48	4,13	9,68	0,67	0,64	3,1
31,5			10,07	85,96	3,96	9,70	0,68	0,67	4,4
32,5	4,77	1,16	10,59	84,36	5,06	9,42	0,67	0,69	4,2
33,5	5,29	1,06	10	85,18	4,82	9,63	0,68	0,70	5,2
34,5			9,68	84,72	5,6	9,73	0,68	0,69	5,7
35,5			9,83	83,18	6,99	9,15	0,66	0,67	3,4
36,5	5,91	0,98	9,34	84,77	5,89	9,07	0,67	0,68	4,5
37,5			8,97	83,89	7,14	9,05	0,66	0,67	4,2
38,5			8,51	83,5	7,98	8,87	0,65	0,66	1,4
39,5			8,34	85,15	6,51	9,05	0,66	0,66	2,2
40,5	5,50	0,76	7,99	79,65	12,36	9,36	0,64	0,68	
41,5			7,75	82,65	9,61	9,17	0,64	0,65	
42,5			8,21	79,9	11,88	9,16	0,65	0,66	1,2
43,5	6,74	0,99	8,05	82,39	9,55	9,39	0,62	0,67	0,7
44,5			9,69	79,64	10,67	9,25	0,64	0,71	1,5
45,5	6,80	0,81	10,22	81,88	7,9	9,14	0,64	0,68	3
46,5			10,35	80,54	9,11	9,51	0,66	0,74	4,6
47,5	6,81	0,73	9,38	84,43	6,19	9,27	0,64	0,73	5,1
48,5			10,96	88,15	0,89	9,35	0,64	0,76	5,2
49,5			9,34	82,41	8,25	9,25	0,65	0,74	3,2
50,5	7,01		10,87	81,71	7,42	9,20	0,65	0,72	3
51,5			8,92	80,2	10,88	9,42	0,66	0,73	2,1
52,5			10,25	78,4	11,35	9,24	0,63	0,71	
53,5	7,18		9,59	78,38	12,03	9,34	0,64	0,71	
54,5			9,6	77,92	12,48	9,16	0,64	0,70	
55,5	6,98		9,12	78,97	11,91	9,17	0,64	0,71	
56,5	7,09		9,67	77,51	12,83	9,33	0,64	0,73	

Table 2. Geochemical and grain size data.

Depth (cm)	Age (CE)	Mass accumulation rate ($\text{g cm}^{-2} \text{yr}^{-1}$)	Dinocyst concentrations (cyst g^{-1})	Gymnosperm concentrations (grain g^{-1})	Angiosperm concentrations (grain g^{-1})	Organic lining concentrations (lining g^{-1})	Flux of dinocyst (cyst $\text{cm}^{-2} \text{yr}^{-1}$)	Flux of gymnosperma (grain $\text{cm}^{-2} \text{yr}^{-1}$)	Flux of angiosperma (grain $\text{cm}^{-2} \text{yr}^{-1}$)	Flux of organic lining (lining $\text{cm}^{-2} \text{yr}^{-1}$)
0,5	2011	0,210	3473	4235	9669	2557	731	891	2034	538
1,5	2009	0,230	3331	2077	8542	938	766	478	1965	216
2,5	2007	0,234	4401	1907	4034	1012	1030	446	944	237
3,5	2004	0,209	2620	1310	2157	2253	547	273	450	470
4,5	1999	0,180	1558	1066	4246	1377	281	192	766	248
6,5	1991	0,176	4649	1749	3351	2142	819	308	591	377
7,5	1986	0,122	2048	1553	4940	2200	250	189	602	268
8,5	1979	0,128	2206	1236	5290	1434	283	159	679	184
9,5	1972	0,110	2921	1163	5119	1675	322	128	565	185
10,5	1966	0,142	2244	1669	5702	1558	320	238	812	222
11,5	1958	0,093	2537	1327	3592	1572	237	124	335	147
12,5	1950	0,087	9510	1039	2740	2299	824	90	237	199
13,5	1941	0,084	13265	1392	2436	2697	1108	116	204	225
14,5	1931	0,076	5265	1728	5888	2784	400	131	447	211
15,5	1920	0,080	16454	2132	3827	3499	1318	171	306	280
16,5	1908	0,058	5373	1559	7171	1559	366	106	489	106
17,5	1900	0,055	10867	1708	3816	1963	598	94	210	108
18,5	1891	0,041	10984	1139	3049	2792	452	47	126	115
19,5	1878	0,072	8214	1585	6444	2139	593	114	465	155
21,5	1859	0,046	10614	1011	4246	4616	488	46	195	212
22,5	1822	0,046	13280	998	2864	5642	611	46	132	260
23,5	1806	0,046	6922	708	1325	3130	318	33	61	144
24,5	1790	0,046	4910	421	1394	1442	226	19	64	66
25,5	1772	0,046	12904	647	2184	3843	594	30	100	177
26,5	1759	0,046	10902	486	1944	2222	502	22	89	102
27,5	1746	0,046	6639	311	1680	1431	305	14	77	66
28,5	1734	0,046	11174	362	2314	1157	514	17	106	53
29,5	1721	0,046	6886	492	3800	805	317	23	175	37
31,5	1695	0,046	4078	490	1642	728	188	23	76	33
32,5	1681	0,046	5682	480	2250	1310	261	22	104	60
33,5	1670	0,046	15791	570	3728	2485	726	26	171	114
34,5	1658	0,046	6735	570	2523	1163	310	26	116	53
35,5	1646	0,046	7074	374	3315	1004	325	17	152	46
36,5	1634	0,046	10091	887	4799	2564	464	41	221	118
37,5	1622	0,046	12466	807	3349	1614	573	37	154	74
39,5	1596	0,046	9533	800	4447	3487	439	37	205	160
41,5	1568	0,046	11873	-	-	-	546	-	-	-
43,5	1540	0,046	11455	413	3080	5634	527	19	142	259
45,5	1514	0,046	14359	1057	3362	6867	661	49	155	316
48,5	1479	0,046	14384	317	2804	3528	662	15	129	162

Table 3. Palynomorph concentrations and fluxes over depth.

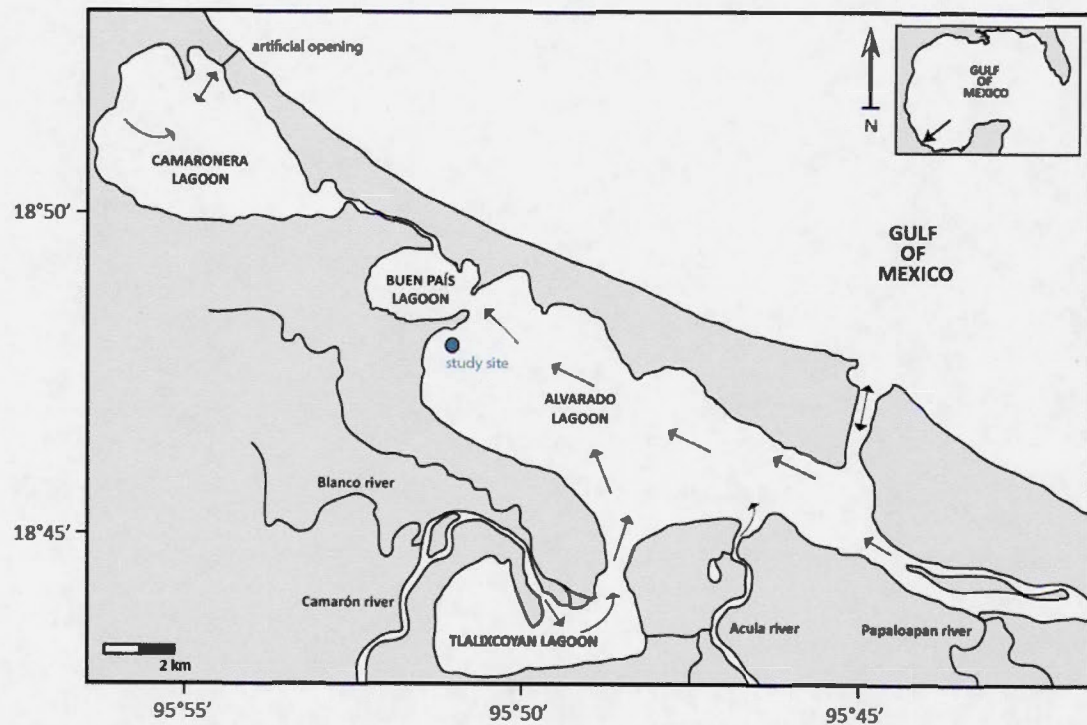


Figure 1. Study area with position of core site and surface circulation. Modified from Castañeda Chávez et al. (2005).

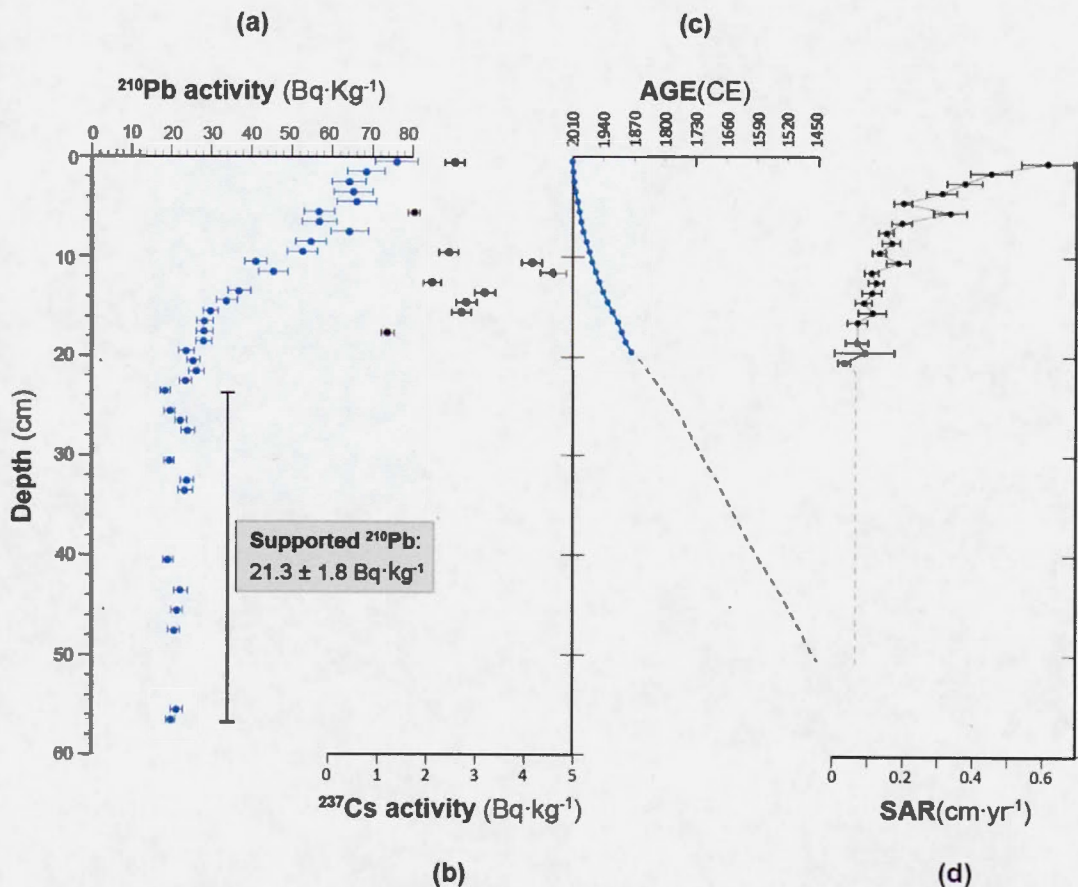


Figure 2. (a) Records of ^{210}Pb activity ($\text{Bq}\cdot\text{kg}^{-1}$) and (b) ^{237}Cs activity ($\text{Bq}\cdot\text{kg}^{-1}$) as function of depth, (c) age model, (d) sediment accumulation rate (SAR) over depth. Dashed line represents extrapolated age model and extrapolated SAR.

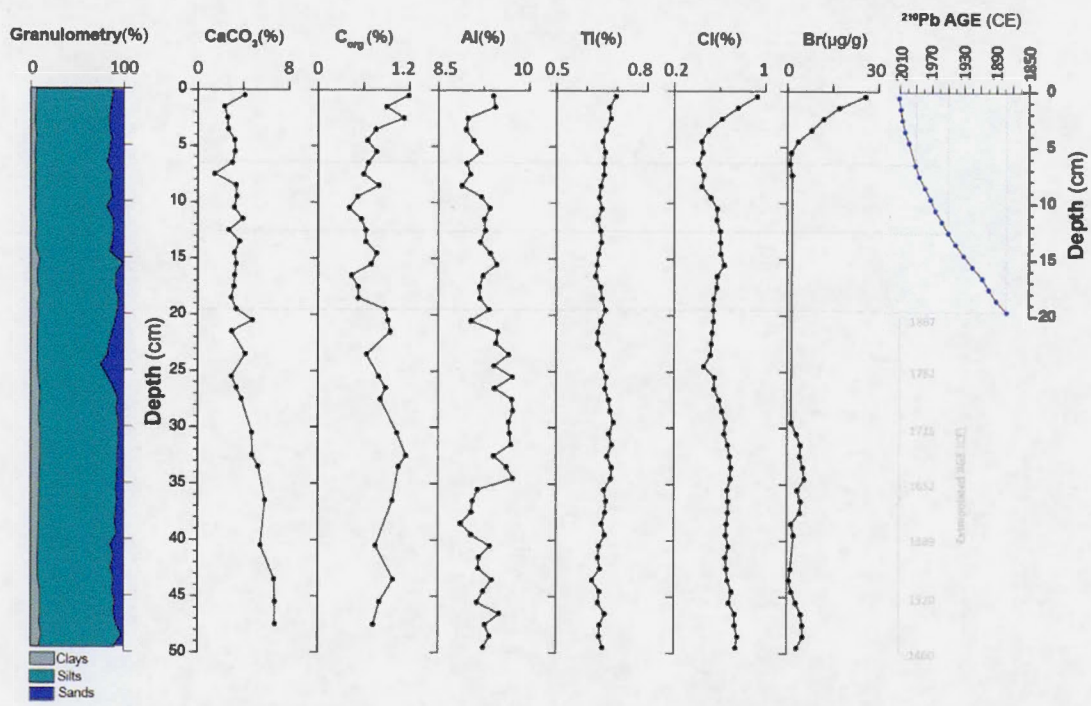


Figure 3. Results of geochemical and grain size analyses, and age model: granulometry (%) and relative abundances of carbonate (CaCO_3 ; %), organic carbon (C_{org} ; %), aluminum (%), titanium (%), chlorine (%), bromine ($\mu\text{g/g}$).

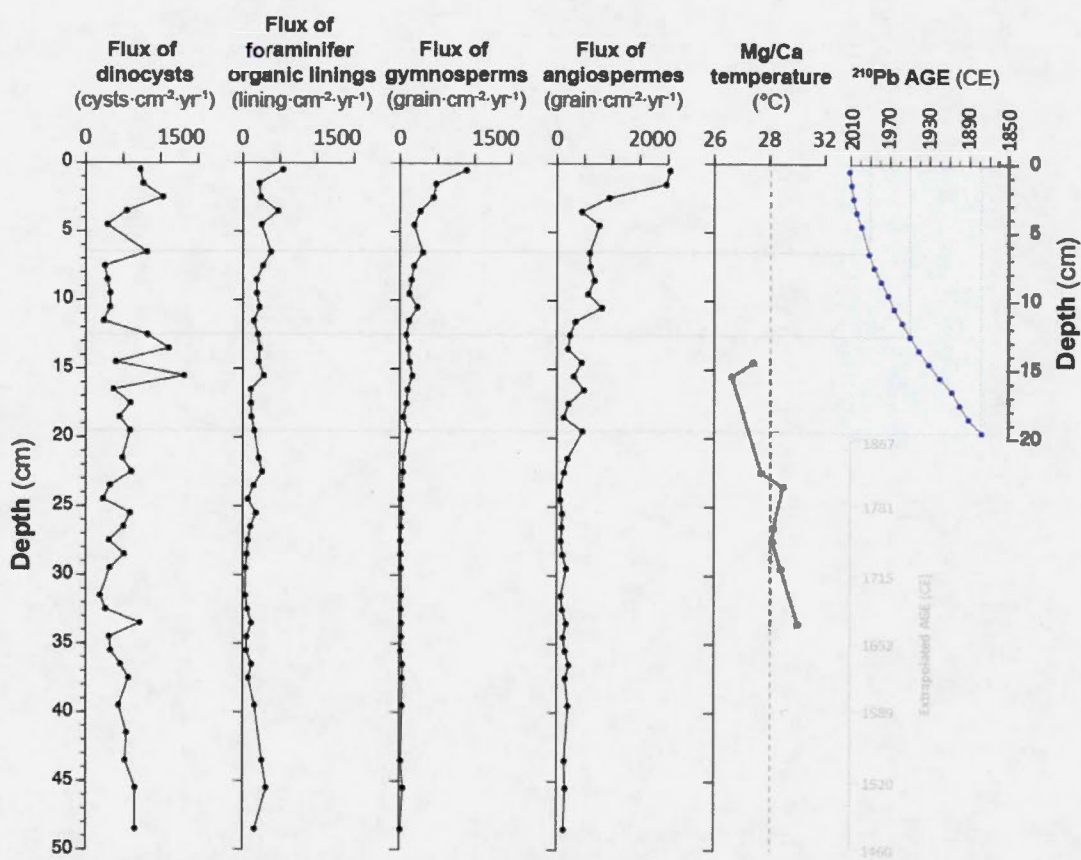


Figure 4. Fluxes of dinocysts ($\text{cysts}\cdot\text{cm}^{-2}\cdot\text{yr}^{-1}$), organic foraminifer linings ($\text{linings}\cdot\text{cm}^{-2}\cdot\text{yr}^{-1}$), gymnosperm pollen ($\text{grains}\cdot\text{cm}^{-2}\cdot\text{yr}^{-1}$) and angiosperm pollen ($\text{grains}\cdot\text{cm}^{-2}\cdot\text{yr}^{-1}$), temperatures inferred from Mg/Ca ratios of foraminifer shells, and age model.

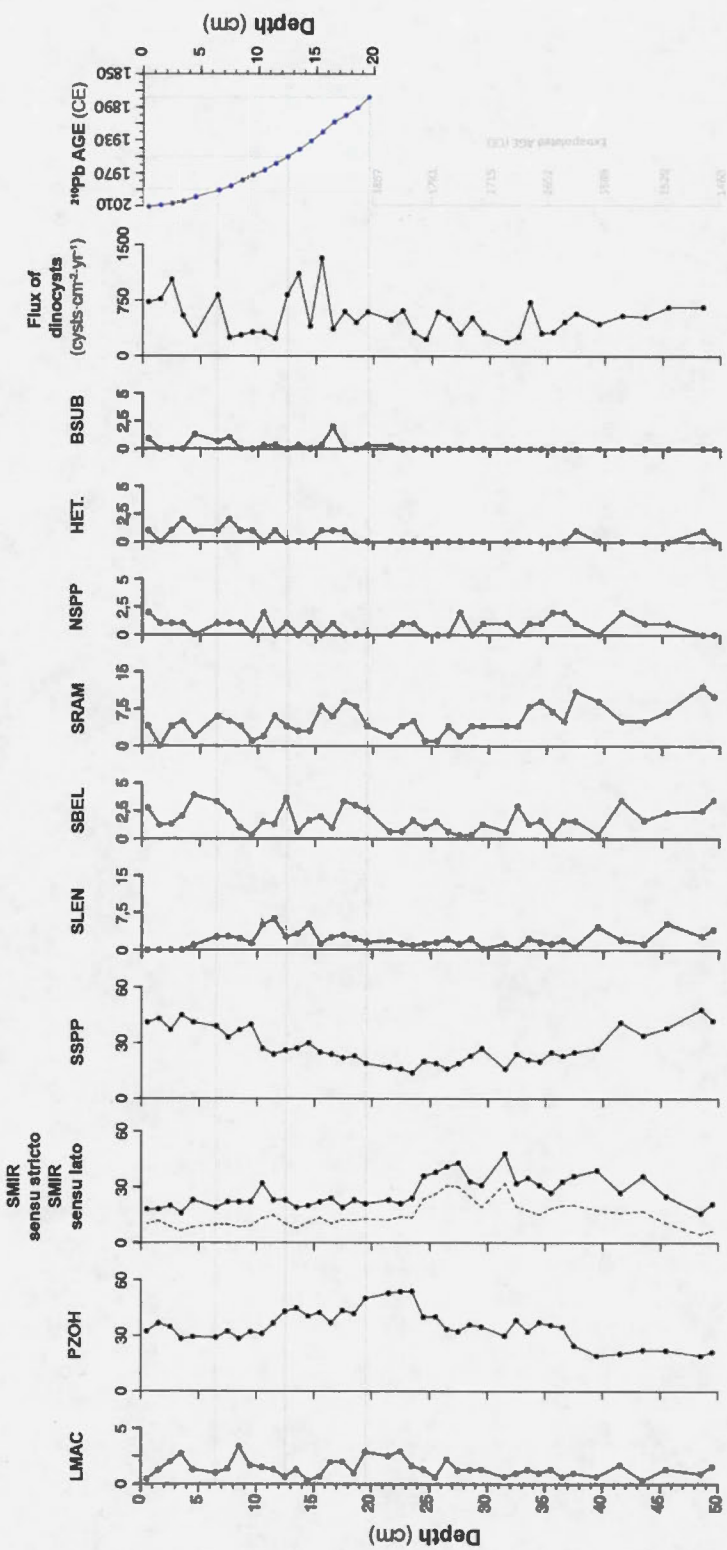


Figure 5. Relative abundance of the main dinocyst taxa (%), total cyst fluxes ($\text{cysts} \cdot \text{cm}^{-2} \cdot \text{yr}^{-1}$), and age model. Abbreviations: LMAC: *Lingulodinium machaerophorum*, PZOH: *Polysphaeridium zoharyi*, SMIR sensu stricto: *Spiniferites mirabilis* only, SMIR sensu lato: *Spiniferites mirabilis* and *Spiniferites hyperacanthus*, SSPP: *Spiniferites* spp., SLEN: *Spiniferites cf. lenzii*, SBEL: *Spiniferites belerius*, SRAM: *Spiniferites ramosus*, NSPP: *Nematosphaeropsis* spp., HET: total heterotrophic taxa and BSUB: remains of *Bryostomatum subsalsum*.

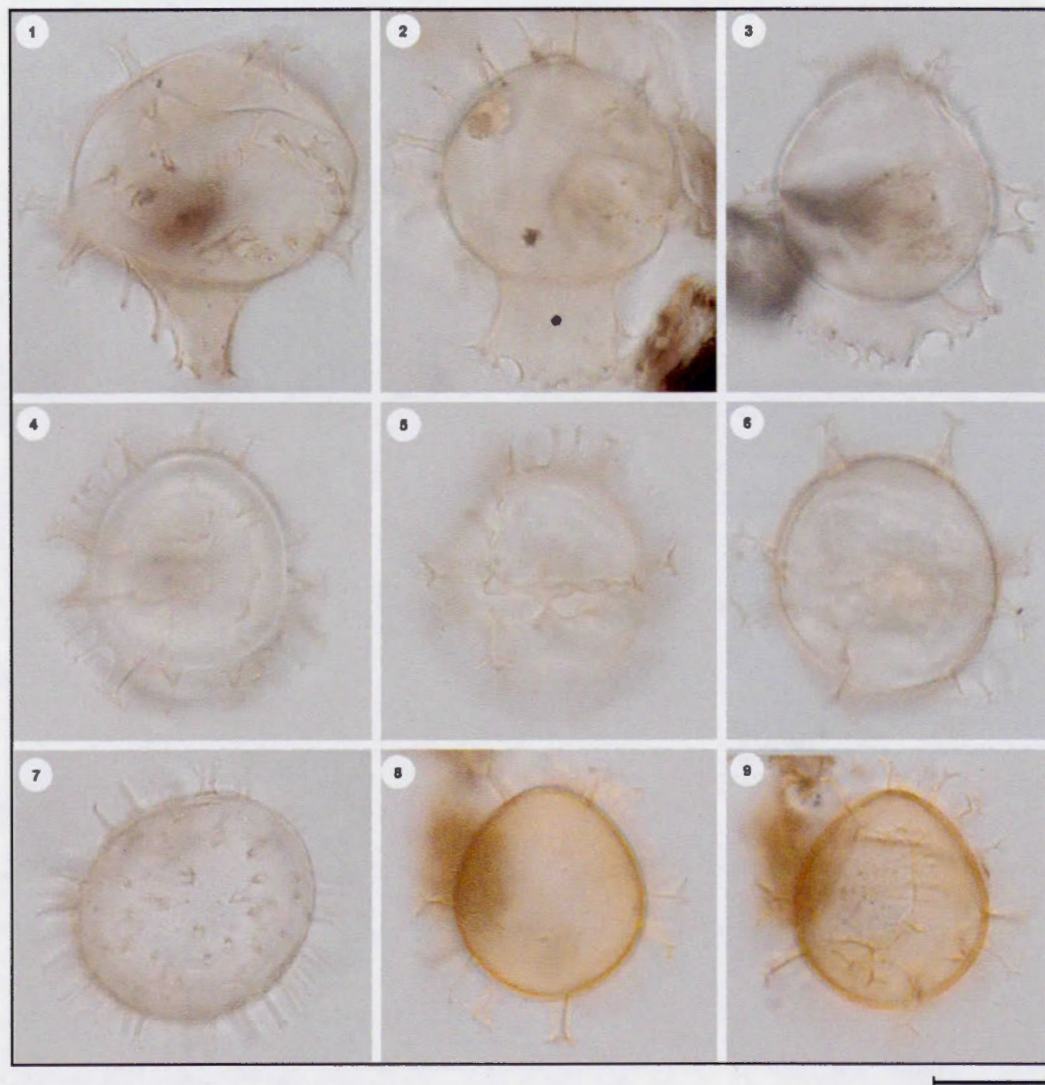


Plate 1. Bright field light micrographs of selected dinoflagellate cyst species (1-3) *Spiniferites mirabilis* sensu stricto. Note the important morphological variations that characterize this taxon. (4-6) *Spiniferites* cf. *lenzii*. High to low focal planes. (7) *Polysphaeridinium zoharyi* (8-9) *Spiniferites* cf. *delicatus*. Scale bar: 20 μm .

Depth (cm)	Concentration dinocysts (Cyst g ⁻¹)																
	Dry weight sediment/slide (g/slide)																
TOTAL	Lycopodium chlorotum counted	Lycopodium chlorotum added	Dry weight sediment (g)	Dry weight sediment (g)	Concentration dinocysts (Cyst g ⁻¹)												
0.5																	
1.5	1	0	0	0	0	0	0	0	0	0	0	0	0	0	3506		
2.5	6	0	2	1	0	104	0	13	4	0	26	34	0	0	3331		
3.5	8	0	3	0	0	83	1	14	6	2	0	19	29	0	0	4401	
4.5	4	0	1	0	0	90	1	7	12	3	0	26	45	1	0	2682	
6.5	3	3	0	0	0	87	2	16	2	10	3	0	29	28	2	1	3903
7.5	4	3	0	0	0	95	0	14	7	4	1	29	35	0	1	0	1138
8.5	10	3	0	0	1	84	0	11	3	5	1	25	40	0	2	0	35791
9.5	5	0	1	0	0	95	0	3	1	27	39	2	0	113	0	0	0
10.5	5	1	4	0	0	102	0	5	5	1	0	44	50	0	0	0	404
11.5	4	0	1	0	0	111	0	12	4	3	1	27	39	1	0	0	31358
12.5	2	0	3	0	0	130	0	12	11	1	1	31	37	0	0	0	3903
13.5	4	1	0	0	0	137	0	7	2	1	2	24	35	0	0	0	0
14.5	1	2	0	1	0	123	0	5	2	3	33	28	1	0	0	0	0
15.5	2	0	0	0	0	128	0	15	6	2	9	41	26	0	0	0	0
16.5	6	2	0	0	0	112	0	14	3	4	31	42	0	1	0	0	0
17.5	6	1	0	0	0	130	1	20	10	0	6	37	21	0	0	0	0
18.5	9	1	0	0	0	125	0	19	9	0	5	36	34	0	1	0	0
19.5	9	1	0	0	0	156	0	11	8	1	3	40	26	0	0	0	0
21.5	14.5	2	0	0	0	167	0	5	2	1	2	39	33	0	51	0	0
22.5	9	4	0	0	0	164	0	8	2	0	4	43	21	0	0	0	0
23.5	5	2	1	0	0	163	0	14	5	0	1	41	31	0	1	0	0
24.5	4	1	0	1	0	121	0	3	3	0	0	71	37	0	0	0	0
25.5	2	0	1	0	0	120	0	3	5	0	0	57	4	0	0	0	0
26.5	7	0	1	0	0	128	0	3	5	0	0	84	36	0	1	0	0
27.5	8	0	2	0	0	163	0	4	1	0	2	97	41	0	0	0	0
28.5	4	0	0	0	0	111	0	4	1	0	7	77	26	0	1	0	0
29.5	4	0	3	0	0	107	0	8	4	0	5	59	38	0	0	1	0
31.5	2	2	0	0	0	92	0	10	2	1	1	62	38	0	0	0	0
32.5	3	0	0	3	0	118	0	10	9	1	2	60	38	1	0	0	0
33.5	4	2	0	1	0	98	0	16	4	3	7	53	54	0	1	55	0
34.5	3	1	1	0	0	114	0	19	5	3	10	47	47	0	0	0	0
35.5	4	7	0	0	0	108	0	14	1	2	7	56	26	0	1	0	0
36.5	2	5	0	1	0	106	0	13	5	1	1	62	38	0	0	0	0
37.5	3	2	0	2	0	76	0	27	5	2	6	63	48	0	0	71	0
39.5	2	0	1	0	0	57	0	18	1	1	9	52	64	0	1	76	0
41.5	5	4	1	0	0	59	0	9	10	0	6	47	33	0	0	110	0
43.5	1	1	2	0	0	68	0	9	5	0	7	52	57	0	1	97	4
45.5	4	3	0	0	0	66	0	14	7	1	7	32	42	0	0	106	16
46.5	3	0	1	0	0	61	0	34	8	1	5	15	36	0	0	143	9
49.5	5	1	0	0	0	67	0	18	11	3	13	21	45	0	0	118	13

Supplementary material. Raw dinocyst counts.

CONCLUSION GÉNÉRALE

Cette thèse avait comme principal objectif de caractériser l'évolution spatiale et temporelle des dinoflagellés nuisibles dans le Golfe du Mexique à partir d'enregistrements sédimentaires. Les analyses palynologiques réalisées dans le cadre de cette étude fournissent de nouvelles informations sur la distribution d'espèces potentiellement toxiques, notamment *Pyrodinium bahamense*, et permettent de souligner le potentiel risque que présentent certaines zones pour le développement de blooms nuisibles. À cet effet, les systèmes lagunaires du Mexique (ex. Lagune Alvarado) sont à la fois caractérisés par des abondances relatives très élevées de *Polysphaeridium zoharyi* (produit par *P. bahamense*) et saisonnièrement soumis à des événements de resuspension sédimentaire. Dans plusieurs autres milieux tropicaux ou subtropicaux similaires (*Indian Lagoon*, Florida ; Baie de Manille, Philippines), ces paramètres jouent un rôle majeur pour le déclenchement d'efflorescences nuisibles. Les réservoirs de kystes de ces lagunes méritent donc une attention particulière puisque ceux-ci représentent une menace potentielle pour l'économie régionale, laquelle repose largement sur les réserves halieutiques. En outre, étant donné que les efflorescences algales sont généralement sporadiques, l'étude des dépôts de kystes dans les sédiments s'avère complémentaire aux observations de microplancton et a le potentiel d'apporter de nouveaux éléments pour la compréhension des paramètres environnementaux régissant leur formation. Ce type d'approche, combinée par exemple à des analyses de biomarqueurs, peut représenter une avenue intéressante pour l'analyse de l'évolution et la surveillance des espèces impliquées dans la formation des efflorescences algales nuisibles.

Cette étude donne également un aperçu de la composition des assemblages de dinokystes sur l'ensemble du Golfe du Mexique. Elle a permis le développement d'une base de données régionale qui pourra éventuellement être utilisée dans le cadre de reconstitutions paléoenvironnementales. Cette dernière représente un complément

important à la base de données de l'hémisphère Nord (<http://www.geotop.ca/fr/bases-de-donnees/dinokystes.html>). De plus, cette étude renforce notre compréhension de l'autoécologie des dinokystes dans les basses latitudes et plusieurs observations importantes en découlent :

- Les assemblages de dinokystes du golfe du Mexique incluent des taxons qui n'ont pas ou n'ont été que très rarement observés dans la flore de dinokystes de l'Atlantique Nord depuis le Pliocène. Parmi ces espèces, l'observation de *Melitasphaeridium choanophorum* est importante puisque cette espèce était auparavant considérée éteinte depuis la fin du Pléistocène. Sa présence moderne dans le Golfe du Mexique suggère que le bassin ait fonctionné comme refuge permettant la persistance d'espèces endémiques. Elle implique également une modification des limites biostratigraphiques qui étaient assignées à *M. choanophorum*.
- Pour la première fois, des kystes fossiles associés à un dinoflagellé benthique ont été identifiés dans la lagune Alvarado. Cette observation est une contribution originale qui permet de documenter le cycle de vie des dinoflagellés benthiques. Le dinoflagellé *Bysmatrum subsalsum*, auquel ils sont associés, est à l'origine d'efflorescences de biomasse élevée et la production de kystes pourrait jouer un rôle dans la dynamique de formation de ses blooms.
- La morphologie des dinokystes examinés dans les milieux côtiers consolide l'hypothèse selon laquelle des conditions variables de salinité et température ainsi que la profondeur de la colonne d'eau exercent une influence significative sur le développement des kystes. Cet aspect est particulièrement bien exprimé chez les différentes espèces de *Spiniferites* dans la lagune Alvarado.

Par ailleurs, les enregistrements sédimentaires ont permis de documenter l'évolution des conditions climatiques au nord du golfe du Mexique au cours de l'Holocène et de la fin du Pléistocène. Une étude multi-proxy effectuée sur la carotte ODP-625B combine des analyses palynologiques à des analyses d'isotopes de l'oxygène et de rapports Mg/Ca sur des tests de foraminifères. Des changements marqués au niveau des assemblages de dinokystes ponctuent le passage des périodes glaciaires vers des périodes interglaciaires. Alors que les stades isotopiques froids sont caractérisés par des assemblages océaniques oligotrophes, les interstades sont dominés par des espèces plus typiques des environnements chauds. Malgré des faibles différences de température entre la dernière période interglaciaire et l'interglaciaire actuel ($\sim 1\text{--}2^\circ\text{C}$, selon les analyses Mg/Ca), les assemblages de dinokystes sont significativement distincts, ce qui souligne des différences dans les paramètres hydrologiques (i.e. circulation de surface, bathymétrie) entre ces deux périodes. L'importance des paramètres environnementaux autres que la température pour la distribution des dinokystes en milieu tropical est en outre illustrée. Cet aspect ouvre notamment la voie à des recherches plus approfondies sur l'influence de l'étendue du plateau continental sur la production de kystes par certaines espèces de dinoflagellés.

Perspectives de recherches futures

L'endémisme et le caractère unique des assemblages de dinokystes du golfe du Mexique soulignent la pertinence d'enrichir la base de données régionale, notamment par l'ajout de sites sur le plateau continental du nord et de l'ouest du bassin. Dans ces régions, il serait intéressant d'étudier l'influence des apports d'eaux douces du Mississippi sur la productivité primaire et la relation entre les processus d'eutrophisation, le développement de zones hypoxiques et les proliférations algales nuisibles. Par ailleurs, puisqu'une distribution spatiale très étendue de *P. bahamense* est déduite des enregistrements sédimentaires microfossiles, il serait pertinent de

mettre cette espèce en culture afin de caractériser sa toxicité locale. Cet aspect serait crucial dans une perspective de surveillance et de sensibilisation à la problématique de blooms nuisibles. Enfin, l'obtention d'une image plus complète de l'évolution à long terme des dinoflagellés nuisibles devrait impérativement lier les travaux palynologiques à d'autres traceurs moléculaires. Cela permettrait d'intégrer également certaines espèces de dinoflagellés nuisibles qui ne produisent pas de kystes fossilisables.

APPENDICE A

FIRST REPORT OF SUB-RECENT FOSSILIZED CYSTS PRODUCED BY THE BENTHIC *BYSMATTRUM SUBSALSUM* (DINOPHYCEAE) FROM A SHALLOW MEXICAN LAGOON IN THE GULF OF MEXICO

Audrey Limoges¹, Kenneth Neil Mertens², Ana-Carolina Ruíz-Fernández³, Anne de Vernal¹

¹ Geotop, Université du Québec à Montréal, Canada

² Research Unit for Palaeontology, Ghent University, Belgium

³ Instituto de Ciencias del Mar y Limnología, Universidad Nacional Autónoma de México, Mexico

Research Note accepté pour publication dans la revue *Journal of Phycology*
[DOI: 10.1111/jpy.12257](https://doi.org/10.1111/jpy.12257)

Résumé

Des kystes produits par le dinoflagellé benthique *Bysmatrum subsalsum* ont été observés dans des échantillons sédimentaires ayant subi des traitements palynologiques, collectés dans la lagune Alvarado (sud-ouest du golfe du Mexique). Ces kystes sont morphologiquement très semblables à la thèque de *B. subsalsum* et l'autofluorescence de leur paroi suggère une composition similaire à celles des kystes produits par des dinoflagellés phototrophes. Ces observations sont très importantes pour notre compréhension du cycle de vie et de l'écologie de cette espèce. Les processus d'enkystement pourraient jouer un rôle déterminant dans la dynamique de formation des blooms nuisibles auxquels cette espèce est associée: la formation d'une réserve de kystes dans les sédiments peut faciliter la réinoculation de la colonne d'eau lorsque les conditions environnementales redeviennent favorables. Il s'agit du premier enregistrement d'un kyste de dinoflagellé benthique fossilisé et récupéré à partir de sédiments sub-récents.

Mots-clés: Dinosporine, Kyste de résistance, Lagune Alvarado, Marée rouge, Palynologie

Abstract

Cysts belonging to the benthic dinoflagellate *Bysmatrum subsalsum* were recovered from palynologically treated sediments collected in the Alvarado Lagoon (southwestern Gulf of Mexico). The cysts are proximate, reflecting the features of the parent thecal stage, and their autofluorescence implies a dinosporin composition similar to the cyst walls of phototrophic species. This finding is important for our understanding of *B. subsalsum* life cycle transitions and ecology. Encystment may play an important role in the bloom dynamics of this species as it can enable the formation of a sediment cyst bank that allows reinoculation of the water column when conditions become favorable. This is the first report of a fossilized cyst produced by a benthic dinoflagellate recovered from sub-recent sediments.

Keywords: Alvarado Lagoon, Dinosporin, Palynology, Red Tide, Resting cyst

Benthic dinoflagellates belonging to the genus *Bysmatrum* are photosynthetic marine species that are typically observed in shallow tropical and subtropical environments (Lombard and Capon 1971, Horiguchi and Chihara 1983, Horiguchi and Pienaar 1988, Faust and Steidinger 1998), where they have been associated with the formation of red tides (Lombard and Capon 1971, Horiguchi and Pienaar 1988, Faust et al. 1996). Although originally classified as *Scrippsiella* (Faust 1996, Steidinger and Tangen 1996), the species were subsequently transferred to the genus *Bysmatrum* on the basis of their reticulated thecal surface and plate configuration: the intercalary plates 2a and 3a are separated from each other by the apical plate 3', a morphological feature that is not present in *Scrippsiella* (Faust and Steidinger 1998, Murray et al. 2006). In addition to these morphological differences, molecular sequencing analyses recently confirmed that *Bysmatrum* is genetically different from *Scrippsiella*, and forms an isolated and uncertain position outside the Thoracosphaeraceae (Gottschling et al. 2012, Jeong et al. 2012).

About 15% of living planktic dinoflagellate species are known to produce fossilizable organic-walled or calcareous resting cysts (Head 1996). However, cysts produced by benthic dinoflagellates have only been reported from culture experiments, but never from sub-surface sediments. For example, hyaline division cysts have been described in cultures of *Prorocentrum* species, but resting cyst descriptions are considered questionable (Hoppenrath et al. 2013). For *Ostreopsis* species, only pellicle cysts have been reported (Bravo et al. 2012), and the cysts described from the related species *Coolia monotis* by Faust (1992) are also probably pellicle cysts (Bravo and Figueroa 2014). In the genus *Bysmatrum*, an ovoid cyst was reported for *Bysmatrum subsalsum* by Ostenfeld (1908, as *Peridinium subsalsum*). However, he did not provide a drawing or photograph, and doubt still persists whether this was indeed a resting cyst instead of pellicle cyst. More recently, coccoid stages of *Bysmatrum subsalsum* were reported from culture experiments (Gottschling et al. 2012) and an unidentified *Bysmatrum* species was germinated from an

undescribed cyst in (sub-)surface sediments from an estuarine bay in the Mediterranean (Satta et al. 2013). Here we report well-preserved cysts of *Bysmatrum subsalsum* extracted from sediments that show autofluorescence and withstand standard palynological processing.

Samples were taken at a 1 cm interval from a 50 cm sediment core recovered from the Alvarado Lagoon (1.5 m water depth) in 2011 (Veracruz, Mexico; 18.7979°N; 95.8579°W). A sampling resolution of ~2-4 years was calculated from average sediment accumulation rates (0.03 to 0.61 cm/yr) from ^{210}Pb measurements (Fig. 1). Sampling was performed using a gravity corer (UWITEC) with a clear PVC liner (9 cm diameter) and samples were kept refrigerated at 4°C until analyses. During palynological treatment, approximately 5g of dried sediment was wet sieved between 106 and 10 μm to remove the coarse and fine fraction. The remaining fraction was then submitted to repeated macerations with warm HCl (10%) and warm HF (49%) in order to remove carbonate and silicate particles, respectively. This treatment includes maceration with HF overnight (for details see de Vernal et al. 1996). The organic residue was sieved again on a 10 μm nylon mesh and the retained fraction was mounted in glycerine gelatin for observation under a Leica DMR light microscope and a Leitz Orthoplan fluorescence microscope. Color staining was not applied to avoid imparting artificial fluorescence. One specimen was isolated using a micropipette onto a glass slide, subsequently air-dried, and observed with a Hitachi S-3400N scanning electron microscope (SEM) (Fig. 2). Specimens were not coated before observation.

Twenty-six cysts were observed in samples during routine palynological counting from the upper 22 cm of the core. This interval corresponds to approximately 170 years (Fig. 1). According to the fairly low to moderate sedimentary organic carbon contents (0.4-1.2%) and palynological observations, there is no reason to believe that the presence of the observed cysts is related to exceptionally good preservation of organic material (Fig. 1). All specimens exhibit yellowish autofluorescence under excitation by blue light and this allows visualization of the

paratabulation (Fig. 3, micrographs 6, 12 and 14). While autofluorescence in living cells is generally associated with chlorophyll or other intracellular bodies (Lessard and Swift 1986), the thecal plates of living cells are not autofluorescent, and need staining with Calcofluor White to observe the bright blue fluorescence of cellulose (Fritz and Triemer 1985, Sekida et al. 1999). On the other hand, the wall material of organic-walled dinoflagellate cysts consists of dinosporin, which in phototrophic species is likely a complex carbohydrate-based polymer (Versteegh et al. 2012, Bogus et al. 2014) that exhibits autofluorescence in the yellow to green spectrum (Brenner and Biebow 2001). All dinoflagellate cysts that show autofluorescence are considered phototrophic (Brenner and Biebow 2001, Bogus et al. 2014). Accordingly, the observed autofluorescence pattern in our specimens is likely due to the carbohydrate composition of the outer wall, which suggests it is a cyst stage produced by a phototrophic species.

Observations with the transmitted light microscope and SEM reveal that the cysts belong to the benthic dinoflagellate *Bysmatrum subsalsum* (Ostenfeld 1908, Steidinger and Balech 1977, Faust and Steidinger 1998), a species that was first observed and described in the Gulf of Mexico by Steidinger and Balech (1977, as *Scrippsiella subsalsa*) (Figs. 2-3). The main characters differentiating *B. subsalsum* from other *Bysmatrum* species (*B. teres*, *B. granulosum*, *B. arenicola* and *B. caponii*) are its general pentagonal morphology, the presence of striations and cross-reticulation on the paraplates, the pentagonal shape of paraplates 1a, 2a and 3a, and the apical pore complex morphology, which resembles a teardrop (see Murray et al., 2006, their Table 1 for a comparison of the five *Bysmatrum* species). Cysts observed herein, are proximate and pentagonal in ventral view with the epicyst and hypocyst being more or less conical and trapezoidal, respectively, and of equal length (Fig. 3, micrographs 9-10). There is a pronounced apical horn and two antapical horns. The cysts are ~35.2-48 μm in length (average 44.0 μm ; SD: 5.65; n=5) and ~35.2-53 μm in width (average 42 μm ; SD: 5.01; n=6). In some cases, the remainder of a red body is observed inside the cyst (Fig. 3, micrograph 4). The formation of such red bodies

has been associated with the breakdown of the cell's metabolic activity (Bravo and Figueroa 2014). The cyst wall is composed of two layers that are often tightly appressed. The paratabulation is readily observable on the outer layer and is characterized by a prominent, teardrop-shaped apical pore complex and tabulation formula typical for the genus: Po, X, 4', 3a, 7'', 6c, 5''', 2''''. Intercalary paraplates 2a and 3a, which are separated by apical paraplate 3', are pentagonal in shape. The paracingulum is relatively narrow and deep, but its vertical displacement is hard to estimate due to compression. Details of the parasulcus and paracingulum are difficult to observe because of the "principle of minority suppression" in cysts (Evitt 1985, p. 157). The surface of the paraplates bears longitudinal striations and sometimes shows smaller cross-reticulations (Fig. 3, micrographs 3, 5, 11, 13). Parasutures are relatively large and also bear striations. The archeopyle is epicystal.

Our results suggest that, over the course of its life cycle, the benthic dinoflagellate *B. subsalsum* produces organic-walled cysts that are preserved in the sediment for at least 170 years. The autofluorescence of the wall suggests that a phototrophic dinoflagellate produced the cysts. Moreover, a good preservation of the cysts after palynological treatment implies some degree of higher preservation potential and suggests a more robust dinosporin composition, similar to what has been described for other resistant phototrophic cysts belonging to planktonic dinoflagellates. Further research will be needed to determine whether encystment occurs during sexual or asexual reproduction (Bravo and Figueroa 2014). However, in both cases, it may allow survival during adverse conditions and play an important role for the seeding strategy of this species. Since *Bysmatrum* species have been associated with the formation of non-toxic red tides, the ability to form cysts could be important with respect to the initiation, dispersion and termination of blooms (Anderson et al. 2004). Finally, the good preservation of these cysts would potentially also enable their use for coastal paleoenvironmental studies.

Acknowledgements

Mona Hoppenrath, Carmen Zinnsmeister, Maria Faust and Øjvind Moestrup are acknowledged for help with identification. Special thanks go to Nicolas Van Nieuwenhove for helpful comments. Raynald Lapointe and Maryse Henry are acknowledged for their help with SEM preparation. Support for sampling activities was provided through grant PAPIIT-DGAPA IN105009. The helpful comments by two anonymous reviewers were greatly appreciated.

References

- Anderson, D. M., Fukuyo, Y. & Matsuoka, K. 2004. Cyst methodologies. In Hallegraeff, G. M., Anderson, D. M. & Cembella, A. D. [Eds.] Manual on harmful marine microalgae. UNESCO, France, pp. 165–89.
- Bogus, K., Mertens, K. N., Lauwaert, J., Harding, I. C., Vrielinck, H., Zonneveld, K. A. F. & Versteegh, G. J. M. 2014. Differences in the chemical composition of organic-walled dinoflagellate resting cysts from phototrophic and heterotrophic dinoflagellates. *J. phycol.* 50:254–66.
- Bravo, I. & Figueroa, R. I. 2014. Towards an ecological understanding of dinoflagellate cyst functions. *Microorganisms* 2:11–32.
- Bravo, I., Vila, M., Casabianca, S., Rodriguez, F., Rial, P., Riobo, P. & Penna, A. 2012. Life cycle stages of the benthic palytoxin-producing dinoflagellate *Ostreopsis cf. ovata* (Dinophyceae). *Harmful Algae* 18:24–34.
- Brenner, W. W. & Biebow, N. 2001. Missing autofluorescence of recent and fossil dinoflagellate cysts- an indicator of heterotrophy? *N. Jb. Geol. Paläont.*, Abh. 219:229–40.
- de Vernal, A., Henry, M. & Bilodeau, G. 1996. Techniques de préparation et d'analyse en micropaléontologie. In Les cahiers du GEOTOP 3. Département des Sciences de la Terre, Université du Québec à Montréal, pp. 16–40.
- Evitt, W.R. 1985. Sporopollenin dinoflagellate cysts: their morphology and interpretations. American Association of Stratigraphic Palynologists Foundation, 333 p.
- Faust, M. A. 1992. Observations on the morphology and sexual reproduction of *Coolia monotis* (Dinophyceae). *J. Phycol.* 28:94–104.
- Faust, M. A. 1996. Morphology and ecology of the marine dinoflagellate *Scrippsiella subsalsa* (Dinophyceae). *J. Phycol.* 32:669–75.
- Faust, M. A. & Steidinger, K. A. 1998. *Bysmatrum* gen. nov. (Dinophyceae) and three new combinations for benthic scrippsielloid species. *Phycologia* 37:47–52.
- Fritz, L. & Triemer, R. E. 1985. A rapid simple technique utilizing calcofluor white M2R for the visualization of dinoflagellate thecal plates. *J. Phycol.* 21:662–4.

- Gottschling, M., Soehner, S., Zinssmeister, C., Uwe, J., Plötner, J., Schweikert, M., Aligizaki, K. & Elbrächter, M. 2012. Delimitation of the Thoracosphaeraceae (Dinophyceae), including the calcareous dinoflagellates, based on large amounts of ribosomal RNA sequence data. *Protist* 163:15–24.
- Head, M. J. 1996. Modern dinoflagellate cysts and their biological affinities. In Jansonius, J. & Mc Gregor, D. C. [Eds.], *Palynology: Principles and Applications*, vol. 3. AASP Foundation, Salt Lake City, UT, pp. 1197–248.
- Hoppenrath, M., Chomérat, N., Horiguchi, T., Schweikert, M., Nagahama, Y. & Murray, S. 2013. Taxonomy and phylogeny of the benthic *Prorocentrum* species (Dinophyceae)- A proposal and review. *Harmful Algae* 27:1–28.
- Horiguchi, T. & Chihara, M. 1983. *Scrippsiella hexapraecingula* sp. nov. (Dinophyceae), a tide pool dinoflagellate from the Northwest Pacific. *Bot. Mag.* 96:351–8.
- Horiguchi, T. & Pienaar, R. N. 1988. Ultrastructure of a new sand-dwelling dinoflagellate *Scrippsiella arenicola* sp. nov. *J. Phycol.* 24:426–38.
- Jeong, H. J., Jang, S. H., Kang, N. S., Yoo, Y. D., Kim, M. J., Lee, K. H., Yoon, E. Y., Potvin, E., Hwang, Y. J., Kim, J. I. & Seong, K. A. 2012. Molecular Characterization and Morphology of the Photosynthetic Dinoflagellate *Bysmatrum caponii* from Two Solar Saltos in Western Korea. *Ocean Sci. J.* 47:1–18.
- Lessard, E. J. & Swift, E. 1986. Dinoflagellates from the North Atlantic classified as phototrophic or heterotrophic by epifluorescence microscopy. *J. Plankton Res.* 8:1209–15.
- Lombard, E. H. & Capon, B. 1971. Observation on the tide pool ecology and behavior of *Peridinium gregarium*. *J. Phycol.* 7:188–194.
- Murray, S., Hoppenrath, M., Larsen, J. & Patterson, D. J. 2006. *Bysmatrum teres* sp. nov., a new sand-dwelling dinoflagellate from north-western Australia. *Phycologia* 45:161–167.
- Ostenfeld, C. H. 1908. The phytoplankton of the Aral Sea and its affluents, with an enumeration of algae observed. *Wissenschaftliche Ergebnisse der Aralsee-Expedition. Lieferung* 8:123–225.
- Satta, C. T., Anglès, S., Lugliè, A., Guillén, J., Sechi, N., Camp, J. & Garcés, E. 2013. Studies on dinoflagellate cyst assemblages in two estuarine Mediterranean

bays: A useful tool for the discovery and mapping of harmful algal species. *Harmful Algae* 24:65–79.

Sekida, S., Horiguchi, T. & Okuda, K. 1999. Direct evidence for cellulose microfibrils present in thecal plates of the dinoflagellate *Scrippsiella hexapraicingula*. *Hikobia* 13:65–69.

Steidinger, K. A. & Balech, E. 1977. *Scrippsiella subsalsa* (Ostenfeld) comb. nov. (Dinophyceae) with a discussion on *Scrippsiella*. *Phycologia* 16:69–73.

Steidinger, K. A. & Tangen, K. 1996. Dinoflagellates. In Tomas, C.R. [Ed.], Identifying Marine Diatoms and Dinoflagellates. Academic Press, New York, pp. 387–598.

Tang, Y. Z. & Dobbs, F. C. 2007. Green Autofluorescence in dinoflagellates, diatoms, and other microalgae and its implications for vital staining and morphological studies. *Appl. Environ. Microbiol.* 73: 2306–13.

Taylor, F. J. R. & Pollingher, U. 1987. The ecology of dinoflagellates. In Taylor, F. J. R. [Ed.], The Biology of Dinoflagellates. Blackwell Scientific Publications, Oxford, pp. 398–529.

Versteegh, G. J. M., Blokker, P., Bogus, K. A., Harding, I. C., Lewis, J., Oltmanns, S., Rochon, A. & Zonneveld, K. A. F. 2012. Infra red spectroscopy, flash pyrolysis, thermally assisted hydrolysis and methylation (THM) in the presence of tetramethylammonium hydroxide (TMAH) of cultured and sediment-derived *Lingulodinium polyedrum* (Dinoflagellata) cyst walls. *Org. Geochem.* 43:92–102.

Wall, D. & Dale, B. 1968. Modern dinoflagellate cysts and evolution of the Peridiniales. *Micropaleontol.* 14:265–304.

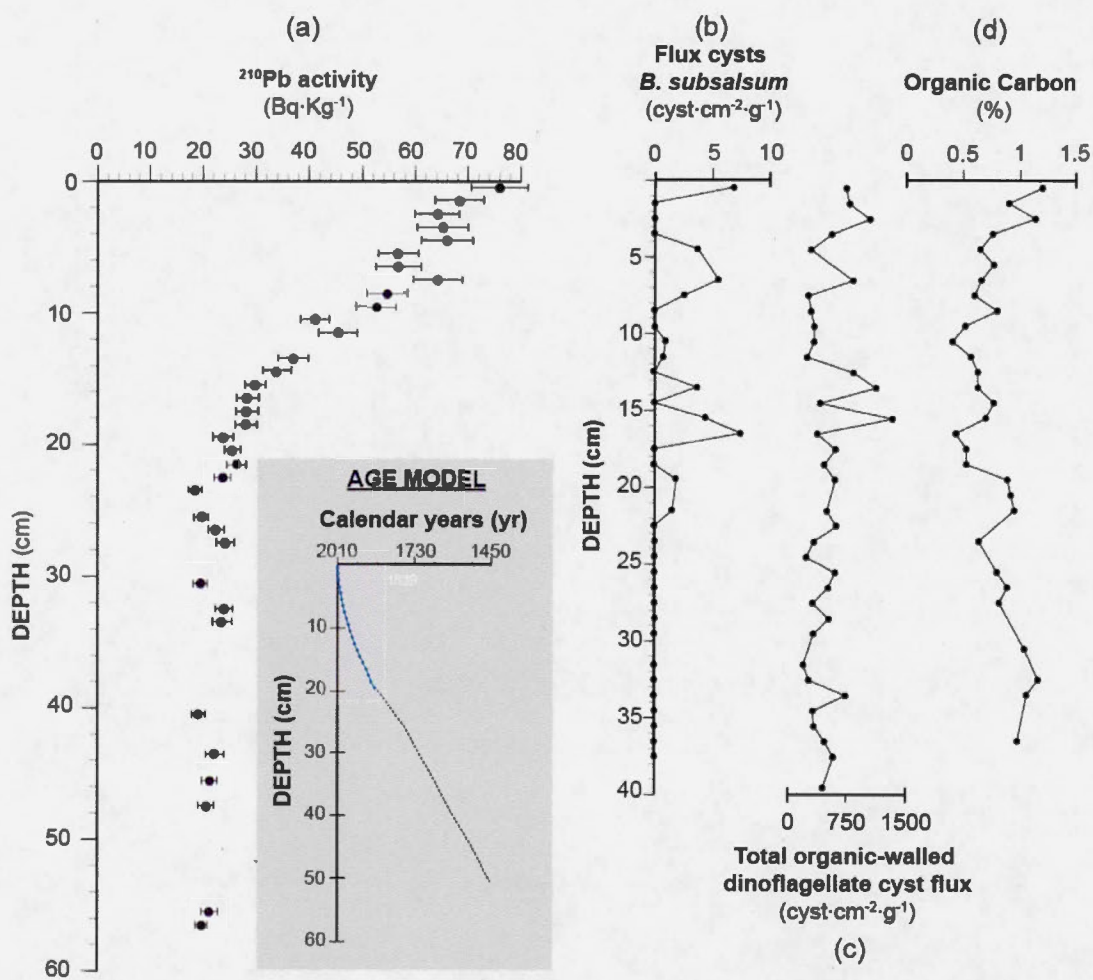


Figure 1: (a) ^{210}Pb activity ($\text{Bq}\cdot\text{Kg}^{-1}$) over depth, and age model, (b) Flux of *Bysmatrum subsalsum* cysts ($\text{cysts}\cdot\text{cm}^{-2}\cdot\text{yr}^{-1}$), (c) Flux of total organic-walled dinoflagellate cysts ($\text{cysts}\cdot\text{cm}^{-2}\cdot\text{yr}^{-1}$) and (d) sedimentary organic carbon (%).

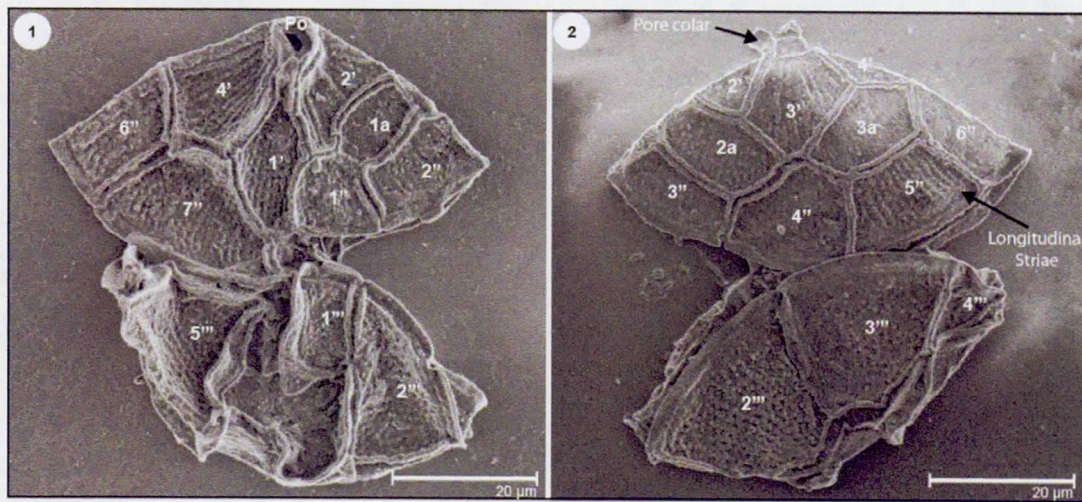


Figure 2: Scanning electron micrographs (SEM) of one specimen of a collapsed cyst of *Bysmatrum subsalsum*, rotated 180 degrees. (1) Ventral view showing apical pore complex and paratabulation. Note that paraplate 1a is pentagonal in shape. (2) Dorsal view showing intercalary paraplates 2a and 3a separated from each other by apical paraplate 3'. Note that paraplates 2a and 3a are pentagonal in shape. Both micrographs clearly illustrate the striated ornamentation of the paraplates. Abbreviations: n': apical plates, n'': precingular plates, n'''': postcingular plates. na: anterior intercalary plates, Po: apical pore plate.

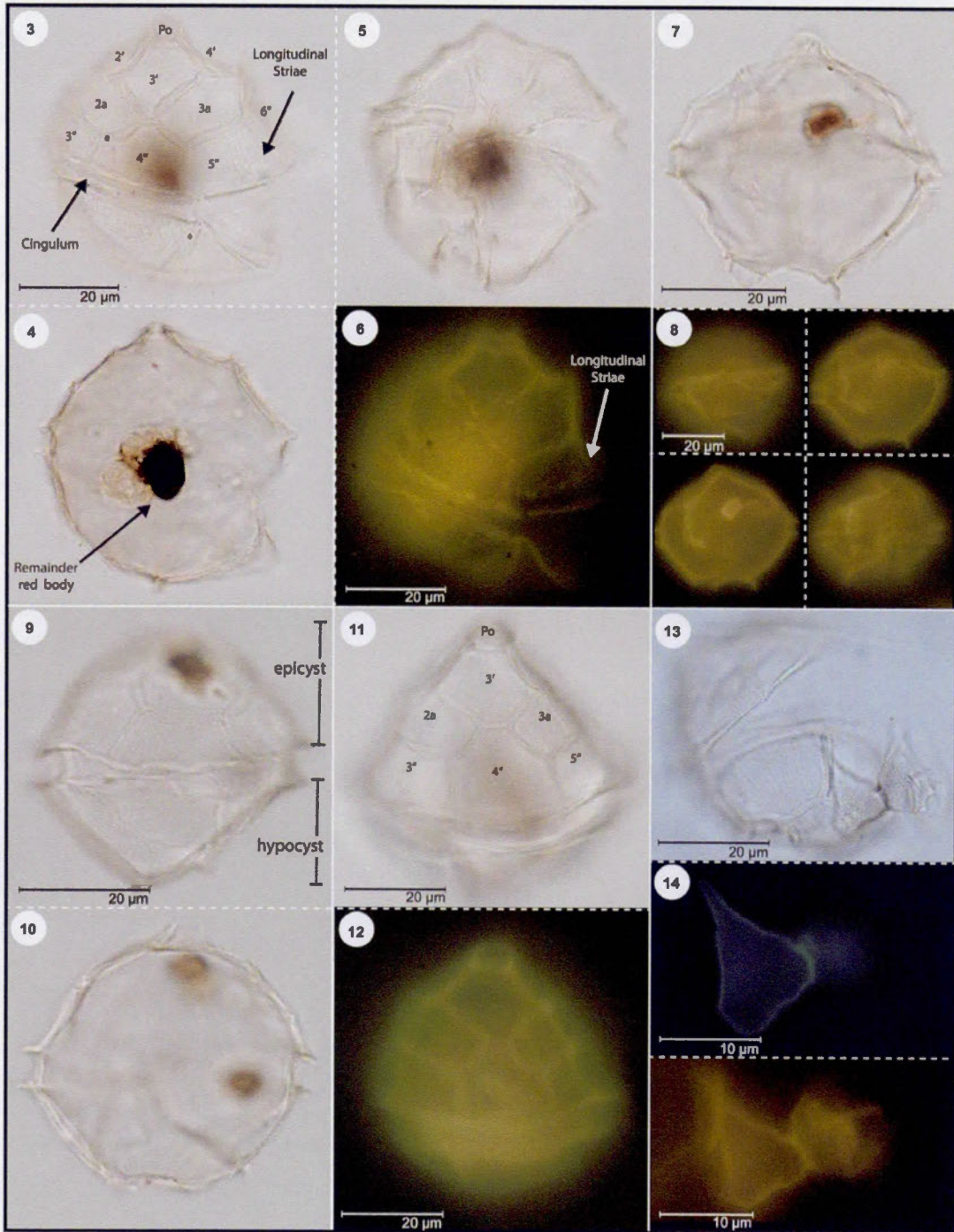


Figure 3: Bright and dark field light micrographs of cysts of *Bysmatrum subsalsum* from palynological slides. (3-6) Specimen from sample 4-5 cm (slide 1, England Finder (EF): Q47-02). 3: Dorsal view, high focal plane. Paratabulation and ornamentation of paraplates (striation) can be seen clearly under optical microscope. 4: Cross-section showing general shape and the remainder of a red body. 5: Ventral view, low focal plane. 6: Fluorescence image. Ornamentation, outline of paraplates and both walls of the cyst show clear yellow autofluorescence. (7-8) Specimen from sample 4-5 cm (slide 1; EF: U47-02). 7: Cross-section. 8: Fluorescence images from high to low focal plane. (9-10) Specimen from sample 0-1 cm (slide 1; EF: R65-02). 9: Dorsal view, high focal plane. Note that epicyst and hypocyst are of equal length. 10: Cross-section. (11-12) Specimen from 7-8 cm (slide 1; EF: R65-02). 11: Dorsal View. High focal plane. 12: Fluorescence image. (13-14) Collapsed specimen from sample 6-7 cm (slide 1: EF: F41-02). 13: High focal plane. Note ornamentation (striations and cross-reticulation) on hypocrystal plates and rupture along the cingulum of the epicystal archeopyle. 14: Fluorescence images with narrow field-of-depth on the two paraplates shown on the lower right of micrograph 13. Outline and ornamentation of paraplates show clear autofluorescence. Abbreviations: see figure 2.

APPENDICE B

RAPPORT DE STAGE : DÉVELOPPEMENT D'UN BIOMARQUEUR POUR LE DINOFLAGELLÉ *KARENIA BREVIS*

Automne 2010

Center for Coastal Environmental Health and Biomolecular Research 2010

Sous la supervision de:

Dr. Marie-Yasmine Bottein

Dr. John Ramsdell

1. Introduction

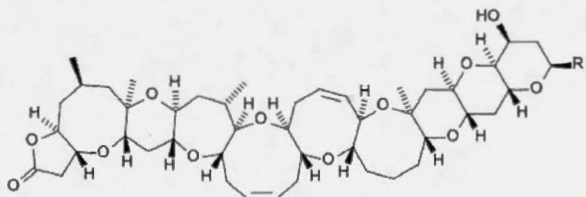
Le dinoflagellé *Karenia brevis* (précédemment *Gymnodinium breve*) est à l'origine des efflorescences algales nuisibles parmi les plus délétères se produisant dans le golfe du Mexique (e.g. Steidinger, 2009; Vargo, 2009; Brand et al., 2012). Il libère une variété de composés nocifs (Kubanek et al, 2005, 2007; Neely and Campbell, 2006; Prince et al, 2010) dont une suite de neurotoxines très puissantes connues sous le nom de brévétoxines (PbTx_s) et regroupées selon leur structure moléculaire sous les type-A et type-B. Ces toxines sont liposolubles et exercent leur toxicité en bloquant la propagation de l'influx nerveux chez les organismes contaminés (Pierce & Henry, 2008). Les efflorescences nuisibles se produisent généralement dans les zones côtières où l'action des vagues et la turbulence peuvent provoquer la rupture des cellules, facilitant la libération des toxines vers le milieu (Van Dolah, 2000). Le long de la péninsule de la Floride, elles se développent communément à l'automne, lors de la saison des pluies (Brand & Compton, 2007). Des larges populations de *K. brevis* ($>100\ 000$ cellules L⁻¹) peuvent mener à des mortalités massives chez les poissons, oiseaux et mammifères marins. Chez l'humain, la consommation des produits de la mer contaminés peut causer des problèmes digestifs aigus, un syndrome nommé *Neurotoxic Shellfish Poisoning* (NSP). Ces toxines peuvent également être létales pour l'humain à de faibles doses, soit (LD₁₀₀) 3ng/ml.

K. brevis se reproduit principalement par fission binaire, mais est capable de reproduction sexuée (Walker, 1982). La production d'un kyste de résistance fossilisable n'est cependant pas associée à cette espèce. Par ailleurs, les toxines qu'il synthétise présentent une très grande stabilité physico-chimique et sont incorporées et préservées dans les sédiments (Baden & Tomas, 1989). Elles constituent donc de potentiels traceurs moléculaires des populations passées de *K. brevis*. Des études *in-situ* et en laboratoire ont permis d'estimer qu'une cellule de *K. brevis* peut produire entre 8 et 25 pg de brévétoxines (PbTx_s) (Baden & Tomas, 1989; Pierce et al, 1990,

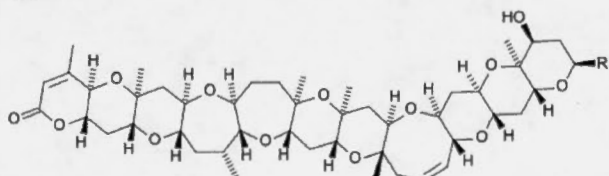
2008; Tester et al., 2008). Les teneurs sédimentaires en brévétoxines pourraient donc potentiellement permettre de caractériser la distribution temporelle et spatiale de cette espèce.

Dans le cadre de cette thèse, l'utilisation des brévétoxines comme potentiel biomarqueur de *K. brevis* a été étudiée lors d'un stage au centre de recherche *Center for Coastal Environmental Health and Biomolecular Research*, sous la supervision de Marie-Yasmine Bottein et John Ramsdell. L'applicabilité des tests immuno-enzymatiques ELISA comme méthode de détection a fait l'objet d'une première démarche exploratoire pour le développement d'une approche méthodologique.

Type-A



Type B



Type-A

- (PbTx-1) R= - CH₂C(=CH₂)CHO
- (PbTx-7) R= - CH₂C(=CH₂)CH₂OH
- (PbTx-10) R= - CH₂CH(-CH₃)CH₂OH

Type B

- (PbTx-2) R= - CH₂C(=CH₂)CHO
- (PbTx-3) R= - CH₂C(=CH₂)CH₂OH
- (PbTx-5) R= the K-ring acetate of PbTx-2
- (PbTx-6) R= the H-ring epoxide of PbTx-2
- (PbTx-8) R= - CH₂CO CH₂Cl
- (PbTx-9) R= - CH₂CH(CH₃)CH₂OH

2. Méthodes et résultats

2.1 Préparation des échantillons

La première étape du projet visait à améliorer le protocole d'extraction des brévétoxines décrit par Mendoza et al. (2008) (taux de recouvrement de 30%). Des échantillons sédimentaires provenant de la côte ouest du Mexique, une région où *K. brevis* est absent, ont d'abord été lyophilisés et ensuite enrichis avec des concentrations prédéfinies de brévétoxines (PbTx-3) (3,10 ou 30 ng/g). Une vaste gamme de solvants, ainsi que plusieurs techniques de séparation ont été évaluées (voir tableau 1). Les échantillons étaient soumis à une analyse immunologique (ELISA) et une détection par chromatographie liquide couplée à un spectromètre de masse (LC-MS). La comparaison des mesures obtenues via les deux méthodes était essentielle puisqu'elle permettait d'une part, de réduire l'effet matrice qui pourrait interférer dans les analyses immunologiques et d'autre part, permettre une calibration pour les analyses subséquentes. Le protocole d'extraction qui présentait le meilleur taux de recouvrement est décrit dans le tableau 2.

DÉVELOPPEMENT PROTOCOLE EXTRACTION	
Solvants testés	
1.	(1 :1) Dichlorométhane : Acétone
2.	Acétone (100%)
3.	Acide Formique (0.1%)
4.	(3 :1) Méthanol : Acétate éthylique
5.	(3 :1) Acetonitrile : Acétate éthylique
6.	Méthanol (100%)
Étapes d'extraction testées	
Extraction effectuée sur 200 mg de sédiment lyophilisé	
1.	Addition initiale de solvant (volume de 40 mL → 5 mL; solvants liste au-dessus); vortex
2.	Ultrasonification (1 min. → 30 sec., amplitude : 60% → 50%); l'échantillon est déposé dans un bain de glace pour éviter d'élever la température de l'échantillon
3.	Centrifugation (2000 rpm → 3000 rpm, 10 minutes)
4.	Surageant transféré dans (a. ballons de verre; b. petites fioles de verre)
Étapes 1-4 répétées 3 à 6 fois consécutives	
5.	Option a.
	<ul style="list-style-type: none"> • Surageant transféré dans ballon un de verre et évaporé au <i>rota-vapor</i> (~20 minutes; température bain : 55°C; rotation : 90; Pression [800 à 500 mbar]) • Resuspension avec MeOH (20%); Extraction en phase solide (EPS) (<i>Varian Bond Elut</i>, 500 mg, 10 mL ; éliminer sels et concentrer les PbTx) ou Filtration 0.45 µm • Séchage sous flux azoté
Option b.	
	<ul style="list-style-type: none"> • Surageant transféré dans petites fioles de verre et évaporé sous flux azoté • EPS ou Filtration 0.45 µm • Séchage sous flux azoté
6.	Resuspension de l'extrait dans MeOH (100%)
7.	Sonification pendant 20 minutes

Tableau 1. Différentes étapes testées pour l'extraction des brévétoxines à partir de sédiments marins.

PROTOCOLE D'EXTRACTION PRÉSENTANT LE MEILLEUR TAUX DE RECOUVREMENT	
Extraction effectuée sur 200 mg sédiment lyophilisé	
1.	Addition 5 mL MeOH (100%); vortex
2.	Ultrasonification (30 secondes, amplitude : 55%); échantillon déposé dans un bain de glace durant sonification
3.	Centrifugation (3000 rpm, 4°C, 10 minutes)
4.	Surageant transféré dans des petites fioles de verres
Étapes 3 à 4, répétées 3 fois	
5.	Filtration 0.45 µm
6.	Sécher sous flux azoté (température : 45°C; pression : 1-5 mbar)
7.	Extrait resuspendu dans méthanol 100% (200ml/200mg)
8.	Bain sonification (20 minutes)

Tableau 2. Protocole d'extraction présentant le meilleur taux de recouvrement.

2.2 Détection des brévétoxines par le test immuno-enzymatique ELISA

2.2.1 Description

La détection quantitative des brévétoxines a été effectuée via un test immuno-enzymatique compétitif ELISA (acronyme de *Enzyme Linked ImmunoSorbent Assay*) basé sur la reconnaissance des brévétoxines par des anticorps spécifiques. Ce test a démontré une grande précision pour la quantification de concentrations très faibles de brévétoxines dans l'eau de mer, les mollusques et les fluides extraits de mammifères marins (Naar et al., 2002). Les toxines produites par *K. brevis* montrent un très grand nombre d'analogues et de congénères, biosynthétisés directement ou issus de séries réactionnelles, pour lesquels les structures moléculaires diffèrent. À cet effet, contrairement aux analyses par LC-MS, ELISA ne permet pas la discrimination des différents types de brevetoxines, mais permet une quantification simple et rapide de l'ensemble des PbTx ainsi que de leurs dérivés.

Dans les premières phases du test, les puits d'une microplaquette immunologique sont tapissés avec une solution d'anticorps capable de se lier spécifiquement aux brévétoxines. Une incubation des plaques pendant 1 heure (35°C) permet aux anticorps de se fixer à la surface plastique des puits par interaction électrostatique. Après incubation, la plaque est rincée 4 fois consécutives avec un détergent pour éliminer l'excès de solution. Les sites actifs restants sont bloqués par l'ajout d'une solution protéinique. Les protéines se fixent également au plastique des puits au cours d'une période d'incubation de 1 heure (35°C). La plaque est de nouveau rincée 4 fois consécutives avec un détergent. L'échantillon à tester est ajouté dans les puits de la microplaquette et s'il contient des brévétoxines, celles-ci se lient aux anticorps. Une concentration prédéfinie d'un antigène conjugué à une enzyme est ensuite ajoutée et permet de catalyser la formation d'un produit coloré. La réaction est arrêtée par l'ajout d'acide sulfurique. Plus l'échantillon est riche en brévétoxines, moins les

antigènes conjugué ne pourront créer des liaisons avec les anticorps et donc plus le signal sera faible. L'obtention d'une mesure quantitative se fait par lecteur de densité optique (450 nm).

Afin de comparer la réponse des PbTx-3 et PbTx-2 au test immunologique, des courbes de calibrations ont été construites à partir de leur dilution en séries (1:3) (20 ng/mL à 0.001 ng/mL) (voir figure 1). Les deux courbes de calibration standard obtenues se superposent, indiquant que les résultats des détections ELISA peuvent être exprimés en équivalents PbTx-2 ou PbTx-3. Ainsi, lors des détections ELISA, la mesure d'absorbance pour chacun des échantillons est reportée à une courbe de calibration standard propre à chaque test et la concentration est exprimée en équivalent PbTx-3. Les valeurs comprises entre les EC80 et EC20 (respectivement 80% et 20% de l'effet maximal) de la courbe de régression se situent dans le registre de détection du test.

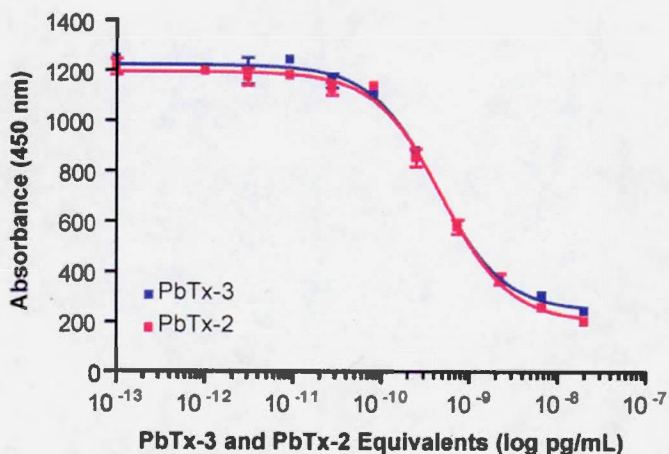


Figure 1. Courbes de calibrations standard à partir de dilutions en séries des PbTx-2 et PbTx-3.

2.2.1 Application sur échantillons TEHUA V 1

Plusieurs aliquotes d'un échantillon de sédiment de surface provenant de la côte Ouest mexicaine (TEHUA V 1) ont été enrichis en PbTx-3 pour générer des concentrations finales en toxines comprises entre 3 et 30 ng/g. Un contrôle a également été préparé (non-enrichi). La procédure d'extraction détaillée dans le tableau 2 a été appliquée à l'ensemble de ces échantillons. La courbe de calibration était construite selon le protocole standard (PbTx-3 dilués dans solution PBST).

2.2.2 Effet matrice

Pour vérifier l'effet matrice des sédiments et/ou étudier le potentiel facteur de correction à considérer lors de mesures ELISA, nous avons comparé une courbe de calibration standard (PbTx-3 dans une solution PBST) à 5 courbes de calibration faites à partir d'un extrait de sédiment (échantillon TEHUA V 1) dilué à différentes concentrations (1 :10, 1 :20, 1 :40 1 :80 et 1 :120).

3. Résultats

3.1 Taux de recouvrement

Les taux de recouvrement en brévétoxines des échantillons enrichis en PbTx-2 et PbTx-3 estimés par LC-MS sont présentés ci-dessous. La méthode d'extraction montre une nette amélioration par rapport à la méthode décrite par Mendoza et al. (2008). Elle n'est cependant pas optimale.

- i. Séđiment enrichi [10ng/mL] **PbTx-2**
Temps de rétention : 24 minutes
Concentration estimée : 3-5 ng/mL
Taux de recouvrement : 25%
- ii. Séđiment enrichi [30ng/mL] **PbTx-2**
Temps de rétention : 24 minutes
Concentration estimée : 9ng/mL
Taux de recouvrement : 30%
- iii. Séđiment enrichi [10ng/mL] **PbTx-3**
Temps de rétention : 19 minutes
Concentration estimée : 6.1 ng/mL
Taux de recouvrement : 61%
- iv. Séđiment enrichi [30ng/mL] **PbTx-3**
Temps de rétention : 19 minutes
Concentration estimée : 21 ng/mL
Taux de recouvrement : 70%

3.2 Application sur échantillons TEHUA V 1

Les échantillons contrôle (non-enrichis en PbTx-3) montrent des concentrations sous la limite de détection. Par ailleurs, les concentrations en brévétoxines sont surestimées pour l'ensemble des échantillons préalablement enrichis. Les mesures sur les duplicates sont relativement constantes. Nos résultats montrent que seul l'ordre de grandeur relatif des concentrations ajoutées en PbTxs est conservé lors de la détection par ELISA. Il n'est actuellement pas possible de déterminer les concentrations absolues présentes dans les échantillons.

Name	Échantillons [PbTx-3]/g	Dilution Avant injection	RESULTATS ELISA		% recouvrement
			Concentrations PbTx _s détectées (ng/mL)		
TEHUA V #1	blank	10	<dl	<dl	-
TEHUA V #1	blank	20	<dl	<dl	-
TEHUA V #1	blank	40	<dl	<dl	-
TEHUA V #1	blank	40	<dl	<dl	-
TEHUA V #1	blank	80	<dl	<dl	-
TEHUA V #1	blank	120	<dl	<dl	-
TEHUA V #1	3	10	8,14	9,88	300
TEHUA V #1	3	20	9,82	8,45	305
TEHUA V #1	3	40	9,20	9,56	313
TEHUA V #1	3	40	<dl	<dl	-
TEHUA V #1	3	80	<dl	<dl	-
TEHUA V #1	3	120	<dl	<dl	-
TEHUA V #1	10	10	>dl	>dl	-
TEHUA V #1	10	20	20,97	18,42	197
TEHUA V #1	10	40	18,70	24,06	214
TEHUA V #1	10	40	19,97	18,24	191
TEHUA V #1	10	80	20,17	22,37	213
TEHUA V #1	10	120	21,16	17,17	192
TEHUA V #1	30	10	>dl	>dl	-
TEHUA V #1	30	20	>dl	>dl	-
TEHUA V #1	30	40	38,08	48,10	144
TEHUA V #1	30	40	49,77	46,53	161
TEHUA V #1	30	80	56,41	58,26	191
TEHUA V #1	30	120	41,36	54,52	160

Tableau 3. Résultats des analyses ELISA.

3.2 Effet matrice

L'ensemble des courbes de calibration construites à partir d'extraits de sédiments est décalé par rapport à la courbe de calibration standard (réalisée dans une solution PBST). Cet effet matrice pourrait expliquer la surestimation des concentrations mesurées dans le test, puisque les mesures d'absorbance des différents échantillons sont normalement reportées à la courbe standard. Il serait donc préférable de :

- Construire la courbe de calibration à partir d'extrait de sédiment lors de l'application du test ou de privilégier l'injection d'extrait dilué par un facteur supérieur à 20 (concentration en sédiment $\leq 0,05$ g/mL)

- Améliorer la méthode d'extraction des sédiments.

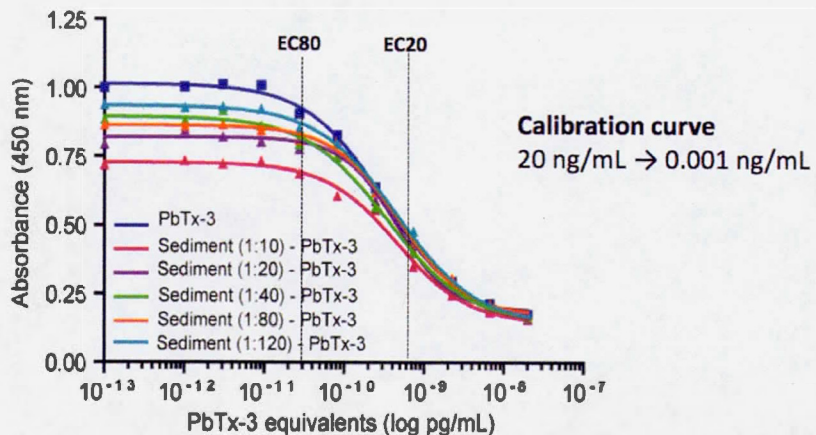


Figure 2. Courbes de calibrations construites à partir d'extraits de sédiments et courbe de calibration standard (PbTx-3).

4. Conclusions préliminaires et perspectives de recherche

Les tests immunologiques ELISA ont le potentiel de permettre un détection rapide et peu couteuse des brévétoxines à partir des sédiments. La méthode d'extraction doit cependant être améliorée afin de réduire l'effet matrice. Il serait également intéressant de vérifier plusieurs aspects liés à la préservation et/ou l'incorporation des toxines dans les sédiments en périodes de blooms.

Ce volet du projet a été pris en charge par Yves Gélinas et Amanda Gabriel (U. Concordia), qui ont travaillé à améliorer la méthodologie d'extraction.

Références

- Baden, D.G. & Tomas, C.R. (1989). Variation in major toxin composition for six clones of *Ptychodiscus brevis*. Dans : Okaichi, T., Anderson, D.M., Nemoto, T. : Red Tides Biology, *Environmental Sciences and Toxicology*, Elsevier, New York, 415-418
- Brand, L.E. & Compton, A. (2007). Long-term increase in *Karenia brevis* abundance along the southwest Florida coast. *Harmful Algae* 7, 232–252.
- Brand, L.E., Campbell, L., Bresnan, E. (2012). *Karenia*: the biology and ecology of a toxic genus. *Harmful Algae* 14, 156–178.
- Kubanek, J., Hicks, M.K., Naar, J., Villareal, T.A. (2005). Does the red tide dinoflagellate *Karenia brevis* use allelopathy to outcompete other phytoplankton? *Limnology and Oceanography* 50(3), 883-895.
- Kubanek, J., Snell, T.W., Pirkle, C. (2007). Chemical defense of the red tide dinoflagellate *Karenia brevis* against rotifer grazing. *Limnology and Oceanography* 52 (3), 1026-1035.
- Neely, T. & Campbell, L. (2006). A modified assay to determine hemolytic toxic variability among *Karenia* clones isolated from the Gulf of Mexico. *Harmful Algae* 5, 592-598.
- Pierce, R.H. & Henry, M. (2008). Harmful algal toxins of the Florida red tide (*Karenia brevis*) : natural chemical stressors in South Florida coastal ecosystems. *Ecotoxicology* 17(7), 623-631.
- Pierce, R.H., Henry, M.S., Proffitt, L.S., Hasbrouck, P.A. (1990). Red tide toxin (brevetoxin) enrichment in marine aerosol. Dans : Graneli, E., Sundstroem, B., Edler, L., Anderson, D.M. : *Toxic Marine Phytoplankton*. Elsevier, New York, 397-402.
- Pierce, R.H., Henry, M.S., Blum, P. (2008). Brevetoxin abundances and composition during ECOHAB-Florida field monitoring cruises in the Gulf of Mexico. *Continental Shelf Research* 28, 45-58.
- Prince, E.K., Poulson, K.L., Myers, T.L., Sieg, R.D., Kubanek, J. (2010). Characterization of allelopathic compounds from the red tide dinoflagellate *Karenia brevis*. *Harmful Algae* 10, 39-48.
- Steidinger, K.A. (2009). Historical perspective on *Karenia brevis* red tide research in the Gulf of Mexico. *Harmful Algae* 8, 549–561.

Tester, P.A., Shea, D., Kibler, S.R., Varnam, S.M., Black, M.D., Litaker, R.W. (2008). Relationship among water column toxins, cell abundance and chlorophyll concentrations during *Karenia brevis* blooms. *Continental Shelf Research* 28, pp.59-72.

Van Dolah, F.M. (2000). Marine algal toxins : origins, health effects, and their increased occurrence. *Environmental Health Perspectives* 208 (1), 133-141.

Vargo, G.A. (2009). A brief summary of the physiology and ecology of *Karenia brevis* Davis (G. Hansen and Moestrup comb. nov.) red tides on the West Florida Shelf and of hypotheses posed for their initiation, growth, maintenance, and termination. *Harmful Algae* 8, 573-584.

BIBLIOGRAPHIE GÉNÉRALE

- Anderson, D.M. & Lindquist, N.L. (1985). Time-course measurements of phosphorus depletion and cyst formation in the dinoflagellate *Gonyaulax tamarensis* Lebour. *Journal of Experimental Marine Biology and Ecology* 86, 1–13.
- Anderson, D.M., Coats, D.W., Tyler, M.A. (1985). Encystment of the dinoflagellate *Gyrodinium uncatenum* temperature and nutrient effect. *Journal of Phycology* 21, 200–206.
- Anderson, D.M. (1998). Physiology and bloom dynamics of toxic *Alexandrium* species, with emphasis on life cycle transitions. Dans : Anderson, D.M., Cembella, A.D., Hallegraeff, G.M. [Eds] : *The Physiological Ecology of Harmful Algal Blooms*. Springer-Verlag, Heidelberg, pp. 29–48.
- Anderson, D.M. & Rengefors, K. (2006). Community assembly and seasonal succession of marine dinoflagellates in a temperate estuary: The importance of life cycle events. *Limnology and Oceanography* 51, 860–873.
- Anderson, D.M., Burkholder, J.M., Cochlan, W., Glibert, P.M., Gobler, C.J., Heil, C.A., Kudela, R.M., Parsons, M.L., Rensel, J.E.J., Townsend, D.W., Trainer, V.L., Vargo, G.A. (2008). Harmful algal blooms and eutrophication: Examining linkages from selected coastal regions of the United States. *Harmful Algae* 8, 30–53.
- Botana, L.M. (2000). Seafood and Freshwater toxins: pharmacology, physiology, and detection. Marcel Dekker, New York, 779 pp.
- Brand, L.E. & Compton, A. (2007). Long-term increase in *Karenia brevis* abundance along the Southwest Florida Coast. *Harmful Algae* 6, 232–252.
- Dale, B. & Fjellså, A. (1994). Dinoflagellate cysts as productivity indicators: state of the art, potential and limits. Dans: Zahn, R. [Eds]: *Carbon Cycling in the Glacial Ocean: Constraints in the Ocean's Role in Global Change*. Springer, Berlin, pp. 521–537.
- Dale, B., 1996. Dinoflagellate cyst ecology: modeling and geological applications. Dans: Jansonius, J., McGregor, D.C. [Eds]: *Palynology: Principles and Applications* 3. American Association of Stratigraphic Palynologists. Foundation, College Station TX, pp. 1249–1275.

- Dale, B. (2001). Marine dinoflagellate cysts as indicators of eutrophication and industrial pollution : a discussion. *The Science of the Total Environment* 264, 235–240.
- de Vernal, A. & Marret, F. (2007). Organic-walled dinoflagellate cysts: tracers of sea-surface conditions. Dans: Hillaire-Marcel, C. & de Vernal, A. [Eds]: *Proxies in late Cenozoic paleoceanography*, Elsevier, Amsterdam, pp. 567–644.
- de Vernal, A., Eynaud, F., Henry, M., Hillaire-Marcel, C., Londeix, L., Magin, S., Matthiessen, J., Marret, F., Radi, T., Rochon, A., Solignac, S., Turon, J.-L. (2005). Reconstruction of sea-surface conditions at middle to high latitudes of the Northern Hemisphere during the Last Glacial Maximum (LGM) based on dinoflagellate cyst assemblages. *Quaternary Science Reviews* 24 (7–9), 897–924.
- Estrada, M., Solé, J., Anglès, S., Garcés, E. (2010). The role of resting cysts in *Alexandrium minutum* population dynamics. *Deep-Sea Research II* 57 (3–4), 308–321.
- Evitt, W.R. (1985). Sporopollenin dinoflagellate cysts, their morphology and interpretation. *American Association of Stratigraphic Palynologists Foundation*, p. 333.
- Flewelling, L.J., Naar, J.P., Abott, J.P., Baden, D.G., Barros, N.B., Bossart, G.D., Bottein, M.Y., Hammond, D.G., Haubold, E.M., Heil, C.A., Henry, M.S., Jacocks, H.M., Leighfield, T.A., Pierce, R.H., Pitchford, T.D., Rommel, S.A., Scott, P.S., Steidinger, K.A., Truby, E.W., Van Dolah, F.M., Landsberg, J.H. (2005). Red tides and marine mammal mortalities. *Nature* 435, 755–756.
- Figueroa, R.I., Bravo, I., Garcés, E., Ramilo, I. (2006). Nuclear features and effect of nutrients on *Gymnodinium catenatum* (Dinophyceae) sexual stages. *Journal of Phycology* 42, 67–77.
- Granéli, E., Weberg, M., Salomon, P.S. (2008). Harmful algal blooms of allelopathic microalgal species: The role of eutrophication. *Harmful Algae* 8, 94–102.
- Hallegraeff, G.M. (1993). A review of harmful algal blooms and their apparent global increase. *Phycologia* 32, 79–99.
- Heisler, J., Glibert, P., Burkholder, J., Anderson, D., Cochlan, W., Dennison, W., Gobler, C., Dortch, Q., Heil, C., Humphries, E., Lewitus, A., Magnien, R., Marshall, H., Sellner, K., Stockwell, D., Stoecker, D., Suddleson, M. (2008). Eutrophication and harmful algal blooms: a scientific consensus. *Harmful Algae* 8, 3–13.

- Hense, I. (2010). Approaches to model the life cycle of harmful algae. *Journal of Marine Systems* 83, 108–114.
- Jacobson, D. & Anderson, D. (1986). Thecate heterotrophic dinoflagellates: feeding behaviour and mechanics. *Journal of Phycology* 22, 249–258.
- Kusek, K.M., Vargo, G., Steidinger, K. (1999). *Gymnodinium breve* in the field, in the lab, and in the newspaper—a scientific and journalistic analysis of Florida red tides. *Contribution Marine Sciences* 34, 1–229.
- Lacasse, O., Rochon, A., Roy, S. (2013). High cyst concentrations of the potentially toxic dinoflagellate *Alexandrium tamarensis* species complex in Bedford Basin, Halifax, Nova Scotia, Canada. *Marine Pollution Bulletin* 66, 230–233.
- Landsberg, J.H. (2002). The effects of harmful algal blooms on aquatic organisms. *Reviews of Fisheries Science* 10, 113–390.
- Licea, S., Zamudio, M.E., Luna, R., Okolodkov, Y., Gomez Aguirre, S. (2002). Toxic and harmful dinoflagellates in the southern Gulf of Mexico. Proceedings of the X International Conference on Harmful Algae. St. Petersburg, FL, 21–25 October, p. 170 (Abstracts).
- Lundholm, N., Ribeiro, S., Andersen, T.J., Koch, T.A., Godhe, A., Ekelund, F., Ellegaard, M. (2011). Buried alive-germination of up to a century-old marine protist resting stages. *Phycologia* 50, 629–640.
- Magaña, H.A., Contreras, C., Villareal, T.A. (2003). A historical assessment of *Karenia brevis* in the western Gulf of Mexico. *Harmful Algae* 2, 163–171.
- Mertens, K.N., Rengefors, K., Moestrup, Ø., Ellegaard, M. (2012). A review of recent freshwater dinoflagellate cysts: taxonomy, phylogeny, ecology and palaeoecology. *Phycologia* 51 (6), 612–619.
- Mudie, P.J., Harland, R., Matthiessen, J., de Vernal, A. (2001). Marine dinoflagellate cysts and high latitude Quaternary paleoenvironmental reconstructions: an introduction. *Journal of Quaternary Science* 16, 595–602.
- Oey, L.-Y., Ezer, T., Lee, H.-C. (2005). Loop current, rings and related circulation in the Gulf of Mexico: a review of numerical models and future challenges. Dans : Sturges, W., Lugo-Fernandez, A. [Eds]: *Circulation in the Gulf of Mexico: Observations and Models*. Geophysical Monograph Series 161. American Geophysical Union, Washington, DC, pp. 31–56.

- Pawlowski, J., Holzmann, M., Fahrni, J.F., Pochon, X., Lee, J.J. (2001). Molecular identification of algal endosymbionts in large miliolid foraminifera. 2. Dinofagellates. *Journal of Eukaryotic Microbiology* 48, 368–373.
- Phlips, E.J., Badylak, S., Lynch, T.C. (1999). Blooms of the picoplanktonic cyanobacterium *Synechococcus* in Florida Bay, a subtropical inner-shelf lagoon. *Limnology and Oceanography* 44, 1166–1175.
- Phlips, E.J., Badylak, S., Youn, S., Kelley, K. (2004). The occurrence of potentially toxic dinoflagellates and diatoms in a subtropical lagoon, the Indian River Lagoon, Florida, USA. *Harmful Algae* 3, 39–49.
- Phlips, E.J., Badylak, S., Bledsoe, E., Cichra, M. (2006). Factors affecting the distribution of *Pyrodinium bahamense* var. *bahamense* in coastal waters of Florida. *Marine Ecology Progress Series* 322, 99–115.
- Pospelova, V., Chmura, G.L., Boothman, W.S., Latimer, J.S. (2002). Dinoflagellate cyst records and human disturbance in two neighboring estuaries, New Bedford Harbor and Apponaugansett Bay, Massachusetts (USA). *The Science of the Total Environment* 298, 81–102.
- Rabalais, N.N., Turner, R.E., Díaz, R.J., Justic, D. (2009). Global change and eutrophication of coastal waters—ICES. *Journal of Marine Science* 66, 1528–1537.
- Radi, T., Pospelova, V., de Vernal, A., Barrie, J.V. (2007). Dinoflagellate cysts as indicators of water quality and productivity in British Columbia estuarine environments. *Marine Micropaleontology* 62, 269–297.
- Rengefors, K., Anderson, D.M. (1998). Environmental and endogenous regulation of cyst germination in two freshwater dinoflagellates. *Journal of Phycology* 34, 568–577.
- Ribeiro, S., Berge, T., Lundholm, N., Andersen, T., Abrantes, F., Ellegaard, M. (2011). Phytoplankton growth after a century of dormancy illuminates past resilience to catastrophic darkness. *Nature Communications* 2 (311).
- Rice, E.L. (1984). Allelopathy, 2nd ed. Academic Press, Orlando, Florida, 423 p.
- Sheng, J., Malkiel, E., Katz, J., Adolf, J.E., Place, A.R. (2010). A dinoflagellate exploits toxins to immobilize prey prior to ingestion. *Proceedings of the National Academy of Sciences of the United States of America* 107 (5), 2082–2087.
- Sierra-Beltrán, A.P., Cortés-Altamirano, R., Cortés-Lara, M.C. (2005). Occurrences

- of *Prorocentrum minimum* (Pavillard) in México. *Harmful Algae* 4, 507–517.
- Smayda, T.J. (1990). Novel and nuisance phytoplankton blooms in the sea: Evidence for a global epidemic. Dans: Graneli, E., Sundstroem, B., Edler, L. and Anderson, D.M. [Eds]: *Toxic Marine Phytoplankton*, Elsevier Science Publishing Co., pp.29–40.
- Smayda, T.J. & Reynolds, C.S. (2003). Strategies of marine dinoflagellate survival and some rules of assembly. *Journal of Sea Research* 49, 95–106.
- Smayda, T.J., (2008). Complexity in the eutrophication-harmful algal bloom relationship, with comment on the importance of grazing. *Harmful Algae* 8, 140–151.
- Sournia, A. (1995). Red tide and toxic marine phytoplankton of the world ocean: an inquiry into biodiversity. Dans : Lassus, P., Arzul, G., Erard-Le Denn, E., Gentien, P. et Marcaillou- Le Baut, C. [Eds]: *Harmful Marine Algal Blooms*. Lavoisier, pp. 103–112.
- Steidinger, K.A., Vargo, G.A., Tester, P., Tomas, C. (1998). Bloom dynamics and physiology of *Gymnodinium breve* with emphasis on the Gulf of Mexico. Dans Anderson, D., Cembella, A., Hallegraeff, G.: *Physiological Ecology of Harmful Algal Blooms*. Springer-Verlag, Berlin, pp. 133–153.
- Taylor, H.H. (1917). Mortality of fishes on the west coast of Florida. *Science* 45, 367–368.
- Taylor, F.J.R., & Pollingher, U. (1987). The ecology of dinoflagellates. Dans: F.J.R. Taylor [Eds]: *The biology of dinoflagellates*, Oxford Blackwell Scientific Publications. pp. 298–529.
- Tester, P.A. & Steidinger, K.A. (1997). *Gymnodinium breve* red tide blooms: Initiation, transport and consequences of surface circulation. *Limnology and Oceanography* 42, 1039–1051.
- Trigueros, J.M. (2000). *Peridiniopsis salina* (Peridiniales, Dinophyceae), a new species of brackish dinoflagellate from Urdaibai estuary, North Spain. *Phycologia* 39 (2), 126–133.
- Van Dolah, F.M. (2000a). Marine Algal Toxins : Origins, health effects, and their increase occurrence. *Environmental perspectives* 108, 133–141.
- Van Dolah F.M. (2000b). Diversity of Marine and Freshwater Algal Toxins. Dans : Botana L. [Eds]: *Seafood Toxicology: Pharmacology, Physiology and Detection*. Marcel Dekker, New York, pp. 19–43.

- Vargo, G.A., Heil, C.A., Fanning, K.A., Dixon, L.K., Neely, M.B., Lester, K., Ault, D., Murasko, S., Havens, J., Walsh, J., Bell, S. (2008). Nutrient availability in support of *Karenia brevis* blooms on the central West Florida Shelf: What keeps *Karenia* blooming. *Continental Shelf Research* 28, 73–98.
- Verleye, T.J., (2011). The late Quaternary palaeoenvironmental changes along the western South-American continental slope: A reconstruction based on dinoflagellate cysts and TEX₈₆. PhD thesis, Ghent University, Belgium, p. 245.
- Versteegh, G.J.M., Blokker, P., Bogus, K.A., Harding, I.C., Lewis, J., Oltmanns, S., Rochon, A., Zonneveld, K.A.F. (2012). Infra red spectroscopy, flash pyrolysis, thermally assisted hydrolysis and methylation (THM) in the presence of tetramethylammonium hydroxide (TMAH) of cultured and sediment-derived *Lingulodinium polyedrum* (Dinoflagellata) cyst walls. *Organic Geochemistry* 43, 92–102.
- Von Stosch, H.A. (1973). Observations on vegetative reproduction and sexual life cycles of two freshwater dinoflagellates, *Gymondinium pseudopalustre* Schiller and *Woloszynskia apiculata* sp. nov. *British Phycological Journal* 8, 105–134.
- Wall, D. (1971). Biological problems concerning fossilizable dinoflagellates. *Geoscience and Man* 3, 1–15.
- Zingone, A. & Enevoldsen, H.O. (2000). The diversity of harmful algal blooms : A challenge for science and management. *Ocean and Coastal Management* 43, 725–748.
- Zonneveld, K.A.F., Versteegh, G., Kodrans-Nsiah, M. (2008). Preservation and organic chemistry of Late Cenozoic organic-walled dinoflagellate cysts: A review. *Marine Micropaleontology* 68, 179–197.